Model-Based Predictive Control Strategies and Renewable Energy Integration for Energy Flexibility Enhancement in School Buildings

Navid Morovat

A Thesis

In the Department of

Building, Civil, and Environmental Engineering

Presented in Partial Fulfillment of the Requirements

For the Degree of

Doctor of Philosophy (Building Engineering)

at Concordia University

Montréal, Québec, Canada

March 2024

CONCORDIA UNIVERSITY

SCHOOL OF GRADUATE STUDIES

This is to certify that the thesis is prepared

By: Navid Morovat

Entitled: Model-Based Predictive Control Strategies and Renewable Energy Integration for Energy Flexibility Enhancement in School Buildings

and submitted in partial fulfillment of the requirements for the degree of

Doctor of Philosophy (Building Engineering)

Complies with the regulations of the University and meets the accepted standards with respect to originality and quality.

Signed by the final Examining Committee:

Dr. Gösta Grahne	Chair
Dr. Jin Wen	External Examiner
Dr. Chunyan Lai	Arm's Length Examiner
Dr. Liangzhu (Leon) Wang	Examiner
Dr. Mohamed Ouf	Examiner
Dr. Andreas K Athienitis	Co-Supervisor
Dr. José Agustín Candanedo	Co-Supervisor

Approved by _____

Dr. Chunjiang An, Graduate Program Director

2024-03-06

Date of defense

_____

Dr. Mourad Debbabi, Dean of Gina Cody School of Engineering and Computer Science

Abstract

Model-Based Predictive Control Strategies and Renewable Energy Integration for Energy Flexibility Enhancement in School Buildings

Navid Morovat, Ph.D.
Concordia University, 2024

This thesis investigates methods to enhance the energy flexibility potential of school buildings through simulation and experimental studies. It contributes a general methodology for the development of data driven grey-box thermal models and the implementation of model-based predictive control (MPC). The methodology is applied to an archetype fully-electric school building near Montréal, Québec, Canada. This approach is scalable and transferable to other institutional or mid-size commercial buildings.

To streamline the implementation of MPC, the proposed approach employs grey-box low-order resistance-capacitance (RC) thermal network models, a clustering of weather conditions to identify typical anticipated scenarios, and several near-optimal setpoint profiles corresponding to each cluster. Archetype control-oriented models for zones with convective systems and zones with radiant floor systems are developed and calibrated with measured data. The calibrated models are used to apply MPC to the school building using the established dynamic tariffs for morning and evening peaks. For the experimental study, the developed MPC framework is applied in six classrooms, and the results are compared with four classrooms with the reactive control system as reference cases. The energy flexibility is quantified based on a proposed building energy flexibility index (BEFI). Results indicated that the school building can provide 45% to 95% energy flexibility (load shifting relative to reference) during on-peak hours while satisfying thermal comfort constraints.

Finally, this thesis presents an MPC methodology for the integration of air-based photovoltaic/thermal (PV/T) systems to further enhance the energy flexibility in school buildings so that in addition to the production of solar electricity, they can be used to preheat fresh air for the classrooms during the heating season. A data-driven grey-box model for the classrooms is calibrated with measured data, and a PV/T model as a renewable energy retrofit measure for energy

efficiency and flexibility is developed. These models are integrated to apply MPC and reduce peak demand during morning and evening. Results show that using an MPC along with PV/T integration can significantly reduce peak demand during morning and evening high demand periods for the grid. The proposed methodology helps institutional buildings to facilitate their integration into future smart grids and smart cities.

ACKNOWLEDGEMENTS

I would like to express my deepest gratitude to my supervisors, Professor Andreas K. Athienitis and Professor José Agustín Candanedo, for their precious guidance and advice. Your expertise, support, and dedication to academic excellence have influenced the results of this research and contributed significantly to my self-development. You have also granted me innumerable enriching experiences: IEA Annex 67, IEA Annex 81, IEA Annex 82, IBPSA 2019, ACEEE 2020, eSim 2021, ASHRAE 2021, IBPSA 2021, Purdue 2021, ASHRAE 2022, COBEE 2022, NSB 2023, and SDEWES 2023, among others.

My participation in the NSERC/Hydro-Québec Industrial Research Chair in Optimized Operation and Energy Efficiency: Towards High-Performance Buildings was an invaluable experience. I was also fortunate to have the opportunity to work at CanmetENERGY-Varennes with bright colleagues within the Intelligent Buildings group and contribute to and learn from their interesting research projects.

Technical support provided by Régulvar and Centre de Services Scolaire des Mille-Îles (CSSMI) is acknowledged with thanks. The comments of our colleagues at CanmetENERGY are gratefully appreciated. I would like to acknowledge the financial support received from Fonds de Recherche du Québec - Nature et Technologies (FRQNT) in the form of a Doctoral Research Scholarship. I could not have carried out this research without their generous contributions.

I want to thank all my colleagues within the Centre for Zero Energy Building Studies (CZEBS). It was very interesting and thought-provoking working in a multidisciplinary team. Thank you all for your friendship, enthusiasm, helpful ideas, and cooperation.

I would also like to thank my family for their constant support during my studies and encouragement to continue my studies in the best way possible. Finally, I would like to thank all my friends who supported me in making my studies and life more beautiful.

Thank you all!

Table of Contents

List of Figures

List of Tables

Nomenclature

A_i	Area of surface represented by node i	(m^2)
C_i	Thermal capacitance of node i	(J/K)
C_a	Thermal capacitance of air	(J/K)
cp_{air}	Specific heat of air	(J/kg°C)
G	Incident radiation	(W/m^2)
h_{c_ins}	Convective heat transfer coefficient from insulation to flowing air	(W/m^2°C)
h_{c_PV}	Convective heat transfer coefficient from PV to flowing air	(W/m^2°C)
h_i	Film coefficient	(W/m^2°C)
J	Objective function	
k	Thermal conductivity of materials	(W/mK)
K_i	Integral control constant	(W/°Cs)
K_p	Proportional control constant	(W/°C)
L	Channel length	(m)
l_i	Thickness of surface i	(m)
$\dot{m}$	Mass flow rate	kg/s
N	Number of time steps	
p	Time step	
P	Power	(W)
PF	Peaking factor	
PH	Prediction horizon	
P_{elec}	Electrical energy produced by the PV/T system	(W)
P_{flex}	Power demand in flexible case	(W)

P_{max}	Maximum power of heating system	(W)
P_{ref}	Power demand in reference case	(W)
$P_{thermal}$	Produced heat	(W)
Q_{aux}	Auxiliary(heating/cooling) source	(W)
Q_{i}	Source entering node i	(W)
Q_{sg}	Solar gains	(W)
Q_{thermal}	Thermal energy produced by the PV/T system	(W)
$R_{\text{i,j}}$	Thermal resistance between nodes i and j	(K/W)
t	Time	(sec)
T	Temperature	(ºC)
T_{a}	Air temperature	(ºC)
T_{i}	Temperature of node i	(ºC)
T_{inlet}	Inlet temperature	(ºC)
T_{ma}	Average air temperature inside the air channel	(ºC)
T_{o}	Outdoor temperature	(ºC)
T_{op}	Operative temperature	(ºC)
T_{outlet}	Outlet temperature	(ºC)
T_{PV}	PV temperature	(ºC)
T_{setpoint}	Air setpoint temperature	(ºC)
T_{STC}	PV module cell temperature at standard test conditions	(ºC)
U_{i}	Thermal conductance at node i	(W/K)
U_{inf}	Infiltration U-value	(W/K)

U_{win}	Window U-value	(W/m^2K)
UA	Conductance	(W/K)
u	Input vector	(-)
$U_{i,j}$	Thermal radiation U-value between surface i and j	(W/K)
$W_{channel}$	PV/T channel width	(m)

Greek letters

α_s	Solar absorptance of the wall	
β_{PV}	PV module temperature coefficient	
Δt	Simulation time step	(s)
ΔT	Temperature difference	(ºC)
η_{PV}	PV electrical efficiency	(%)
η_{STC}	PV module electrical coefficient under standard testing conditions	(%)

Abbreviation and Acronyms

ACH	Air change per hour
ADR	Active demand response
AHU	Air handling unit
ASHP	Air source heat pump
ASHRAE	American society of heating refrigeration and air-conditioning engineers
BAS	Building Automation System
BAU	Business as usual
BEFI	Building Energy Flexibility Index
BEMS	Building Energy Management System
PV/T	Building Integrated Photovoltaic / Thermal system
BOPTEST	Building Optimization Performance Test
C&I	Commercial and Institutional
COP	Coefficient of Performance
CO_2	Carbon Dioxide
CV-RMSE	Coefficient of variation of the root mean squared error
DHW	Domestic Hot Water
DR	Demand response
DSM	Demand-side management
EUI	Energy use intensity
EV	Electric Vehicle
GHG	Green House Gas
GSHP	Ground Source Heat Pump
HP	Heat pump
HVAC	Heating, Ventilation and Air Conditioning
IAQ	Indoor Air Quality
IEA EBC	International Energy Agency in Buildings and Communities
MPC	Model predictive control

NMBE	Mean biased error
PCM	Phase Change Material
PID	Proportional-Integral-Derivative
PV	Photovoltaic
PV/T	Photovoltaic/Thermal system
RBC	Rule Based Control
RES	Renewable Energy Sources
RC model	Resistance capacitance model
RFH	Radiant floor heating
RL	Reinforcement Learning
RMSE	Root mean squared error
ROM	Reduced-order model
SLSQP	Sequential Least Squares Quadratic Programming
SSEC	Solar Simulator and Environmental Chamber
STPV	Semi-transparent PV
TES	Thermal Energy Storage
TOU	Time-of-use

Chapter 1: Introduction

Buildings are responsible for approximately 32% of the energy use worldwide, 17% of direct CO_2 emissions, and 33% of indirect CO_2 emissions (Policy 2013). Thus, building energy efficiency and ways to reduce CO_2 emissions are of primary importance. Using on-site renewable energy systems such as photovoltaics (PV) and heat pumps (HPs) is an efficient way to decarbonize and increase building energy efficiency, particularly in green-powered grids (Liu et al. 2023, Pochwała et al. 2023). Additionally, heat pumps can be integrated with intelligent building management systems to optimize energy usage and further enhance overall sustainability in the built environment (Gibbons and Javed 2022, Mitterrutzner et al. 2023). However, incorporating renewable energy sources (such as PV systems) and HPs into an already strained electric grid presents a challenge, especially in locations where the peak demand is associated with extreme cold weather events. Therefore, utilizing the energy flexibility of the building load is critical for reducing peak grid demand.

Demand-side management (DSM) is considered one of the most effective ways to reduce peak electricity demand (Tang et al. 2021). Demand-side management strategies can be classified into three categories: energy efficiency measures, demand response (DR), and energy flexibility (Farrokhifar et al. 2021, Fernández Bandera et al. 2023). *Energy efficiency* measures are characterized by reductions in energy consumption compared to a reference system or baseline. *DR*, an approach that curtails building electrical demand during grid on-peak hours, is a strategy for reducing electric loads in buildings without significant capital investment. *Energy flexibility*, in turn, is characterized by shifting energy demand profiles to satisfy grid and local objectives, including energy availability, cost management, and carbon emission reduction (Reynders et al. 2018). It is typically executed in a planned and optimized manner (Reynders et al. 2018, Finck et al. 2019). Annex 67 of the International Energy Agency-Energy in Buildings and Communities Programme (IEA-EBC) defined energy-flexible buildings as those with "the ability to manage [their] demand and generation according to local climate conditions, user needs and grid requirements" (Jensen et al. 2017).

In smart electricity grids, buildings are increasingly recognized as flexible loads that can act as energy generators (Li et al. 2019), energy storage devices (Le Dréau and Heiselberg 2016), and

demand controllers (Wang et al. 2023). Improving energy flexibility and reducing the peak demand will reduce the need to build new peaking fossil fuel power plants and their accompanying environmental concerns (Diakaki et al. 2008, Huang et al. 2021). Buildings can provide different flexibility services to reduce peak loads and shift demand in accordance with local renewable energy sources production, e.g., utilization of thermal mass (Foteinaki et al. 2018, Weiß et al. 2019) storage in batteries, charging of electric vehicles (Zhou and Cao 2019) and adjustability of the heating, ventilation, and air conditioning (HVAC) system use (Jensen et al. 2017).

According to the published literature and presented in IEA-EBC Annex 67 (Figure 1-1), increasing energy flexibility for the design of smart energy systems and buildings is influenced by four important factors (Reynders et al. 2014, Jensen et al. 2017):

- Physical characteristics of the building,
- HVAC systems and storage equipment,
- Adequate control systems and strategies,
- Comfort requirements.

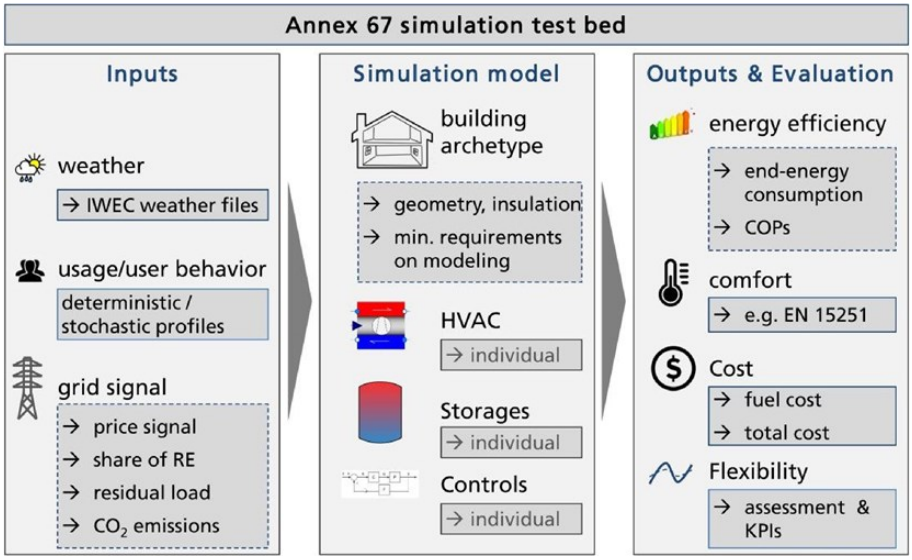

Figure 1-1: Sketch of the simulation test bed proposed for modelling work in Annex 67 (Jensen et al. 2017).

In this context, the appropriate application of control strategies in HVAC systems is a key factor in improving the energy performance (Braun 2003, Tabares-Velasco et al. 2012, Afroz et al. 2018, Morovat et al. 2019) and energy flexibility of buildings (Le Dréau and Heiselberg 2016, Jensen et

al. 2017, Reynders et al. 2018) by reducing the time mismatch between supply and demand for heating or cooling (Klein et al. 2017).

1.1 Grid Requirements

Energy flexibility is critical to addressing the grid's challenges of balancing supply and demand and incorporating renewable energy capacity. Buildings can play an important role in DR. The magnitude and flexibility of buildings' energy demand can become a key asset for smart grids if well managed (Li et al. 2017).

Québec generates most of its electricity (94%) from hydroelectric plants (Canada energy regulator 2021), and most commercial buildings rely on electricity as their primary or only energy source (Distribution.). In Québec, the morning and evening peaks in winter put a great deal of strain on the electrical grid to provide electric power during extremely cold weather (Hydro-Québec 2020). Therefore, controlling energy use is essential to reduce the time mismatch between supply and demand (Klein et al. 2017, Afroz et al. 2018). Figure 1-2 shows the peak electricity demand from 2020 to 2022 in Québec, called "Beaver curve" by this thesis. It depicts that the highest peak demand occurred in the morning between 6:00 to 9:00 a.m. Also, it shows a power demand of 40,178 MW in 2022, which is the highest power demand in the history of Hydro-Québec (Hydro-Québec 2023).

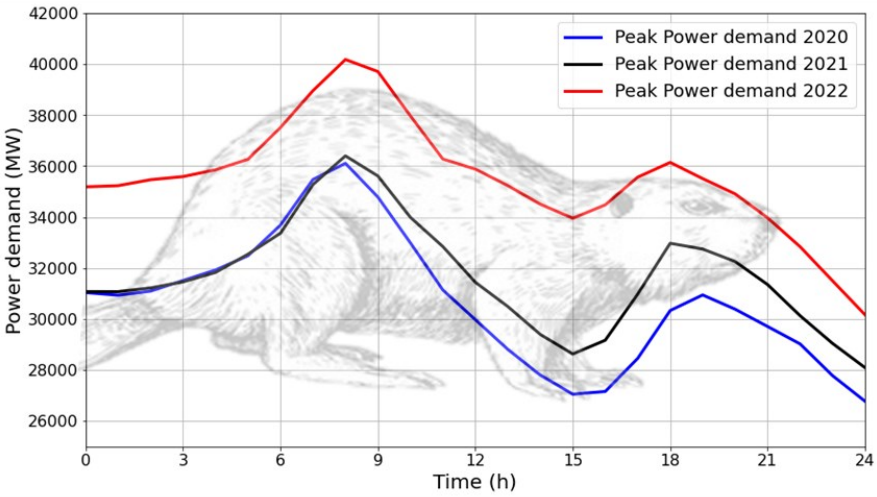

Figure 1-2: Example of peak electricity demand in Québec (Hydro-Québec 2023), "Beaver curve"

This shape of daily demand profile (shown in Figure 1-2), with a morning peak, an afternoon dip, and another evening peak, is very typical. When a large amount of generation from PV panels

adds to the grid on a sunny day, the system curve displays an even more apparent "belly" appearance in the midday and a steep rise after the sunset, portraying the silhouette of a duck. This phenomenon of grid demand profile is also known as the "duck curve" (Denholm et al. 2015). Figure 1-3 presents the California grid duck curve between 2015 and 2023.

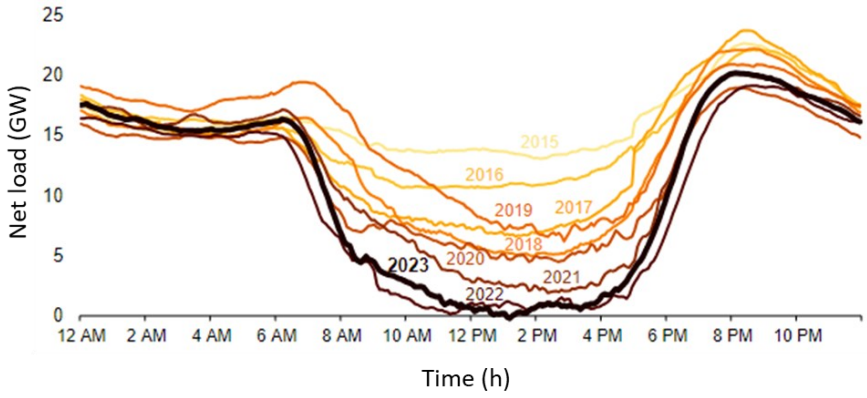

Figure 1-3: The California grid duck curve between 2015 to 2023 (US Energy Information Administration 2023)

The duck curve has created opportunities for energy storage. For commercial and institutional (C&I) buildings installing electric battery storage would be costly. Thus, buildings with flexible electricity demand offer grid-responsive support, especially for large C&I buildings (Chen et al. 2019, Fu et al. 2022).

School buildings represent a sizeable portion of the C&I building stock. There are over 15,500 schools in Canada, with over 5 million students and nearly 700,000 teachers and other employees (Statistic Canada 2017). Thus, quantification of energy flexibility in school buildings has a significant role in providing a safe and efficient operation of the future resilient grid. Furthermore, school buildings provide an interesting example of the potential of other C&I buildings. Improving learning and teaching performance in schools requires higher indoor environmental quality (IEQ), which can significantly impact students' and teachers' health and well-being. However, HVAC systems are often far from optimal energy performance in school buildings (Droutsa et al. 2021). Enabling communication and control technology in these buildings is the key to enhancing energy flexibility and actively involving commercial HVAC loads in future electricity grid scheduling. Figure 1-4 presents the electricity demand of a typical school on a cold day in Québec. This graph depicts that the school's peak load is in the early morning, which is simultaneous to the grid's peak

load. Thus, appropriate control strategies and renewable energy retrofits are needed to enhance energy flexibility in schools or other institutional buildings.

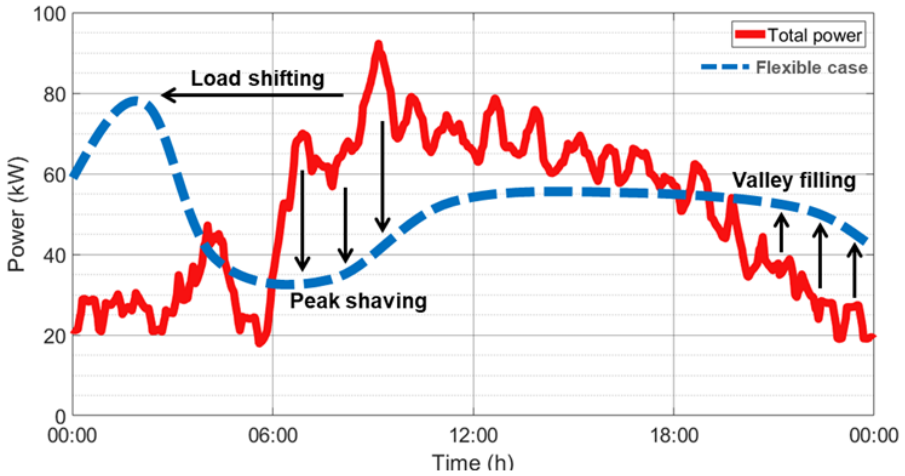

Figure 1-4: Electricity demand of a typical school in a cold day.

In summary, the new operating conditions (e.g., RES integration, oversupply risk) of the electric grid require novel concepts and methodologies to tackle the associated problems. With the advancement of internet and communication technologies, school buildings, with their embedded energy flexibility, can contribute significantly to the process of grid modernization, as well as being an indispensable part of the smart grid.

1.2 Case study

Building energy performance simulation (e.g., EnergyPlus and TRNSYS) is a popular approach to studying school buildings. However, studies based on control-oriented models and measured sensor data of schools are relatively rare (Ham et al. 2023). This research investigates measured field data in an archetype school building in Québec, Canada. The case study is an elementary school (Figure 1-5) located in Sainte-Marthe-sur-le-Lac, near Montreal, Québec, Canada. The school is under the jurisdiction of the CSSMI school board (Centre de services scolaires des Mille-Îles).

The location of the school makes it an ideal site for studying the impact of flexibility events on power demand in educational institutions in cold climate regions. This two-storey school is about 80 m by 44 m and oriented 35° west of south. The first floor consists of 10 classrooms, offices, a kitchen, daycare, a music room, a kindergarten, and a gym, while the second floor has 13

classrooms and a library. It is an archetype of new school buildings in Québec, with a 60% window-to-wall ratio of double-glass windows with an air gap.

The classrooms are heated with local water-to-air HPs in their ceilings, using a geothermal system as their heat source, and an individual thermostat controls each classroom. Each classroom has a smart controller panel to adjust the temperature and lighting level and monitor CO_2 ppm, relative humidity, and energy consumption (Figure 1-6). The offices and the gym also have radiant floor systems connected to a geothermal water-to-water heat pump. The school's design incorporates energy-efficient LED lighting and motion sensors to reduce energy consumption further when classrooms are unoccupied. The whole system is closely monitored with sensors. Thermostat and power meter data were collected at 15-minute intervals in CopperCube, an on-site trend log archiver, through the BACnet network. These datasets include setpoint temperature, indoor temperature, CO_2 level, air and water flow rate, and electricity power of HVAC systems.

Figure 1-5: Horizon-du-Lac school building (left) and a classroom with the control panel (right)

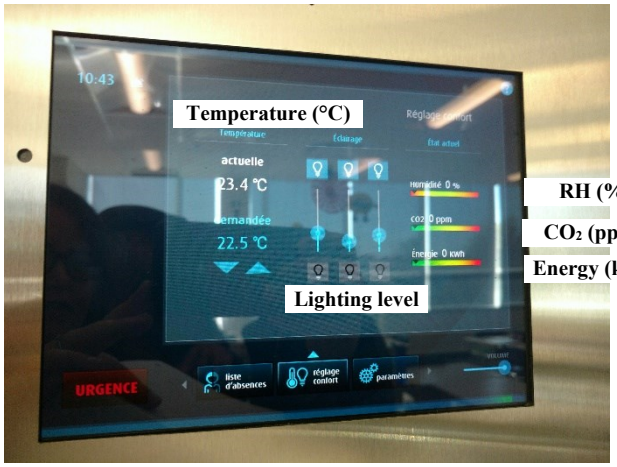

Figure 1-6: Control panel for adjusting setpoint temperature and monitoring measured data in classrooms

The summary of building information, including general information, mechanical system, school's schedule, and utility tariffs is listed in Table 2.

Table 2. Key features of the school building and utility tariff

General Information	Site	Sainte-Marthe-sur-le-Lac, Québec, Canada
	In operation	since 2017
	Net floor area	2596 m^2/floor
	Number of floors	2
	Number of classrooms	23
	Number of students	576
	Window type	Double-glazed argon Low-e
Mechanical	Space heating/cooling	Hydronic radiant floor heating system, Convective system
	Heating/cooling equipment	Ground source water-water HP and local water-air HPs
	Ventilation system	Centralized dual-core heat recovery system modulated based on schedule and CO_2 threshold
	Domestic Hot water source	Two electricity boilers with a capacity of 15 kW each
	Thermal Energy Storage	An electrical thermal storage unit with a maximum capacity of 80 kW on the source side. (ThermElect)
Default Schedule	Occupied hours	From 06:00 to 18:00, 20-24 °C
	Unoccupied hours	From 18:00 to 6:00, 18-20 °C
Utility rate Flex M during winter	Consumption during off-peak hours	3.29¢/kWh
	Consumption during on-peak hours: • Morning: 06:00 to 9:00 • Evening: 16:00 to 20:00	51.97¢/kWh

The school BAS programs the default thermostat schedule, but an end-user (e.g., teachers) can override it by changing the setpoint. It should be noted that during the experiment, access to override the indoor temperature is restricted by obtaining permission from the school board. This restriction ensures that the experiments are conducted under controlled conditions and minimizes potential disruptions to the control strategies.

1.3 System description

Figure 1-7 presents the schematic of the building heating systems. The system consists of an integrated geothermal system, an electrically heated thermal energy storage device (ThermElect), a water-to-water HP, 36 terminal local water-to-air HPs in classrooms, and a floor heating system in offices and gym. All heating systems are electrical devices, providing a link to the electrical grid. A predictive controller can exploit this link to help balance electricity production and demand, among other potential uses.

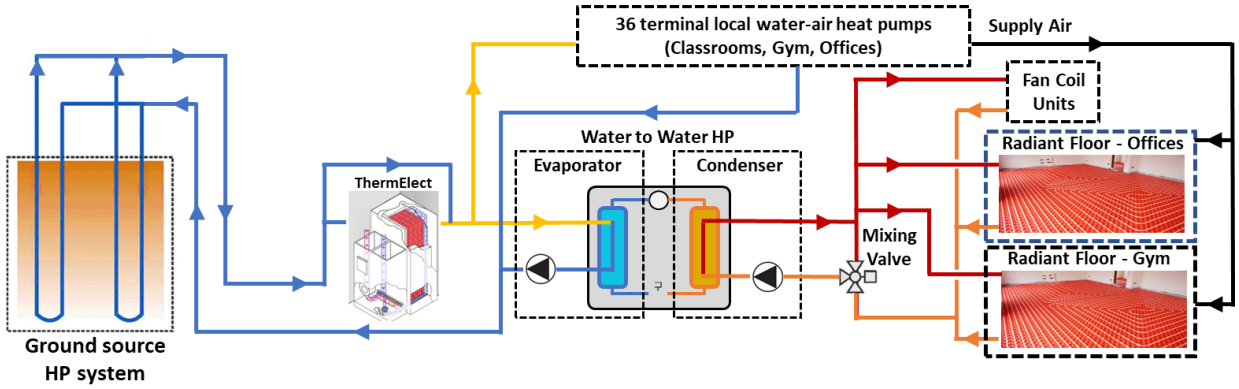

Figure 1-7: Schematic of the building heating systems.

The main water-to-water HP for space heating has a nominal heating output of 33 kW in two stages (16.5 kW per stage) and a maximum water supply temperature of 48.8 °C. Low-temperature heat on the evaporator side of the HP is generated by a geothermal system with 28 loops. The ThermElect can preheat the water inlet to local water-to-air HPs and the water-to-water HP. The sensor data from the ground heat exchanger, the thermal storage device, and the water-to-water HP are collected (fifteen-minute time step) and then used as the inputs for the modelling. A thermostatic three-way valve regulates the temperature of the supply water of the HP to the zones, with a maximum setting of 60 °C. An integrated floor heating system supplies space heating and

a convective ceiling system throughout the offices and the gym. Thermostats regulate the indoor temperature in each zone separately.

1.4 Objectives

The overall goal of the dissertation is to investigate the energy flexibility potential in school buildings through simulation and experimental studies. It contributes a general methodology for the development of data-driven grey-box thermal models and the implementation of model-based predictive control (MPC). The methodology is applied to an archetype fully-electric school building near Montréal, Québec, Canada. This approach is scalable and transferable to other institutional or mid-size commercial buildings.

More specifically, the objectives of the work can be summarized as follows:

1. **Develop data-driven grey-box thermal models:** Create reliable and robust data-driven archetypical control-oriented models for (a) zones with convective systems and (b) zones with radiant floor systems.
2. **Develop model predictive control (MPC):** Apply MPC techniques to develop advanced control strategies for HVAC systems in school buildings, under a regime of established dynamic tariffs for morning and evening peak periods.
3. **Introduce energy flexibility KPIs:** Introduce key performance indicators (KPIs) as a function of key parameters to quantify energy flexibility at both the zone level and the whole building level, while also considering IEQ.
4. **Implement the developed MPC in an archetype school building:** Test the effectiveness of the MPC strategy by conducting experiments in an archetype school building.
5. **Assess the potential of MPC for energy flexibility enhancement:** Evaluate the potential of the proposed approach to activate and harness the energy flexibility inherent in fully electric, occupied school buildings.
6. **Evaluate the potential of PV/T and MPC as a renewable energy retrofit in existing school buildings:** Design a model predictive control methodology for integrating retrofitted air-based PV/T systems in school buildings.

These objectives aim to contribute to the development of an innovative and scalable approach for optimizing energy flexibility in school buildings, with broader applicability to institutional buildings in general.

1.5 Outline of the thesis

In view of the aforementioned objectives, this thesis is structured as follows:

Chapter 1 Introduction. Presents an overview of the thesis, which illustrates the background and objective of the study.

Chapter 2 Literature Review. Methods for assessing building performance and simulation methods are presented. Emphasis is given to control-oriented models. Data-driven grey-box models are identified as a suitable approach for application in the context of demand-side management in smart grids. Model-based predictive control, energy flexibility, and recent works on school buildings are reviewed. The need to apply MPC strategies and energy retrofit with PV/T in school buildings is shown, and limitations in existing buildings are analyzed, followed by the current research needs.

Chapter 3 Methodology. First, the grey box modelling approach is described. Then, the time series clustering and its application in preprocessing of data for the control-oriented models is explained. MPC as an advanced control strategy is presented, and the KPIs for quantification of energy flexibility at zone level and building level are proposed.

Chapter 4 Archetype Control-Oriented Modelling. Modelling and calibration of the grey-box models with measured data are presented. Then, it explores the testing of different control scenarios to assess the impact on electricity demand and energy performance. The results obtained using flexible scenarios are compared to the current operation of the building as a reference case.

This chapter is based on the following peer-reviewed journal articles and published refereed conference papers:

- **Morovat, N.,** Athienitis, A. K., Candanedo, J. A., Delcroix, B. (2022). “Data-driven model-based control strategies to enhance energy flexibility in electrically heated school buildings”, Buildings, 12(5), 581. (Published)

- Candanedo, J. A., Vallianos, C., Delcroix, B., Date, J., Saberi, A., **Morovat, N.,** John C., and Athienitis, A. K. (2022), "Control-oriented archetypes: a pathway for the systematic application of advanced controls in buildings", Journal of Building Performance Simulation, 1-12. (Published)
- **Morovat, N.,** Athienitis, A. K., Candanedo, J. A. (2021). "Modeling energy performance and real-time energy flexibility of a floor heating system in a school building", Building Simulation 2021 Conference, Bruges, Belgium, September 1-3. (Presented)
- Athienitis, AK., Dumont, E., **Morovat, N.,** Lavigne, K., Date, J. (2020), "Development of a dynamic energy flexibility index for buildings and their interaction with smart grids", ACEEE Summer Study on Energy Efficiency in Buildings, California, USA, August 17-2. (Presented)
- **Morovat, N.,** Candanedo, J. A., Athienitis, A. K. (2021). "Application of grey-box models for the quantification of the energy flexibility of a school building in Canada", 2021 ASHRAE Annual Conference, Phoenix, USA, June 28-30. (Presented)

Chapter 5 Model Predictive Controls and Field test. This chapter illustrates the development and implementation of a model predictive control methodology to activate the energy flexibility of fully-electric school buildings to reduce electricity demand during peak demand periods of the electric grid. A data-driven grey-box approach is used to create archetype models for different thermal zones in a typical school building. The weather data are clustered into several categories, representing different weather conditions. For each MPC scenario, a simulation is run using forecast weather data to quantify and enhance energy flexibility in response to grid requirements. The developed MPC framework is then applied in six classrooms, and the results are compared with four classrooms with the reactive control system as reference cases.

This chapter is based on the following journal article and published refereed conference papers:

- **Morovat, N.,** Athienitis, A. K., Candanedo, J. A. (2023). "Energy Flexibility Activation in School Buildings: Heuristic Model Predictive Control Method", Energy Journal. (Under review)
- **Morovat, N.,** Athienitis, A. K., Candanedo, J. A. (2023). "Field test of model predictive control in occupied all-electric school buildings located in a cold climate region", Building and Environment journal. (Submitted)

- **Morovat, N.,** Athienitis, A. K., Candanedo, J. A. (2023), "Model predictive control for demand response in all-electric school buildings", 13th Nordic Symposium on Building Physics (NSB 2023), Aalborg, Denmark, 12-14 June 2023. (Presented)
- **Morovat, N.,** Athienitis, A. K., Candanedo, J. A. (2022), "Enhancing energy flexibility of a school building using local setpoint adjustment in classrooms", 5th International Conference on Building Energy and Environment, Concordia University, Montreal, Québec, Canada, July 25-29. (Presented)
- **Morovat, N.,** Athienitis, A. K., Candanedo, J. A. (2022), "A Model Predictive Control Method to Activate the Energy Flexibility of School Buildings", 7th International High-Performance Buildings Conference 2022, Purdue University, West Lafayette, IN, USA, July 10-14. (Presented)
- **Morovat, N.,** Candanedo, J. A., Athienitis, A. K. (2020), "Data analysis, modelling, and energy flexibility assessment of an educational building in Canada", eSIM 2021 Conference, Vancouver, BC, Canada, June 14 -16. (Presented)

Chapter 6 Modelling PV/T with MPC. This chapter presents an MPC approach for integrating PV/T systems as a renewable energy retrofit for energy efficiency and flexibility in school buildings. In this chapter, three scenarios are investigated and compared: 1) Reference case without a PV or PV/T system, 2) Flexible case integrating a PV system and MPC strategies, and 3) Flexible case integrating of a PV/T system and MPC strategies.

This chapter is based on the following journal article and published refereed conference papers:

- **Morovat, N.,** Athienitis, A. K., Candanedo, J. A. (2023), "Design of a model predictive control methodology for integration of retrofitted air-based PV/T system in school buildings", Journal of building performance simulation (Under review)
- **Morovat, N.,** Athienitis, A. K., Candanedo, J. A. (2023), "Model Predictive Control for Integration of PV/T system in School Buildings", The 18th Conference on Sustainable Development of Energy, Water and Environment Systems (SDEWES), Dubrovnik, Croatia, 24–29 September 2023. (Presented)

Chapter 7 Conclusion and Directions for Future Work. This chapter concludes the thesis and provides recommendations for future work. References and appendices follow Chapter 8.

Chapter 2: Literature review

This chapter discusses existing literature on the topics of building thermal modelling, model parameter identification, model-based predictive control, building energy flexibility, previous works on the field test of MPC, and renewable energy retrofit in buildings. Section 2.1 presents an overview of building thermal modelling approaches. Section 2.2 discusses previous work on MPC for buildings. Section 2.3 outlines previous work on the implementation of MPC in real buildings. Section 2.4 discusses research on building-grid interaction and building energy flexibility. Section 2.5 presents the literature on school buildings; Section 2.6 discusses renewable energy retrofits using PV systems in buildings. Finally, Section 2.7 discusses research needs and proposed work.

2.1 Modelling methods

In general, three main approaches are used to create building energy models (Coakley et al. 2014, Li and Wen 2014, Chen et al. 2022):

- *White-box models:* In this approach, physical principles simulate the heating and cooling demand. Most building simulation programs utilizes this approach. However, the accuracy of control strategies relying on these physical models has not been satisfactory since some real building parameters in existing buildings are often unknown and tend to deviate significantly from the design values (Crawley et al. 2001, Hensen and Lamberts 2012).
- *Black-box (purely data-driven) models:* In recent years, this approach with self-learning capabilities has become popular. Black-box models rely on statistics and machine learning methods. However, a substantial amount of data might be required to achieve the accuracy needed for a control-oriented model, and the resulting parameters may lack a clear physical interpretation (Chen et al. 2022).
- *Grey-box (partly data-driven) models*: With this approach, both physical insight and the trustworthiness of real data are maintained. To implement MPC in building automation systems, it is essential to identify thermal models with sufficient resolution, robust performance, and low computation time (Candanedo et al. 2022).

Proper identification of building thermal models with adequate resolution, robustness, and acceptable computation time is fundamental for the widespread implementation of MPC or other

advanced control strategies in building automation systems. In grey-box models, choosing an appropriate level of resolution is essential as it directly affects the parameter tuning and calculation time. A high-order model containing too many parameters requires information that is not often available with adequate accuracy. An oversimplified model may not be accurate enough to be helpful as a decision-making tool. Thus, considering the control objectives and constraints, such as thermal comfort criteria, model complexity should be carefully chosen.

Smart grids integrate real-time communication between both demand and supply sides to enable demand-side management and leverage storage technologies (Battaglini et al. 2009). According to the published literature review, grey box models are suitable for application in the context of demand-side management in smart grids. The model structures are derived from low order Resistance-Capacitance (RC) thermal networks that use an electric circuit analogy to describe the thermal dynamics of building systems. Gouda et al. (2002) proposed a second-order model in which each construction element is modelled using three resistances and two capacitances. Braun and Chaturvedi (2002) presented a simplified reduced-order RC models that uses a transfer function for building energy modelling. They found that one to two weeks of data are sufficient to accurately predict cooling/heating demand. Candanedo et al. (2013) proposed a methodology to create simplified reduced-order RC models for control studies. Their methodology can be implemented in building simulation tools to generate simplified models automatically.

The accuracy of the reduced-order models depends on their characteristic parameters (resistances and capacitances), so they must be appropriately adjusted. Bacher and Madsen (2011) proposed a statistical procedure for model identification suited to different applications in building thermal studies. Fraisse et al. (2002) proposed other methods to obtain the effective thermal parameters, but these methods require complex mathematical modelling. Reynders et al. (2014) analyzed two detached single-family houses in Belgium. These two buildings represent two extreme cases of detached single-family houses in Belgium regarding insulation level (high and low insulation level). They used data obtained from detailed building simulations with the IDEAS library in Modelica software. This study investigated five grey-box model types, ranging from first to fifth-order models (As shown in Figure 2-1).

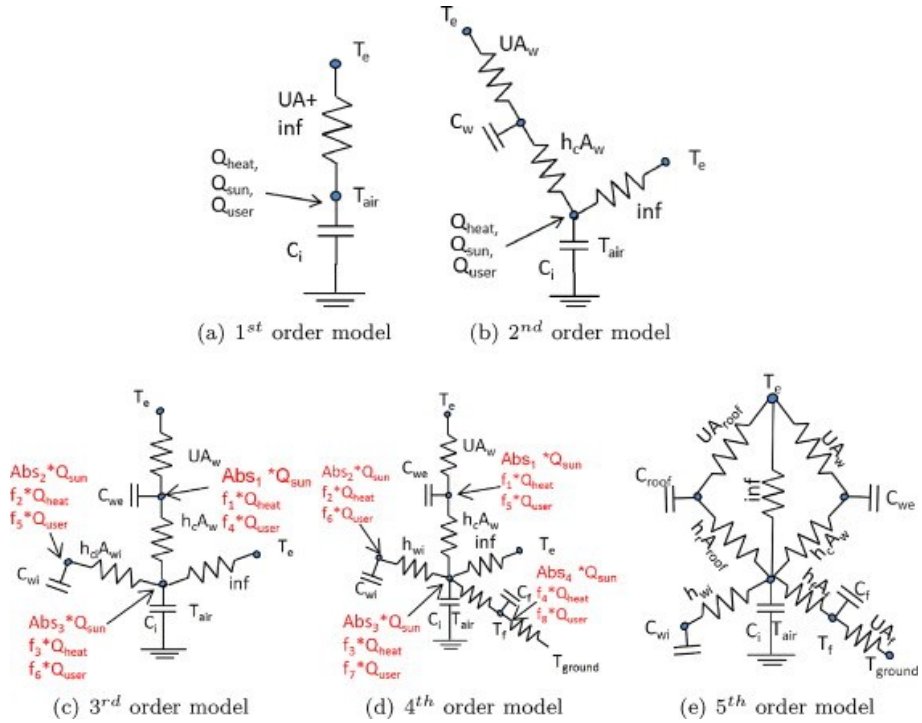

Figure 2-1: RC-analogy of reduced order building models (Reynders et al. 2014)

In the first-order model (Figure 2-1(a)), the entire thermal mass of the house is modelled with a single capacity. There is no distinction between fast-dynamic signals (i.e., indoor air temperature) and slow dynamic signals (i.e., structural mass). The 2nd order model (Figure 2-1(b)) considers this difference by including a second capacity. The 3rd order model (Figure 2-1(c)) has a thermal capacitance for the envelope, the internal walls and floors, and the indoor air. The 4th order model (Figure 2-1(d)) extends the 3rd order model by including a different capacity for the floor. In the 5th order model (Figure 2-1(e)), additional capacitance is included for the roof. Since a lightweight structure is used for the pitched roof, the dynamics of the roof can be expected to differ significantly from the heavy-weight brick walls. Therefore, the potential model improvement by separating the dynamics of the roof and the exterior walls is investigated.

Bacher and Madsen (2011) presented a method for determining effective heat dynamics models based on a single-story residential building as a case study. A hierarchical model complexity framework and forward selection strategy were applied for iterative model selection. Likelihood ratio tests compared model performance, and validation involved statistics and physical interpretation. Leprince et al. (2022) introduced an automated stochastic model identification method for scalable deployment in residential buildings. They applied a forward model selection

process with a residual auto-correlation indicator. Testing on 247 residential buildings revealed distinct fit-quality groups, indicating the approach's potential for city-scale modeling, energy disaggregation, and demand-side management. Vallianos et al. (2022) presented a method for automatically generating thermal models in residential buildings using data from smart thermostats. The methodology incrementally increased model complexity by adding or removing parameters based on their impact on model quality, which was assessed using the Bayesian Information Criterion. This approach was applied to a residential building in Québec, Canada, demonstrating effective 24-hour predictions based on zone-specific thermal dynamics and solar gain factors.

2.2 Model predictive control (MPC)

Classical control techniques such as thermostat control (On/Off control with predefined setpoints and PID control) are popular in Building Energy Management Systems (BEMS). Large commercial buildings usually have significant thermal mass in the form of exposed concrete or tiled concrete floors. Typically, feedback methods, such as proportional-integral (PI) control, are used in the local control of these buildings. These approaches are suitable for fast responding local loops but fail to control slow responding dynamic processes efficiently (e.g., radiant floor systems which are used for energy storage) (Afram and Janabi-Sharifi 2014). The time lag of the temperature response and the associated occupant discomfort is a function of many parameters, including the amount of effective thermal mass and its thermal coupling with the occupied space (Chen 2013). The materials used as interior room layers, such as carpets, tiles, or wooden surfaces, also affect the thermal coupling between the surfaces and the indoor air and, therefore, the peak heating/cooling loads (Papachristou and Athienitis 2016). For this reason, anticipatory controls can be beneficial since they address the delay between the supplied heating/cooling and its effect on the room temperature. Li and Wen (2014) outlined three types of energy forecasting models (white-box, black-box, gray-box) and reviewed optimization methods for building energy systems.

In this context, model-based predictive control (MPC) is a promising approach to alternative feedback-only control strategies. MPC uses weather forecast and occupancy patterns and a mathematical model of the thermal space to choose the best action for the near future (Athienitis and O'Brien 2015). Additionally, upgrading the control strategy can be implemented relatively quickly compared to retrofitting HVAC systems or building envelopes, making it a cost-effective

solution for improving building energy flexibility (Taheri et al. 2022). MPC is particularly suitable for slow-responding systems (e.g., thermally massive buildings (Henze 2003, Sakellariou 2011, Hu and Karava 2014). Energy storage capacity—such as that provided by a thermal energy storage (TES) device or a significant thermal mass— enhances the potential of MPC since it allows planning the capture and release of energy as a function of the expected power load and energy cost profiles (Candanedo et al. 2013).

The proactive "look ahead" approach of MPC can provide significant improvements in energy efficiency, comfort conditions, load management, building-grid interaction, and energy flexibility of the building. Figure 2-2 provides a conceptual representation of MPC.

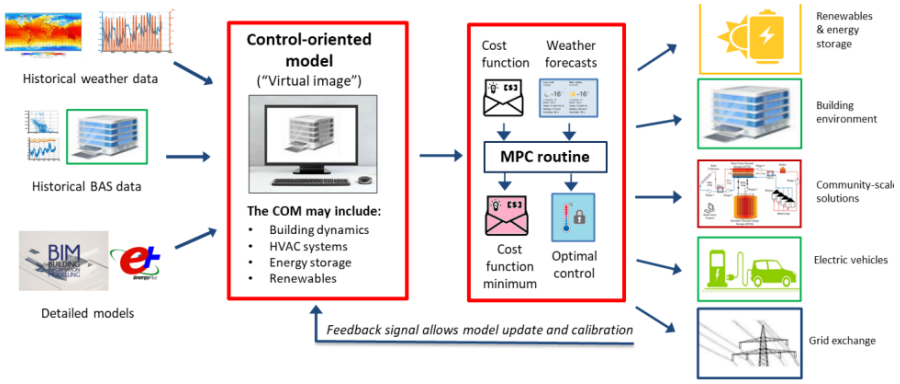

Figure 2-2: Conceptual representation of Model-based Predictive Control (MPC) (David Blum 2023)

Because of the number of variables and constraints that must be considered, optimization can become quite complex. Setting up a suitable building control model is crucial for MPC. An alternative way to tackle this problem is to employ approximations of the MPC solution. The gains from using only the most relevant features are threefold: first, improved performance, second, reduced complexity, and third, improved interpretability of the developed models. This is, however, typically where most of the effort in an MPC project goes.

Joe and Karava (2019) proposed an MPC approach that uses dynamic estimates and predictions of zone loads and temperatures, outdoor weather conditions, and HVAC system models to minimize energy consumption and cost while meeting equipment and thermal comfort constraints. Their study focuses on the comparison between theoretical MPC, experimental MPC, and simple feedback control for the floor heating system and air-based system. The study was carried out in three offices located in Herrick Building at Purdue University campus for both cooling and heating

seasons. They proposed a data-driven grey-box building model (Figure 2-3) based on the state-space formulation.

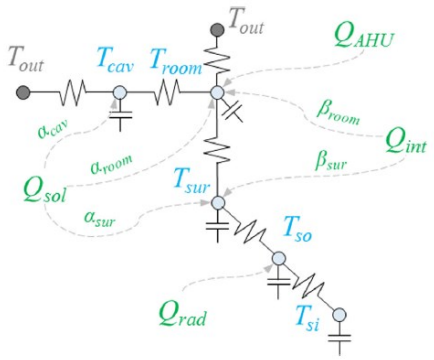

Figure 2-3: Grey box model structure (Joe and Karava 2019)

In general, previous research reports challenges associated with the control of radiant systems due to:

1) *Large thermal inertia*: it is difficult to handle conventional control strategies to respond to changes in weather or room temperature.
2) *Low heating/cooling power:* to overcome condensation and discomfort constraints.

MPC provides a systematic operation approach using a system model and an optimization algorithm to adjust the control setpoints dynamically while automatically satisfying steady-state and dynamic components and operation constraints related to building dynamics, HVAC equipment, etc. Compared to machine learning approaches that rely on input-output relations, MPC takes advantage of prior knowledge: on the building system and shows better performance in terms of energy savings as well as computational time (Wang and Ma 2008).

Li et al. (2022) studied the demand flexibility of a commercial HVAC system with an ice storage tank, and they found that MPC reduced the energy cost by up to 16% and the peak power demand by up to 25% compared with RBC in this case study. Liu et al. (2023) established a model predictive control method in residential buildings with a radiator heating system. The result of their numerical study showed that a predictive controller performs better than a conventional control in maintaining indoor temperature and can reduce energy consumption by 5%. Wang et al. (2022) proposed a clustering-based optimization method for regulating air conditioning system operation in office buildings. Results showed about 18% and 35% energy savings in summer and winter, respectively. Chen et al. (2023) developed an artificial neural network method combined

with MPC to decrease energy cost and consumption in an office zone in Edinburgh, Scotland. Their results showed that energy consumption decreased by 26%, and the cost decreased by 28%. Wang et al. (2023) compared the performance of reinforcement learning (RL) and MPC in enhancing building energy efficiency and operational flexibility. They found that the MPC controller outperformed the baseline controller, reducing discomfort by 100% and energy consumption by 22%. (Hu et al. 2019) investigated the control of floor heating systems in the context of smart grids. Through a testbed simulation, their results demonstrated that the MPC controller effectively reduces peak energy demand and saves electricity costs for residential users. Wang et al. (2023) explored using MPC in residential buildings to optimize air conditioner performance. Their results demonstrated that the MPC controller reduced cooling costs by 22% in the bedroom and 27% in the living room, outperforming traditional rule-based control. Merema et al. (2022) implemented an MPC controller for all-air systems in two lecture rooms at a university located in Ghent, Belgium. Their results showed a 40% reduction in electric energy use and up to 55% reduction in thermal energy.

2.3 Field test of MPC

Cotrufo et al. (2020) proposed an MPC framework based on machine-learning techniques for institutional buildings. Their results showed a 22% reduction in natural gas consumption and a 4% reduction in heating demand. Hu et al. (2019) simulated an MPC controller for the living room of a residential apartment in Denmark. Their results demonstrated that the MPC controller reduces electricity costs by 19% compared to conventional on-off controllers. Zhao et al. (2022) compared the operation of a radiation air conditioning system using MPC with conventional rule-based control and PID control. They showed that the overall energy consumption is reduced by 15% compared to conventional rule-based control and 9% compared to the PID.

Although numerous studies of using MPC for building applications have been carried out and published over the last decades, most of them are still based on pure simulation studies, and only a limited number of papers have reported MPC demonstrations at actual buildings (Afroz et al. 2018). This indicates the need for more studies that involve real-world measurements and demonstrations to validate the effectiveness of MPC in real building environments. A recent study by (Ham et al. 2023) presented a field demonstration of MPC at a K–12 school in California, US. Their results showed that using the MPC could achieve a 24% reduction in peak demand

during the cooling season and up to 16% during the heating season while allowing end users to override thermostat setpoints. Zhang et al. (2022) investigated an MPC controller in a convenience store equipped with photovoltaics and batteries in California, US. The results show that the MPC controller achieved 12% annual electricity cost savings and 34% peak demand reduction compared to a constant setpoint temperature. Bruno et al. (2019) implemented MPC in a public school equipped with Battery and PV systems in southern Italy. They found that 4%-7% electricity cost savings can be achieved compared to commercial rule-based control. (Wang et al. 2023) compared the performance of MPC and rule-based controllers for air conditioners in a residential building in Shenzhen, China. Their results showed that the MPC controller reduced cooling costs by 22% in the bedroom and 27% in the living room. Merema et al. (2022) implemented an MPC controller for all-air systems in a university located in Ghent, Belgium. Their results showed a 10%–40% reduction in electric energy use and 21%–55% in thermal energy use.

Drgoňa et al. (2020) developed an MPC framework for an office in Belgium equipped with a ground-source heat pump and thermally activated building structures. Their study found that the MPC approach reduced the energy consumption of the building by 54% and improved thermal comfort by 37%. Aswani et al. (2011) investigated the implementation of an MPC controller for an air conditioner that cools a computer laboratory on the Berkeley campus in California, US. Results showed that the MPC controller results in a 30%-70% reduction in cooling energy consumption compared to the traditional controller. Bengea et al. (2014) developed an MPC controller for a multi-zone, variable-volume HVAC system in a mid-size commercial building, which resulted in 75% reductions in heating costs over the heating season. Kim and Braun (2022) presented an MPC framework to coordinate multiple rooftop units for medium-sized commercial buildings located in Los Angeles, U.S. They concluded that cooling energy savings of 15%–30% can be achieved through applying MPC. Vivian et al. (2022) reported the results of MPC performed in a lightweight building lab in Piacenza, Italy. They found that this strategy allows to obtain savings on electricity in a range of 10–17% compared to a conventional control.

Table 1 summarizes some of the MPC field implementations in real buildings.

Table 1: Studies on the implementation of MPC in real buildings

Year	Ref	T_{out}	Building Type	Test duration	Systems controlled	Summary of results
2023	(Ham et al. 2023)	18 – 28 °C	School classrooms	One month	RTUs	24% reduction in total power and 30% in HVAC power
2023	(Wang et al. 2023)	26 – 34 °C	Residential	30 Days	Air conditioner	22-29 % cooling energy saving
2023	(Vivian et al. 2022)	0 – 5 °C	laboratory	Three days	Fan coils	10–17% electricity cost saving
2022	(Kim and Braun 2022)	NA	University lab	Two months	RTUs	3.6%-8.7% energy cost savings; 36% demand savings
2022	(Zhang et al. 2022)	NA	Small Commercial	Several months	RTUs, refrigeration, battery	12% energy cost savings; 34% demand reductions
2022	(Blum et al. 2022)	8 – 22 °C	Office	Two months	Rooftop units, underfloor air distribution system	40% energy saving
2021	(Knudsen et al. 2021)	-2 – 12 °C	Laboratory	32 days	hydronic radiator	22.5% energy cost saving
2020	(Bünning et al. 2020)	13 – 39 ◦C	Residential	Six days	Cooling ceiling panels	24.9% cooling energy saving
2019	(Joe and Karava 2019)	0 – 30 °C	Office	20 days	Hydronic radiant floor	50% cooling, 29% Heating energy saving
2018	(Kim and Braun 2018)	15 – 30 °C	Conference room	Four months	Packaged air conditioners	12% HVAC energy savings and 18% HVAC peak demand
2016	(De Coninck and Helsen 2016)	2-12 °C	Office	Winter season	Heat pumps, gas boiler	34-40% energy cost savings; 20-30% primary energy reduction
2014	(Bengea et al. 2014)	16 – 38 °C	Laboratory	Several months	Multi-zone HVAC unit	20% energy savings during the transition season, 70% during heating season, and 10% peak power reduction
2011	(Široký et al. 2011)	3.4 °C	Large building	Winter season	Ceiling radiant heating	Energy saving between 15% and 28%
2005	(Henze et al. 2005)	12 – 28 °C	Small room	Five days	Chillers and an ice-based TES	17% to 27% Cost saving

Our review of the literature shows that field studies on energy flexibility, especially in school buildings, are rare. Energy efficiency still dominates field investigations as the main goal. With the trend toward building electrification and grid-interactive buildings, buildings' energy flexibility will become increasingly important and call for more field validation work. By leveraging MPC in school buildings, educational institutions can create a more sustainable, comfortable, and cost-effective environment for students and staff. Moreover, the literature review shows that most of the field tests on MPC are conducted in hot regions during the cooling season, and there is no study about the implementation of MPC in schools in very cold climate regions (with an average outdoor temperature of -10 °C during winter), as to the authors' knowledge.

2.4 Energy flexibility in buildings

Energy flexibility in building net electricity demand is an essential part of the solution to address the electrical future grids requirements. Buildings are important components of smart electricity grids; they can provide energy flexibility services to reduce peak loads and shift demand in accordance with local RES production. These energy flexibility services include energy storage in thermal mass and batteries (Foteinaki et al. 2018, Weiß et al. 2019), charging of electric vehicles (Afram and Janabi-Sharifi 2014), and HVAC system adjustments (Jensen et al. 2017).

Torres Ruilova (2017) defined Energy flexibility in buildings as “the possibility to deviate the electricity consumption of a building from the reference scenario at a specific point in time and during a certain period”. Annex 67 of the IEA *Energy in Buildings and Communities Programme* (IEA-EBC) defined energy flexible buildings as those with “the ability to manage [their] demand and generation according to local climate conditions, user needs, and grid requirements” (Jensen et al. 2017). Energy flexibility takes into consideration two-way communications between buildings and the power grid. In this way, buildings are regarded not as consumers but as “prosumers” (Ilic et al. 2012).

Energy flexibility can be activated in two ways: by leveraging thermal energy storage and by shifting equipment operation. According to the first approach, energy storage can be used to shift the operation of electrically-driven devices. In the second approach, some electrical devices can be controlled to shift the electricity demand to periods with lower electricity prices or greater renewable energy generation (Lopes et al. 2016). In this context, an effective application of control

strategies within HVAC systems is essential for increasing the buildings' efficiency (Tabares-Velasco et al. 2012, Afroz et al. 2018, Morovat et al. 2019) and energy flexibility (Klein et al. 2017).

Energy flexibility in buildings refers to the ability of a building to modify its energy consumption in response to external signals, such as grid electricity prices or renewable energy availability (Junker et al. 2018, Luo et al. 2022). This adaptability can be achieved through various means, including demand-side management and advanced control strategies (Farrokhifar et al. 2021). Energy flexibility is also instrumental for providing contingency reserve for emergencies (e.g., cold load pickup after a power outage) and for enabling dynamic electricity trading. Energy flexibility is a time-varying quantity: in the context of this discussion, real-time energy flexibility must be calculated at short notice (e.g., kW available over the next few hours) and predicted ahead of time. Electric utilities consider Demand Side Management (DSM) a key solution to reduce peak power demand. In periods of peak power demand, using DSM is more cost-effective than operating peaking power plants or purchasing power from other jurisdictions (Davito et al. 2010). DSM can have an even more significant effect on the grid when integrated with renewable energy sources (RES).

Finck et al. (2020) developed a method and tested it under real-life conditions, including the stochastic behaviour of occupants and the dynamic behaviour of the building and heating system. They used key performance indicators to quantify energy flexibility by considering: (1) energy and power, (2) energy efficiency, and (3) energy costs. They found that this categorization helps to make clear the benefits of using flexibility indicators in real-life applications. Junker et al. (2018) presented a methodology for evaluating energy flexibility based on the flexibility function, to describes how a particular smart building or cluster of smart buildings reacts to a penalty signal. De Coninck and Helsen (2016) developed a methodology to quantify flexibility in buildings based on the cost curve. The methodology returns the amount of energy that can be shifted and the costs of this load shifting. Tumminia et al. (2021) proposed a multidisciplinary approach to finding trade-offs between the need to limit environmental impacts and the trend toward higher building energy performance. They found that an oversized photovoltaic (PV) system is not the best solution for load matching, grid interactions, and environmental impacts in the absence of storage systems. They noted that installing a storage system in conjunction with the appropriate size of a

PV system would result in an improved load-matching of the building and reduce grid dependence at low generation times.

How can real-life applications benefit from the quantification of flexibility indicators for control?

In the past, investments have been made by utilities in the distribution system. The resulting cost has spread to consumers, slowing the rate of de-carbonization. New electric technologies allow facing those challenges in a more affordable way. It is possible today to consider the optimization of the entire electric system from the generation units to the final end-uses. Buildings are part of this system and can bring flexibility to it. Recent international efforts have recognized the need for a methodology to assess the flexibility for demand response in buildings, such as by (O'Connell et al. 2019), who developed a methodology consisting of four steps:

1. System and load identification.
2. Flexibility characterization.
3. Scenario modelling to visualize the impact on demand profiles.
4. Key performance indicators (KPIs) labeling to enable contract negotiation between building operators and aggregators or utilities.

Other important considerations are the scalability of the assessment methodology and ease of implementation. In general, the energy flexibility KPIs are categorized into three domains (Finck et al. 2020):

- *Energy and power:* When using the instantaneous power flexibility as a KPI, it is possible to identify the demand flexibility completely. The instantaneous power flexibility is defined as the evolution of electrical and heating power during a flexibility event.
- *Energy efficiency:* Refer to the effective utilization of available sources such as the heat pumps and the storage heat tank.
- *Energy costs:* Conventional KPIs for demand flexibility integrate operational costs of electricity consumption of the heat pump.

This categorization helps to make clear the benefits of using flexibility indicators in real-life applications, including detailed information on demand flexibility concerning the power grid, demand flexibility for retrofitting and design of new energy systems, and optimal control of demand flexibility.

Can building energy systems provide short-term demand flexibility in balancing and spot markets?

The contingency reserve is an amount of power the utility may call when needed to face the loss of a generation unit or other unexpected load unbalance. To address this need, real-time thermal load flexibility is predicted ahead of time or calculated continuously and should be available at short notice (e.g., 10 minutes) over a time duration of about an hour or a few hours. Around 40 % of the world's energy is consumed by buildings, so buildings must play an important role in providing a safe, reliable, and efficient operation of the future resilient energy systems. Energy flexibility takes into consideration two-way communications between buildings and the power grid. In this way, buildings are regarded not as consumers but as prosumers (Ilic et al., 2012).

2.5 School buildings

School buildings account for a large portion of the building stock and a significant portion of the total energy use. Schools account for 30% of the public sector's energy consumption (Natural resources Canada 2022) and have an average energy intensity of 200 kWh/m^2/year in Canada (Ouf and Issa 2017). Also, HVAC energy accounts for 46% of school energy consumption (U.S. Energy Information Administration (EIA)). Additionally, implementing energy-efficient control strategies can improve indoor air quality and occupant comfort, creating a healthier learning environment for students and staffs (Cabovská et al. 2022, Sadrizadeh et al. 2022). Thus, transitioning to "energy flexible" buildings responding to grid requirements is an important and urgent research topic (Le Dréau and Heiselberg 2016, Torres Ruilova 2017, Li et al. 2022).

Although school buildings constitute a large proportion of the nation's building stock and contribute considerably to the total energy needs, few studies have been focused on these buildings in Canada. According to the published literature, the Energy use intensity (EUI) of junior high schools and elementary schools ranges from 20 to 405 kWh/m^2/year worldwide (Wang 2019). Ouf and Issa (2017) investigated the EUI of 129 junior high and elementary schools, using data collected over ten years from 30 schools' buildings in Manitoba, Canada. Their results show that the average EUI in an elementary school is 270 kWh/m^2/year; in a junior high school is 264 kWh/m^2/year, and in the K-12 schools is 127 kWh/m^2/year. They mentioned that the difference

between K-12 and elementary and secondary schools in energy consumption might be attributed to their equipment and activities.

Another study by (Ouf et al. 2016) examined both electricity and natural gas use in schools in Canada. They divided the schools into three groups based on the year they were built: before 2004, between 2004 and 2013, and after 2013. They found that the electricity EUI of the schools built before 2004 was 58 kWh/m^2/year, between 2004 and 2013 was 116 kWh/m^2/year, and after 2013 was 125 kWh/m^2/year. Although newly constructed schools are more energy efficient in heating and cooling, school electricity use has increased due to the electrification of heating systems and additional teaching equipment. Energy-retrofitted and green schools spent 37% more on electricity than conventional schools. Nevertheless, green schools spent 56% and 41% less on gas than conventional and energy-retrofitted schools, respectively. Their total energy costs were also 28% lower than conventional and energy-retrofitted schools.

Golshan et al. (2018) evaluate the indoor environmental conditions of 10 energy-conscious schools in the Netherlands by focusing on the thermal comfort and indoor air quality (IAQ) conditions. The results from the study indicate that the situation is less than desirable in some cases, and the focus had been placed mostly on the energy aspect rather than the comfort or healthy indoor environment of the occupants. In more than 40% of the existing schools, the IAQ is insufficient while the energy consumption is high. It was concluded that inadequate ventilation is a common problem in primary school classrooms all over the world. In the Netherlands, the situation is that in around 70% of the existing classrooms, the requirements for healthy ventilation are not met. However, around 40% of the school's classroom ventilation is seriously insufficient during the winter.

A study by (Lourenço et al. 2014) analyses the energy consumption patterns of eight Portuguese case-study schools with a methodological approach that integrates quantitative and qualitative data analysis. The approach made it possible to link the energy consumption patterns of the schools with the user behavior and management strategies. As a result, six Key Performance Strategies (KPS) were identified to potentially enhance the energy performance of school buildings through use and management. Some of the identified KPSs can be implemented directly through school management policies to reduce energy use and enhance efficiency. Others can be incorporated in

future building design strategies. Some have the potential for being hereafter integrated into the simulation models of buildings' energy performance.

Droutsa et al. (2021) investigates available data from energy audits of about 350 Hellenic school buildings from the national electronic repository that have been performed for issuing energy performance certificates. They found that, on average, actual thermal energy use is about twenty percent higher than calculated, while the actual electricity consumption is about half of the calculated value. The majority of educational buildings do not meet the current energy performance requirements, requiring considerable energy retrofits.

2.6 Renewable Energy Retrofits

Retrofitting school buildings is expected to be a major undertaking in the next few years. School buildings are well placed to set the course for future energy use, since enhancing the energy performance of school buildings is essential for spreading a culture of energy efficiency throughout the community. The question on the school building sector is: should retrofit strategies be limited to improving energy performance, or should sustainability be the ultimate goal?

In the building sector, sustainability refers to the impact of the building on the environment and energy generation and usage, as well as the well-being of its inhabitants and the economic factors. These issues become even more important when referring to school buildings, where occupants are students/children pursuing a learning activity. The sustainability protocols, aimed at making schools sustainable, evaluate the building in terms of energy efficiency, health and comfort, and how the structure can serve as a learning tool for sustainability strategies.

There is an increased interest in decarbonizing buildings by replacing fossil fuels with renewable electricity. As a retrofit measure, on-site photovoltaic (PV) generation could contribute to this goal. Solar panels may be installed as part of a new construction project or a retrofit strategy to offset the energy demands of a school building. Using photovoltaic/thermal (PV/T) systems to provide electricity and thermal energy is one of the most important retrofit technologies for supply-side management. The Varennes Library, the first institutional net-zero building in Canada, utilizes an on-site renewable system that includes a 110 kW_p PV/T system where 15% of the heat is recovered and used to pre-heat the fresh air intake (Dermardiros and Scott Bucking PhD 2019). Figure 2-4 shows the HVAC system and the PV/T system installed in the Varennes Library.

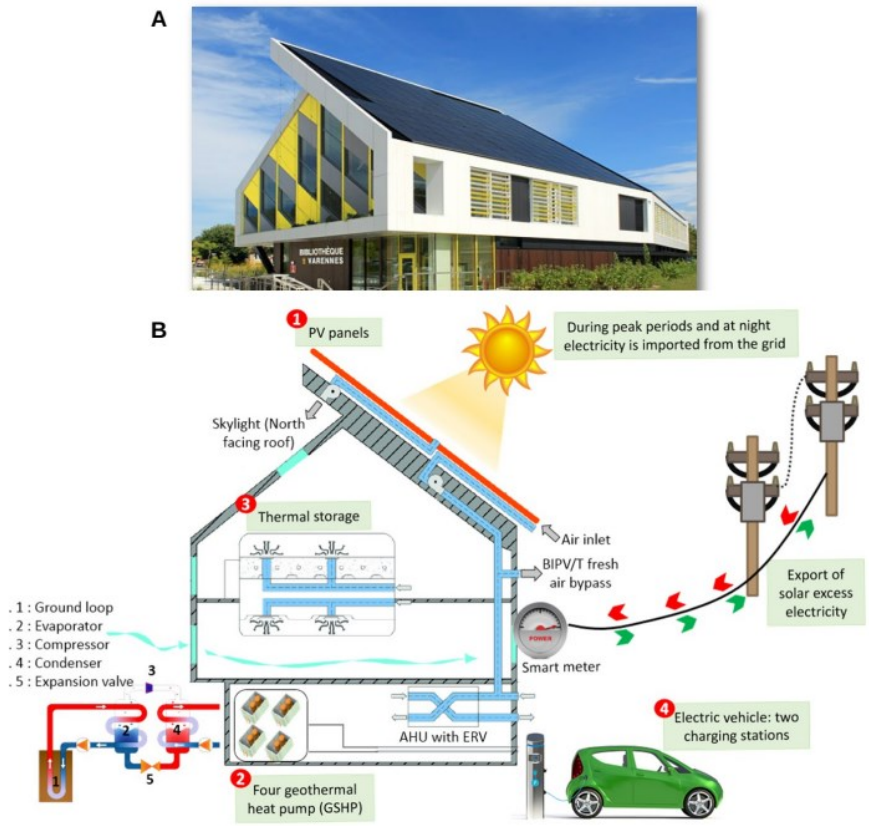

Figure 2-4: Varennes library schematic, A) Front view, B) plan view (Amara et al. 2019)

Due to the rapid reduction in the cost of PV modules and the increase in their efficiency, grid-connected PV systems could be the key to a sustainable energy transition. However, the optimal design of these systems is a major challenge, especially for existing buildings that have not incorporated renewable supply systems from the start of the design process. If a time-of-use electricity price and demand charge are applied to utility rates, renewable energy technologies may benefit school buildings. In this context, obtaining a control-oriented model that provides reliable predictions and can be implemented in smart controllers is crucial for optimal building performance and renewable energy integration (De Coninck et al. 2016, Arroyo et al. 2020, Candanedo et al. 2022).

2.7 Research needs and proposed work

The transition to smart grids has raised the need to investigate and enhance building energy flexibility. Energy flexibility is critical to address the grid's challenges of balancing supply and demand and integrating renewable energy sources. To achieve these goals, developing

control-oriented models able to provide reliable predictions, to be implemented in smart controllers, and generalizable for widespread deployment in buildings is necessary.

To achieve these goals, research needs to:

- **Develop control-oriented models based on measured data:** that provide reliable predictions and can be generalized for widespread school deployment. Control systems used in traditional school buildings react to changes in weather and occupancy conditions as they occur without making any predictions. In contrast, MPC can enable programming the building operation based on future weather and occupant behaviour, resulting in significant improvements in energy flexibility, IEQ, and building-grid interaction.
- **Develop a general model predictive control framework in school buildings:** The literature studying MPC applications needs a theoretical framework and detailed experimental investigation. Consequently, there is an essential need for a practical and comprehensive methodology that facilitates the modeling, design, and widespread implementation of MPC strategies in schools. This thesis presents an MPC framework and investigates the implementation of developed MPC in a real-used school building. Also, although several studies have investigated the application of MPC in buildings, most focused on energy consumption in cooling-dominated regions. However, in cold regions, the peak load in the morning and evening strains the electrical grid. It is thus essential to reduce peak demand for the grid by using the energy flexibility of building load.
- **Develop a general method to quantify the energy flexibility potential of buildings:** Recent international efforts have recognized the need for a methodology to assess the flexibility for demand response in buildings. This methodology should consist of four steps: 1. System and load identification, 2. Flexibility characterization, 3. Scenario modelling to visualize the impact on demand profiles, and 4. Key performance indicators (KPI) labeling to enable contract negotiation between building operators and aggregators or utilities. Other important considerations are the scalability of the assessment methodology and ease of implementation.
- **Integrate PV/T systems with MPC:** optimal control with MPC will help the large-scale integration of RES (e.g., PV/T) technologies and reduce the energy cost of school buildings. Many new schools need to be built soon, and old ones need renovation, but a few studies have been performed on integrating PV systems in school buildings. Therefore,

minimizing the research gap regarding the potential of integrating PV systems in schools to provide on-site electricity generation in educational buildings is essential.

Therefore, this thesis investigates the energy flexibility potential in school buildings through simulation and experimental studies. It contributes a general methodology for the development of data-driven grey-box thermal models and the implementation of MPC. The methodology is applied to an archetype fully-electric school building near Montréal, Québec, Canada. The approach is scalable and transferable to other institutional or mid-size commercial buildings. The proposed methodology helps school buildings adapt smoothly to the necessities of the future smart grid and smart cities.

Chapter 3: Methodology

In this chapter, the thermal modelling approach employed in this thesis is presented as part of an overall modelling methodology that can be applied to buildings equipped with convective heating systems and radiant floor heating system. This modelling approach is used for model-based predictive control and building energy flexibility quantification. These models use a grey-box modelling approach, in which physically meaningful parameters can be calibrated with measured data or identified using optimization techniques.

The general methodology in this thesis is as follows:

1. **Experimental data in real school:** Exploration of the experimental data measured by smart meters installed in the school.
2. **Data analysis:** Investigate the effect of data quality and resolution on the calibration or training of the most promising models.
3. **Control-oriented model:** Develop a methodology to create control-oriented building models in Python programming language, i.e., models that facilitate developing and assessing the impact of alternative control strategies in the schools.
4. **Simulation scenarios for assessment of control strategies:** Evaluation of the different control strategies aimed to enhance energy flexibility potential of school buildings while considering indoor environmental quality.
5. **Model predictive control:** Develop a MPC framework to investigate predictive control strategies in school building and integration of PV/T systems as a renewable energy retrofit measure.
6. **Energy flexibility quantification:** Present a methodology for defining and calculating dynamic building energy flexibility for school buildings and their interaction with smart grids.
7. **Renewable Energy Retrofit:** Integration and sizing of PV/T system to enhance energy efficiency and flexibility in school buildings.

3.1 Governing equations

Grey-box models rely on physical knowledge about the system dynamics to define the model structure. Statistical methods are then used to estimate the unknown parameters. These parameters may be directly linked to the physical properties of the building, given that the model structure correctly represents the physical behavior of the system.

The thermal modelling approach followed here is based on the lumped parameter finite difference method and implemented in Python. A fully explicit finite difference approach is used to solve the energy balance equations at each node in the models. The fully explicit approach assumes that the current temperature of a given node depends only on its temperature and the temperature of the surrounding nodes at a previous time step. By performing a heat balance on the control volume, the differential equation of a node can then be written as (Athienitis 2013):

$$C_i \frac{dT_i}{dt} = Q_i + \sum_{ij}^{n} \frac{(T_j - T_i)}{R_{i,j}} \qquad 3\text{-}1$$

Each node's energy balance is solved using an explicit finite difference method. The discretization of the time derivative term is as follows:

$$C_i \frac{dT_i}{dt} \approx C_i \frac{\Delta T_i}{\Delta t} = C_i \frac{(T_i^{t+1} - T_i^t)}{\Delta t} \qquad 3\text{-}2$$

Temporal discretization of Equation 3-3 can be rearranged in the following explicit manner:

$$T_i^{t+1} = \frac{\Delta t}{C_i}\left[\sum_j U_{ij}^t (T_j^t - T_i^t) + \sum_j U_{ik}^t (T_k^t - T_i^t) + \dot{Q}_i^t\right] + T_i^t \qquad 3\text{-}3$$

Where:

- U_{ij}: Conductance between nodes i and j,W/K;
- U_{ik}: Conductance between nodes i and k where node k has a defined or known temperature, W/K;
- T: is the temperature at node i or adjacent nodes, °C;
- C_i: Capacitance of the node ($C_i = \rho C_p A dx C_T$) , J/K;
- $\dot{Q}$: Heat flow into the node, W;
- Δt: Time step, s.

The capacitance of the air node contains a factor C_T (air thermal capacitance multiplier) that accounts for phenomena (furniture and objects, the time required for air mixing, delay due to ducting and other factors) that in a low-order model result in capacitance with an observed effective value significantly larger than the one calculated using only the physical properties of the air. The air thermal capacitance multiplier range between 6 to 10 (Hong and Lee 2019). The Equations 3-4 in matrix form is:

$$\begin{Bmatrix} T_1 \\ \vdots \\ T_N \end{Bmatrix}^{t+1} = \begin{Bmatrix} \frac{\Delta t}{C_1} \\ \vdots \\ \frac{\Delta t}{C_N} \end{Bmatrix} \odot \left(\begin{bmatrix} -\sum_j^N U_{1j} - \sum_k^M U_{1k} + \frac{C_1}{\Delta t} & U_{12} & \dots & U_{1N} \\ \vdots & \vdots & \ddots & \vdots \\ U_{N1} & U_{N2} & \dots & -\sum_j^N U_{Nj} - \sum_k^M U_{Nk} + \frac{C_N}{\Delta t} \end{bmatrix} \begin{Bmatrix} T_1 \\ \vdots \\ T_N \end{Bmatrix}^t + \begin{Bmatrix} \dot{Q}_1 + \sum_k^M (U_{1kk} T_{kk}) \\ \vdots \\ \dot{Q}_N + \sum_k^M (U_{Nkk} T_{kk}) \end{Bmatrix} \right) \quad 3\text{-}4$$

where,

- $\odot$: is an element-wise multiplication operator.
- N: is the number of nodes.
- M: is the number of nodes with known temperatures.

To assure numerical stability in the solution, the time step must be chosen according to the stability criterion defined in Equation 3-5:

$$\Delta t \leq \min \left(\frac{C_i}{\sum U_i} \right) \quad 3\text{-}5$$

Equation 3-6 calculates the heat provided by the heating system with proportional-integral control (PI controller) at each time step, which the integral part should be reset periodically.

$$\dot{Q}^{t+1} = k_p \left(T_{sp}^t - T_{air}^t \right) + k_i \int_0^t \left(T_{sp}^t - T_{air}^t \right) dt \quad 3\text{-}6$$

where:

- k_p, proportional gain of the controller, $\mathrm{W/K}$
- k_i, Integral gain of the controller, $\mathrm{W/(K \cdot s)}$

Model identification is the process of determining the physical properties of unknown systems according to some experimental data or training data. The objective of the optimization algorithm is to find the equivalent RC circuit parameters by minimizing *CV (RMSE)*. Equation 3-7 and Equation 3-8 (ASHRAE Guideline 14 2002) are used to calculate this index where T_i ,$\hat{T}_i$, n, and $\overline{T}$

represent the measurements data, simulation results, a total number of observations, and the average of all measurements, respectively.

$$CV(RMSE)(\%) = \frac{\sqrt{\sum_{i=1}^{n}(T_i - \hat{T}_i)/n}}{\bar{T}} \times 100 \quad 3\text{-}7$$

$$NMBE(\%) = \frac{\sum_{i=1}^{n}(T_i - \bar{T})}{(n-1) \times \bar{T}} \times 100 \quad 3\text{-}8$$

According to ASHRAE Guideline 14 (Measurement of Energy and Demand Savings), the model shall have a CV(RMSE) of not more than 30%, NMBE of 10%, and R^2 higher than 0.75 relative to hourly calibration (measured) data (ASHRAE Guideline 14 2002). Table 2 summarizes the criteria of the three main documents to validate a model as calibrated.

Table 2: Calibration criteria based ASHRAE guideline 14 (ASHRAE Guideline 14 2002)

Index	Monthly	Hourly
NMBE	±5%	±10%
CVRMSE	15%	30%
R^2	0.75	

3.1.1 State-space representations

State-Space representations describe systems of linear differential equation in a compact manner, as shown in Equation 3-9, where (**x**) is the state matrix, (**u**) is input, (**w**) is disturbance, and (**y**) represent output vectors.

$$\dot{x}(t+1) = A\mathbf{x}(t) + B\mathbf{u}(t) + E\mathbf{w}(t)$$
$$y(t) = C\mathbf{x}(t) + D\mathbf{u}(t) \quad 3\text{-}9$$

Where:

- x(t) is system variables to track.
- u(t) is controllable variable, e.g., heating/cooling, fan on/off, etc.
- w(t) is uncontrollable inputs, e.g., weather.
- y(t) is model output.

In this approach, the temperatures of nodes with thermal capacitances are usually considered as the states of the system since they have certain physical meaning and are relatively easy to measure (Candanedo et al. 2013). The aspect of control-oriented archetypes will be discussed in Chapter 4.

3.1.2 Weather clustering

In this research a centroid-based approach (time series *K*-means clustering) in Python is implemented. *K*-means clustering is a commonly used unsupervised machine learning algorithm for partitioning a given data set into a set of k clusters. It classifies objects in multiple clusters, such that objects within the same cluster are as similar as possible (high intra-class similarity), whereas objects from different clusters are as dissimilar as possible (low inter-class similarity) (Heidrich-Meisner and Wimmer-Schweingruber 2018). Each cluster is represented by its centroid, which corresponds to the mean of points assigned to the cluster. Then, system identification is carried out to identify appropriate reduced-order models. Time-series databases are extensive, and there are always difficulties in treating them separately. Clustering is a very useful tool to simplify the time-series data by grouping similar time-series into aggregated clusters. This approach can be a pre-processing step for other models. The *k*-means clustering algorithm is as follows:

Algorithm 1: *k-means clustering algorithm*

Data: number of clusters, data set X
Result: cluster centers $C = (c_1,\ldots,c_k)c$
Begin
  Randomly select k data points as initial cluster centers;
  Repeat
    Reinitialize all partition subsets as empty:
    $S_1 = S_2 = \ldots = S_k = ()$;
    Assign each data point to the closest cluster center:
    for $i \in (1,\ldots,N)$ **do**
      $l = \text{argmin}_{j\in(1,\ldots,k)} \left\| x_i - c_j \right\|^2$;
      $S_l = S_l \cup x_i$;
    end
    Define new cluster centers based on current partition
    for $j \in (1,\ldots,k)$ **do**
      $c_j = \sum_{i \in (1,\ldots,N),\, x_i \in S_j} x_i / |S_j|$
    end
  until the cluster assignment converges;
end

3.2 Model predictive control (MPC)

MPC is a multi-variable control method that incorporates several additional aspects with the controller: a dynamic model of the system to be controlled, forecasts of future disturbances such as weather, a cost function that is minimized over a prediction horizon, and sometimes a history of past control sequences. The basis of MPC in buildings is that better control of the building energy systems and planning of resources is possible due to insights into forecast weather, expected occupancy, and the thermal response of the building.

Typically, in MPC, the optimal control problem is solved at each defined control step by looking ahead at forecast weather and occupancy schedules over the prediction horizon (PH). The prediction horizon is a time period over which has reasonably reliable information about the future, ranging from a few hours to a couple of days. Using data available from the prediction horizon period, an optimization routine is solved, and an optimal sequence of control moves is identified through the implementation of MPC. The identified schedules and control moves are applied to the building over a "control horizon", which can be the same length or be shorter than the prediction horizon. Once the current control horizon has ended, the optimization exercise is performed again for the following prediction horizon. This process is repeated until the end of the simulation time (e.g., one day or one year). The controller's objective is to minimize a cost function that may incorporate energy and/or power while maintaining the zone within reasonable comfort limits.

The overall MPC formulation is presented in Equation 3-10 (Drgoňa et al. 2020): an objective function is to be minimized over a prediction horizon, subjected to various constraints where some describe the dynamics of the system to control while others define limits and boundary conditions.

$$\min_{u^0,\dots,u^{N-1}} \sum_{i=1}^{N} l(x^i, u^i, w^i)$$

Subject to $x^{i+1} = f(x^i, u^i, w^i) = Ax^i + Bu^i + Ew^i$ System dynamics

$$h(x^i, u^i, w^i) = 0$$

$$g((x^i, u^i, w^i) \geq 0$$

$x^1 = x,$ Current state

3-10

Where,

- x^t system variables track the system dynamics,
- u^t control variables which can be manipulated in order to improve the building performance,
- w^t exogenous inputs representing time series that can be observed but cannot be controlled, such as weather,
- l(x, u, w) loss or cost function which could be to minimize the utility cost, or the grid interaction, or some other cost,
- h(x, u, w) = 0 equality constraints; here, the system dynamics of the system (next-step interior temperature) is given by the trained model,
- g(x, u, w) ≥ 0 inequality constraints, here, the inequality constraints are the boundaries of the problem: can include the capacity of the heating system, toggling limitations to reduce wear, the comfortable temperature range, an allowance for discomfort, etc.

In this thesis, two cost functions incorporating the utility rate structures were implemented, and their results were compared to the typical manual control currently in operation. Equation 3-11 shows the optimization problem, where the objective is to minimize energy when the electricity cost is constant. Equation 3-12 presents the objective function, where the objective is to minimize the peak load when the energy cost varies over the day, with higher prices during peak hours in the morning (from 6:00 to 9:00) and evening (from 16:00 to 20:00), as shown in Table 3.

$$\min_P J$$

$$where\ J = \left(\sum_{i=1}^{N-1} P_i \Delta t\right) \cdot \left(Cost_{\text{Energy},i}\right) \qquad 3\text{-}11$$

$$\text{Subject to} \quad \underline{T} \le T_{in} \le \overline{T}$$

$$0 \le P \le P_{max}$$

$$where\ J = \left(\sum_{i=1}^{N-1} P_i \Delta t\right) \cdot \left(Cost_{\text{Energy},i}\right) + max(P_i) \cdot \left(Cost_{\text{Demand},i}\right) \qquad 3\text{-}12$$

$$\text{Subject to} \quad \underline{T} \le T_{in} \le \overline{T}$$

$$0 \le P \le P_{max}$$

where P_i is the power demand at the time, N is the number of time steps across the prediction horizon PH, and Δt is the time step. The space heating demand (P) is limited by the maximum capacity of the heating equipment (P_{max}). In this study, MPC performs optimization starting midnight with a 24-hour prediction horizon, timestep 15 minutes, and control horizon of three hours.

3.2.1 Québec Electricity Rates for medium-power customers

This study concentrates on the electricity rates called *Rate M* and *Rate Flex M*, applied in Québec to the medium-sized commercial building sector (Hydro Québec 2022). These rates are summarized in Table 3.

Table 3: Utility rate for medium commercial buildings (Hydro Québec 2022)

Rate M	
Demand charge	$15.16/kW
First 210,000 kWh	5.23¢/kWh
Remaining energy used	3.88¢/kWh
Rate flex M	
Winter: 1 Dec. – 31 Mar.	
Demand charge	$15.16/kW
Consumption outside peak hours	3.29¢/kWh
Consumption during peak hours: Morning (6:00 to 9:00) and Evening (16:00 to 20:00)	51.97¢/kWh
Summer: 1 Apr. – 30 Nov.	
Demand charge	$15.16/kW
First 210,000 kWh	5.23¢/kWh
Remaining Energy used	3.88¢/kWh

When the maximum power demand during a consumption period included in the last 12 months exceeded 50 kW, then *Rate M* applies to the contract. The rate includes a demand charge and two energy prices: one for the first 210,000 kWh and another for any remaining energy use. Power prices are applied to the billing demand, which is determined by the maximum of two quantities: 1) the maximum power measured during the month, or 2) 65% of the previous winter's peak (minimum billing demand). A minimum billing demand refers to the minimum amount a customer must pay for every consumption period, regardless of how much power is consumed. Due to the large space heating loads during the winter, operation strategies must be carefully considered.

Under *Rate Flex M*, the cost of electricity is cheaper than *Rate M* most of the time. However, during peak demand events, electricity is billed at a much higher price (51.97 ¢/kWh). Thus, it is necessary to shift electricity use or limit it to reduce costs. The day before a peak demand event, customers will receive a notification. Peak demand events can occur Monday to Friday from December 1 to March 31, from 6 to 9 a.m. and 4 to 8 p.m., as shown in Figure 3-1. The Rate M (base rate) price is applied for the rest of the year.

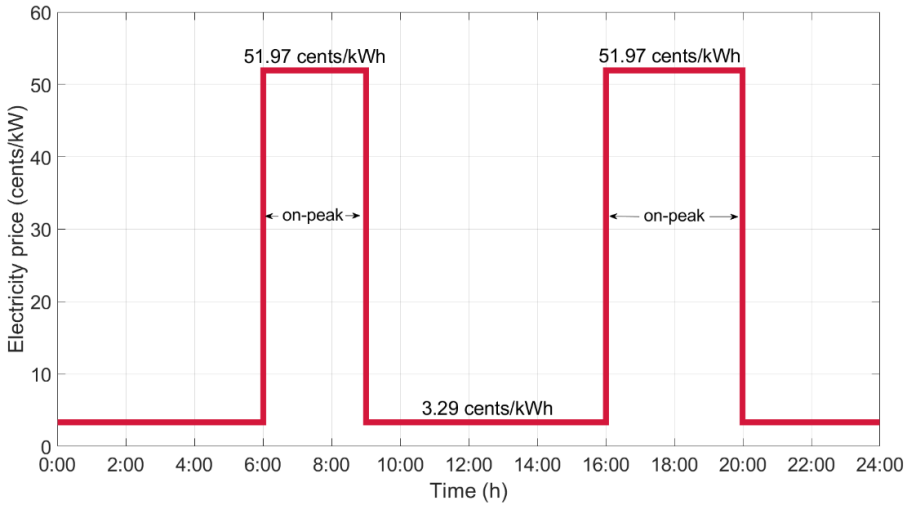

Figure 3-1: Electricity price – Rate flex M (Hydro Québec 2022)

3.3 Energy Flexibility

Energy flexibility in building net electricity demand is an essential part of the solution to address the electrical future grids requirements. A Building Energy Flexibility Index (BEFI) would help to define the amount of power variation over a fixed duration that is available from a building. A well designed BEFI would help to quantify the flexibility from a building, to improve building design to increase the potential flexibility, to control the building to get maximum available flexibility when needed and to compare different systems, designs and operational strategies. The prediction accuracy for BEFI within ±10% error is considered optimal for smart grid applications (MacDougall et al. 2017), but errors of up to 36% have been reported in flexibility available through operation of heat pumps. Energy flexibility in building net electricity demand and possible onsite energy production is an essential part of the solution to address the electrical grid's challenges of grid balancing, renewable energy capacity, as well as increasingly important challenges such as providing a contingency reserve to be used for emergencies (e.g. cold load

pickup after power outage) and dynamic electricity trading facilitated with building-to-grid-related communication protocols such as OpenADR.

This section presents the quantification of a dynamic building energy flexibility index (BEFI) for the school building and its interaction with smart grids. Equation 3-13 calculates the average BEFI under the implementation of the flexibility strategy and the reference as-usual profile, and equation 3-14 presents the BEFI as a percentage and equation 3-15 quantifies BEFI at the building level.

$$\overline{BEFI}(t, Dt) = \frac{\int_t^{t+Dt} P_{ref}\,dt - \int_t^{t+Dt} P_{flex}\,dt}{Dt} \quad 3\text{-}13$$

$$BEFI = \frac{P_{ref} - P_{flex}}{P_{ref}} \quad 3\text{-}14$$

$$BEFI_{Buidling} = \sum_{1}^{n} BEFI_{zone} \quad 3\text{-}15$$

where: $\overline{BEFI}$ is the average Building Energy Flexibility Index at time t for duration Dt. It should be noted that BEFI at time t may vary according to time of notice and notice before a signal may allow preconditioning the building to maximize available flexibility when needed. The flexibility available may be quantified by using a model to establish the power demand difference between the reference case (P_{ref}) with a case where the temperature is allowed to drop for one hour or a few hours. This calculation gives the available flexibility at time t. The calculation is repeated every hour to give the available flexibility over the period (BEFI (t+Dt)).

- *Rebound power:* The power surge before or after the flexibility event, either positively or negatively, is called rebound power. The rebound power P_{rb} is defined below:

$$P_{\mathrm{rb}} = max|BEFI| \quad 3\text{-}16$$

Domain: $(0\,, t)$ and $(t + Dt\,, PH)$

The time range (0, t) indicates the extra power used before the demand response (DR) event, the range (*t*+*Dt*, *PH*) denotes the additional power use after the event until prediction horizon (PH).

This information is important for the grid to ensure that the grid remains stable and balanced outside the DR period.

Figure 3-2 shows the estimated power and BEFI due to a flexible setpoint temperature in a school building.

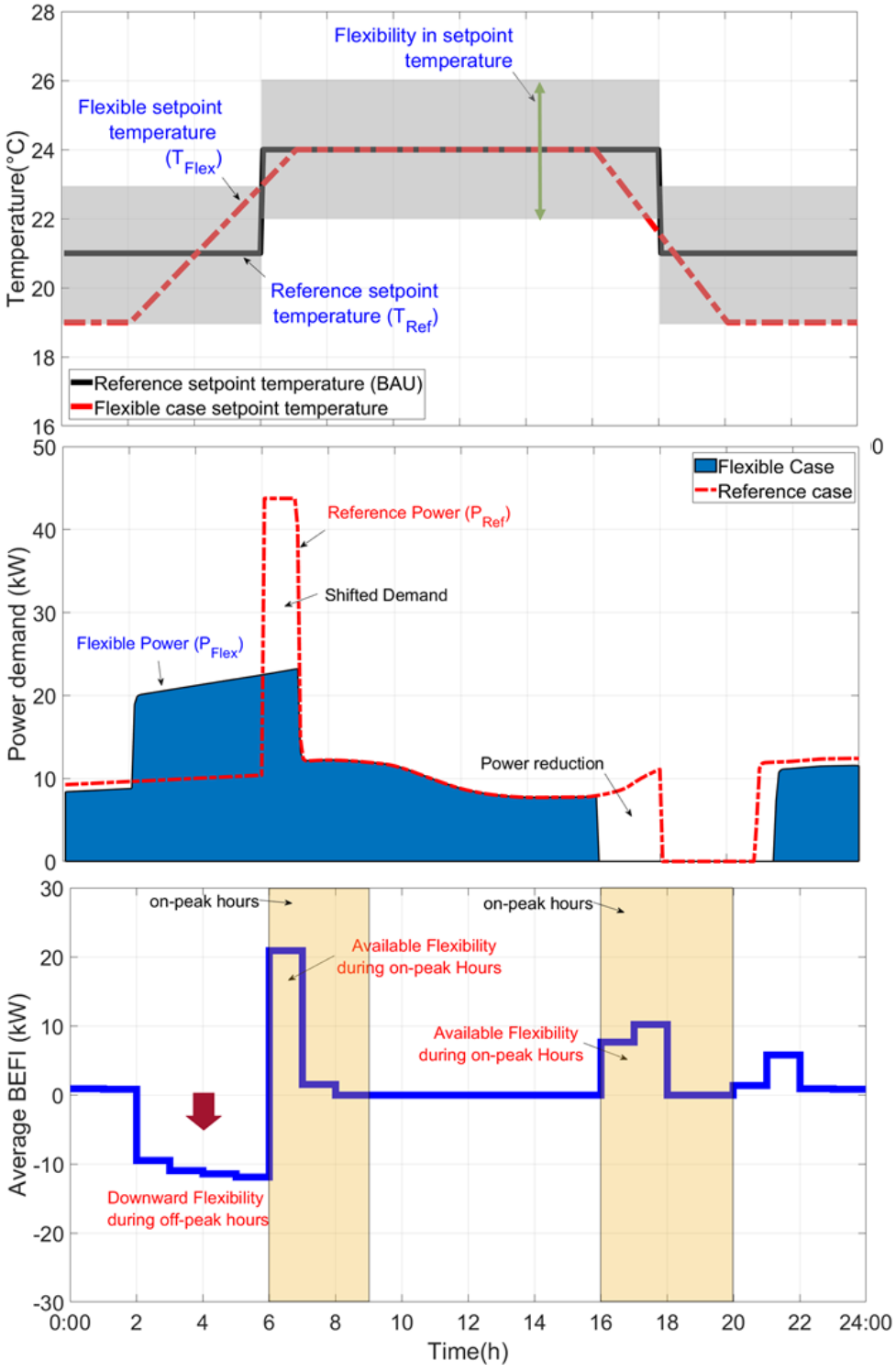

Figure 3-2: Concept of BEFI available to the grid

This figure illustrates how by using flexible setpoint temperature, we can shift the power demand or reduce the power. Also, using Flexible power and reference power profile, we can

predict the available energy flexibility of the building to the grid. The following sections present the case study building and the results for different control strategies to enhance the energy flexibility of the building.

3.4 Energy performance of the school building

Figure 3-3 presents the measured total power electricity in the case study school. This figure shows that the peak power demand was 120.7 kW on 11 February 2020. According to measured data, the average total power during the heating season (November – April) is 52 kW, with an average monthly energy consumption of 37,440 kWh.

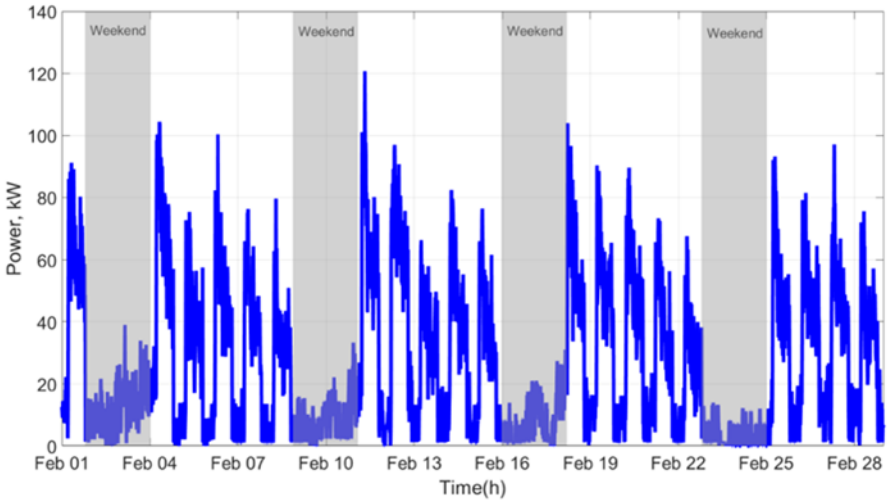

Figure 3-3: Power demand of the school for cold winter days, February.

Based on data collected from energy bills, the EUI in the school is 145 kWh/m^2/year, which is about 27% lower than the national average, which is 200 kWh/m^2/year for schools in Canada (Ouf and Issa 2017). This performance could be explained by using efficient new equipment (e.g., high-efficiency heat pumps), efficient windows, proper control systems, and high insulation levels in the school. Energy use can be further reduced with additional (ongoing) commissioning effort.

Figure 3-4 presents the electrical load duration curve of the school during the heating season. This graph shows the hourly power demand sorted descending. By intercepting the curve with the x-axis, the percentage of time where the school has a high peak load can be determined.

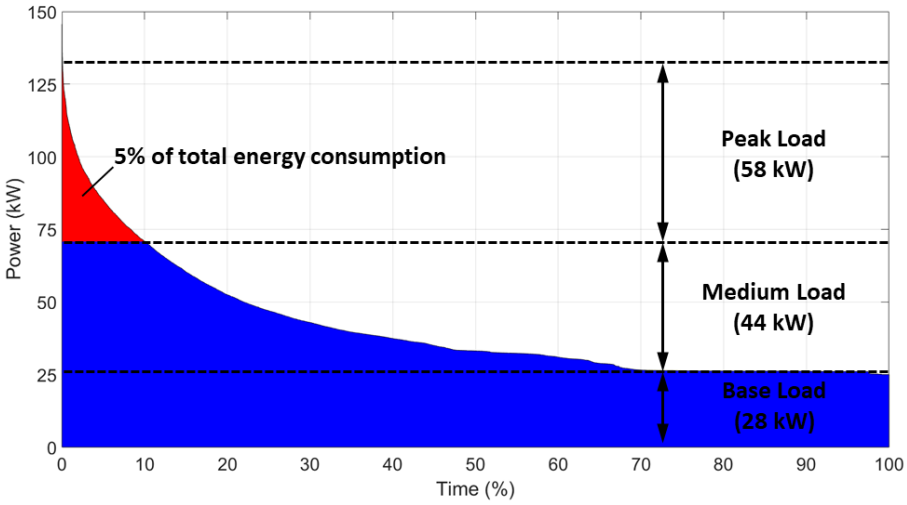

Figure 3-4: Electrical load duration curve - Heating season

For the given period, 50% of the peak load occurred less than 10% of the time. Therefore, it is important to have promising predictive control strategies to reduce peak demand and quantify the energy flexibility potential of the school building studied.

3.4.1 Energy signature

Energy signature diagram estimates energy use as a function of outdoor temperature and may include other parameters. Daily energy signatures can generate more robust energy consumption benchmarks and provide additional insight into unusual energy demand patterns than monthly or weekly signatures, requiring slightly more data. In particular, they distinguish between weekday and weekend consumption. As shown in Figure 3-5, regression analysis is used to define the relationship between energy use and outdoor temperature.

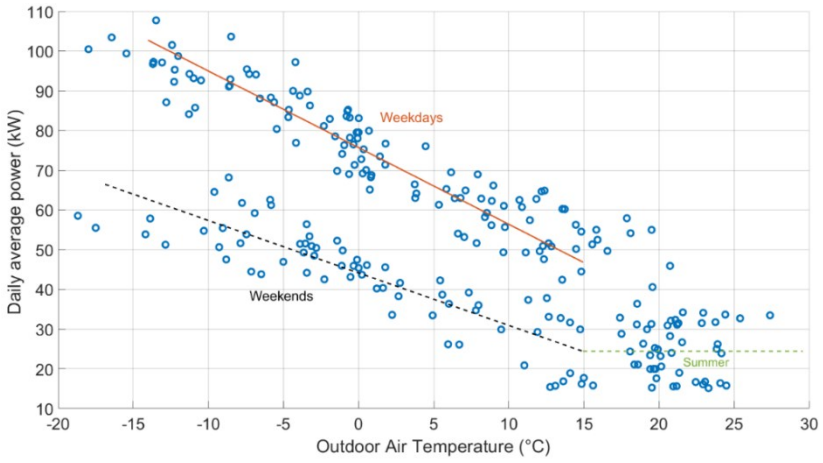

Figure 3-5: Energy signature of the school building

The energy signature diagram indicates a baseline demand of 25 kW, which occurs when the outdoor air temperature exceeds 15 °C. For an outdoor air temperature of 15 °C to -15 °C, the difference between the mean power demand on weekdays and weekends ranges from 20 kW to 45 kW, respectively. There are variations of average daily power beyond those related to mean outdoor temperature or weekday/weekend differences. These variations can be caused by variations in solar heat gain, equipment and lighting usage, occupancy, and possibly other factors.

3.4.2 Energy consumption and end-use breakdown

Figure 3-6 presents the measured power consumption of major subsystems on a typical cold sunny day at the school. In winter, the peak electricity grid demand occurs in Québec during the morning (6:00 a.m. to 9:00 a.m.) and evenings (4:00 p.m. to 8:00 p.m.). This graph shows that the average electricity demand during morning on-peak hours is 65kW, and during the afternoon is 58 kW. It should be noted that this graph does not include all electrical loads in the school. Therefore, there is a difference between electric billing and the measured electric load of the school.

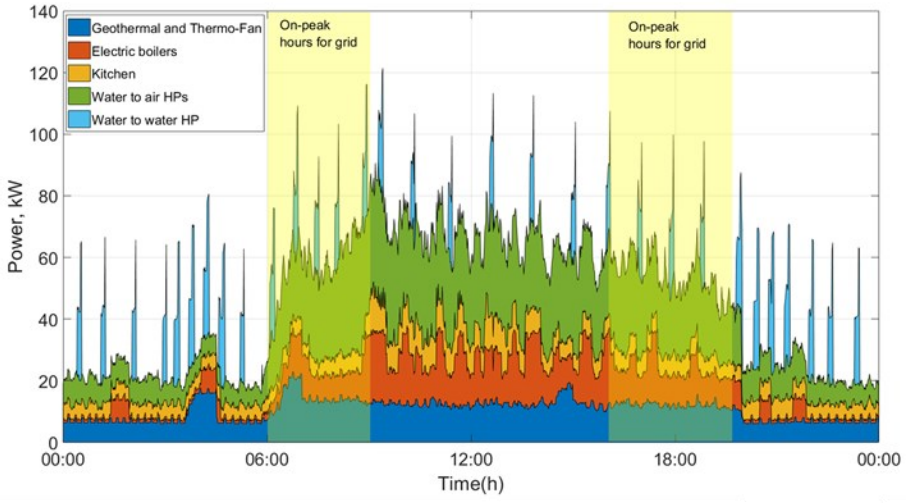

Figure 3-6: Measured power consumption distribution for different subsystems on a typical cold sunny day.

Figure 3-6 shows that water to air HPs and water to water HP account for a significant portion of the peak load. Many strategies could be effective for peak heating demand reduction, including the effect of appropriate predictive control strategies by adjusting setpoint profiles to fully exploit the storage capacity of the concrete slab in zones equipped with radiant floor systems and convective systems. The detail of the energy end-use breakdown is shown in Table 4. Measurements show that the local water-to-air heat pumps use 38% of total energy, and water-to-

water heat pumps consume around 15 % of total energy (in the heating mode of operation). Fan and pump power take up a significant portion due to the radiant slab systems requiring circulation pumps and the fan coil units having their own fans.

Table 4: End-use breakdown in equipment level.

End use breaker	**Energy used (%)**
Electric boiler for hot water	14
Kitchen & lighting	12
Pumps and fans	18
Water to air HPs	38
Water to water HP	15

Measured data shows that around 45% of total energy is consumed by the zones equipped with the convective system (i.e., classrooms, library, kindergarten), and 25% by the zones equipped with radiant floor and convective system (i.e., offices and gym), which is 70% of the total energy used.

Chapter 4: Archetype Control oriented modeling[1]

4.1 Introduction

Data-driven grey-box models ensure both physical insight and the reliability of measured data. Literature review indicates that grey-box models are also suitable for demand-side management in smart grids (Gouda et al. 2002, Bacher and Madsen 2011, Candanedo et al. 2013, Reynders et al. 2014). In grey-box models, choosing an appropriate level of resolution is essential as it directly affects the parameter tuning and calculation time. A high-order model containing too many parameters requires information that is not often available with adequate accuracy. An oversimplified model may not be accurate enough to help make decisions. Therefore, obtaining a model that provides reliable predictions and can be implemented in smart controllers is crucial for optimal building performance.

This chapter investigates the impact of model resolution and structure on the energy flexibility quantification. The methodology is based on the use of archetypes of resistance-capacitance thermal networks for representative thermal zones calibrated with measured data. Providing a closer link between smart grids and smart buildings requires appropriate control strategies. Thus, this study presents an application of the developed model for control purposes based on smart grid requirements. This methodology has been implemented in the fully-electric school building located in Québec, Canada. This school has several features (geothermal heat pumps, hydronic radiant floors, and energy storage) that make it ideal for the purpose of this study. The following steps are used to develop grey-box models and quantify energy flexibility:

- Real building measurement data are collected from the smart meters installed in the archetype zones. Data included variables such as power demand (kW), zone air

[1] This work is based on peer-reviewed journal articles and published refereed conference thesis: (a) Morovat, N., Athienitis, A. K., Candanedo, J. A., Delcroix, B. (2022). "Data-driven model-based control strategies to enhance energy flexibility in electrically heated school buildings", Buildings, 12(5), 581. (b) Candanedo, J. A., Vallianos, C., Delcroix, B., Date, J., Saberi, A., Morovat, N., John C., and Athienitis, A. K. (2022), "Control-oriented archetypes: a pathway for the systematic application of advanced controls in buildings", Journal of Building Performance Simulation, 1-12. (c) Athienitis, AK., Dumont, E., Morovat, N., Lavigne, K., Date, J. (2020), "Development of a dynamic energy flexibility index for buildings and their interaction with smart grids", ACEEE Summer Study on Energy Efficiency in Buildings, California, USA, August 17-2. (d) Morovat, N., Candanedo, J. A., Athienitis, A. K. (2021). "Application of grey-box models for the quantification of the energy flexibility of a school building in Canada", 2021 ASHRAE Annual Conference, Phoenix, USA, June 28-30.

temperature (°C), weather data, and specific data related to each zone (e.g., floor heating temperature). All measurements were taken at intervals of 15 minutes.

- Numerical models of thermal building control are developed. These models are based on RC thermal network models.
- The developed models are calibrated using the collected data. The important parameters are identified using the Sequential Least Squares Programming (*SLSQP*) in Python.
- Appropriate control strategies for zones with the convective system and zones with radiant floor system are presented to enhance the energy flexibility available from the building to the grid at specific times, depending on the grid requirement.
- A Building energy flexibility index (BEFI) is applied to quantify dynamic building energy flexibility at the zone and building levels.

4.2 Archetype zones with convective system: classrooms

Figure 4-1 shows two of the classrooms in this school. Each classroom has a ceiling water-to-air heat pump (1.5-2 tons each) and has Proportional-Integral control (PI) in the local-loop control of room air temperature. The local heat pumps are ground source water to air HPs; therefore, the COP of the HPs as the heating system are almost constant and is equal to 3.2 in this school. The typical classrooms are 9.1 m long by 7.2 m wide, and the ceiling-floor height is 3.0 m.

Figure 4-1: Horizon-du-Lac School – Classrooms with convective from ceiling

A schematic of the HVAC system in one of the school's classrooms is shown in Figure 4-2. The air handling unit used in this school is an energy recovery unit that provides preheated fresh air to all classrooms. Each classroom has a local water-to-air HP with local thermostat control.

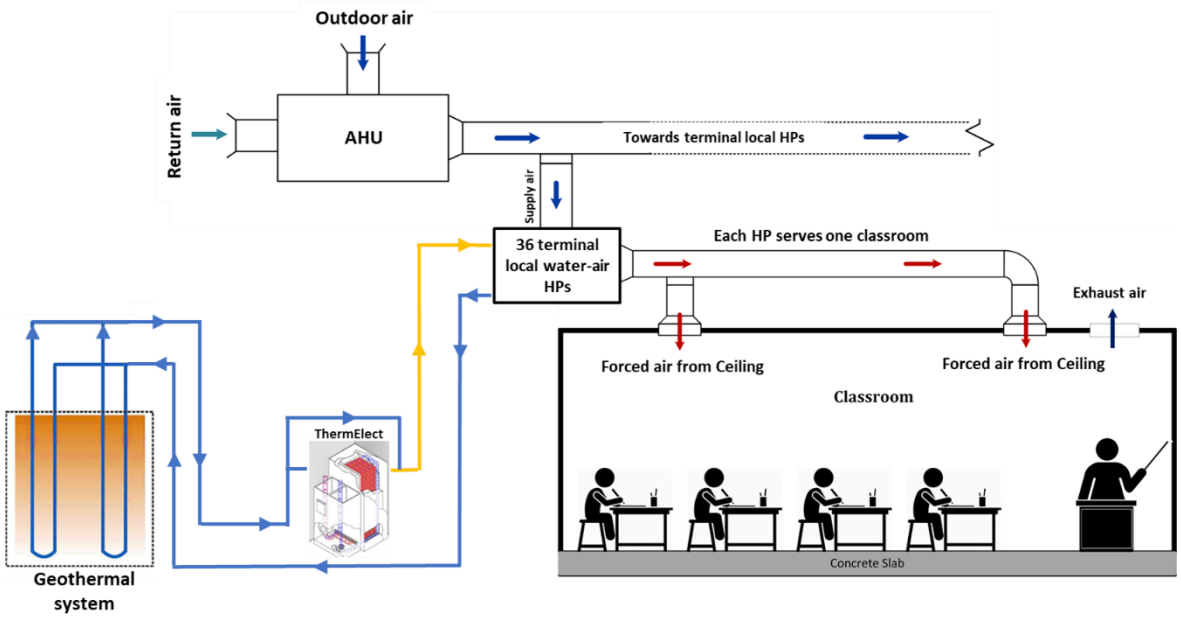

Figure 4-2: Schematic of the heating system, AHU, and classrooms

Figure 4-3 presents the thermal network RC model structures for zones with convective systems. Figures 6a to 6c show the first-order model (1R1C), second-order (3R2C), and the third-order model (4R3C), respectively. The inputs for the analyzed models include outdoor temperature (T_{ex}), solar heat gain (q_{SG}), internal heat gain (q_{IG}), and heat delivered by water-air heat pumps (q_{aux}). Montreal weather data is used to determine outdoor temperature and solar radiation. In the measured data, the heat supplied by water-air HP is calculated by multiplying measured electricity demand by COP of the HP and is used for comparison of models and measurements (Figure 4-4). The solar heat gains, internal gains, and heating for the third-order model are distributed over the thermal capacitances (Figure 4-3(c)). The performance of the simplified RC models from the first order to the third-order model is validated with measured data, as shown in Figure 4-4 (a-c).

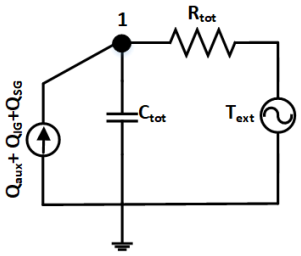

(a)

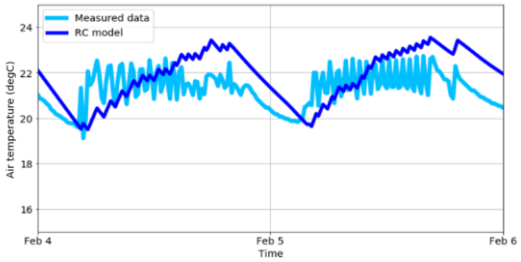

(a)

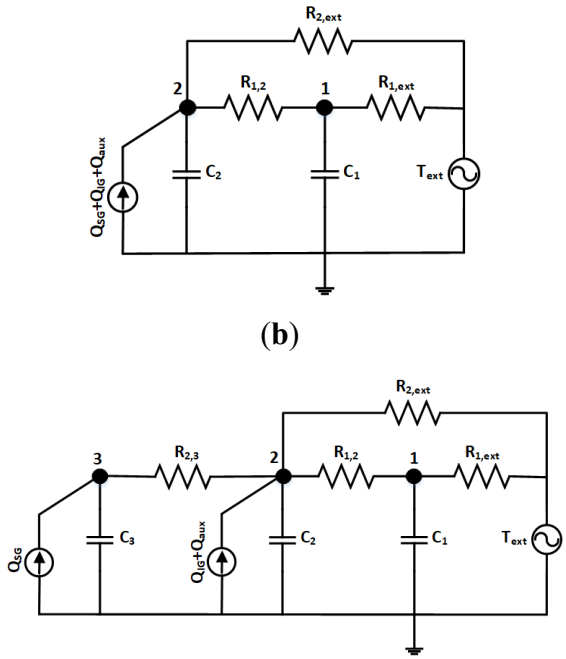

Figure 4-3: RC thermal network model: (a) First order (b) Second order, and (c) Third order model

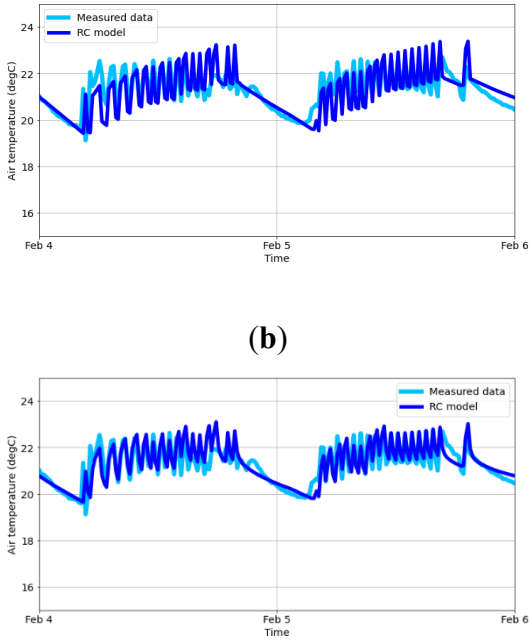

Figure 4-4: Calibration of RC thermal network models with measured data: (a) First order (b) Second order, and (c) Third order model

As shown in Figure 4-4a, the first-order model cannot capture the system's dynamics well. The second-order model has better calibration results than the first-order model, but it still cannot capture details of the thermal dynamics of the system (Figure 4-4b). The calibration of the third-order model (Figure 4-4c) shows good accuracy and adequate statistical indices (CV-RMSE of 8 % and a maximum difference of 0.4 °C). It should be noted that higher-order models require additional inputs, such as heat flux measurements, to guarantee observability. Since these measurements will not be available in most buildings, higher-order models' identity cannot be guaranteed (Reynders et al. 2014).

4.3 Available energy flexibility in contingency event

Contingency reserves are amounts of power that a utility can use in the event of the loss of a generation unit or unexpected load imbalance. To address this need, Real-time thermal load flexibility should be predicted ahead of time or calculated continuously and should be available at short notice (e.g., 10 minutes) over an hour or several hours. This section presents the contingency strategy to quantify the energy flexibility available from the zones with convective system to the grid at specific times. In this case, a tolerance band setpoint profile is proposed. A flexible

approach is proposed within the tolerance limits where the temperature is allowed to deviate from the reference setpoint. For example, during a flexibility event occurring at 2 pm for one hour, the temperature is allowed to drop by 2 degrees to provide a “temporary relief” to the heating system (Figure 4-5). At this point, the setpoint is lowered two degrees (from 24 to 22 °C).

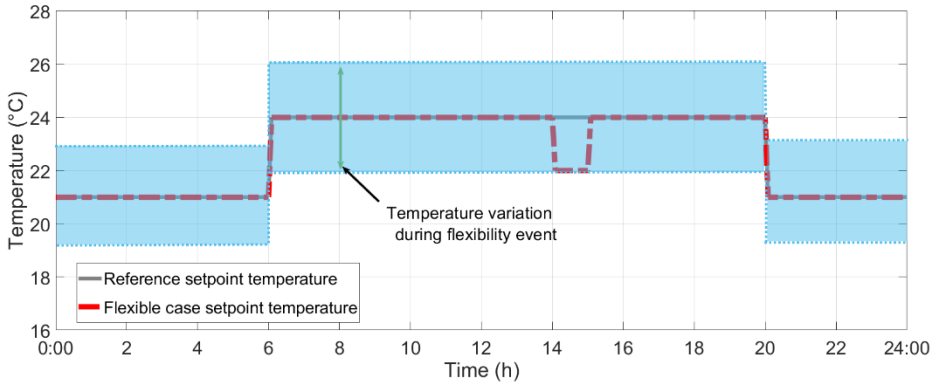

Figure 4-5: Daily setpoint profile with acceptable temperature band and a flexibility event with a duration of 1h.

Figure 4-6 and Figure 4-7 present setpoint temperature and indoor temperature with 1-hour flexibility (from 14:00 to 15:00) and 3 hours flexibility (from 14:00 to 17:00) as an example. As shown in Figure 4-6, indoor temperature does not reach minimum acceptable setpoint temperature with 1-hour flexibility. It can be expected to discharge less thermal energy stored in the building and therefore less flexibility. However, in the case with 3 hours flexibility (Figure 4-7) it can reach the minimum acceptable setpoint temperature and therefore uses more of the energy stored in the thermal mass of the building.

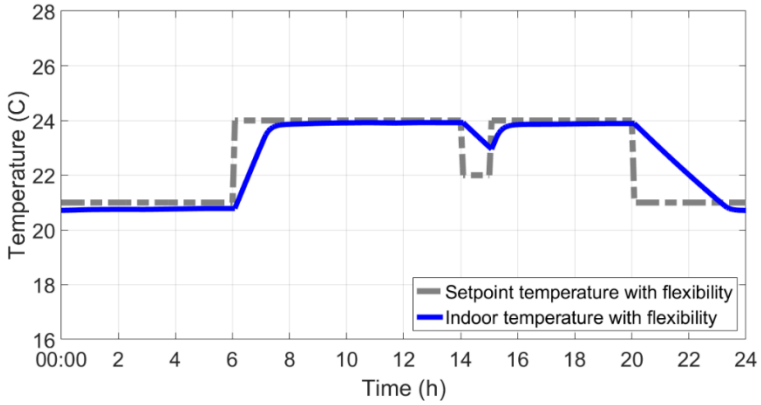

Figure 4-6: Setpoint and indoor air temperature with 1-hour flexibilty

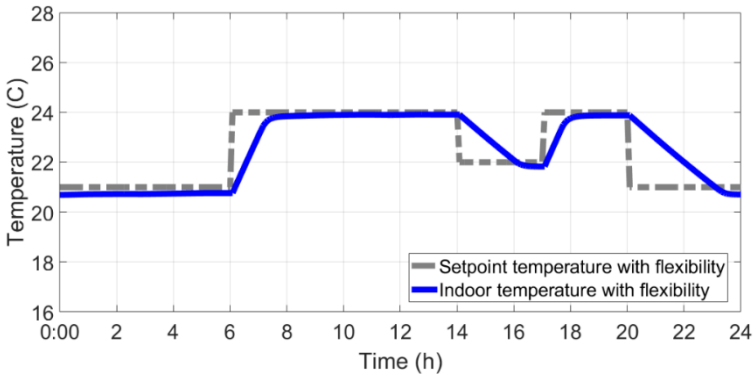

Figure 4-7: Setpoint and indoor air temperature with 3-hour flexibilty

Energy flexibility of a classroom within a short notification time, for a duration of one hour and three hours during day is quantified in Figure 4-8 and Figure 4-9 which present average BEFI (*t*, 1 hr) and BEFI (*t*, 3 hr) for a classroom at the school.

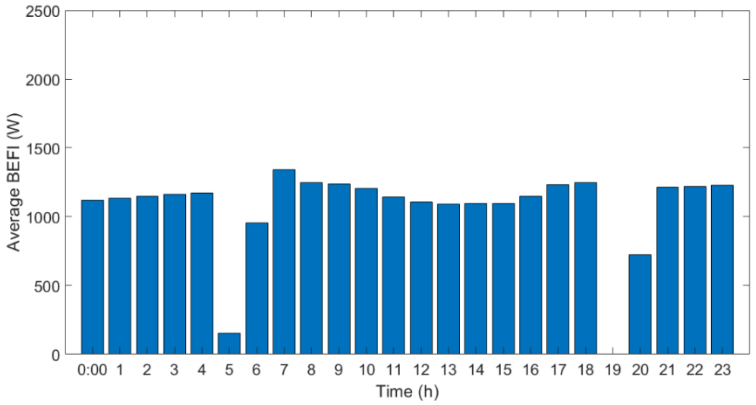

Figure 4-8: BEFI (t, 1 hr) in one classroom, updated every 1 hour

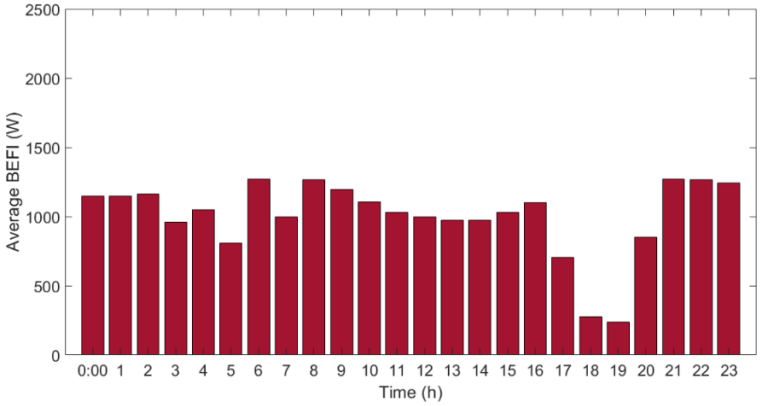

Figure 4-9: BEFI(t, 3 hr) in one classroom, updated every 1 hour

Figure 4-10 and Figure 4-11 show BEFI (t, 1 hr) and BEFI (t, 3 hr) respectively with updating every 15 minutes (as a continues BEFI) for the classroom considered at the school.

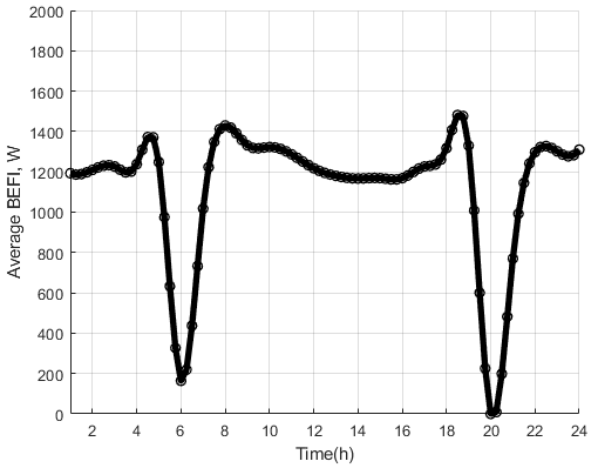

Figure 4-10: BEFI (t, 1 hr) in one classroom - updated every 15 minutes

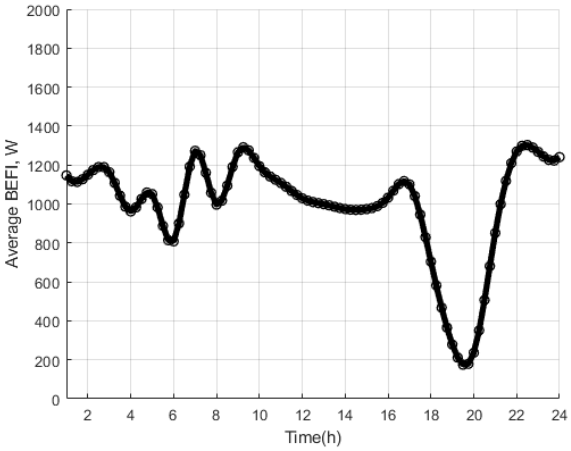

Figure 4-11. BEFI (t, 3 hr) in one classroom - updated every 15 minutes

As shown in Figure 4-10, hourly BEFI for a classroom is around 1200 W for most of the time but at step changes in reference setpoint temperature, this amount decreased sharply. This result shows that when reference setpoint increases in the morning, flexibility is limited because the room temperature gets too close to the acceptable temperature. Also, in the evening, when reference setpoint temperature is lowered, the power demand of the building is negligible due to release of energy stored in the building envelope and floor slab. Therefore, reduction of setpoint temperature could not at this moment provide more flexibility for the grid and average BEFI will be negligible. Based on these observations, it would be possible to propose a new reference setpoint within acceptable limits that will allow a more stable flexibility availability during the whole day. In the case of BEFI (6 a.m., 1 hr), there is almost no flexibility at that time because it takes almost an hour to go from the night set back temperature to the new minimum acceptable temperature. In the case of BEFI (6 a.m., 3 hr) (Figure 4-11), it takes about the same time to reach the acceptable temperature, but then it has two hours more where it can benefit from the flexibility.

If this flexibility strategy is applied to all classrooms, total hourly BEFI that can be provided to the grid is as shown in Figure 4-12 and Figure 4-13:

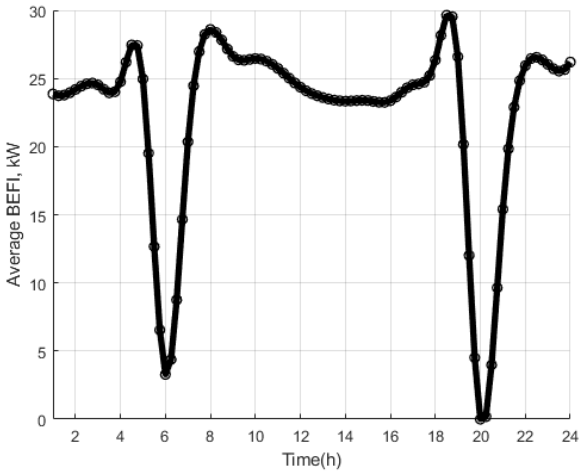

Figure 4-12: BEFI (t, 1 hr) in all classroom - update every 15 minutes

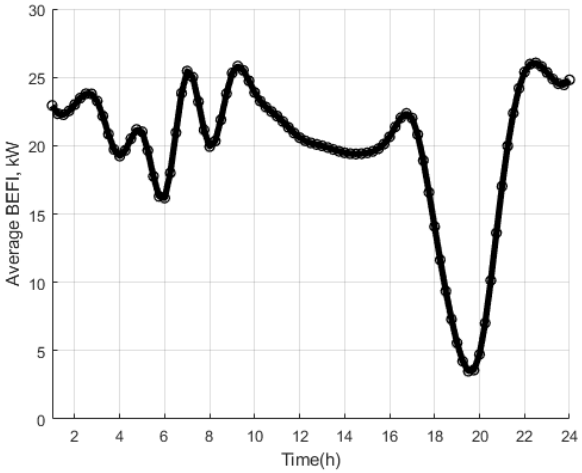

Figure 4-13: BEFI (t, 3 hr) in all classroom - update every 15 minutes

As shown in Figure 4-12 and Figure 4-13, an energy flexibility of around 25 kW can be provided to the grid when needed to face the loss of a generation unit or other unexpected load unbalance. Figure 15 shows that using flexible setpoint for a duration of three hours during the day can provide more stable flexibility (around 20 kW) for the grid. According to Figure 4-14, energy flexibility of around 20 W/m^2 can be provided to the grid in the event of loss of a generation unit or other unexpected power outages. It should be considered that when we add all the classrooms, we have more flexibility in the individual setpoint profiles based on occupancy, therefore the available flexibility would be able to be flattened and more stable flexibility can be provided for the grid.

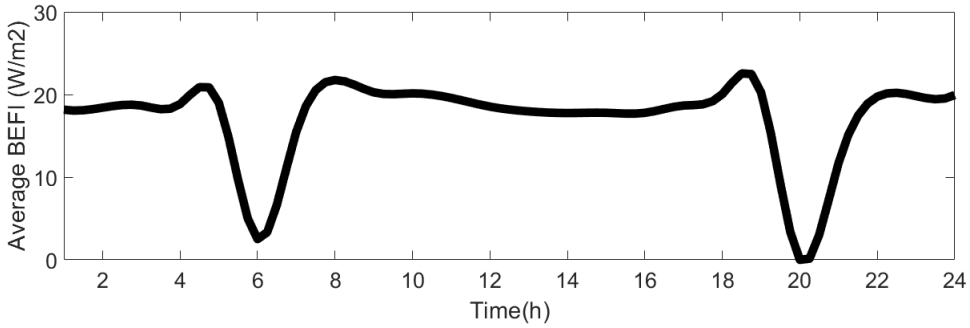

Figure 4-14: Energy flexibility profile, 1-hour event

It should be noted that BEFI at time *t* may vary according to time of notice and a notice prior to signal may allow to precondition the building to maximize available flexibility when needed. The BEFI can be implemented in the BAS with a predictive model controller, which can optimize power flexibility for a known period of high demand. This makes BEFI appropriate for various grid requirements, from contingency reserves to load shifting.

4.4 Archetype zones with hydronic radiant floor and convective heating systems

Figure 4-15 presents a schematic of the office zones equipped with local water-air HP and a hydronic radiant floor system on the school's first floor.

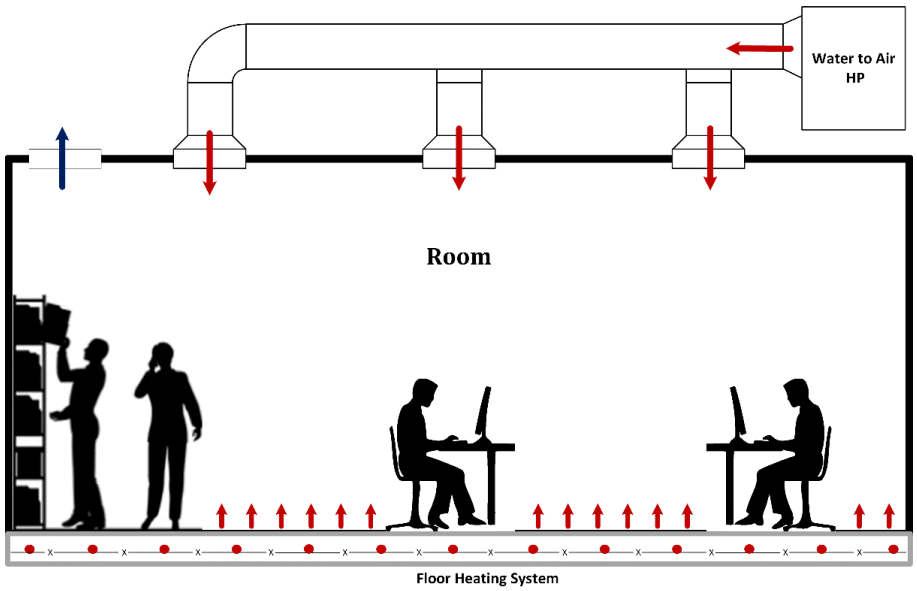

Figure 4-15: Schematic of the office zone equipped with hydronic radiant floor and convective systems

The plan view of the offices and piping of the hydronic radiant floor system is shown in Figure 4-16. These offices are heated with hydronic radiant and local convective systems. Proportional-integral thermostats control heating systems. The thermocouples in the offices are T-types with a standard accuracy of 0.2 °C for the temperature range of 0 to 70 °C. In addition to air temperatures, floor temperatures are also measured at eight different locations, as shown in Figure Figure 4-16.

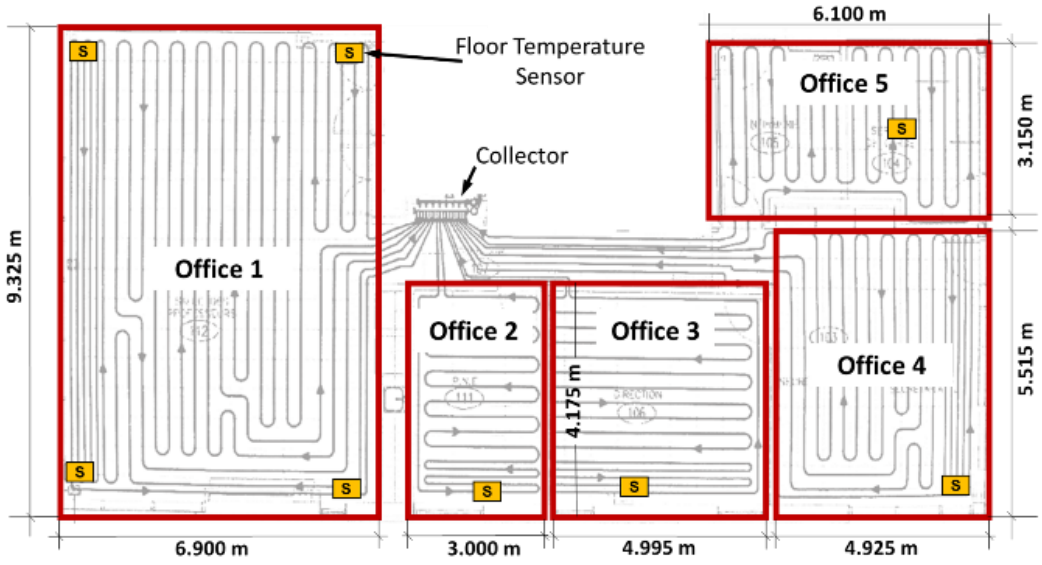

Figure 4-16: Plan view of the offices with hydronic radiant floor system.

Table 5 presents the radiant hydronic floor area in each zone and the piping length.

Table 5: Floor area and piping length of the offices with hydronic radiant system.

Thermal zone	Area (m^2)	Piping length (m)
Office 1	64	244
Office 2	12	69
Office 3	21	91
Office 4	27	176
Office 5	19	87
Total	143	667

A front view of the slab with hydronic radiant piping can be seen in Figure 4-17. The floor is a concrete slab 15 cm thick insulated at the bottom with total thermal resistance of 5.64 m^2K/W. The pipe is made of cross-linked polyethylene (PEX), has a diameter of 1.25 cm, and is in the depth of 6 cm. The pipes were kept in place by a wire mesh before casting concrete, and the distance between the pipes was 30.4 cm.

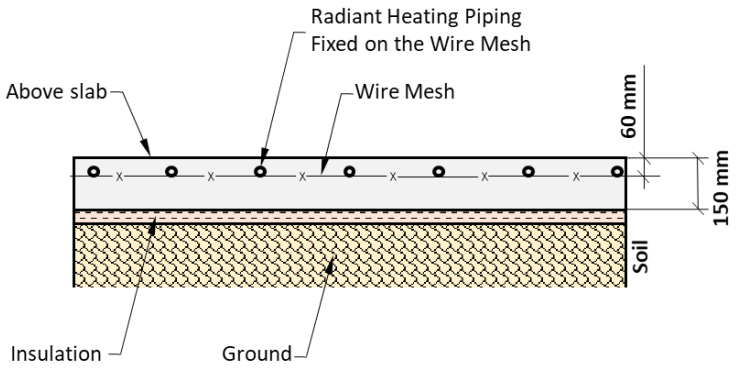

Figure 4-17: Slab cut with hydronic radiant heating piping.

Concrete's properties are affected by its age, temperature, humidity, and moisture content (Marshall 1972). Following ASHRAE (ASHRAE 2009), a normal-density concrete has a conductivity of 1.7 W/(mK), the specific heat of 800 J/(kgK), and a density of 2200 kg/m^3. A water-water HP provides a controlled flow rate of 0.29 L/s with a maximum temperature of 48.8 °C. The HP has a nominal COP of 2.7 under full load conditions at 48.8 °C. Heating power to the hydronic radiant system is calculated by Equation 4-1:

$$Q = \dot{m} \times c_p \times \Delta T \qquad 4\text{-}1$$

According to the ASHRAE standard 55, the floor temperature must not exceed 29 °C (ASHRAE 55 2017). Thus, a floor surface temperature of 26 °C is considered in this study. Several floor sensors and control valves protect the floor from overheating and enhance thermal comfort. The RC thermal network for the zones with hydronic radiant and convective heating/cooling systems is shown in Figure 4-18. The inputs are outdoor temperature (T_{ext}), solar gain (Q_{SG}), internal heat gain (Q_{IG}), the heat delivered by hydronic radiant system (Q_{RF}), and heat delivered by the convective system (Q_{aux}). These inputs can be:

- *Controllable:* such as the heat delivered by the heating systems and the ventilation airflow rate.
- *Uncontrollable:* such as the outdoor temperature, solar gains, and internal gains.

The performance of the simplified RC model is validated with measured data, as shown in Figure 4-19.

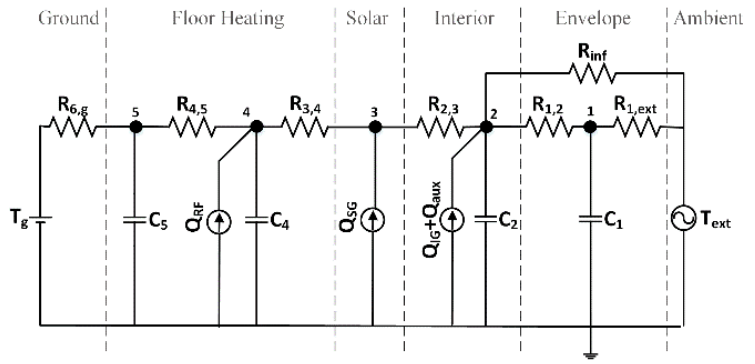

Figure 4-18: RC thermal network model of the zones with hydronic radiant floor system and convective system

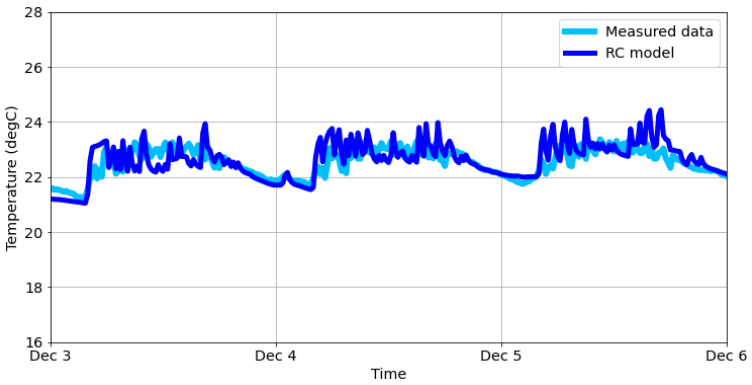

Figure 4-19: Calibration of RC thermal network model with measured data, zones with hydronic radiant floor system and convective system

Table 6 provides an overview of the thermal network model parameters:

Table 6: Description of RC thermal network model parameters (7R4C).

Parameter	Description	Parameter	Description
1	Node of Envelope	$R_{1,ext}$	Resistance of wall, (K/W)
2	Node of indoor air	$R_{1,2}$	Resistance between wall and air node, (K/W)
3	Node of floor surface	$R_{2,3}$	Resistance between floor and air node, (K/W)
4	Node of Pipe	R_{inf}	Resistance of Infiltration, (K/W)
5	Node of concrete (top)	$R_{3,4}$	Resistance between pipe and floor surface, (K/W)
T_{ext}	Temperature of outdoor, (°C)	$R_{4,5}$	Resistance between concrete and pipe, (K/W)
T_g	Temperature of ground, (°C)	$R_{6,g}$	Resistance between ground and concrete, (K/W)
Q_{SG}	Solar heat gain, (W)	C_1	Capacitance of envelope, (J/K)
Q_{IG}	Internal heat gain, (W)	C_2	Capacitance of effective Air, (J/K)
Q_{aux}	Heating power, (W)	C_4	Capacitance of Floor (top), (J/K)
Q_{RF}	Heating of radiant floor, (W)	C_5	Capacitance of Floor (below), (J/K)

4.2.1. Control Scenarios for zones with hydronic radiant floor and convective systems

This section investigates the heat supplied to the zones with hydronic radiant and convective systems. It will be possible to develop simple predictive control strategies that use thermal storage potential while also considering peak load and thermal comfort. In the reference case (a business-as-usual case), the hydronic radiant floor temperature setpoint (21.8 °C) is always lower than the air temperature setpoint (23 °C) during the daytime (Figure 4-20a). As a result, the convective system is the primary heating system, and the floor acts as a heat sink. In this study, alternative control scenarios for a cold winter day are examined and compared to current building operations as a reference case. Assumptions considered in designing control strategies include:

- To maintain the slab temperature within the comfort range, the slab surface is set to a maximum of 26°C.
- The water-water HP can deliver up to 15 kW of heat to the radiant floor heating system, according to the observation from measured data.
- The operating temperature is considered to be the effective indoor temperature.
- During unoccupied hours (nighttime), the slab is charged and discharged during occupied hours (daytime).

1. Control scenario 1 (Reference case)

The reference case is presented in Figure 4-20a, which is the current operation of zones with hydronic radiant heating. In this scenario, the convective system is the primary heating system, and the hydronic radiant system is not commonly used. As seen in Figure 4-21, in this case, the peak load is 10 kW and occurs during the on-peak hours (6 a.m. to 9 a.m.). Thus, in order to improve the energy flexibility of the building, the following two control scenarios are presented.

2. Control scenario 2 (constant air setpoint temperature)

This control scenario involves preheating the slab from midnight to 8:00 a.m. with a setpoint temperature of 26°C (Figure 4-20b). During occupied hours (from 8:00 a.m. to 5:00 p.m.), the slab's set point temperature is 18 °C, and then it is raised to 22 °C. It is considered that the air setpoint temperature is always constant and equal to 20 °C during occupied and non-occupied hours.

According to Figure 4-20(b), the operative temperature varies between 21 and 24 °C, which is within the thermal comfort range for the occupants. In Figure 4-21(b), the heat delivered to the

thermal zones is calculated using the control scenario 2. In this control scenario, the radiant floor system is the primary heating system, and the heating demand during occupied hours is reduced. It should be noted that in this control scenario, the ventilation system is off, resulting in poor air quality in the offices. Therefore, control strategy 3 is presented to address the air quality of the zones during occupied hours.

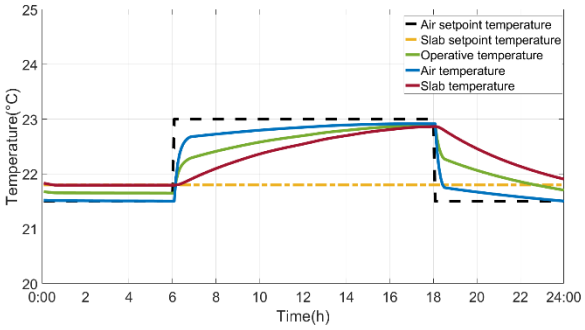

(a) Control strategy 1 (Reference case)

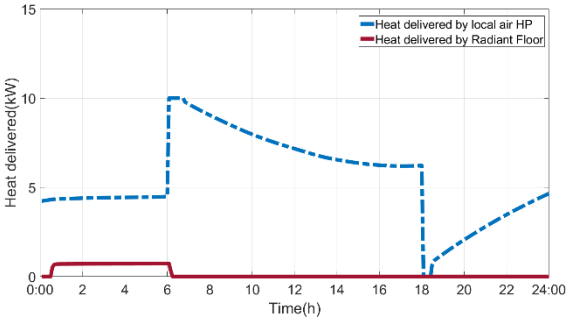

(a) Control strategy 1 (Reference case)

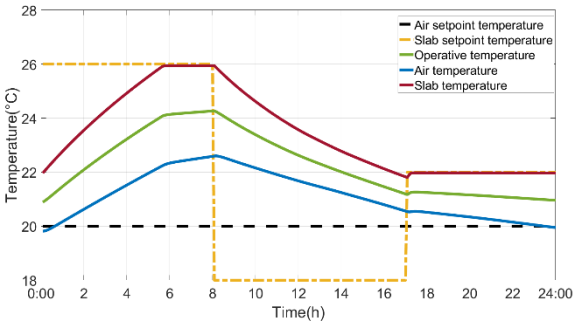

(b) Control strategy 2

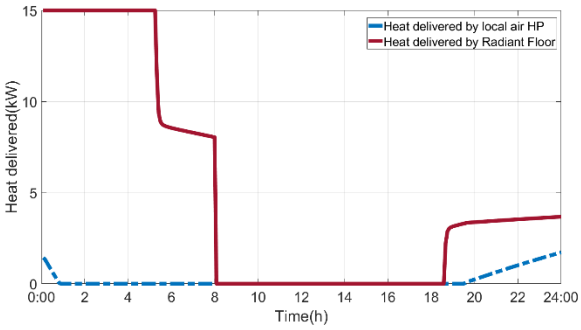

(b) Control strategy 2

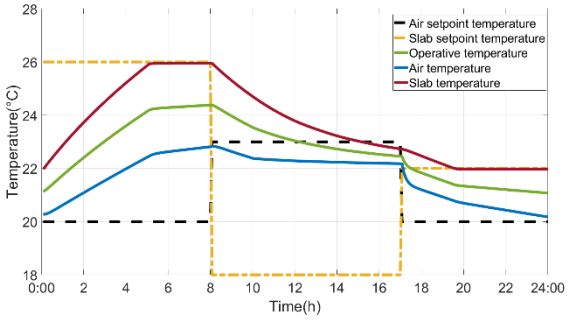

(c) Control strategy 3

Figure 4-20: Temperature profile in different control strategies

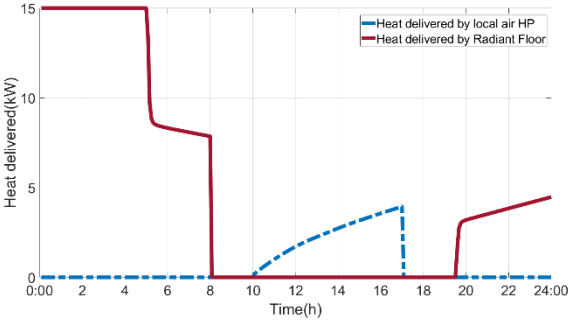

(c) Control strategy 3

Figure 4-21: Heat delivered to the thermal zones in different control strategies

3. Control scenario 3 (variable air setpoint temperature)

As part of this control scenario, the air setpoint temperature is increased to 23 °C during occupied hours (Figure 4-20c). As a result, the morning peak load can be reduced, and fresh air can be provided to the zones from 10:00 a.m. to 5:00 p.m. The energy consumption in this flexible scenario is 133.5 kWh, which is less than the reference case (136.6 kWh). The following section will address the slab's state of charge (SOC) (i.e., thermal storage), as well as the flexibility associated with reducing peak loads and energy consumption over peak periods.

4.5 State of Charge (SOC) of the slab

The thermal inertia in the slab can provide the flexibility to reduce peak loads and shift the heat production of the radiant heating system in time. State of Charge (SOC) is a concept that describes how much energy is stored at time t relative to the total capacity, as shown in Equation 4-2 (Reynders et al. 2018):

$$SOC = \frac{E_{th}(t) - E_{th,min}(t)}{E_{th,max}(t) - E_{th,min}(t)} \quad 4\text{-}2$$

The SOC is the percentage of the stored thermal energy as a function of the minimum and maximum slab surface temperatures, as given by (Qu´ebec).

$$SOC = \frac{T_{slab}(t) - T_{th,min}(t)}{T_{th,max}(t) - T_{th,min}(t)} \quad 4\text{-}3$$

Where $T_{\text{th,max}}$ is the maximum slab surface temperature, set at 26 °C for indoor thermal comfort, and $T_{\text{th,min}}$ is the minimum slab surface temperature, considered equal to the average indoor air temperature.

Figure 4-22 and Figure 4-23 illustrate heat storage and SOC of the slab in the reference case (control strategy 1) and flexible case (control strategy 3). It can be observed that in the reference case, the slab cannot be fully charged. Thus, the thermal energy storage capacity of the slab is not fully utilized; while using a flexible case (control strategy 3), the slab is fully charged during unoccupied hours and discharged during on-peak hours. This approach activates the thermal load flexibility of the school and allows the electricity grid to manage electricity demand when needed.

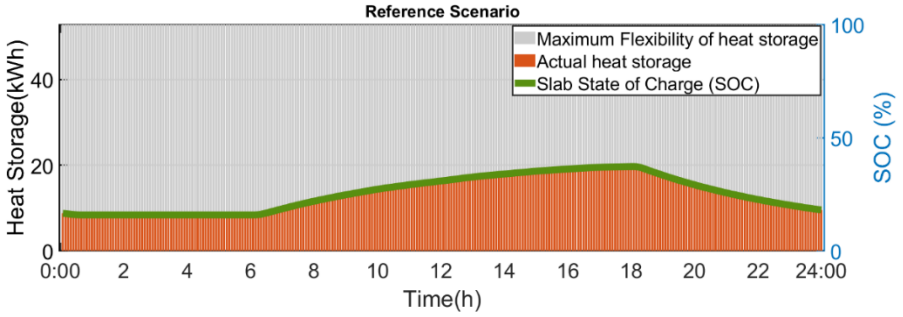

Figure 4-22: Heat storage and State of Charge (SOC) of the slab - reference case

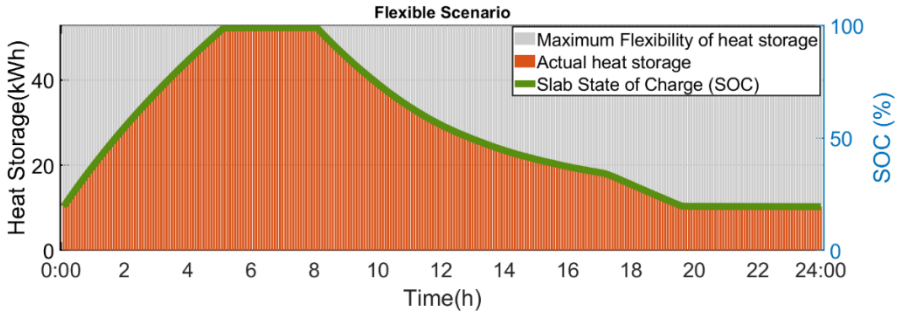

Figure 4-23: Heat storage and State of Charge (SOC) of the slab – flexible case

4.5.1 Thermal load flexibility in archetype zones with hydronic radiant system

In Figure 4-24, a flexibility strategy is applied to zones with hydronic radiant and convective heating systems to calculate the hourly BEFI.

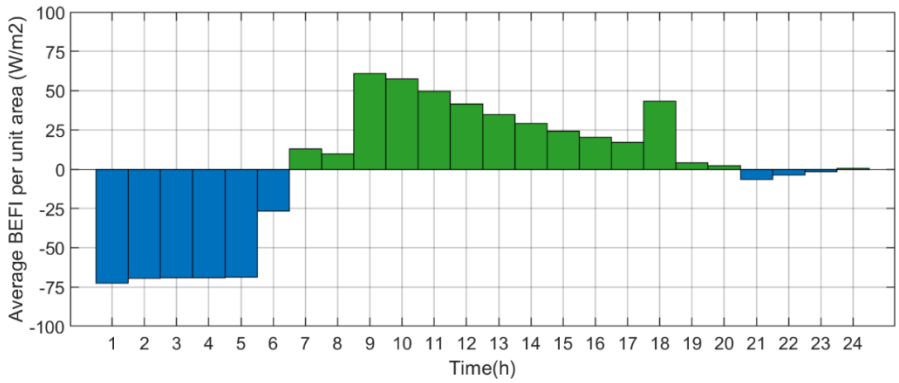

Figure 4-24: Average hourly BEFI – Flexible control strategy.

By applying a flexible control strategy, available hourly BEFI provided to the grid during on-peak hours is positive, indicating the power reduction value available compared to the reference case. During nighttime (off-peak hours), the BEFI is negative, showing a higher power demand for charging the slab and preheating the zones. Based on Figure 4-24, around 60 W/m^2 energy flexibility can be provided to the grid in the morning and 45 W/m^2 in the evening (on-peak hours).

4.6 Building Level Energy Flexibility

Figure 4-25 presents energy flexibility at the building level. Zones with radiant floor and convective heating systems can provide around 60 W/m^2 energy flexibility. Also, classrooms and the library with convective heating systems can provide 20 W/m^2 during on-peak hours. In total, by implementing appropriate control strategies, the school building can provide energy flexibility from between 30 W/m^2 to 80 W/m^2 when needed by the grid.

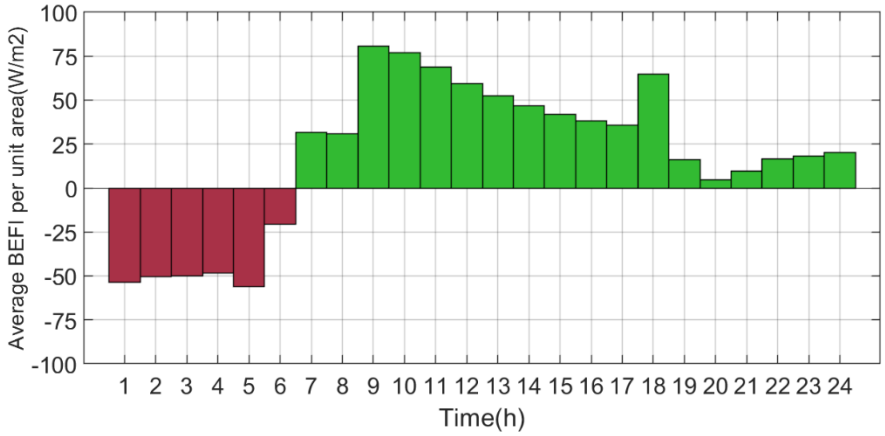

Figure 4-25: Hourly building energy flexibility in school

In this school, the gym and offices floor area are 586 m^2, and the classrooms, libraries, and kindergartens floor area are 2054 m^2. Therefore, the school at the building level has potential flexibility of between 50 to 80 kW, representing 40% to 65% building energy flexibility. This bottom-up approach opens the path towards labelling energy flexibility in school buildings as part of the future smart grid and smart cities.

4.7 Conclusion

School buildings are an important part of the building stock; they also represent a sizeable portion of the total energy use in the building sector. Therefore, quantification of energy flexibility in school buildings has a significant role in providing a safe and efficient operation of the future resilient grid. This chapter presented a practical methodology that facilitates the modelling and implementation of appropriate control strategies in school buildings. It also presented a methodology for defining and calculating a dynamic energy flexibility index for buildings. The dynamic building energy flexibility index (BEFI) is defined in terms of key performance indicators relative to a reference energy consumption profile at zone level, building level, and as a percentage.

The application of the BEFI was presented for a fully-electric school building in Canada. This study illustrated how low-order lumped parameter thermal network models could be utilized to calculate the BEFI. Furthermore, the activation of energy flexibility through a rule-based approach with near-optimal setpoint profiles is investigated. Results showed that applying appropriate control strategies can enhance the school building energy flexibility by 40% to 65% during peak-demand periods. In addition to improving energy flexibility in school buildings, these control strategies could reduce the size of HVAC units at the design stage, thereby lowering their operating and initial capital costs.

Chapter 5: Model Predictive Control and Field Test[2]

5.1 Introduction

Model predictive control (MPC) is one of the key approaches in activating energy flexibility in buildings to meet smart grid needs (Killian and Kozek 2016, Drgoňa et al. 2020). MPC allows the building operation to be programmed based on the weather forecast, expected schedules, and occupants' behavior. With MPC's proactive "look ahead" approach, the building operation can be optimized, activating energy flexibility while maintaining satisfactory indoor environmental quality.

Although several studies have investigated the application of MPC in buildings, most focused on energy consumption in cooling-dominated regions. In cold regions, the peak load in the morning and evening strains the electrical grid. For example, during winter, the electrical grid of Québec (Canada) is heavily stressed by peak morning (6:00 to 9:00) and evening (16:00 to 20:00) loads (HydroQuebec 2023). It is thus essential to reduce peak demand for the grid by using the energy flexibility of building load (Klein et al. 2017, Afroz et al. 2018).

Recent international efforts have recognized the need for a systematic approach to assess the flexibility for demand response in buildings (Tang et al. 2021, Bai et al. 2023, Liu et al. 2023). The methodology of the present chapter includes following steps:

- Developing data-driven grey-box models for representative zones and calibration of these models with real data,
- Clustering weather data based on the outdoor temperature and solar irradiance,
- Creating predefined setpoint profiles for each weather cluster,

[2] This work is based on a published refereed conference thesis and a peer-reviewed journal article: (a) Morovat, N., Athienitis, A. K., Candanedo, J. A. (2023). "Energy Flexibility Activation in School Buildings: Heuristic Model Predictive Control Method", Energy Journal. (Under review), (b) Morovat, N., Athienitis, A. K., Candanedo, J. A. (2022), "A Heuristic Model Predictive Control Method to Activate the Energy Flexibility of School Buildings", 7th International High-Performance Buildings Conference 2022, Purdue University, West Lafayette, IN, USA, July 10-14. Morovat, N., Athienitis, A. K., Candanedo, J. A. (2023), "Model predictive control for demand response in all-electric school buildings", 13th Nordic Symposium on Building Physics (NSB 2023), Aalborg, Denmark, 12-14 June 2023.

- Testing of different control scenarios to assess the impact on electricity demand and energy performance,
- Energy flexibility quantification to enable interaction between buildings, aggregators, and utilities.

Following these steps, this chapter presents an MPC methodology to control the HVAC system using the established dynamic tariffs for morning and evening peaks. Also, it demonstrates its potential to activate the energy flexibility of an occupied fully electric school building in a cold climate region. This clustering methodology to identify typical weather scenarios and room types and using predefined setpoint profiles is a practical approach that simplifies the implementation of MPC in real buildings while reducing the time and costs of modeling and optimization. Also, this methodology helps the utility to plan ahead based on the weather clusters while limiting the number of decisions. The approach presented here is scalable and can be transferable to other school buildings.

5.2 Methodology

As shown in Figure 5-1, the school building's zones are divided into the archetype zones with convective heating systems and zones with radiant heating systems. Then, archetype models for representative zones are developed. The input data, such as indoor temperature and power demand, are measured and collected. These data are used as inputs for the calibration of archetype data-driven grey-box models and parameter identification. Then, the weather data (e.g., outdoor temperature, solar radiation) are clustered into several categories, representing different weather conditions (6 clusters representing two ambient temperature ranges and three solar radiation ranges). The developed MPC methodology uses predefined setpoint profiles to shift the building load from on-peak to off-peak hours. For each MPC scenario, the model runs a simulation to provide an optimal setpoint profile for the building and quantify energy flexibility in response to grid requirements.

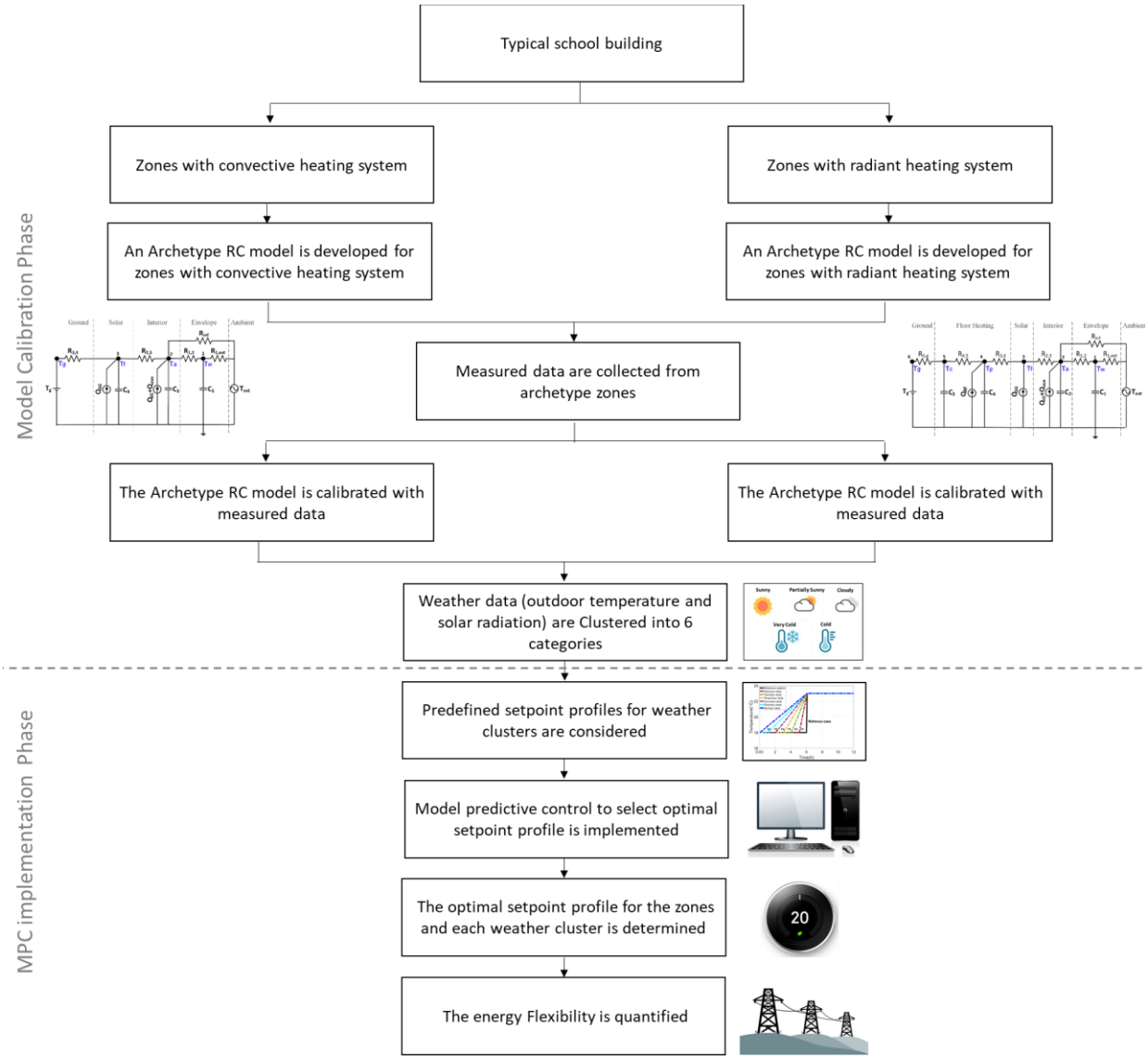

Figure 5-1: General overview of the proposed control methodology.

5.3 Model Creation

5.3.1 Data-Driven Grey-Box Model

The challenges of generating an accurate and generalized model are one of the most significant limitations of MPC and have led to MPC largely being constrained to the research field to date (Killian and Kozek 2016, Drgoňa et al. 2020) (Amadeh et al. 2022). Building energy models are typically categorized into three types: white box, black box, and grey box models. White-box models simulate the heating/cooling demand using physical principles, black-box models use data-driven models, and grey-box models use physical insight and real data. Data-driven grey-box models have been identified as a practical approach for addressing challenges associated with

implementing MPC in intelligent buildings (Li et al. 2021, Joe et al. 2023). Selecting an appropriate level of resolution in a grey-box model is essential, as it directly impacts the tuning of the model parameters and, particularly, the calculation time of MPC. A high-order model containing too many parameters requires information that is not often available with adequate accuracy. An oversimplified model may not be accurate enough to be useful as a decision-making tool. Thus, model complexity should be chosen carefully considering the control objectives and constraints, such as the assessment of energy use and comfort criteria.

Figure 5-2 shows a third-order RC thermal network with three capacitances for the zones with convective heating, and Figure 5-3 presents a fourth-order RC thermal network for zones with radiant heating system. In these thermal network models, *R* indicates the lumped thermal resistance between the connected temperature nodes; *C* represents the lumped capacitance of the nodes, and *Q* represents the heat addition to the nodes. Table 1 provides an overview of thermal network parameters and their description.

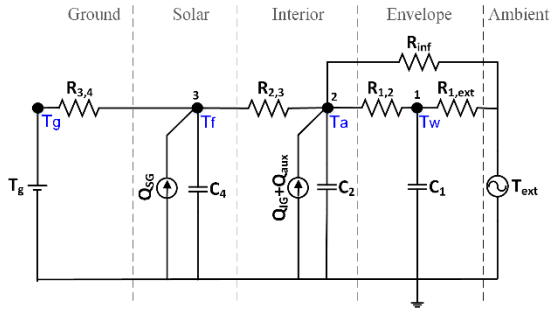

Figure 5-2: RC thermal network model of the zones with convective system.

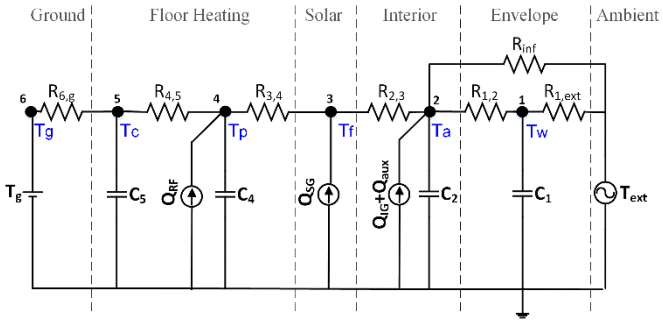

Figure 5-3: RC thermal network model of the zones with convective and radiant floor heating systems.

The RC models are calibrated with measured data in zones with convective heating systems (i.e., Classrooms) and zones with radiant floor systems (i.e., gym and offices). The accuracy of the reduced-order models depends on their characteristic parameters (resistances and capacitances), so they must be appropriately adjusted. The optimization approach establishes the equivalent parameters for RC circuits by minimizing the coefficient of variation of the root mean square error (CV-RMSE).

Table 7: Thermal Network Parameter Description

Third-order model		**Fourth-order model**	
Parameter	**Description**	**Parameter**	**Description**
1	Envelope temperature node	1	Envelope temperature node
2	Indoor air temperature node	2	Indoor air temperature node
3	Floor temperature node	3	Floor surface temperature node
4	Ground temperature node	4	Pipe temperature node
$R_{1,\,ext}$	Wall resistance, (K/W)	5	Concrete temperature node
$R_{1,2}$	Resistance between wall and air node (K/W)	6	Ground temperature node
$R_{2,3}$	Resistance between floor and air node, (K/W)	$R_{1,ext}$	Wall resistance, (K/W)
$R_{2,\,ext}$	Infiltration, (K/W)	$R_{1,2}$	Resistance between wall and air node, (K/W)
C_1	Envelope capacitance, (J/K)	$R_{2,3}$	Resistance between floor and air node, (K/W)
C_2	Effective Air capacitance, (J/K)	R_{inf}	Infiltration, (K/W)
C_4	Floor capacitance, (J/K)	$R_{3,4}$	Resistance between pipe and floor surface, (K/W)
T_{ext}	Outdoor temperature, (°C)	$R_{4,5}$	Resistance between concrete and pipe, (K/W)
Q_{SG}	Solar heat gain, (W)	$R_{5,6}$	Resistance in concrete, (K/W)
Q_{IG}	Internal heat gain, (W)	$R_{6,g}$	Resistance between ground and concrete, (K/W)
Q_{aux}	Heating power, (W)	C_1	Envelope capacitance, (J/K)
T_g	Ground or connecting zone temperature, (°C)	C_2	Effective Air capacitance, (J/K)
		C_4	Floor capacitance (top), (J/K)
		C_5	Floor capacitance (below), (J/K)
		T_{ext}	Outdoor temperature, (°C)
		T_g	Ground or connecting zone temperature, (°C)
		Q_{SG}	Solar gain, (W)
		Q_{IG}	Internal gain, (W)
		Q_{aux}	Heating power, (W)

5.3.2 Data clustering as a simplification approach

A conventional optimization approach has a high computational complexity when applied to all classrooms and for all weather conditions; this complexity hinders its practical implementation. Therefore, we propose finding the optimal setpoint profiles for representative days and zones instead of performing a complex optimization for all conditions. To this end, we adopt a time-series clustering technique that determines the representative zones and weather conditions. The weather forecasts are divided into clear, partly cloudy, and overcast days using the *k*-means clustering technique in Python programming language. The clustering quality is assessed using the *Silhouette index*. Silhouette analysis is a method of interpretation and validation of consistency within data clusters. The silhouette index (ranging between +1 and -1) measures how similar an object is to its cluster (cohesion) compared to other clusters (separation). An average silhouette

index of 1 indicates dense, well-separated clusters; negative values indicate incorrect grouping. A cluster with the maximum average silhouette (within a specific range) is considered optimal. The forecast weather data was obtained from the CanMETEO® program from Natural Resources Canada (NRCan 2021). This approach is a pre-processing step for other models.

5.3.3 Model predictive control formulation

Model predictive control is a method for controlling a system that incorporates a dynamic model, predictions of impending disturbances (e.g., weather), and a cost function that minimizes over time (e.g., electricity price). An illustration of the MPC strategy employed in this study is shown in Figure 5-4.

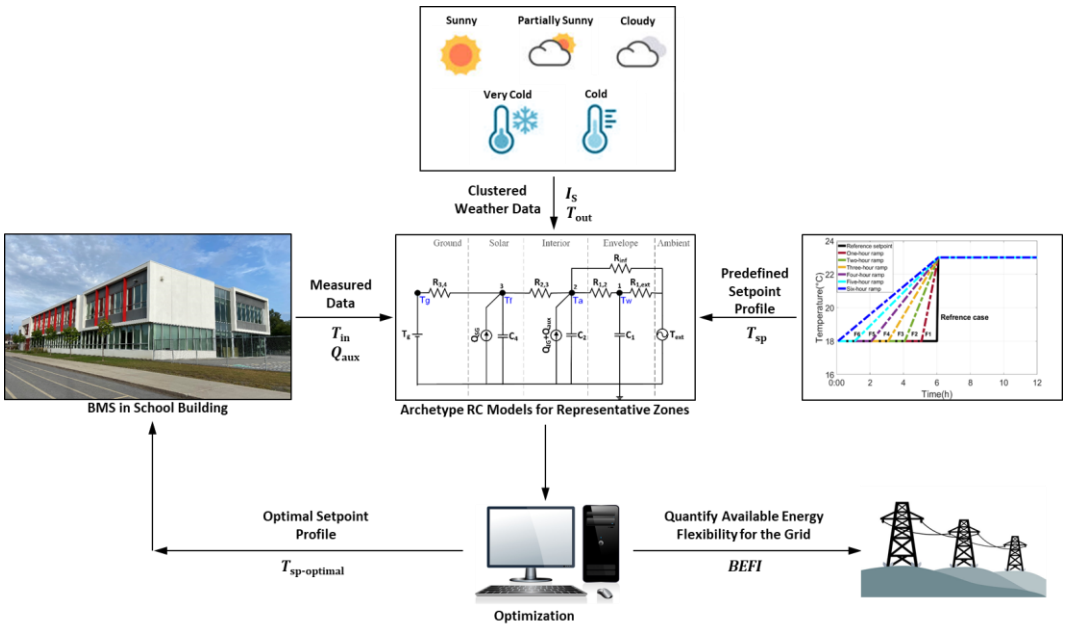

Figure 5-4: Diagram of the heuristic model predictive control employed.

The weather forecast over the prediction horizon is used to solve the optimal control problem in MPC. The prediction horizon ranges from a few hours to a few days of generally accurate information about the future. The prediction horizon period is used to solve an optimization routine. The overall MPC framework is presented in Eq. 1 (Drgoňa et al. 2020), where some sections describe the system dynamics for control, and others establish boundary conditions.

A general optimal MPC formulation is given as follows:

$$\text{Objective: } \min_{u^0,\ldots,u^{N-1}} \sum_{i=1}^{N} l(x^i, u^i, w^i)$$

$$\text{Subject to } h\left(x^i, u^i, w^i\right) = 0 \qquad \text{5-1}$$

$$g(\left(x^i, u^i, w^i\right) \geq 0$$

$$x^1 = x, \qquad \text{Current state}$$

$$x^{i+1} = f\left(x^i, u^i, w^i\right) = Ax^i + Bu^i + Ew^i, \text{ System dynamics}$$

Where,

- x^i: State variables describe the current state of the system,
- u^i: controllable input variables (such as heating setpoints) that can be changed to enhance the building's performance,
- w^i: Uncontrollable inputs ("disturbances") such as weather (outside temperature, solar radiation),
- l (x, u, w): cost function,
- h (x, u, w) = 0: equality constraints,
- g (x, u, w) ≥ 0: inequality constraints (boundary conditions).

In this study, MPC performs optimization starting at midnight with a 24-hour prediction horizon, timestep of 15 minutes. The rest of the constraints force the MPC formulation to use the building model and restrict the heating output to the installed capacity of each zone. The prediction horizon of 24 hours allows for a comprehensive forecast of future electricity prices and heating requirements. The convex optimization problem was solved using the cvxpy library in Python (Diamond and Boyd 2016). The optimization results in optimum heating output values for each water-to-air heat pump and the equivalent zone temperatures.

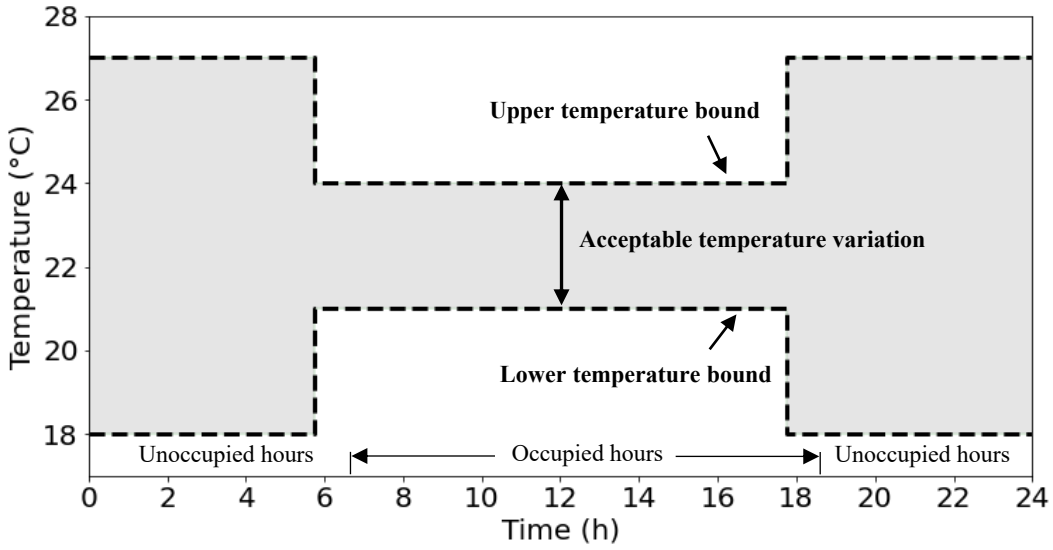

Figure 5-5: Boundary of indoor temperature for cold winter days

In an MPC framework, enforcing a specific temperature range is a common way to achieve thermal comfort. Figure 5-5 presents the set point temperature for the classrooms. The indoor zone temperature is constrained by a lower bound, which is 18 °C at night and 21 °C during the day, and an upper bound, which is 27 °C at night and 24 °C during the day, in order to maintain a level of thermal comfort for the zone occupants. The upper bound generates the desired setpoint target to minimize the energy cost through load shifting by considering future weather and utility price signals. A lower bound constrains the minimum indoor temperature to maintain thermal comfort in the zone.

The literature on optimization prefers convex models and constraints to ensure quick and reliable convergence to a global minimum. This thesis uses state-space representations with convex cost functions, models, and constraints to formulate a convex optimization problem. In Québec, the operating cost includes the price of the peak energy demand, which can be represented as a 1-norm within a convex prediction horizon. Hence, MPC is implemented in Python using routine CVXPy (Diamond and Boyd 2016), a convex optimizer that is solved using ECOS (Domahidi et al. 2013). The two key simplifications in this methodology are: (a) a clustering approach is used to identify typical weather scenarios and room types and (b) predefined optimal setpoint profiles for each cluster are considered to facilitate implementation of MPC in real buildings. Eq. 3 shows the optimization problem, where the objective is to minimize the electricity cost based on weather data clusters and predefined setpoint profiles. For each MPC scenario, the

model runs a simulation using one day ahead forecast weather data to quantify and activate energy flexibility in response to grid requirements. In Equation 5-2, the energy cost varies over the day, indicated by sub-index i, with higher prices during peak hours.

$$\begin{aligned} &\text{Objective: } \min J \\ &\text{Where: } J = \left(\left(\sum_{i=1}^{N} P_i \Delta t \right) \cdot \left(Cost_{\text{Energy},i} \right) + max(P_i) \cdot \left(Cost_{\text{Demand},i} \right) \right) \\ &\text{Subject to } \quad T_{sp} \in \left[T_{sp,1}, T_{sp,2}, \dots, T_{sp,n} \right] \\ &\qquad\qquad 0 \le P \le P_{max} \\ &\qquad\qquad \underline{T} \le T_{in} \le \overline{T} \end{aligned} \tag{5-2}$$

Where P_i is the power demand at the time, N is the number of time steps across the prediction horizon PH, and Δt is the time step. The objective is to determine the room setpoint temperature profile (T_{sp}) from predefined setpoint profiles (one for each weather cluster) that reduce the energy cost of the based on the heuristic optimization. The space heating demand (P) is limited by the maximum capacity of the heating equipment (P_{max}), and the interior zone temperature T_{in} needs to be kept within the allowable limits for comfort.

5.4 Simulation results: heuristic MPC in zones with convective heating system

5.4.1 Weather clustering

The coldest months of the year in Montreal (January and February) are selected because this is when peak energy demand occurs. The solar irradiance (SI) and outdoor temperature data are clustered using *k*-means clustering method. The closest match with the centroids is then identified using this model. According to the average Silhouette index, the optimal number of clusters is three for solar radiation and two for outside temperature, as shown in Figure 5-6 and Figure 5-7.

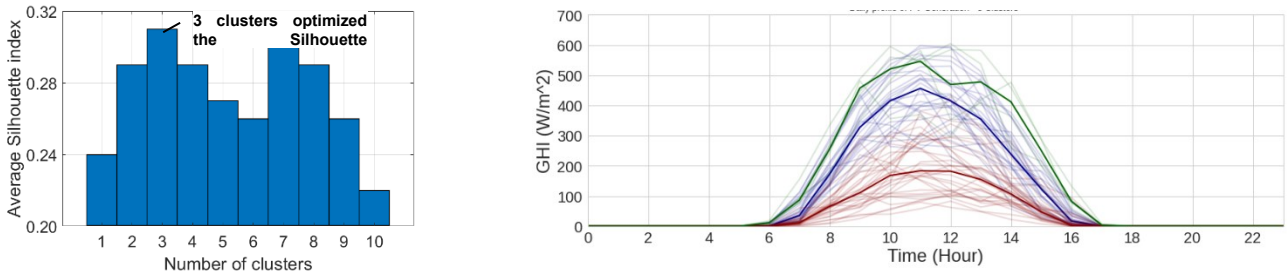

(a) (b)

Figure 5-6: a) The average silhouette index for solar irradiance and b) corresponding clusters

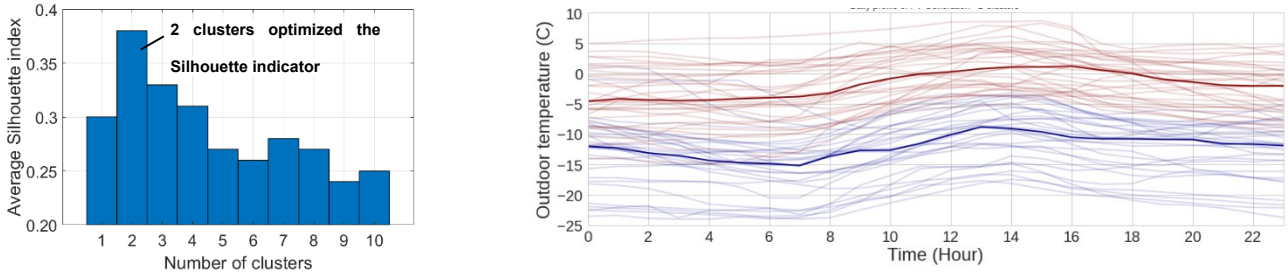

(a) (b)

Figure 5-7: a) The average silhouette index for outdoor temperature and b) corresponding clusters

In this way, we can classify possible weather conditions into six groups (2 x 3). Table 8 presents forecast scenarios according to the clustered outdoor temperature and solar irradiance.

Table 8: Clustering scenarios for weather forecasts

	Level of Cloudiness		
Outdoor Temperature	Cloudy ($SI < 250$ W/m^2)	Semi-Cloudy ($250 < SI < 500$ W/m^2)	Sunny ($SI > 500$ W/m^2)
Cold day (Average temperature = -2.5 °C)	Cluster 1	Cluster 2	Cluster 3
Very cold day (Average temperature = -12.5 °C)	Cluster 4	Cluster 5	Cluster 6

This methodology makes it possible to calibrate archetype RC thermal networks for representative clusters. Such a clustering-based approach enables the development of archetype control-oriented models for decision-making while reducing the number of choices/decisions, thus avoiding the high computational time and costs of modelling and optimization.

5.5 Energy Flexibility Assessment: Predefined 6:00 a.m. event

A Building Energy Flexibility Index (BEFI) has been proposed to quantify the energy flexibility of the building (Athienitis et al. 2020). A description of the concept of the BEFI is presented in

chapter 2. Using outdoor air temperature and solar radiation as inputs, these benchmarking models predict daily power demand. The Six predefined profiles (shown in Figure 5-8) were tested on different clusters of weather forecasts (presented in Table 3). Figure 5-9a and Figure 5-10a present indoor air setpoint temperature and the power demand for classrooms under business-as-usual (BAU) control to evaluate the peak load reduction due to heuristic MPC implementation. For example, Figure 5-9b and Figure 5-10b show the power demand under a four-hour transition ramp in setpoint temperature during very cold and cold days.

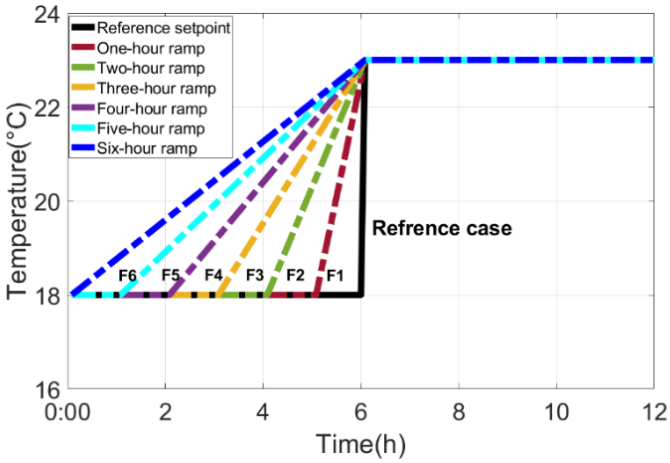

Figure 5-8: Predefined setpoint profiles and the reference case

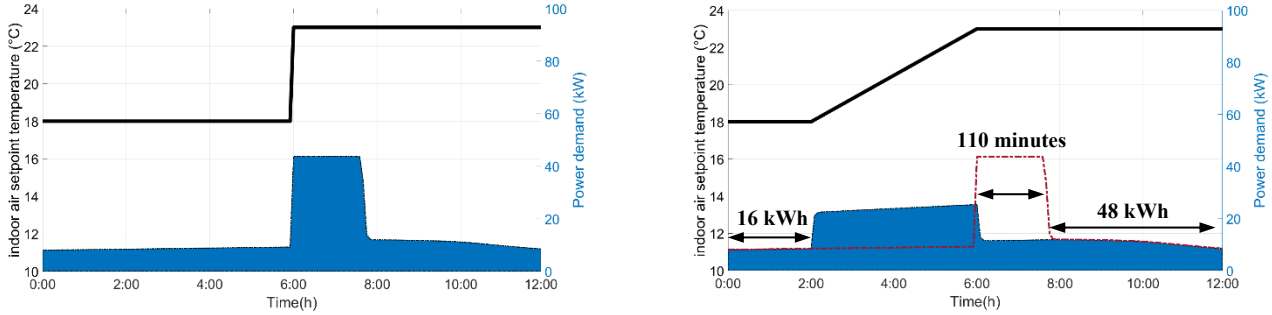

(a) Step-change (b) four-hour ramp

Figure 5-9: Indoor air setpoint temperature and power demand during a very cold sunny day

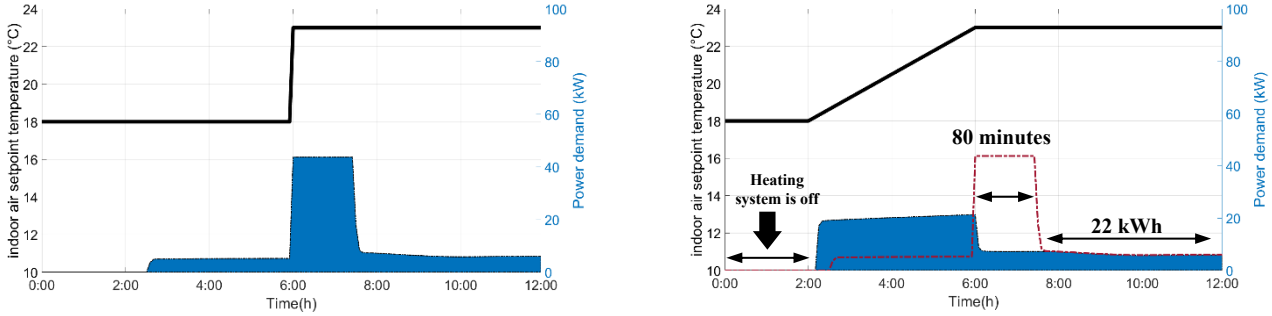

(a) Step-change (b) four-hour ramp

Figure 5-10: Indoor air setpoint temperature and power demand during a cold cloudy day

For very cold days (OAT = -12.5 °C), simulations show that a lower night set-back value is advantageous to prevent peak load rise during on-peak hours. Building heating demand can be switched from peak to off-peak hours using a nearly flat set point (nighttime). Additionally, MPC increased thermal comfort for occupants by gradually raising the internal temperature at night rather than abruptly changing the set point right before occupancy began.

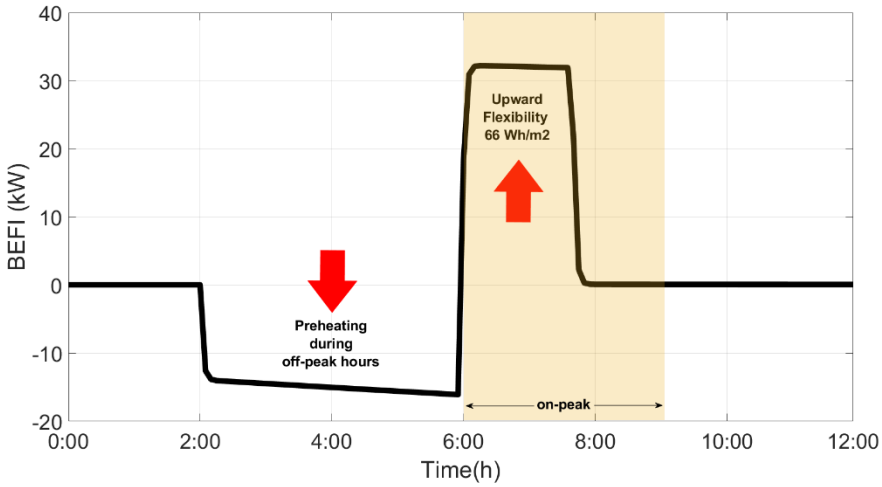

Figure 5-11: Available flexibility with four hours ramp in setpoint temperature.

As shown in Figure 5-11, applying a four-hour ramp during on-peak hours results in a positive BEFI (33 kW), indicating power reduction compared to the reference case. The BEFI is negative during off-peak hours (2:00 a.m. to 6:00 a.m.), meaning a higher power demand to preheat the zones. Figure 5-11 shows that 66 W/m^2 of floor area of energy flexibility can be provided to the grid during morning on-peak hours.

5.6 Energy Flexibility Assessment: Contingency Reserve

The “contingency reserve” refers to the ability of buildings to either reduce their electrical load or provide additional power back to the grid in situations where the power balance between supply and demand is disrupted (e.g., due to a power outage). This concept is part of energy flexibility, where buildings actively participate in the energy system to support grid stability and efficiency.

The first objective is to study the dynamic response of the classrooms to a downward temperature step change during on-peak hours of a very cold day while maintaining adequate comfort. Figure 5-12 and Figure 5-13 present setpoint temperature, room air temperature, power demand, and price signal for the reference and “flexible” scenarios, respectively.

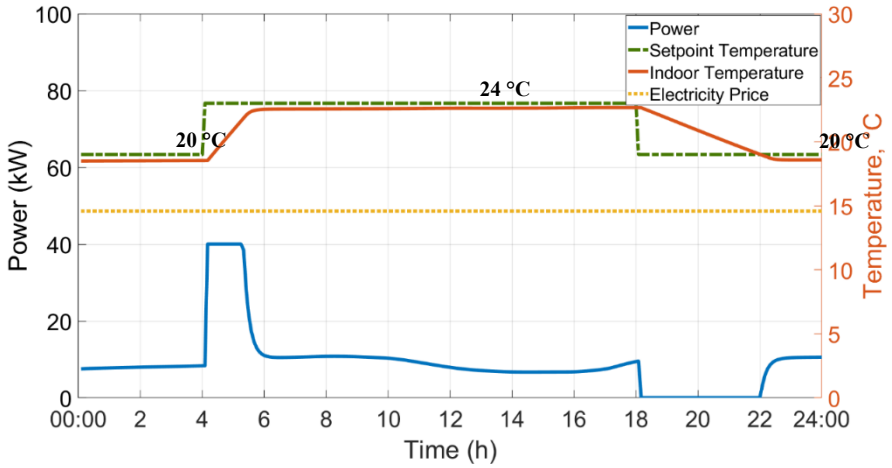

Figure 5-12: Power demand, setpoint temperature, and room temperature - Reference scenario.

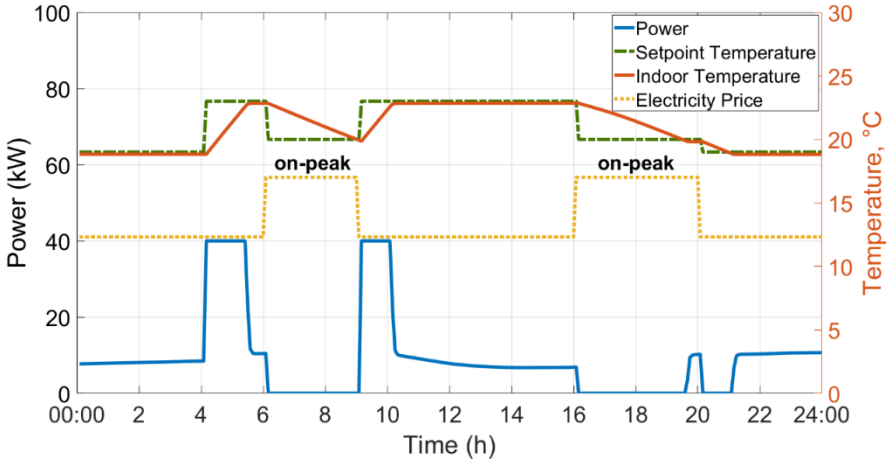

Figure 5-13**:** Power demand, setpoint temperature, and room temperature - Flexible scenario.

Figure 5-14 shows that significant peak reduction can be achieved by replacing a step change with a simple 1, 2, or 3-hour ramp.

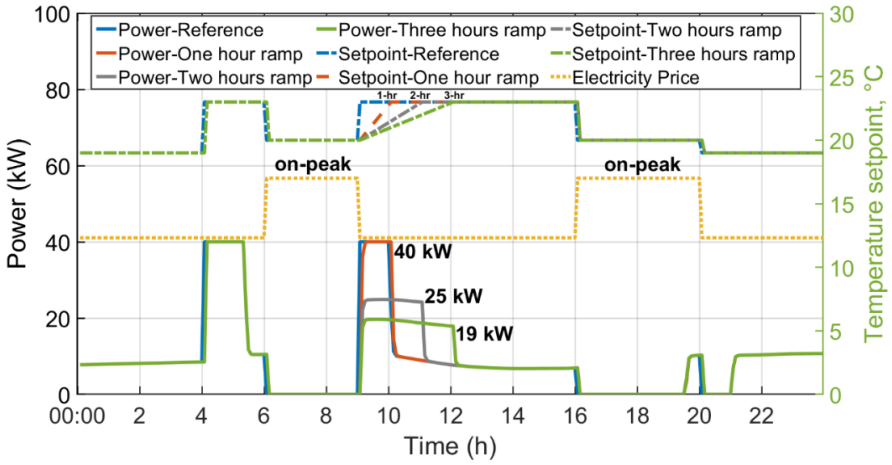

Figure 5-14: Impact of ramping temperature setpoint on rebound power

The results presented in Figure 5-14 show that by increasing the ramp in temperature setpoint from 1 hour to 3 hours, the rebound power decreases by around 50%, which causes the peak values of efficiency. The total BEFI provided to the grid without a ramp and three hours ramp after the flexibility event in the morning are shown in Figure 5-15 and Figure 5-16, respectively.

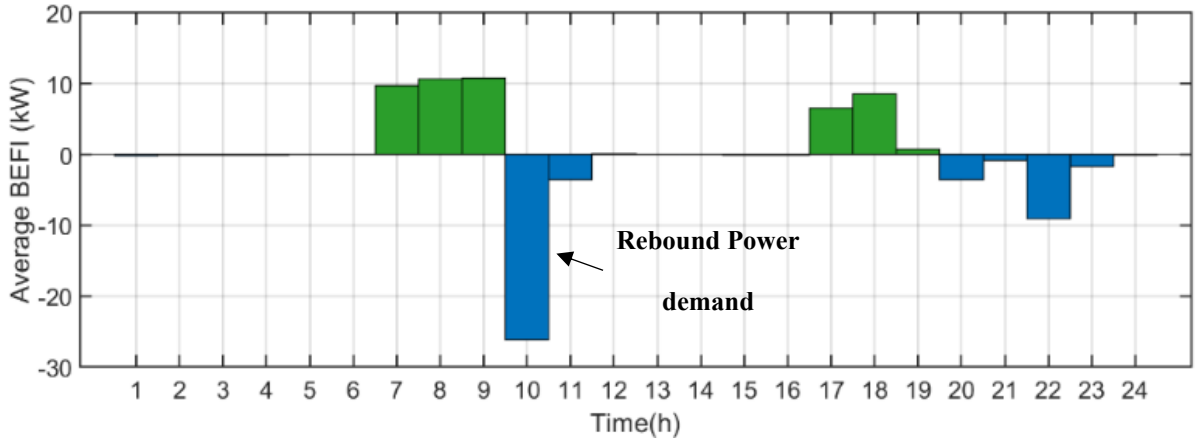

Figure 5-15: Average hourly BEFI – Reference scenario with upward step change

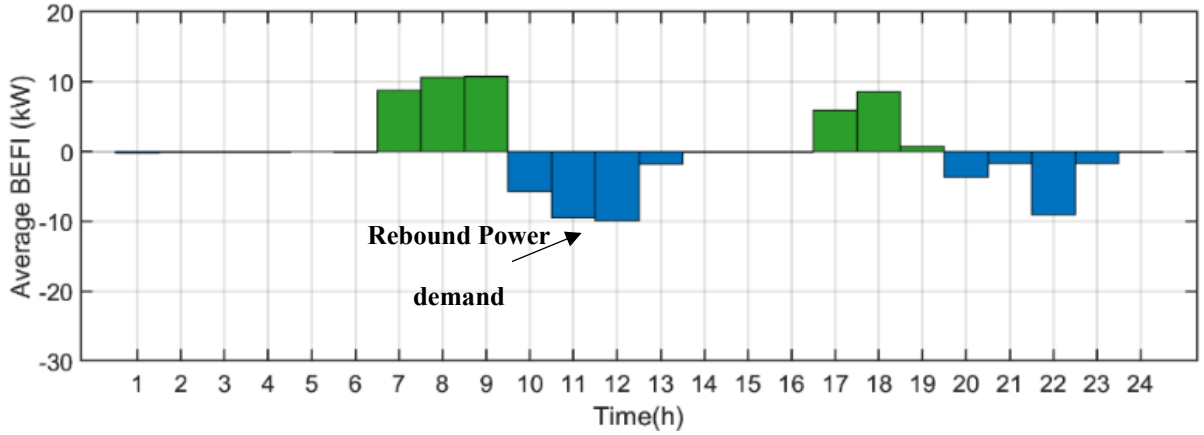

Figure 5-16: Average hourly BEFI – Flexible scenario with three hours ramp

The results show that the BEFI is positive during peak hours by applying the proposed setpoint profiles, making power available for the grid. During off-peak hours (after DR events), the BEFI is negative, which shows higher power demand due to the power rebound for the classrooms. Energy flexibility of 11 kW in the morning and 8 kW in the evening can be achieved when the grid needs. Using the developed control strategies, achieving up to a 35% reduction in peak power demand during peak-demand periods while maintaining acceptable comfort levels is possible. According to Figure 5-16, using a ramp in setpoint temperature has an important effect on the potential energy flexibility. Results show that using a three-hour ramp after on-peak hours could

reduce the negative BEFI (rebound power) by 63 % and thus reduce the rebound effect. This action is essential for the stability and balance of the grid.

5.7 Simulation results: MPC in zones with convective heating system

In this section, the predictive control strategies in zones with convective system are presented. Different control strategies are investigated, including:

a) The reference case: which is the current operation of classrooms. Figure 5-17 shows the classrooms to start being heated around 4:30 am until reach the lower boundary of setpoint temperature at 6 am. In this scenario, as seen in Figure 5-20, the peak load is 49 kW and occurs during the on-peak hours (6:00 to 9:00 am). Thus, in order to improve the energy flexibility of the building, the following control scenarios are presented.

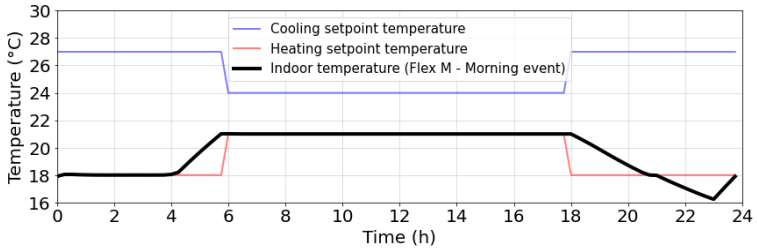

Figure 5-17: Indoor air temperature with flat price rate

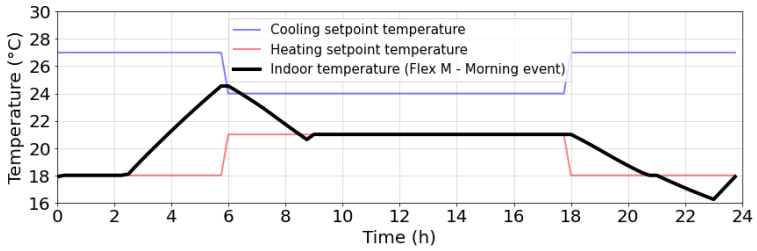

Figure 5-18: Indoor air temperature with rate flex M applied during morning peak hours

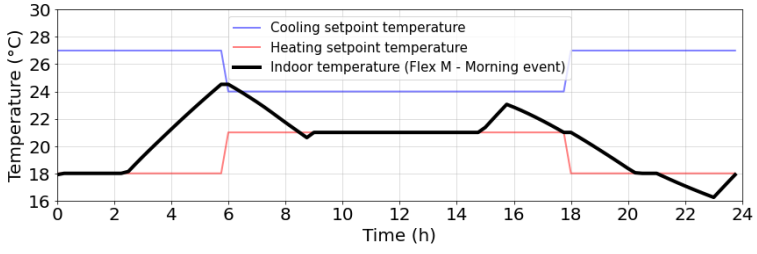

Figure 5-19: Indoor air temperature with rate flex M applied during evening peak hours

b) *Rate flex M in the morning:* To consider a case of a morning peak in a time-of-use tariff structure, the energy cost between 6:00 and 9:00 am is increased by a factor of 15. Figure 5-18

show the classrooms to start being heated around 2:30 am until heating is completely shut off at 6 am. The over-heated space can free float during the peak period and remain within the comfort boundaries. As shown in Figure 5-22 the heating system can be off during morning peak hours, resulting in peak load reduction up to 49 kW. This pre-heating and system staging strategy has emerged through the minimization of operational costs. Compared to the uniform pricing case, this case consumes 77 kWh less than the BAU case.

c) *Rate flex M in the morning and evening:* If there is an evening peak from 4:00 to 8:00 pm, the evening behavior is affected by a slight preheating but not as aggressively as in the morning. The indoor temperature is back to 21°C (Figure 5-19). This case consumes 815 kWh energy less than the BAU.

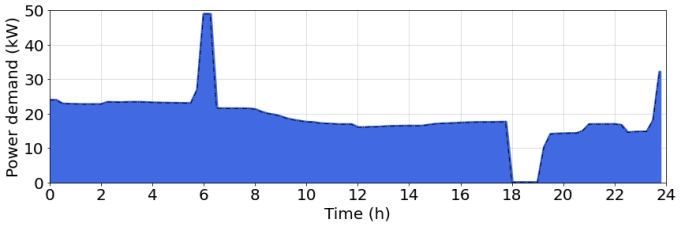

Figure 5-20: The reference case, business-as-usual operation

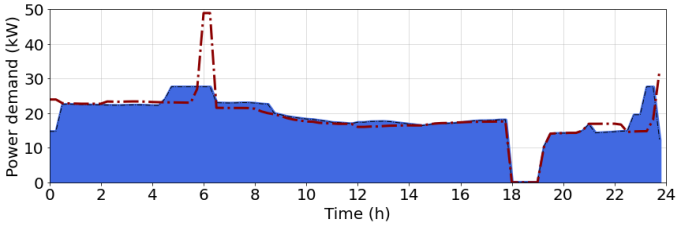

Figure 5-21: Under demand response program with flat rate

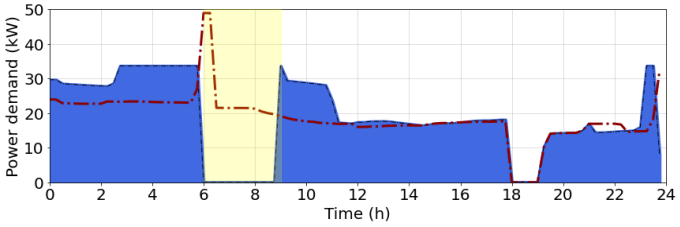

Figure 5-22: Flexible case, Rate flex M during morning

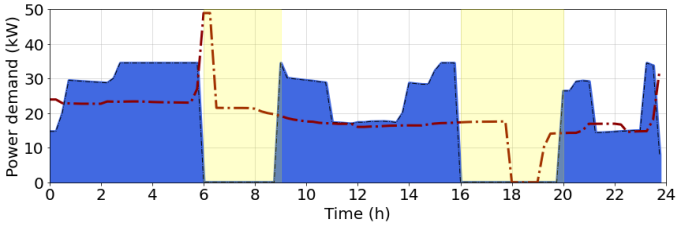

Figure 5-23: Flexible case, Rate flex M during morning and evening

5.8 Simulation results: MPC in zones with radiant floor heating system

Radiant floor systems integrate high thermal inertia into the heating/cooling system and can be used to peak-shave and load-shift the building's thermal load. This section proposes near-optimal setpoint profiles for zones with radiant floor systems to increase energy flexibility while considering thermal comfort constraints. The maximum heating output is limited to the size of the system, which is 16 kW.

To preheat the slab, four predefined control strategies are considered: preheating the slab at 20, 22, 24, and 26 °C from 12:00 a.m. to 6:00 a.m. on both day clusters. Then, the slab temperature was reduced to 18 °C during the daytime (from 6:00 to 17:00) to discharge the slab. During unoccupied hours from 18:00 to 24:00, the setpoint temperature is raised to 22 °C to charge the slab again. Applying these predefined setpoint strategies shifts the power demand from on-peak hours to off-peak hours. Figure 5-24b and Figure 5-25b show the power demand on very cold and cold days, respectively, when the slab is preheated at 22°C during unoccupied times. It is beneficial to have a higher night set-back value when the outdoor air temperature is very low (for example, OAT = -15 °C) to avoid peak load during on-peak hours. It should be considered that using a high night set-back value of 26 °C on cold days (for example, OAT = -2 °C) paves the need for higher energy consumption and increases the risk of overheating during daytime.

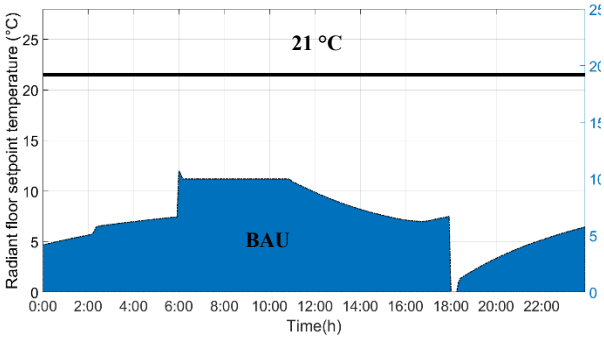

(a) Flat setpoint temperature

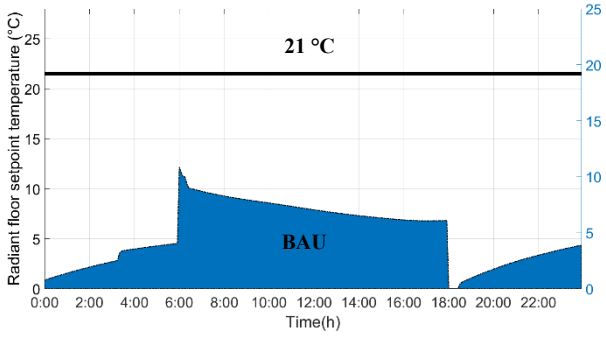

(a) Flat setpoint temperature

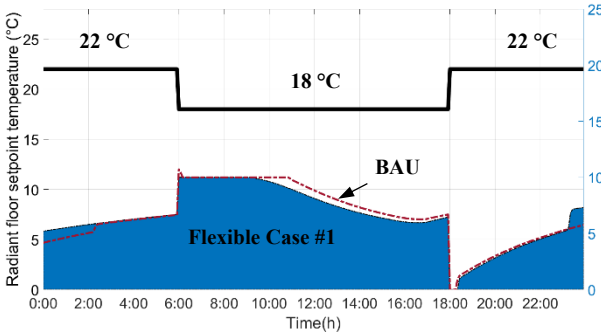

(b) Preheating at 22 °C

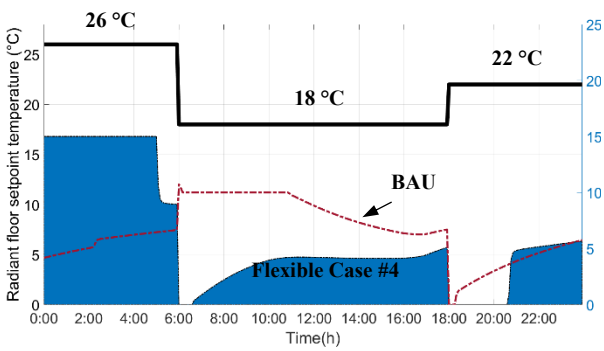

(c) Preheating at 26 °C

Figure 5-24: Power demand in zones with floor heating systems during very cold sunny days

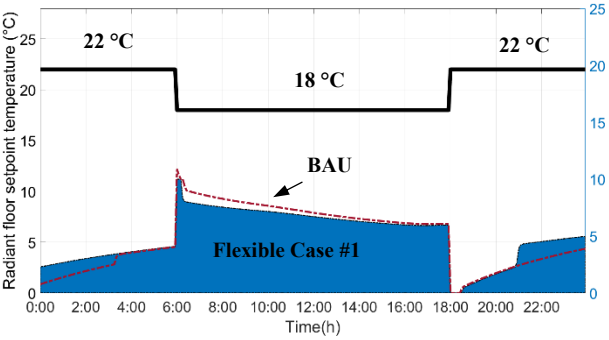

(b) Preheating at 22 °C

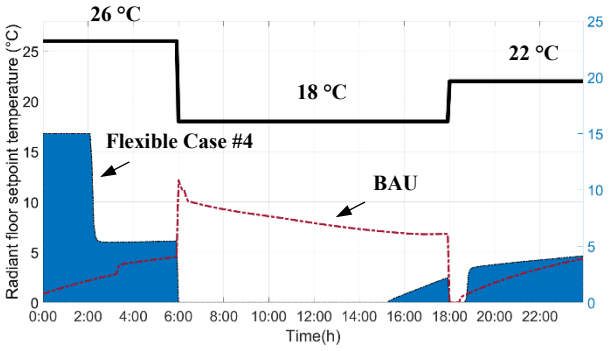

(c) Preheating at 26 °C

Figure 5-25: Power demand in zones with floor heating system during cold cloudy days

5.9 Energy flexibility in zones with radiant floor system

This section calculates such a BEFI to quantify the real-time thermal load flexibility of the building. Eq. (B.1) – (B.3) calculate BEFI by implementing the flexibility strategy and comparing it with the reference case. The average BEFI per unit area in hourly intervals in zones with radiant hydronic floor and convective heating system is shown in Figure 5-26 for a very cold sunny day (OAT = -12.5 °C) and Figure 5-27 for a cold cloudy day (OAT = -2 °C).

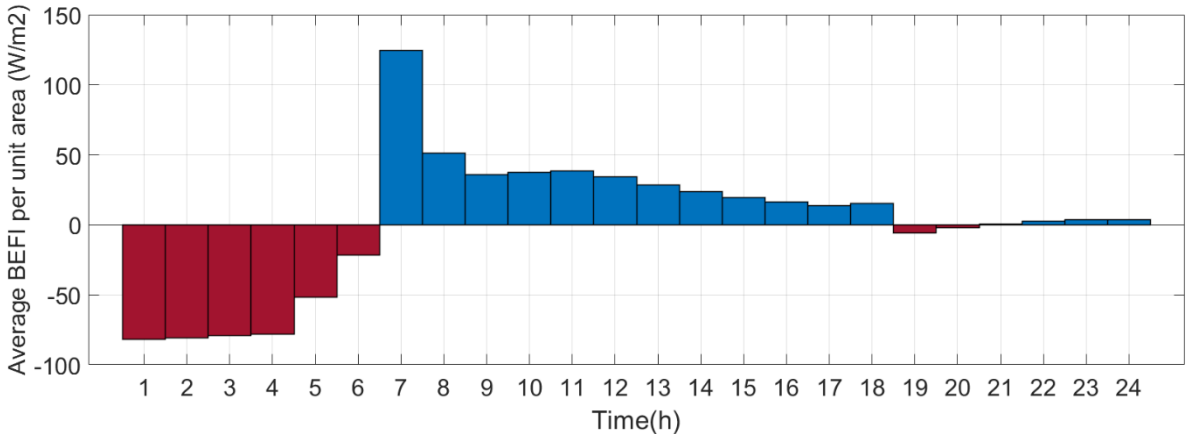

Figure 5-26: Average BEFI in an hourly interval for a very cold sunny day

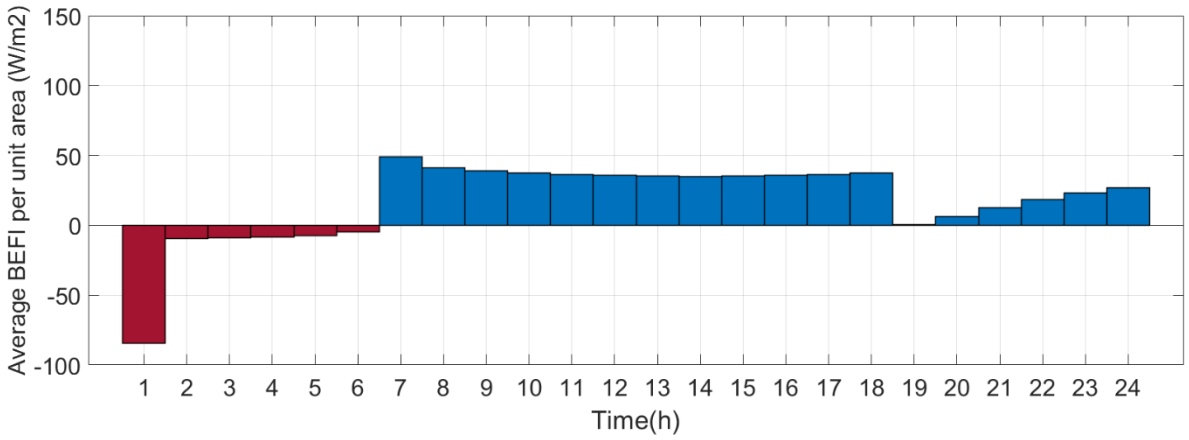

Figure 5-27: Average BEFI in hourly intervals for a cold cloudy day

Both preheating options at 24 °C and 26 °C yielded favorable results, with an average BEFI of up to 9 kW (65 W/m^2) for three h. The BEFI values are highest in the early morning because the abrupt switch from night setback to daytime temperature results in the most considerable reduction in peak demand. The potential power reduction can significantly (45%) downsize the heating systems. A BEFI of around zero shows that flexibility is not available from the building to the grid.

5.10 Field implementation results

The developed MPC methodology was implemented through BACnet (Haakenstad 1999) in the case study building to test its actual performance. Ten classrooms are investigated, including five on the first floor and five on the second floor, with different orientations (as much as possible). Four classrooms are considered as the reference cases (Blue highlights in Figure 5-28), and six are

the flexible cases using MPC (Yellow highlights in Figure 5-28). In this way, we could compare the results of the flexible case with the business-as-usual one. Each classroom is 9 m × 7 m × 3.5 m with a floor area of 63 m^2.

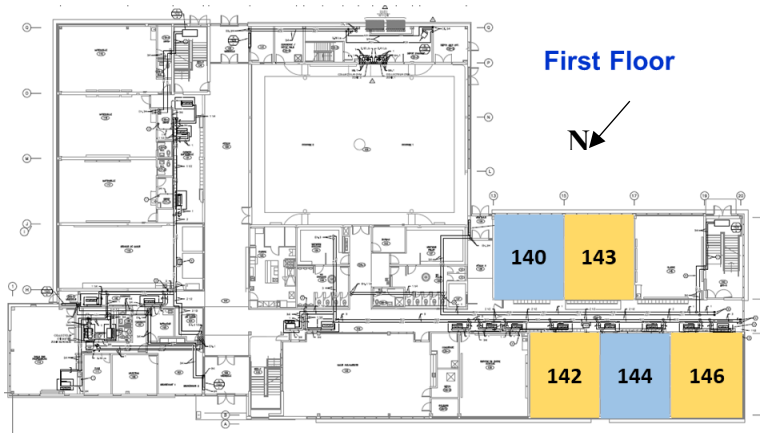

(a)

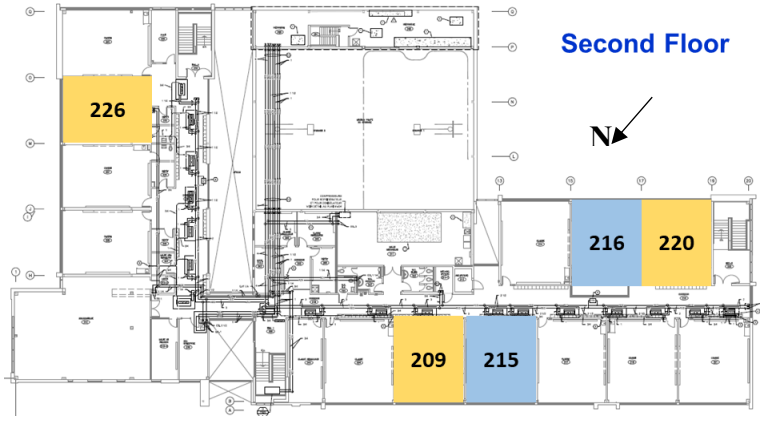

(b)

Figure 5-28: Selected classrooms for experiment at a) the first and b) second floor of the school

By including classrooms on both floors with varying orientations, we aimed to capture various thermal conditions and evaluate the MPC in different scenarios. Table 9 presents each classroom's control strategy, location, and installed heating capacity.

Table 9: Characteristics of the selected classrooms and control strategies applied.

Room	Control strategy	Location	Orientation	Heating capacity (kW)
Class 140	Reference case	First Floor	Southeast	4.84
Class 142	With MPC	First Floor	Northwest	4.84
Class 143	With MPC	First Floor	Southeast	4.84
Class 144	Reference case	First Floor	Northwest	4.84
Class 146	With MPC	First Floor	Northwest	5.89
Class 209	With MPC	Second Floor	Northwest	4.84
Class 215	Reference case	Second Floor	Northwest	4.84
Class 216	Reference case	Second Floor	Southeast	4.84
Class 220	With MPC	Second Floor	Southeast	4.84
Class 226	With MPC	Second Floor	Northeast	4.84

As an example of results, Figure 5-29 and Figure 5-30 show power demand and average BEFI for two of the tested classrooms on a sunny cold day in winter with an average outdoor temperature of -10 °C (reaching -16 °C in the early morning).

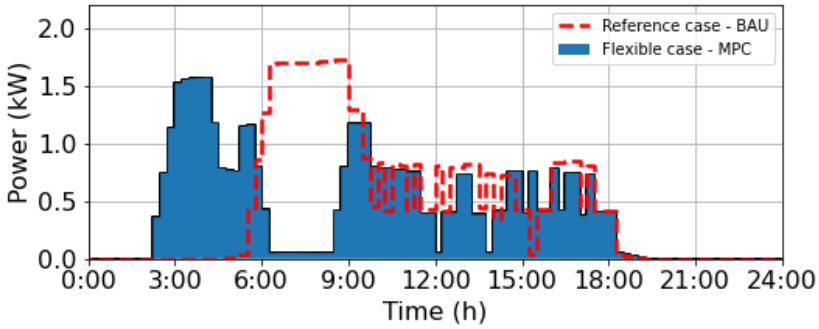

(a)

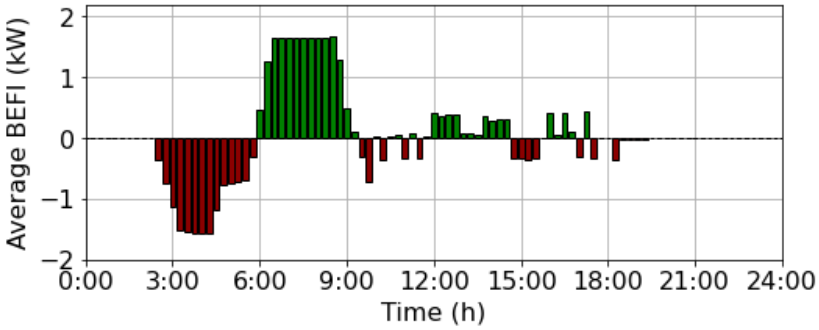

(b)

Figure 5-29: Reference (BAU) and Flexible (with MPC) classrooms in the first floor, a) power demand and b) Average energy flexibility

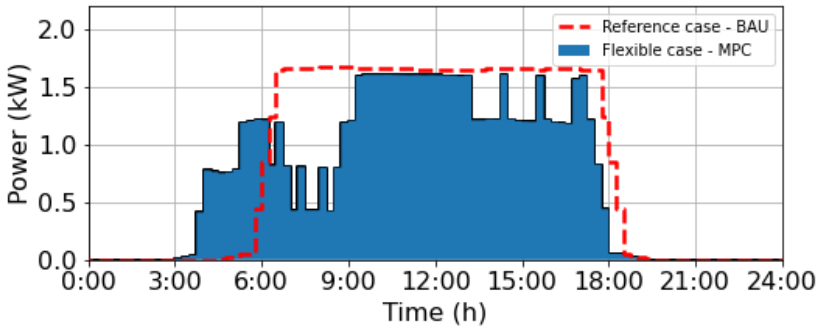

(a)

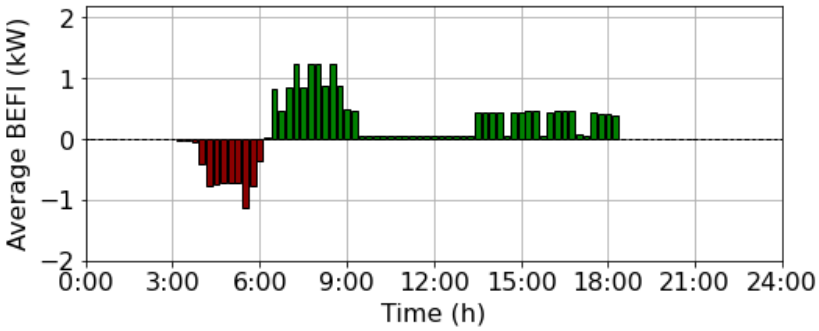

(b)

Figure 5-30: Reference (BAU) and Flexible (with MPC) classrooms in the second floor, a) power demand and b) Average energy flexibility

Figure 5-29 presents the results for south-facing classrooms located on the first floor (i.e., class 143 as the flexible case and class 140 as the reference case), and Figure 5-30 shows the results for north-facing classrooms on the second floor (i.e., class 209 as the flexible case and class 215 as the reference case). The results show that the power demand during on-peak hours is reduced by 1.65 kW in the classroom on the first floor and 0.95 kW in the classroom on the second floor. Thus, the average energy flexibility has increased between 58% to 95%. One reason for the different available flexibility is that each classroom has an individual heat pump controlled by a separate PI controller. Thus, heat pumps have various heating responses in each classroom, which results in different energy flexibility. Another observation is that the power demand after peak hours (i.e., after 9:00 a.m.) is higher in the north-facing classroom. This could be due to the solar radiation effect in the south-facing zones.

Table 6 presents the average BEFI (kW) and percentage of BEFI (%) during the morning effect in flexible classrooms with MPC. These results are obtained by comparing the power demand with their adjacent classrooms as reference cases (refer to Figure 5-28). In the case of class 226, the

adjacent classrooms have not been appropriately measured. Therefore, for this classroom, class 215 is considered as the reference case. As shown in Table 10, by applying the developed MPC in the school, the average BEFI of between 0.8 to 1.65 kW and the average energy flexibility of 47 % to 95 % could be achieved.

Table 10: Average BEFI and percentage of BEFI in the flexible zones with MPC.

Room	Average BEFI – Morning Event	BEFI – Morning Event (%)
Class 142	1.25 kW	73 %
Class 143	1.65 kW	95 %
Class 146	1.10 kW	68 %
Class 209	0.95 kW	58 %
Class 220	1.30 kW	82 %
Class 226	0.80 kW	47 %

The proposed control methodology builds upon data-driven models and enhances school buildings' energy flexibility. Nonetheless, it was built to be scalable to similar mid-size school and commercial buildings. Moreover, it would facilitate the integration of school buildings in the future smart grid by adjusting the objective function in the optimization routine (e.g., peak demand, energy costs, and carbon intensity). Other new challenges for the grid, such as the integration of renewable energy sources and resiliency, could also be tackled with such a predictive control approach.

5.10.1 Field test results under different control scenarios

Three control scenarios for cold winter days are investigated. The first scenario involves reactive controllers in selected rooms that are considered business as usual. The second scenario investigates the MPC without occupancy in the classrooms (This test was conducted during spring break). The third scenario explores the MPC application while considering occupancy in the classrooms. In MPC scenarios, the objective is to minimize the peak load during peak hours in the morning (from 6:00 to 9:00). The reactive controllers in the first scenario are designed to respond to real-time data and changing conditions in the selected rooms. This approach is commonly used and represents the baseline control strategy. In the second scenario, without occupancy in the classrooms, the MPC system can optimize energy consumption by adjusting temperature setpoints based on real-time data and weather forecasts. Lastly, in the third scenario, considering occupancy in the classrooms allows for more realistic control of temperature, leading to further energy savings during peak hours in the morning. The summary of control scenarios is as follows:

Control scenario 1) Reference case (Business as usual)

Control scenario 2) Flexibility scenario I: MPC in classrooms without occupancy (during spring break in February and March)

Control scenario 3) Flexibility scenario II: MPC in classrooms with occupancy (during normal operation of the school)

5.10.2 Reference case (Business as usual)

The current classroom operation, considered as the reference case, is based on a reactive controller for the local HPs. In this scenario, as shown in Figure 5-31, the indoor temperature is around 24 °C during occupied hours (6:00 to 18:00), and the peak load occurs during the morning peak hours (6:00 to 9:00 am) shown in Figure 5-32. The energy consumption during high-price periods for the reference case was in the range of 2.3 kWh to 3.1 kWh, with an average of 2.5 kWh. These high-price periods can significantly impact energy costs for the schools. Also, during the reference scenario, the reactive controller started heating the zones as soon as the setpoints changed. The time it took for the zones to reach the setpoints resulted in some thermal discomfort. This thermal discomfort was particularly noticeable during the morning peak hours when the reactive controller struggled to heat the zones to the new setpoints quickly. This delay in reaching the desired temperature could decrease productivity and create discomfort for students and staffs. Therefore, it is crucial to find a solution that minimizes this thermal discomfort while still optimizing energy consumption during high-price periods. By implementing a more proactive approach that considers occupancy patterns, weather conditions, and utility tariffs, energy consumption during these high-price periods can be optimized. This would reduce energy costs and improve comfort levels for the occupants throughout the day.

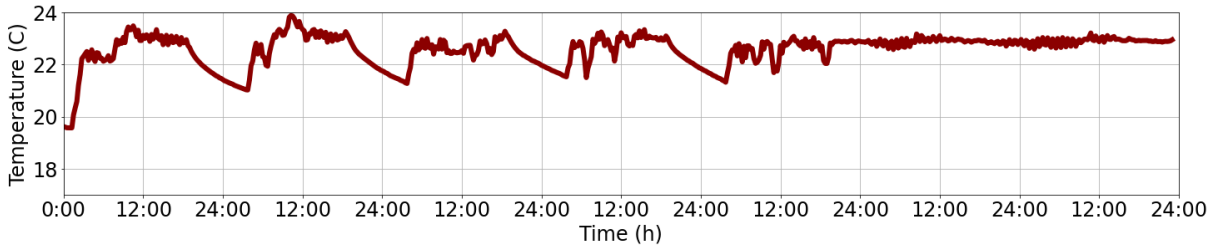

Figure 5-31: Indoor air temperature for control scenario 1 (reference case)

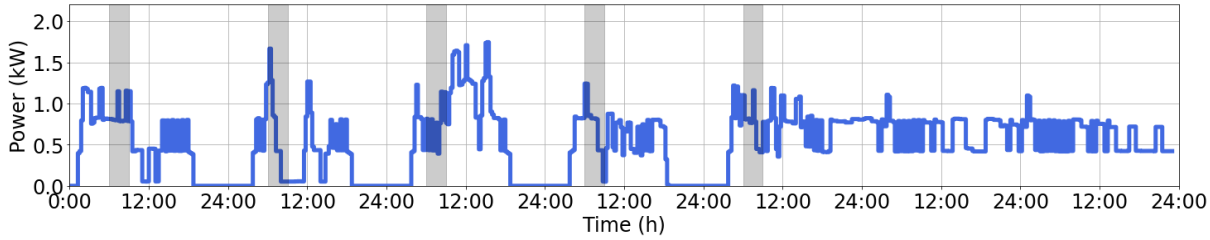

Figure 5-32: Power demand for control scenario 1 (reference case)

5.10.3 Flexibility scenario I (MPC without occupant):

Figure 5-33 shows the indoor temperature profile of the reference case and the flexible case without occupancy for each day of the experiment. During the reference case, the indoor temperature is almost constant during occupied hours, while in the flexible case, the indoor temperature drops by about 2 °C to reduce peak load and energy consumption during morning peak hours. This temperature reduction is achieved by leveraging the flexibility of the building through the implementation of MPC. By actively adjusting the indoor temperature based on the predicted demand, the building contributes to load shifting and reduces strain on the grid during peak hours. Figure 5-34 compares the power demand in the reference case and the flexible case with MPC. This figure shows that peak load and energy consumption are reduced during on-peak hours. To consider a case of a morning peak in a time-of-use tariff structure, the energy cost between 6:00 and 9:00 a.m. is increased by a factor of 15. To minimize the cost, the MPC controller followed the same 'strategy' for all days: preheating the zones before the high-price periods. The preheating can also be seen in Figure 5-34, which shows the power demand in a week without occupancy in the classrooms. Results show that the classrooms start being heated around 3:00 a.m. until the heating is completely shut off at 6 a.m. The heated space can free-float during the peak period and remain within its comfort boundaries. The heating system can be off during morning peak hours, resulting in a peak load reduction of up to 65%. This pre-heating and system staging strategy has emerged by minimizing operational costs. Compared to the uniform pricing case, this

case consumes 50% less than the BAU case. This pre-heating and system staging strategy reduces operational costs and ensures that the classrooms are comfortably heated during the peak period. Allowing the heated space to free-float within comfort limits optimizes energy usage and enhances energy flexibility.

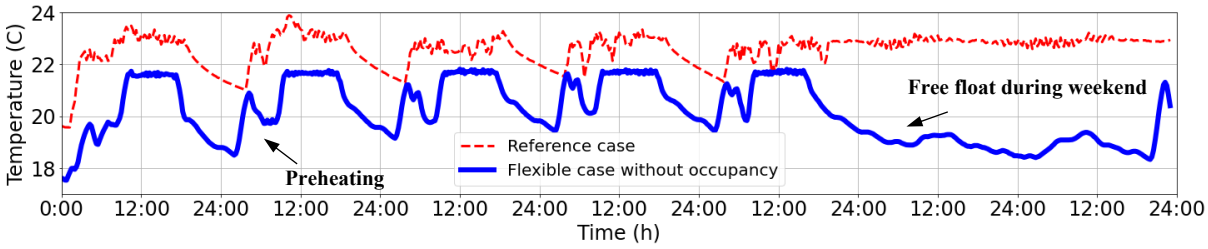

Figure 5-33: Indoor air temperature for the flexible case without occupancy compared to the reference case

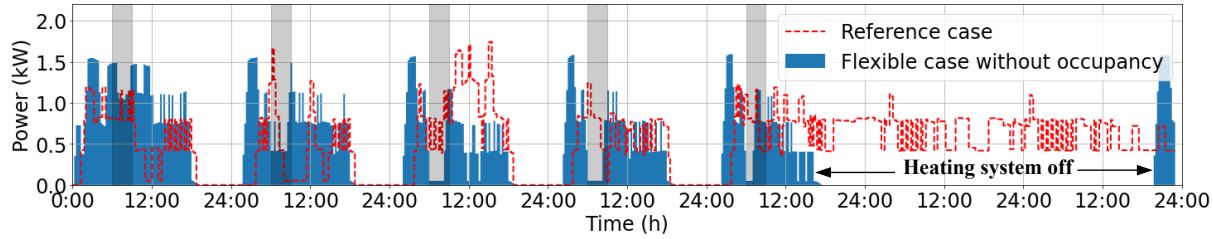

Figure 5-34: Power demand for the flexible case without occupancy compared to the reference case

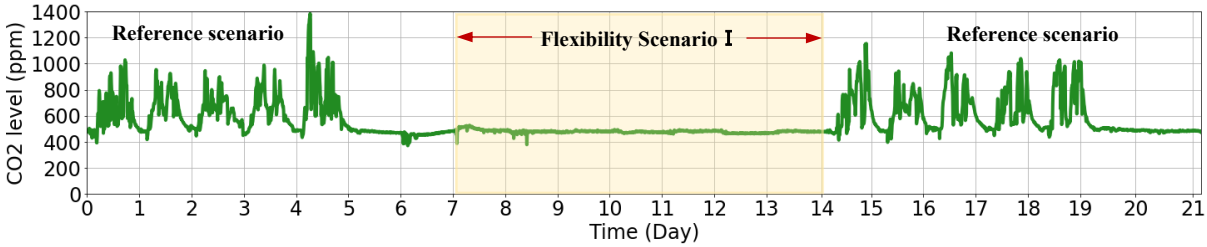

Figure 5-35: CO_2 level for the flexible case without occupancy compared to the reference case

5.10.4 Flexibility scenario II (MPC with Occupant):

In this case, the field test was conducted during normal operation of the school, when all students and teachers were in the classrooms. Each classroom has 25 students and a teacher equipped with occupancy detection and CO_2 sensors. MPC is usually designed to minimize energy-related terms (e.g., energy cost) while maintaining room temperatures within a comfort band. However, when an end-user (e.g., a teacher) overrides the setpoint schedule, the comfort band constraint in MPC should be updated to reflect personal preference. Otherwise, the end user's action will be overridden by the MPC again, resulting in conflicts with control actions and loss of credibility between the technology and the end user. Thus, during the experiment, access to override the

indoor temperature is restricted by obtaining permission from the school board. This restriction ensures that the experiment is conducted under controlled conditions and minimizes potential disruptions to the control strategies.

Figure 5-37 shows the power demand suddenly decreased near 12:30 because the students had lunchtime at noon and came back to the classrooms near 12:30, i.e., increasing internal heat gain. Another important observation is that the power demand with occupancy is 30% less compared with the unoccupied scenario. Also, energy consumption in flexibility scenario II is 45% lower compared to flexibility scenario 1. These results show the importance of considering occupancy in MPC applications.

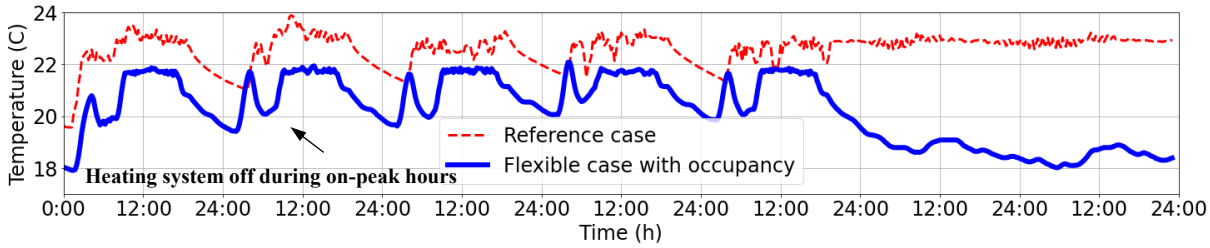

Figure 5-36: Indoor air temperature for the flexible case with occupancy compared to the reference case

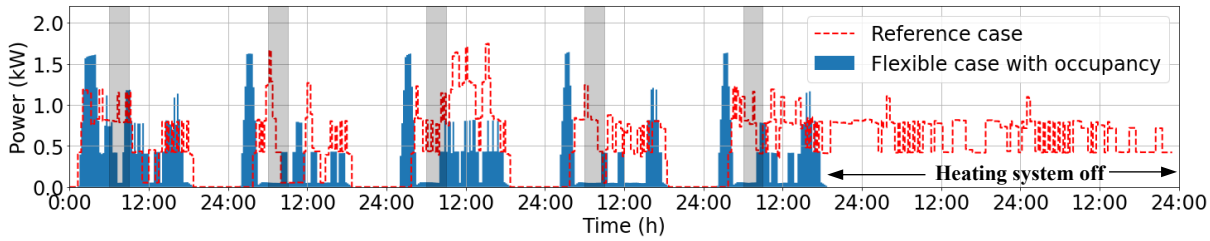

Figure 5-37: Power demand for the flexible case with occupancy compared to the reference case

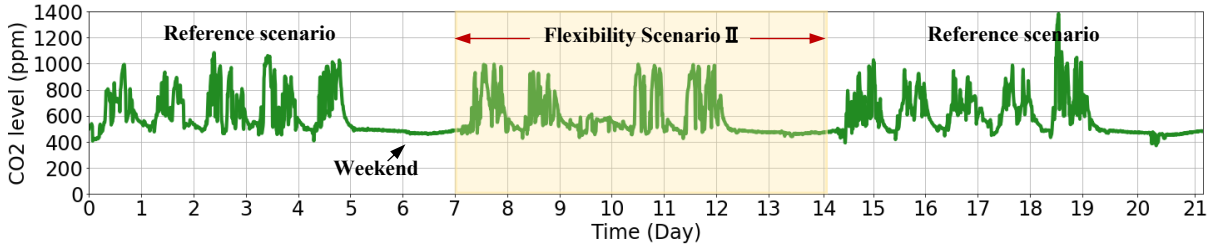

Figure 5-38: CO_2 level for the flexible case with occupancy compared to the reference case

Figure 5-39 shows the distribution of the power demand. Comparison of the power demand between the reference, MPC without occupancy, and MPC with occupancy days in a classroom during the experiment days. Another observation is that the median power demand in the unoccupied scenario is up to 90% higher than in the flexibility scenario with occupancy. The

distribution of power demand during flexibility scenarios is less than the reference scenario, indicating smoother power demand by using MPC in the control system. Another observation is that the MPC scenario with flexibility has the lowest median and quartile ranges, among others. This suggests that the use of MPC in the control system leads to smoother power demand but also helps in reducing overall energy consumption. Additionally, the lower quartile range indicates that the flexibility scenario with occupancy and MPC is more consistent in power demand, further highlighting its effectiveness in optimizing energy usage. Also, the significant energy savings achieved through the proposed approach demonstrate the effectiveness of considering occupancy in control methods. The MPC controller achieved an average reduction of 49% compared to the reference case by reducing energy consumption to the range of 10.1 kWh to 18.3 kWh without occupancy and 7.3 kWh to 12.6 kWh for the flexible scenario with occupancy. The use of MPC controllers significantly reduced energy usage during both occupied and unoccupied times. It's important to note that the total peak power demand is moved to off-peak times. If more customers switch to MPC controllers to cut expenses, this demand shift might put pressure on the grid. Smart grids can help efficiently manage the shifted demand by dynamically adjusting electricity prices based on real-time supply and demand conditions. This would incentivize customers to shift their energy usage to times when the grid is less strained, ensuring a more balanced distribution of power and preventing overload situations.

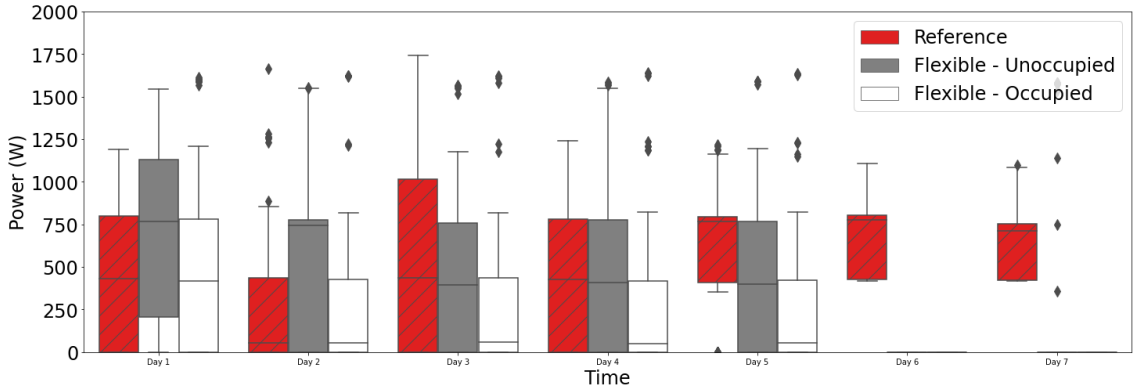

Figure 5-39: Comparison of the power demand between Baseline, MPC without occupancy, and MPC with occupancy days in a classroom.

5.10.5 Flexibility quantification

Figure 5-40 and Figure 5-41 show the BEFI per floor area for the days of the experiment in flexibility scenarios I and II. Results show that in scenario flexibility I, the building can provide up to 30 W/m^2 of energy flexibility during off-peak hours and up to 22 W/m^2 during on-peak hours,

meaning a 60% and 44% power demand reduction, respectively. However, in scenario flexibility II, the available energy flexibility increases to up to 38 W/m^2 (i.e., 76% power demand reduction), significantly improving grid energy flexibility. The increase in energy flexibility during scenario II is primarily attributed to the additional internal heat gains from occupancy. The BEFI is negative in the early morning when the school is preheating in anticipation of the morning peak. This effect is more intense in the case of the MPC controller without occupancy, which preheats significantly more and earlier than the MPC controllers with occupancy. The presence of occupancy in the MPC controllers allows for a more accurate heat demand prediction, resulting in more efficient preheating. Additionally, the MPC controllers without occupancy may experience higher energy consumption due to excessive preheating, leading to a larger negative BEFI. Additionally, including occupancy data enables the MPC controllers to better adapt to real-time changes in heat demand, further enhancing grid energy flexibility.

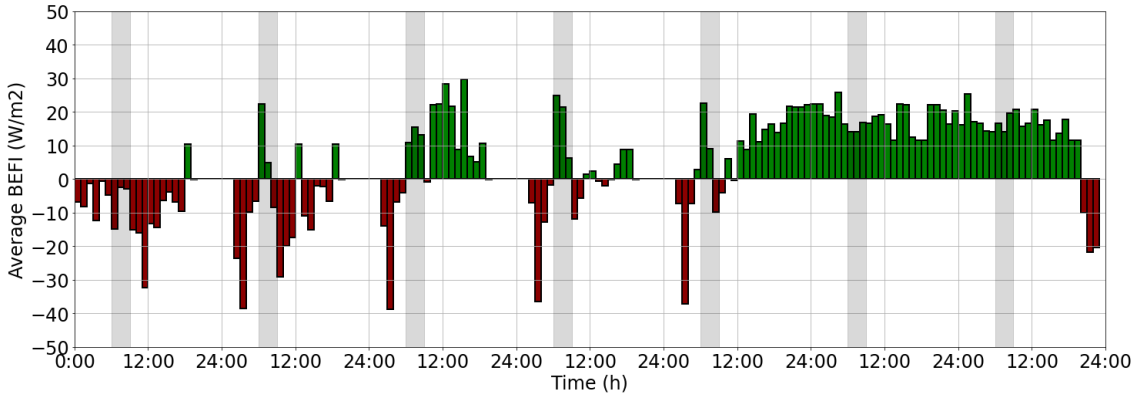

Figure 5-40: Average BEFI for the flexible case without occupancy by using MPC. The shaded areas correspond to high-price periods.

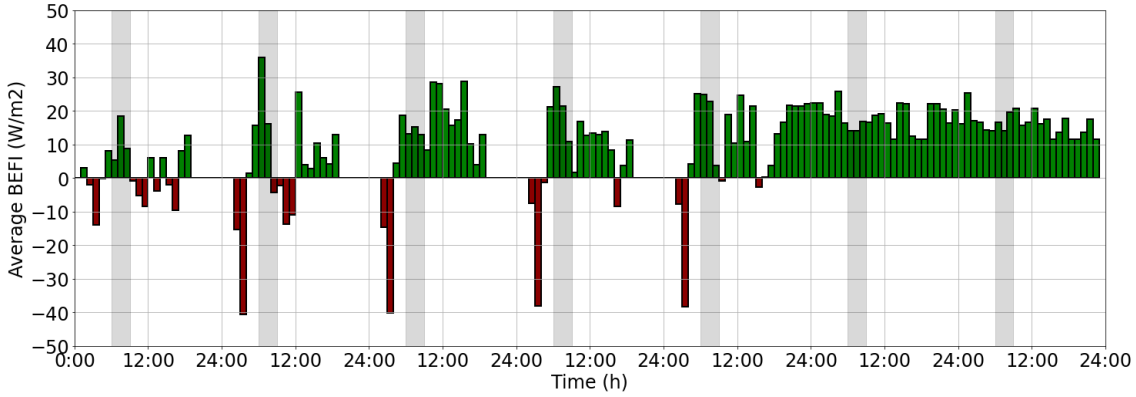

Figure 5-41: Average BEFI for the flexible case with occupancy by using MPC. The shaded areas correspond to high-price periods.

By effectively managing school energy usage, the MPC can contribute to overall grid stability and reliability. Additionally, the ability to tap into the demand response resources of schools can help support the integration of renewable energy sources into the grid, which is presented in chapter 6.

5.11 Conclusion

This chapter presented an MPC methodology based on data-driven grey-box models and weather data clustering in electrically heated school buildings. A *k*-means clustering algorithm was applied to the solar irradiance and outdoor temperature data. The weather data are clustered into several categories, representing different weather conditions (6 clusters representing two ambient temperature ranges and three solar radiation ranges). The clustering results were further implemented into data-driven grey-box models. A third-order resistance-capacitance network for zones with convection systems and a fourth-order model for radiant floor systems were developed and calibrated using measured data. The developed MPC framework was then implemented in an occupied school building near Montreal, Canada. Ten classrooms are investigated, with six using the MPC and four as reference cases. Results showed that using MPC energy flexibility of 32 W/m^2 of floor area for the zones with a convective heating system and 65 W/m^2 of floor area for the zones with radiant heating can be achieved during a demand response event. Moreover, using a three-hour ramp in setpoint temperature after peak hours could reduce the negative BEFI (rebound power) by 63%, which is essential for the stability and balance of the grid. According to the results, the school building can provide up to 100% energy flexibility (load shifting relative to reference) during on-peak hours while satisfying thermal comfort constraints. The proposed approach is scalable and can be transferable to other commercial and institutional buildings.

Moreover, three control scenarios have been implemented and compared: 1) Reference case with a reactive controller, 2) Flexible scenario using MPC in Unoccupied classrooms, and 3) Flexible scenario using MPC in occupied classrooms. Remarkable achievements of the MPC include an energy flexibility of 44% in unoccupied classrooms and an energy flexibility of 76 % with MPC in occupied classrooms. These results underscore the MPC's potential to harness the substantial demand response resources available in schools, simultaneously reducing utility costs and maintaining comfort.

Chapter 6: Model Predictive Control for Integration of air-base PV/T System[3]

6.1 Introduction

The increasing global demand for renewable energy sources has accelerated the development of photovoltaic/thermal (PV/T) systems, which simultaneously generate both electricity and heat (Dumoulin et al. 2021, Gaucher-Loksts et al. 2022, Aspetakis and Wang 2023). School buildings often have large roofs, and high energy demand due to ventilation air heating during the daytime and are thus an attractive type of building for integration of PV/T systems. To this purpose, system design, control strategies, and energy management must be developed to integrate these systems into existing buildings. Many new schools need to be built soon, and the old ones need renovation; in both cases, PV/T could be helpful as a renewable energy retrofit to enhance energy efficiency and flexibility. However, relatively few studies have been performed on integrating PV/T systems into school buildings and their optimized operation and grid interaction; it is thus essential to address this research gap to provide on-site electricity and heat generation in schools. Traditionally, on-site generation brings to mind batteries as the energy storage device; however, given the size of a school, such a storage system would be costly. For this reason, we are considering incorporating the thermal mass of the school for thermal energy storage and demand-side management strategies.

This chapter presents an MPC methodology for integration of air-based photovoltaic/thermal (PV/T) system in school buildings so that in addition to production of solar electricity they can be used to preheat fresh air for the classrooms during the heating season. The methodology is developed based on the case study school building. The PV/T system electrical capacity is set

[3] This work is based on a published refereed conference thesis and a peer-reviewed journal article: (a) Morovat, N., Athienitis, A. K., Candanedo, J. A. (2023), "Design of a model predictive control methodology for integration of retrofitted air-based PV/T system in school buildings", Journal of building performance simulation. (b) Morovat, N., Athienitis, A. K., Candanedo, J. A. (2023), "Model Predictive Control for Integration of PV/T system in School Buildings", The 18th Conference on Sustainable Development of Energy, Water and Environment Systems (SDEWES), Dubrovnik, Croatia, 24–29 September 2023.

equal to peak electricity demand in the classrooms. A data-driven RC thermal network model for the classrooms is calibrated with measured data, and a PV/T model as a renewable energy retrofit for energy efficiency and flexibility is developed. These models are integrated to apply MPC to the school building using the established dynamic tariffs for morning and evening peaks. Three scenarios are investigated and compared: 1) A reference case without a PV or air-based PV/T system, 2) Integration of a PV system and MPC strategies under a demand response scenario, and 3) Integration of an air-based PV/T system and MPC strategies under a demand response scenario.

6.1.1 PV/T system

Generally, solar energy technology can be categorized into two major classes: 1) PV modules that can convert a portion of available solar power directly into electrical energy, and 2) solar thermal systems that transform solar energy into thermal energy (Sari and Said 2021). In the latter, electric energy is required to drive a working fluid through the solar thermal installation. By combining photovoltaics with the solar thermal design as an integrated photovoltaic/thermal (PV/T) system it is possible to eliminate or significantly reduce purchased electric energy. When such systems are integrated into the building, they are called building-integrated photovoltaic/thermal (BIPV/T).

A typical commercial crystalline PV module converts about 15–20% of the incident solar energy into electricity, with the rest either reflected (5–10%) or primarily converted into heat (Abdelrazik et al. 2022). For a large installation of the PV/T system, such as institutional and commercial roofs, the peak PV temperature could reach up to 70 °C on hot sunny days (Sari and Said 2021). The rise in PV temperature not only reduces electricity generation but also reduces the lifespan of the module itself. Integrating the PV and solar thermal technology into a single component could reduce the overheating of PV and provide useful thermal energy for the building. This energy can be used for ventilation air pre-heating, water heating for direct floor heating systems, domestic hot water heating, and heat storage for later use.

PV/T systems could offer a variety of potential benefits for school buildings, including:

- **Reduced energy costs:** PV/T systems generate electricity and heat simultaneously, which can significantly reduce school energy costs (Tripanagnostopoulos et al. 2006, Delisle and Kummert 2016, Mehigan et al. 2018, Gaucher-Loksts et al. 2022, Zhao et al. 2023).

- **Improved indoor air quality:** PV/T systems can provide preheated fresh air and improve indoor air quality, especially during cold winter days when windows remain closed.
- **Reduced carbon footprint:** PV/T systems help reduce school buildings' carbon footprint, which is essential for mitigating climate change (Buker and Riffat 2015, Asaee et al. 2017, Maghrabie et al. 2021, Sohani et al. 2022).
- **Improved indoor comfort:** PV/T systems can be integrated into building envelopes, such as facades and roofs, providing shading, insulation, and ventilation, which can regulate indoor temperature and reduce mechanical heating and cooling (Yang et al. 2019, Yang et al. 2021, Zhao et al. 2022).

Moreover, PV/T systems can provide valuable educational opportunities for students, allowing them to learn about renewable energy technology and its application in real-world settings (Attoye et al. 2018, Abdelrazik et al. 2022).

One of the simplest and most efficient thermal applications for PV/T is preheating the supply air through the PV/T (Rounis et al. 2022). This reduces the thermal load on the HVAC system. Depending on the PV/T outlet temperature and the indoor setpoint temperature, the PV/T can either fully supply preheated ventilation air or boost the heating system's operation by providing air at a higher temperature. If the outlet air temperature exceeds the setpoint, it can be mixed with cool fresh air to reach the required temperature. If the heated air temperature is lower than the specified setpoint, it is further heated by heating coils supplied by a ground source heat pump. The solar-heated air can further heat by passing through a heat recovery ventilator (HRV). In the Varennes library, Canada's first institutional net-zero building, 110 m^2 of the south-facing roof is covered by a BIPV/T system. This library utilizes an on-site renewable system with a 110 kWp BIPV system where 15% of the PV arrays have heat recovery (Dermardiros and Scott Bucking PhD 2019). Preheated air is directed to the fresh air supply during the heating season and vented to the environment during summer. Oviedo-Cepeda et al. (2021) explored strategies for energy flexibility in a net-zero solar energy institutional building in Québec, Canada, using a machine learning algorithm and model predictive control. The study quantifies the impact of horizon selection on the building's flexibility during critical grid periods. It shows reductions in energy consumption ranging from 20% to 49% and 10% to 28% in morning and evening peak periods using MPC. Rounis et al. (2021) conducted a numerical investigation on the performance comparison between

single and multiple-inlet BIPV/T systems with an example of a large-scale installation on an office building. They developed a flow distribution model to compare thermal and electrical performance for cold winter and hot summer under varying wind conditions. Results indicated that the multiple-inlet BIPV/T system might have up to 1% higher electrical efficiency and up to 24% higher thermal efficiency, with lower and more uniform PV temperatures.

Gao et al. (2023) explored the use of MPC for building energy systems that combine batteries and PV in an office building in Japan. Results showed that the proposed framework improved battery safety by 81.6% and combined heat and power operation by 36.4%. It also enhanced off-grid operation optimization by 69% compared to conventional control while maintaining thermal comfort. Maurer et al. (2013) investigated the integration of transparent solar thermal collectors into high-rise building facades, aiming to balance renewable energy generation and visual transparency. They addressed modelling challenges using transient systems simulation (TRNSYS) and evaluated the overall performance, measuring non-renewable primary energy demand, while exploring possibilities for energy savings through building mass as thermal storage. Hao et al. (2022) studied the economic performance of integrating renewable energy and storage systems into the electrical grid. It compared ice storage and batteries, utilizing model predictive control and optimal sizing for a case study in commercial buildings with chillers and on-site PV systems. Ice storage had lower costs but limited load-shifting capability, while batteries offered consistent efficiency with higher initial costs and a shorter lifespan.

6.1.2 PV electricity self-consumption in school buildings

School operational activities generally take place from early morning to late afternoon when solar electricity and heat generation are available. Hence, school buildings are excellent candidates for the high self-consumption of on-site electricity produced by PV. Self-consumption is “the fraction of photovoltaic-generated electricity consumed by the producer on-site or by associates directly contracted to the producer” (Villar et al. 2017). Excess electricity can be injected into the grid or stored to be consumed when needed. A 100% self-consumption rate means no photovoltaic generation is fed to the grid. PV power self-consumption has manifold benefits, such as enhancing grid stability with less fluctuating loads, reducing consumers’ energy costs through self-sufficiency, and enabling the downsizing of traditional power plants in the long term to facilitate renewable energy integration. PV self-consumption can be improved by 1) shifting the generation

by using batteries (Merei et al. 2016, Yu 2021) and 2) shifting the load by controlling demand and thermal energy storage (Manojkumar et al. 2021, Koskela and Järventausta 2023, Zhan et al. 2023).

This study presents an MPC methodology for integrating PV/T systems as a renewable energy retrofit to enhance energy efficiency and flexibility in school buildings. The methodology is developed based on a case study for an archetype fully-electric school building in Québec, Canada. The PV/T system electrical capacity is set equal to peak electricity demand in the classrooms. A data-driven resistance-capacitance (RC) thermal network model for the classrooms is calibrated with measured data, and a PV/T model is developed. These models are integrated to apply MPC to the school building using the established dynamic tariffs for morning and evening peaks. Energy performance is determined during a typical heating season in Montreal, Canada. This methodology is scalable and can be transferable to other institutional buildings.

The outline of this chapter is structured as follows: Section 2 explains the methods used for model development, MPC implementation, and energy flexibility quantification; Section 3 describes the case study school; Section 4 presents and discusses the results; and Section 5 provides the conclusion and future work.

6.2 Methodology

Figure 6-1 presents the methodology in this chapter, which consists of a) a resistance-capacitance (RC) thermal network model for the classrooms is developed and calibrated with measured data, b) a model for PV and a model for PV/T system is established, c) an MPC methodology for obtaining optimal control strategies is developed, d) Optimal control strategies for different scenarios (i.e., reference case, with PV and with PV/T) are obtained, e) Building load for different scenarios is calculated, and f) energy flexibility is quantified.

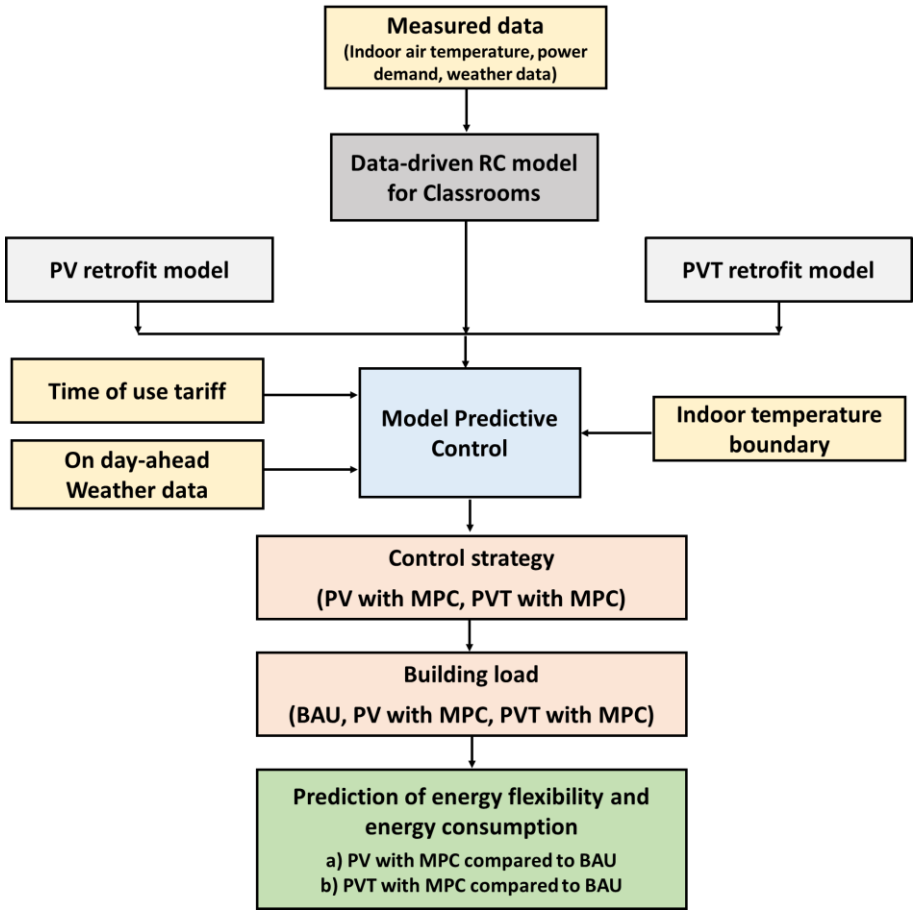

Figure 6-1: Methodology flowchart.

Three scenarios are investigated and compared: 1) A reference case without a PV or air-based PV/T system, 2) Integration of a PV system and MPC strategies under a demand response scenario, and 3) Integration of an air-based PV/T system and MPC strategies under a demand response scenario. The schematics of each configuration studied are shown in Figure 6-2.

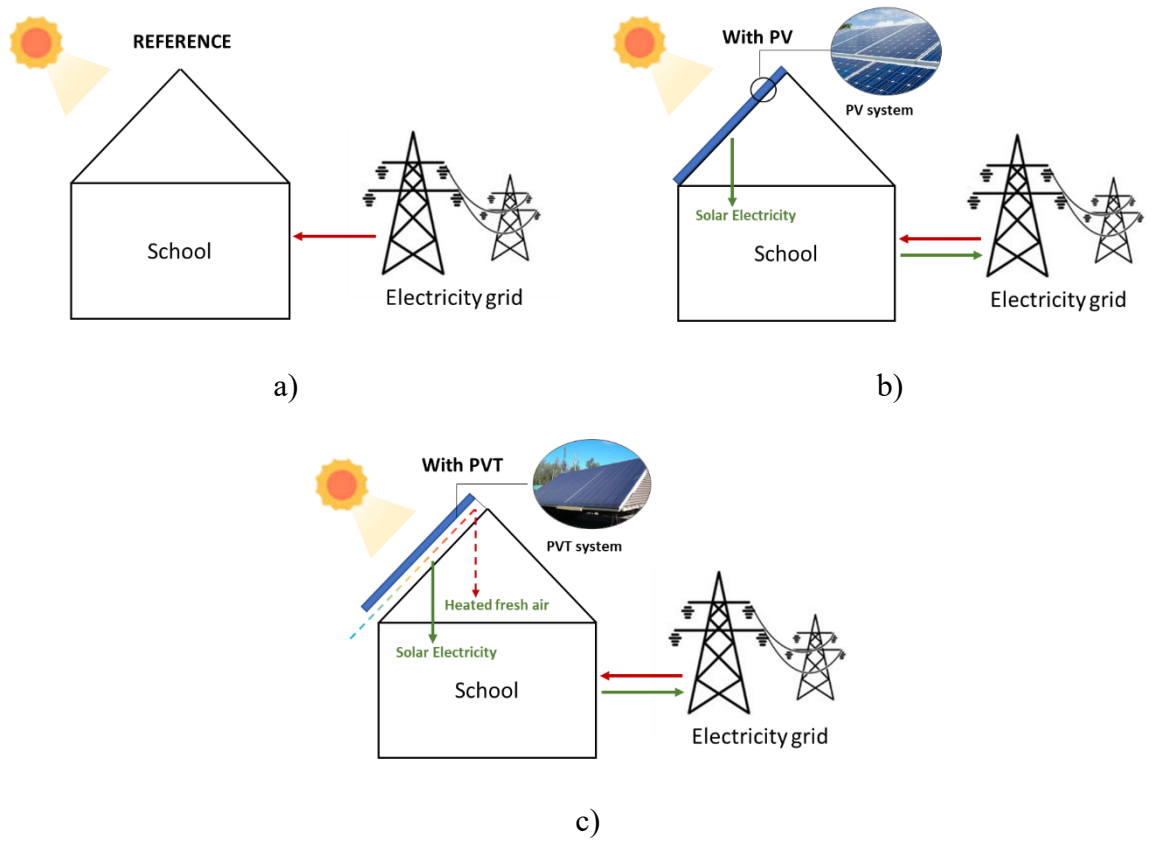

Figure 6-2: Schematic of a) reference case, b) with PV retrofit, and c) with PV/T retrofit system.

Configuration 1 serves as a baseline for comparison in the absence of solar electricity generation and solar heat, providing a reference point for the study. In Configuration 2, we explore integrating a PV system using MPC methodology. The primary objective is to enhance the energy flexibility and efficiency potential associated with MPC when integrating PV systems. This involves prioritizing on-site PV electricity consumption within the building, with any additional power demand being supplemented by the grid. Configuration 3 includes the option of reducing the heating load of the building with instantaneous heat and electricity production from PV/T, along with MPC as a controller. The ideal operation of this configuration is to utilize and transfer the solar-heated air from the PV/T cavity on a sunny day to preheat the fresh air to the building.

Figure 6-3 presents a schematic of the PV/T system concept for the roof of the school. As shown in this figure, the air is mechanically driven by variable-speed fans through a 70 mm-high air channel, used as preheated ventilation air during the heating season, and discarded in summer.

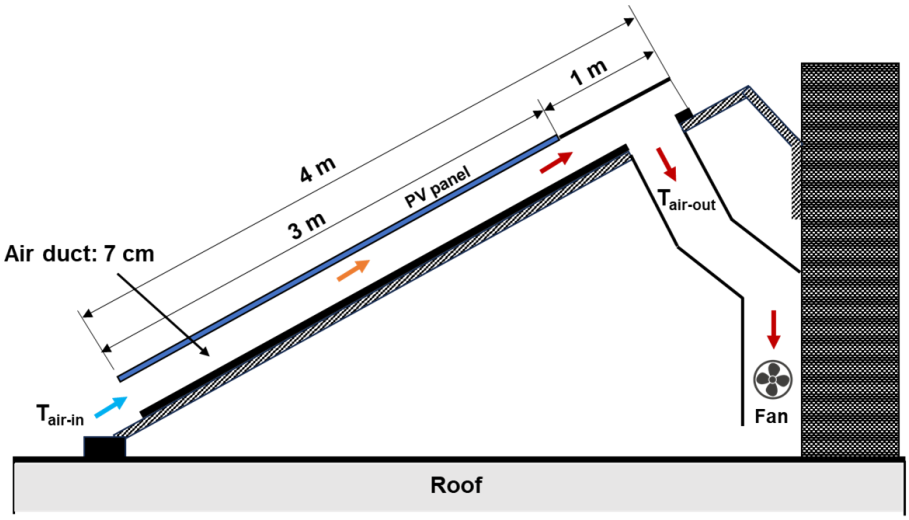

Figure 6-3: Schematic of the PV/T retrofit system concept for the roof of the school

The following section details the mathematical models of each key component developed in the Python programming language.

6.2.1 Classrooms thermal model

Data-driven grey-box models ensure both physical insight and the reliability of measured data (Candanedo et al. 2013, Arroyo et al. 2020, Li et al. 2021). Literature review indicates that grey-box models are suitable for control applications and demand-side management in smart grids (Gouda et al. 2002, Bacher and Madsen 2011, Candanedo et al. 2013, Reynders et al. 2014). The model structure is derived from low-order RC thermal networks analogous to electric circuits to describe the thermal dynamics of building systems. The unknown parameters are then estimated using optimization techniques. Figure 6-4 presents a third-order RC thermal network model for classrooms.

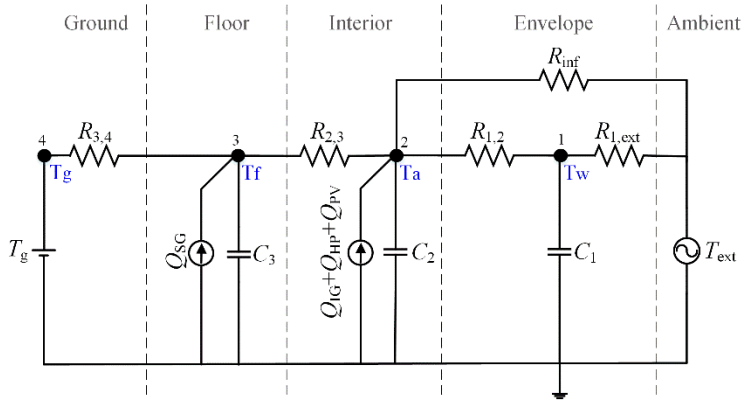

Figure 6-4: RC thermal network for a typical classroom

The zone envelope capacitance in this model is represented by C_1, the air capacitance by C_2, and the floor capacitance by C_3. Thermal resistance $R_{1,ext}$ describes the resistance between the envelope and the exterior air, $R_{1,2}$ describes the resistance between the envelope and the interior air, R_{inf} represents the infiltration between the interior air and the outside air, $R_{2,3}$ refers to the resistance between the interior air and the floor, $R_{3,4}$ refers to the floor resistances. Node 1 is the wall temperature node, node 2 is the indoor air temperature node, and node 3 *is* the floor temperature node. Q_{IG} is the internal heat gain added to the space from occupants, equipment and lighting, Q_{HP} is the heat provided by heat pump, Q_{PV} is the heat generated by PV/T, and Q_{SG} is heat from solar radiation. α_1 is the solar absorption coefficient for the envelope, and α_3 is the solar absorption coefficient for the floor. Equations 6-1 to 6-3 present the energy balance differential equations for each node:

$$C_1 \frac{dT_w}{dt} = \frac{(T_{\text{ext}} - T_w)}{R_{1,\text{ext}}} + \frac{(T_a - T_w)}{R_{1,2}} + \alpha_1 \cdot Q_{\text{SG}} \qquad 6\text{-}1$$

$$C_2 \frac{dT_a}{dt} = \frac{(T_{out} - T_a)}{R_{\text{inf}}} + \frac{(T_w - T_a)}{R_{1,2}} + \frac{(T_f - T_a)}{R_{2,3}} + Q_{\text{IG}} + Q_{\text{HP}} + Q_{\text{PV}} \qquad 6\text{-}2$$

$$C_3 \frac{dT_f}{dt} = \frac{(T_a - T_f)}{R_{2,3}} + \frac{(T_g - T_f)}{R_{3,4}} + \alpha_3 \cdot Q_{SG} \qquad 6\text{-}3$$

Equations 6-4 to 6-6 are obtained by discretizing the above equations using an explicit finite difference scheme. In these equations, the current and the next time step are represented by the variables i and i+1, respectively, and the simulation's time interval is denoted by Δt.

$$T_w^{i+1} = \frac{\Delta t}{C_1}\left(\frac{(T_{\text{ext}} - T_w)}{R_{1,\text{ext}}} + \frac{(T_a - T_w)}{R_{1,2}} + \alpha_1 \cdot Q_{\text{SG}}\right) + T_w^i \quad 6\text{-}4$$

$$T_a^{i+1} = \frac{\Delta t}{C_2}\left(\frac{(T_{out} - T_a)}{R_{\text{inf}}} + \frac{(T_w - T_a)}{R_{1,2}} + \frac{(T_f - T_a)}{R_{2,3}} + Q_{\text{IG}} + Q_{\text{HP}} + Q_{\text{PV}}\right) + T_a^i \quad 6\text{-}5$$

$$T_f^{i+1} = \frac{\Delta t}{C_3}\left(\frac{(T_a - T_f)}{R_{2,3}} + \frac{(T_g - T_f)}{R_{3,4}} + \alpha_3 \cdot Q_{SG}\right) + T_f^i \quad 6\text{-}6$$

The performance of the model is assessed by comparing model predictions with BAS measurements. The optimization strategy utilized in this study aims to identify equivalent parameters for RC circuits by minimizing the coefficient of variation of the root mean square error (CV-RMSE), shown in Equation (6-7):

$$CV(RMSE)(\%) = \frac{\sqrt{\sum_{i=1}^{n}(T^i - \hat{T}^i)/n}}{\bar{T}} \times 100 \quad 6\text{-}7$$

Where n is the total number of data points T^i is the measured temperature, $\hat{T}^i$ is the predicted temperature in time step I, and $\bar{T}$ represents the average of all measurements. As per ASHRAE Guideline 14, which addresses the Measurement of Energy and Demand Savings, the model is required to maintain a CV(RMSE) of no more than 30% in relation to hourly calibration (measured) data (Haberl et al. 2005).

The measured data from February 1st to February 15th is used for model calibration (Figure 6-5). The dataset is divided into two datasets: 60% of the dataset was used for training, while 40% was kept for validation purposes.

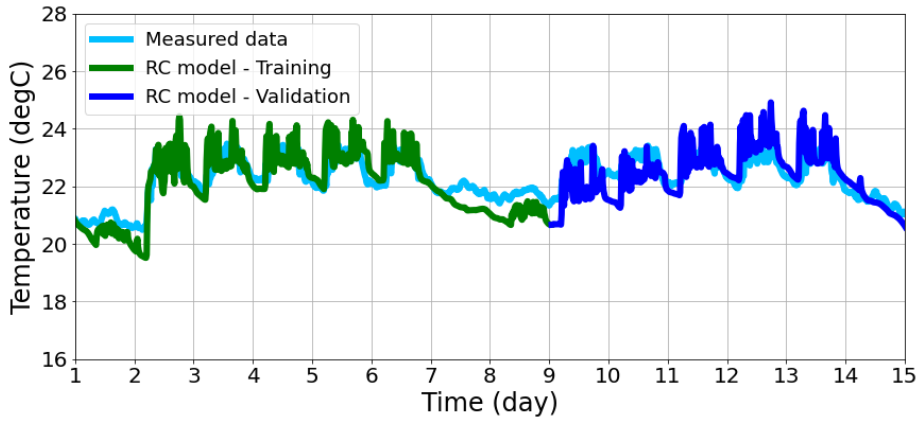

Figure 6-5: Calibration of thermal network model with measured data

The calibration result complies with ASHRAE Guideline 14 with an hourly CV-RMSE of 8%. It should be mentioned that additional inputs are needed for higher-order models, like heat flux measurements, which are typically not measured in buildings. Thus, it is not possible to guarantee the identity of higher-order models.

6.2.2 PV/T model

Typically, air-based PV/T systems consist of the PV modules and the air channel underneath them. In this air channel, the air circulates and extracts heat from the PV modules and the back layer, which is part of the building envelope (exterior wall or roof with insulation). A thermal network model is commonly used for analyzing solar thermal systems. Figure 6-6 illustrates a thermal network schematic for the PV/T system studied in this thesis. The PV panel, insulation, air channel, and ambient surroundings of the PV/T system make up a network in which their interactions achieve a balanced steady state in the experiment.

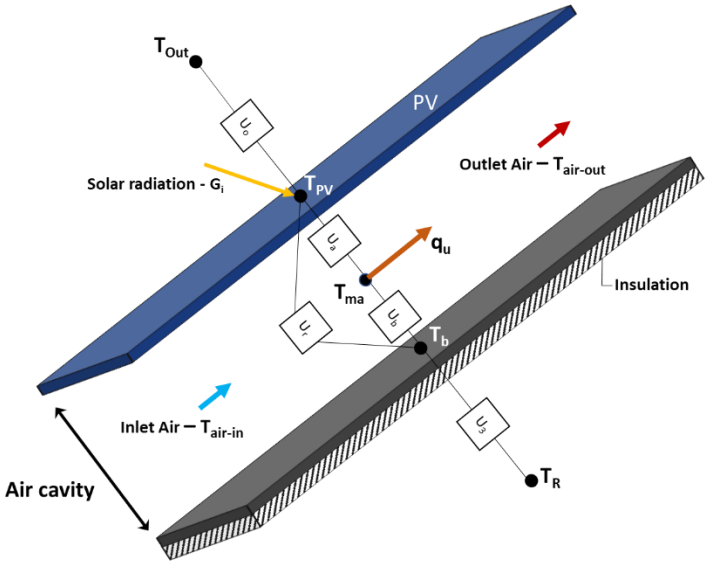

Figure 6-6: Thermal network for PV/T models

Where:

- T_o: the ambient temperature (°C).
- T_{PV}: the PV temperature (°C).
- T_{ma}: the average air temperature inside the air channel (°C).
- T_b: the insulation temperature (°C).
- T_R: the temperature of the adjacent room (°C).
- U_a, U_b: the convective heat transfer coefficients from the PV and the insulation surface to the flowing air (W/m^2·°C).
- U_r: the radiative heat transfer between the PV and the insulation surfaces (W/m^2·°C).
- q_u: Heat transfer inside the air channel
- U_o: the outside convective heat transfer coefficients.

At each node, the temperature is calculated using the following explicit finite difference approach:

$$T_i^{t+1} = \frac{\Delta t}{C_i}\left[\sum_j U_{ij}^t (T_j^t - T_i^t) + \dot{Q}_i^t\right] + T_i^t \qquad 6\text{-}8$$

The electrical efficiency of PV modules is related to its temperature and can be determined from Equation (6-9):

$$\eta_{\mathrm{PV}} = \eta_{\mathrm{STC}} + \left(1 - \beta_{\mathrm{PV}} \cdot (T_{\mathrm{PV}} - T_{\mathrm{STC}})\right) \quad 6\text{-}9$$

Where:

- η_{STC}: the PV module electrical coefficient under standard testing conditions (%)
- β_{PV}: the PV module temperature coefficient (usually between 0.004 – 0.006)
- T_{PV}: the measured PV module cell temperature (°C)
- T_{STC}: the PV module cell temperature at standard test conditions (25 °C)

The electrical efficiency of the module decreases as its temperature increases over 25 °C; this effect highlights the importance of efficiently cooling the PVs. The absorbed solar radiation and the electric production can be calculated as:

$$S_{Total} = \alpha_{PV} \cdot A_{PV} \cdot G \quad 6\text{-}10$$

$$P_{Electricity} = \eta_{\mathrm{PV}} \cdot A_{PV} \cdot G_{incident} \quad 6\text{-}11$$

The equations corresponding to a representative control volume in the state-space model are shown below. Equations 6-12 correspond to energy balances at the air node. Equations 6-13 shows the PV surface temperature, Equation 6-14 shows thermal energy absorbed by the PV and Equation 6-15 presents the temperature in the wall node. Equation 6-16 presents the recovered heat by PV/T and Equation 6-17 calculates outlet temperature from PV/T arrays.

$$T_{\mathrm{ma}} = \frac{1}{\Delta x} \cdot \int_0^{\Delta x} \left[\frac{h_{c_{PV}} \cdot T_{PV_b} + h_{c_{ins}} \cdot T_{ins\_t}}{h_{c_{PV}} + h_{c_{ins}}} + \left(T_{inlet} - \frac{h_{c_{PV}} \cdot T_{PV_b} + h_{c_{ins}} \cdot T_{ins\_t}}{h_{c_{PV}} + h_{c_{ins}}} \right) \cdot e^{-\frac{W_{channel} \cdot \left(h_{c_{PV}} + h_{c_{ins}}\right)}{\dot{m} \cdot c_{p_{air}}}} \right] \quad 6\text{-}12$$

$$T_{PV} = \frac{U_o T_0 + U_a T_{ma} + U_r T_b + S_{total} - P_{electricity}}{U_o + U_r + U_r} \quad 6\text{-}13$$

$$P_{Thermal} = \eta_{\mathrm{PV}} \cdot A_{PV} \cdot G_{incident} - \eta_{\mathrm{PV}} \cdot A_{PV} \cdot PF \cdot G_{incident} \quad 6\text{-}14$$

$$T_b = \frac{U_r T_{PV} + U_b T_{ma} + U_3 T_r}{U_r + U_b + U_3} \quad \text{6-15}$$

$$q_{Air} = h_{c_{PV}} \cdot \left(T_{PV_b} - T_{\mathrm{ma}}\right) + h_{c_{ins}} \cdot \left(T_{ins_t} - T_{\mathrm{ma}}\right) \quad \text{6-16}$$

$$T_{\mathrm{outlet}} = T_{inlet} + \frac{q_{air}}{\dot{m} \cdot c_{\mathrm{p_{air}}}} \quad \text{6-17}$$

Following the steady-state approach, resolution is achieved through iterative processes. Assumptions are made regarding the PV and the back temperatures and then substituted. Python programming language is used to implement the iterative process, and temperatures are reached to an average convergence of ±0.3 °C. After installation of the PV/T system, a data-driven grey-box model could be developed based on measured data.

6.2.3 MPC development for integration of PV/T

MPC is a control strategy that uses a mathematical model of the system to predict its behavior and optimize its performance. The MPC algorithm generates a control signal that considers the system's current state and predicted behavior over a future time horizon. Figure 6-7 shows the schematic of the PV/T retrofit system in this study. The power imported from the electric grid and PV/T electricity and heat generation are input to the MPC algorithm. The PV/T system provides preheated fresh air for classrooms through a heat recovery ventilator (HRV) system. The thermal efficiency of the HRV system is 80 %. The HRV system exchanges heat between the delivered heat from PV/T and the return air from the classrooms to minimize heat loss when the output temperature of the PV/T system ($T_{\mathrm{PV/T}}$) is lower than the classroom's return air temperature (T_{RA}). The MPC algorithm minimizes the objective function and determines optimal control strategies based on the weather forecast and time of use tariff. The school's local heat pumps operate using optimal control strategies derived from the MPC routine.

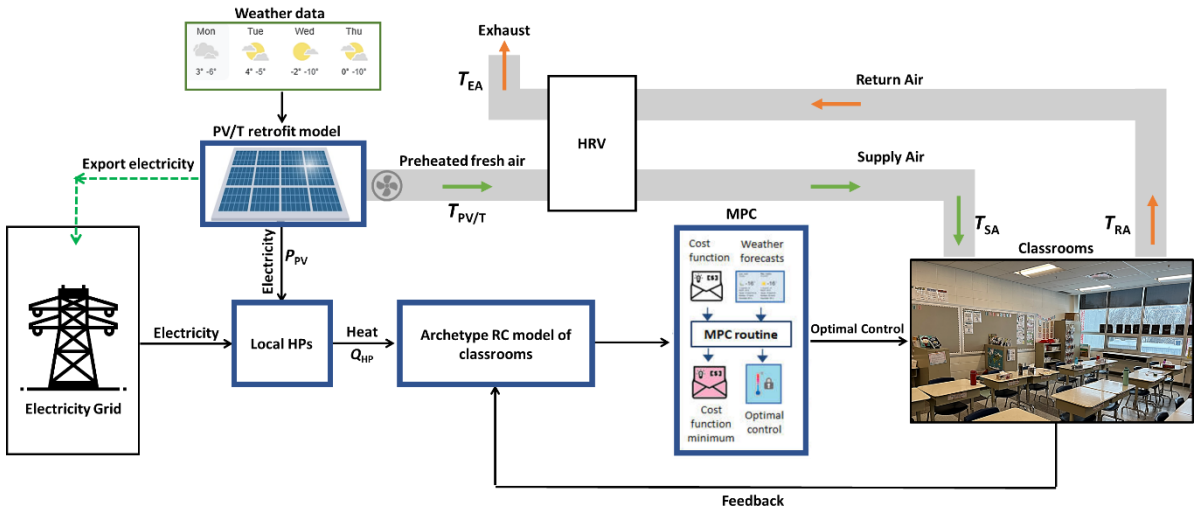

Figure 6-7: Conceptual representation of MPC employed

The overall MPC formulation is presented in Equation 18 (Drgoňa et al. 2020):

$$\min_{u^0,\ldots,u^{N-1}} \sum_{i=1}^{N} l(x^i, u^i, w^i)$$

Subject to $x^{i+1} = f(x^i, u^i, w^i) = Ax^i + Bu^i + Ew^i$ System dynamics

6-18

$$h(x^i, u^i, w^i) = 0$$

$$g((x^i, u^i, w^i) \geq 0$$

$$x^1 = x, \qquad \text{Current state}$$

Where x is system variables, u indicates controllable variables, w is uncontrollable inputs such as weather, l is the cost function, h is equality constraints, and g presents inequality constraints (boundary conditions).

The indoor air temperature (T_{in}) is chosen as the state function, and the heating power of the heat pump (P) is selected as the control variable. A cost function incorporating the utility rate structure is implemented, and its result is compared to the typical manual control currently in operation. The minimization problem is performed in Python using routine CVXPy. Equation (19) presents the objective function, where the objective is to reduce the peak load when the energy cost varies over the day, with higher prices during peak hours in the morning (from 6:00 to 9:00) and evening (from 16:00 to 20:00), as shown in Table 1.

$$\min_{P} J$$

$$where\ J = \left(\sum_{i=1}^{N-1}(P_i - P_{PV})\Delta t\right) \cdot (Cost_i) \qquad 6\text{-}19$$

$$\text{Subject to} \quad T^{i+1} = AT^i + Bu^i + Ew^i, i \in \{0,1,\dots,N-1\}$$

$$\underline{T} \le T_{in} \le \overline{T}$$

$$0 \le P \le P_{max}$$

where P_i is the total power demand (kW) and P_{PV} is the electricity generation of the PV/T system (kW). N is the number of time steps across the prediction horizon PH, and Δt is the time step. T_{in} is indoor temperature, $\overline{T}$ is the upper temperature bound and $\underline{T}$ is the lower temperature bound, shown in Figure 6-8. The space heating demand (P) is limited by the maximum capacity of the heating equipment (P_{max}).

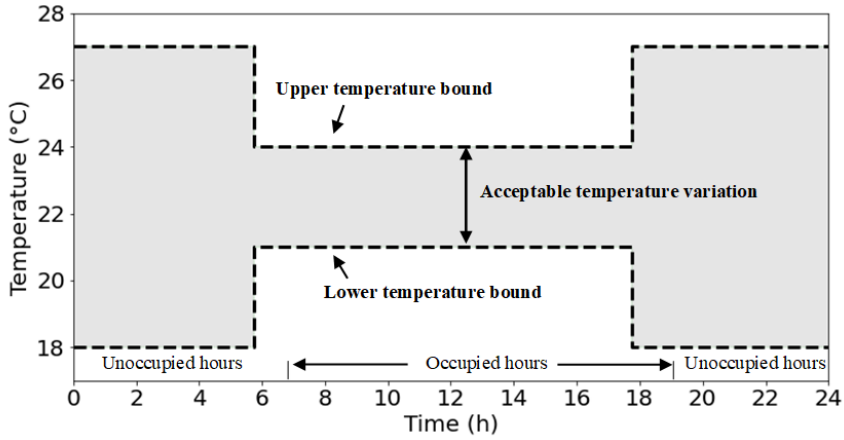

Figure 6-8: Allowable temperature variation

The indoor zone temperature is constrained by a lower bound, which is 18 °C at night and 21°C during the day, and an upper bound, which is 27 °C at night and 24 °C during the day, in order to maintain a level of thermal comfort for the zone occupants. The upper bound generates the desired setpoint target to minimize the energy cost through load shifting by considering future weather and utility price signals. A lower bound constrains the minimum indoor temperature to maintain thermal comfort in the zone.

The developed MPC framework performs optimization starting at midnight with a 24-hour prediction horizon and timestep of 15 minutes. The rest of the constraints force the MPC formulation to use the building model and restrict the heating output to the installed capacity of each zone. The prediction horizon of 24 hours allows for a comprehensive forecast of future electricity prices and heating requirements. The optimization results in optimum heating output values for each water-to-air heat pump and the equivalent zone temperatures.

Table 11: Utility rate for medium commercial buildings in Québec, Canada (Hydro Québec 2022)

Rate flex M- During winter (1 Dec. – 31 Mar)	
Demand charge	$15.16/kW
Consumption outside peak hours	3.29¢/kWh
Consumption during peak hours: Morning (6:00 to 9:00) and Evening (16:00 to 20:00)	51.97¢/kWh

6.2.4 Energy flexibility

Dynamic energy flexibility is defined as the capability of a building to reduce or increase its electricity demand for a period of time needed for the grid. Energy flexibility has been calculated based on Equation 20. This equation calculates the building energy flexibility index (BEFI) under the implementation of the flexibility strategy and the reference as-usual profile. In this equation, the P_{ref} refers to the power demand (i.e., HVAC loads) under business-as-usual operation, which is the current operation of the school. The P_{flex} represents the HVAC power demand under the MPC controller, considered the flexible case, and the Dt is the duration of the flexibility event needed by the grid. We presented the details of BEFI in (Athienitis et al. 2020). The calculation of the BEFI as a percentage compares the peak power under the flexible case and the reference as usual profile (Equation 21). The energy flexibility is reflected in the consumption of PV generation, quantified by self-consumption, which is a fraction of the total PV power generation consumed by the building (Equation 22).

$$\overline{BEFI}(t, Dt) = \frac{\int_t^{t+Dt} P_{\text{Ref}} dt - \int_t^{t+Dt} P_{\text{Flex}} dt}{Dt} \qquad 6\text{-}20$$

$$BEFI\% = \frac{\overline{BEFI}(t, Dt)}{P_{\text{Ref}}} \times 100 \quad \text{6-21}$$

$$SC\% = \frac{P_{self\ consumption}}{P_{PV\ generation}} \quad \text{6-22}$$

6.3 Case study

The case study is a two-story fully-electric school building school (Figure 6-9) located in Sainte-Marthe-sur-le-Lac (near Montreal), Québec, Canada. There are 23 classrooms with dimensions of 9.1 m by 7.6 m (1590 m^2 total). Each classroom is equipped with a water-to-air HP and a dedicated thermostat, and the whole system is closely monitored with sensors. T-type thermocouples are used with an accuracy of 0.2 °C for a temperature range of 0 to 70 °C. Thermostat and power meter data were collected at 15-minute intervals in CopperCube, an on-site trend log archiver, through the BACnet network.

Figure 6-9: Horizon-du-Lac school building

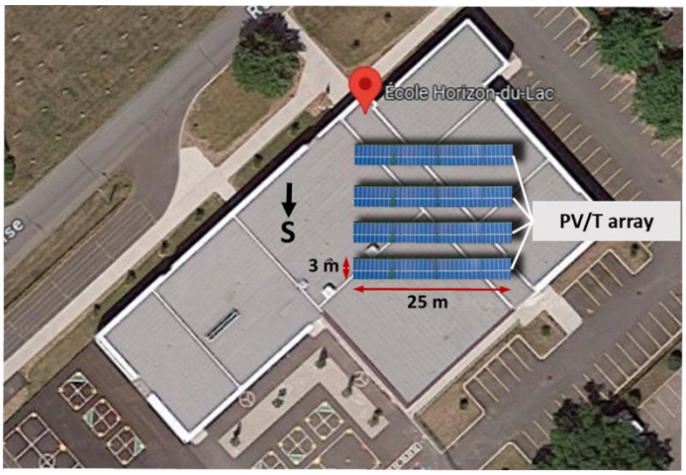

Figure 6-10: Horizon-du-Lac school's roof with PV/T retrofit (Adapted from Google Maps©)

The maximum capacity of the water to air HPs installed in the classrooms is 38 kW. A 38 kW PV system is considered as retrofit to cover this load. The PV/T system is 3 m long and 25 m wide in four arrays (300 m^2 total), shown in Figure 6-10, with a PV efficiency of 18%. The total roof area of the school is 2596 m^2, which provides enough space for the installation of the PV/T system. This size of PV panel could generate up to 54 kWp DC electricity. Considering a load ratio of 1.25 and an efficiency of 0.9 for the invertor, this PV system could provide around 38kW of electricity for the school.

6.4 Results

Weather data for typical cold days in the winter is selected as the simulation scenario since the electrical power demand tends to peak under these conditions. Figure 6-11 presents the outdoor temperature and global horizontal irradiance (GHI). The *Simulation Energetique Des Batiments* (SIMEB) weather data service provided measurements of ambient temperature, relative humidity, wind speed and direction, and GHI for the selected location.

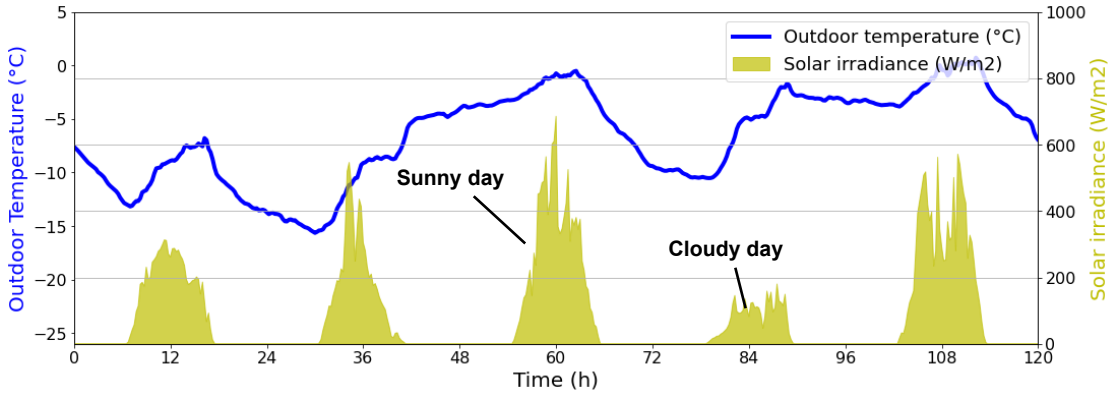

Figure 6-11: Montreal weather data – outdoor temperature and GHI in typical winter days

The consideration of providing energy flexibility to the grid in the renewable energy retrofit of a building can led to a range of benefits. Buildings that are retrofitted for energy flexibility are more likely to be efficient, using fewer resources to meet the same needs. They are also more likely to be resilient in changing energy demands, as they can more easily adapt to shifting energy use. This flexibility is also beneficial for building owners, as it can reduce their energy bills over time.

Figure 6-12 presents the total power demand of the classrooms and PV electricity generation for five working days in winter in a business-as-usual (BAU) case. As shown in Figure 6-12, the maximum power demand is 38 kW during peak hours. Also, the green area represents the PV electricity self-consumption, and the yellow represents the PV surplus electricity generation, which can be stored or used in the rest of the building or exported to the grid. A 100% self-consumption rate means no photovoltaic generation is fed to the grid. As seen in this Figure, PV generation could cover the power demand for sunny days and export surplus electricity to the grid. During cloudy days, PV electricity generation covers part of the power demand, which can be very useful to enhance the energy flexibility of the building. Therefore, an appropriate control strategy is needed to shift electricity demand and maximize PV electricity self-consumption in the school building.

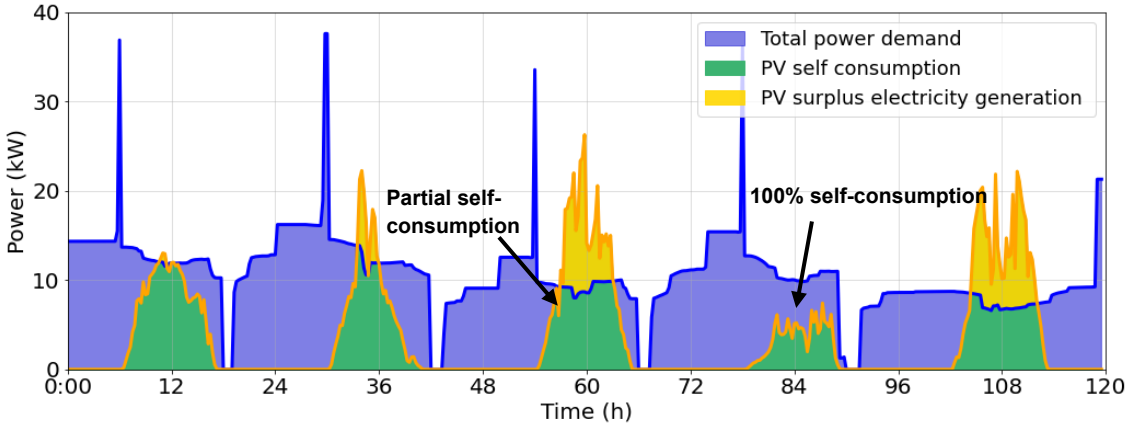

Figure 6-12: Power demand and power generation in the school building

6.4.1 Integration of PV system

In Québec, Canada, winter's morning and evening peaks significantly strain the electrical grid to provide electric power during extremely cold weather (Hydro-Québec, 2020). Integrating renewable energy into power grids creates challenges in balancing fluctuations and ensuring reliable grid operations. Therefore, it is imperative to provide predictive control strategies in school buildings to reduce and/or shift peak electricity demand.

Three control scenarios for cold cloudy and cold sunny days in winter are investigated. The effect of PV electricity production on the net power demand has been studied in all scenarios. In MPC scenarios, the objective is to minimize the peak load during peak hours in the morning (from 6:00 to 9:00) and evening (from 16:00 to 20:00). The control scenarios presented are as follows:

Case 1) Reference case (Business as a usual case)

Case 2) MPC with rate flex M and morning event from the grid

Case 3) MPC with rate flex M and morning and evening events from the grid

a) Case 1. Reference case (Business as usual case)

This control scenario is the current operation of the classrooms, which is considered the reference case. In this scenario, as shown in Figure 6-13, the peak load is 34 kW on sunny days and 38 kW on cloudy day and occurs during the morning peak hours (6:00 to 9:00 am). The PV system could produce a maximum of 28 kW on sunny days and 5 kW on a cloudy day, which peaks at noon. Results show that for the BAU scenario on a sunny day, by using a PV system, the

building could export/store up to 18 kW of electricity during sunny days, while it cannot export/store any electricity during cold days. In this scenario, the peak power occurs when there is no PV production. Thus, to improve the energy flexibility of the building, the following control scenarios are presented.

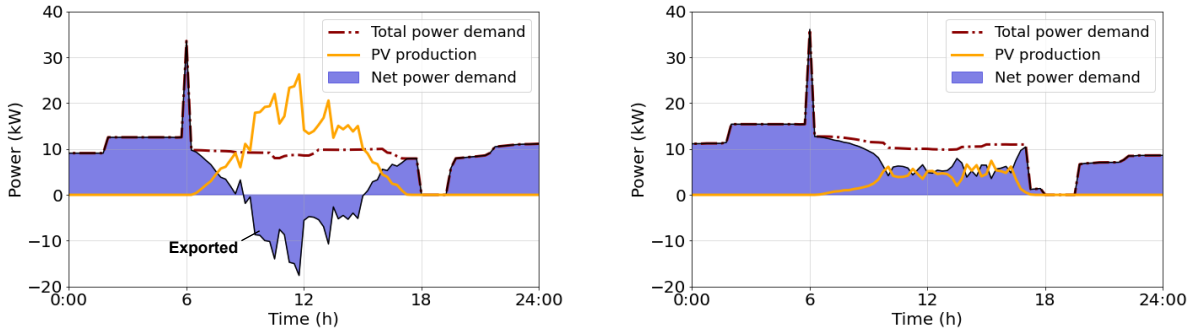

a) Sunny day b) Cloudy day

Figure 6-13: Power demand under BAU

b) *Case 2. Rate flex M in the morning:* To consider a case of a morning peak in a time-of-use tariff structure, the energy cost between 6:00 and 9:00 am is increased by a factor of 15. Results in Figure 6-13 show that on sunny days, the classrooms start being heated around 4:00 am until the heating is completely shut off at 6 am. The over-heated space can free float during the peak period and remain within the comfort boundaries. The heating system can be off during morning peak hours, reducing the peak load to 34 kW. This pre-heating and system staging strategy has emerged by minimizing operational costs. Compared to the uniform pricing case, this case consumes 30 kWh less than the BAU case. Considering the PV production, it is possible to achieve power export during morning on-peak hours.

Rebound power. The rebound power refers to the power surge before or after the flexibility event, either positively or negatively. Using the PV production, the rebound power due to turning on the heating systems at 9:00 am could be reduced from 28 kW to 15 kW (46% reduction). This rebound power is an important factor for the grid, especially after cold-load pick-up due to power outages during cold winter days. Figure 6-14b presents the results for a cloudy day, which shows that same as sunny days, the heating system could be turned off during morning peak hours. In this case, the heating system starts preheating the classrooms at 3:00 am, one hour earlier than on sunny days. Moreover, the rebound power is still high (28 kW) since the PV production is not high at 9:00 am.

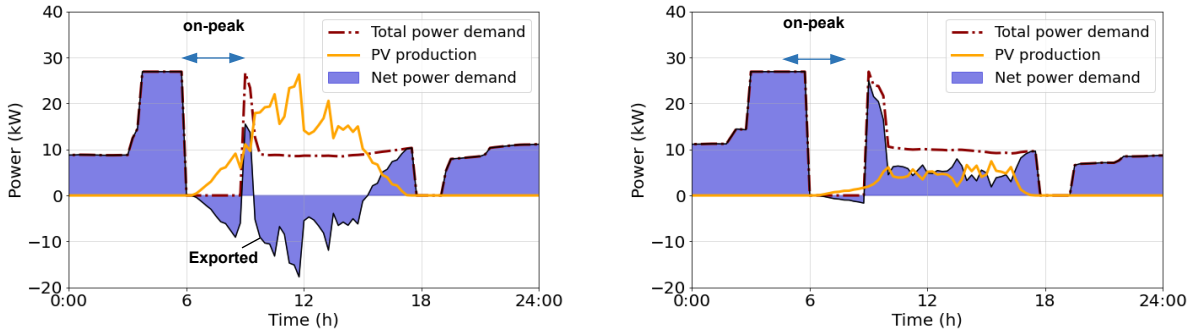

a) Sunny day b) Cloudy day

Figure 6-14: Power demand under morning event

c) *Case 3. Rate flex M in the morning and evening:* If there is an evening peak from 4:00 to 8:00 pm, the evening behavior is affected by a slight preheating but not as aggressively as in the morning since the school is not occupied after 8 pm. The peak power is before evening peak hours, which by using the PV production it, can be reduced from 28 kW to 21 kW, a 25% peak load reduction, as shown in Figure 6-15. Also, an average of 8 kW for 8 hours can be exported to the grid. This case consumes 122 kWh of energy less than the BAU.

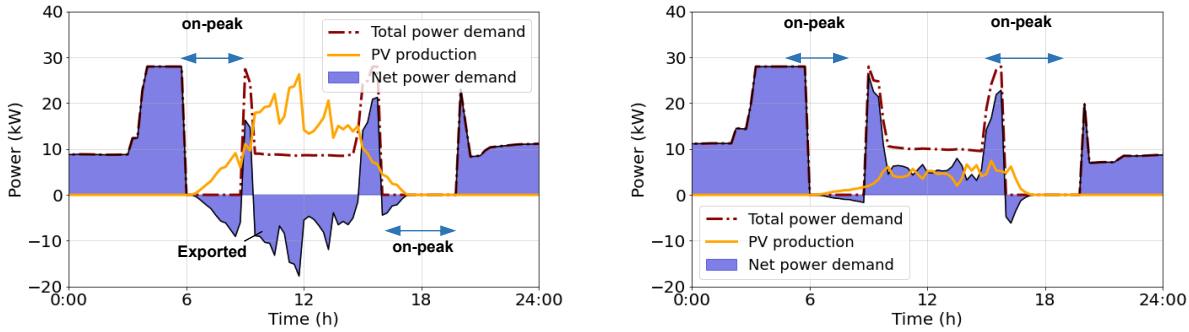

a) Sunny day b) Cloudy day

Figure 6-15: Power demand under morning and evening event

6.4.2 Integration of PV/T system

The three control scenarios mentioned in the previous section for cold cloudy, and cold sunny days in winter are investigated. The effect of PV/T electricity and heat production on the net power demand has been studied in all scenarios.

Figure 6-16 to Figure 6-18 show the effect of PV/T and MPC control strategies on the power demand and export from the building to the grid. The exported power can be increased up to 30

kW at noon, which is 55% more than the building with only a PV system. Also, the rebound power can be decreased to 10 kW, which is 50% less than the case with the PV system. In this case, the energy consumption is 167 kWh less than BAU, which is 36% less than the case with the PV system. Moreover, using PV/T during cloudy days, the power demand will decrease from 5 kW to 2.5 kW, a 50% power demand reduction during the day.

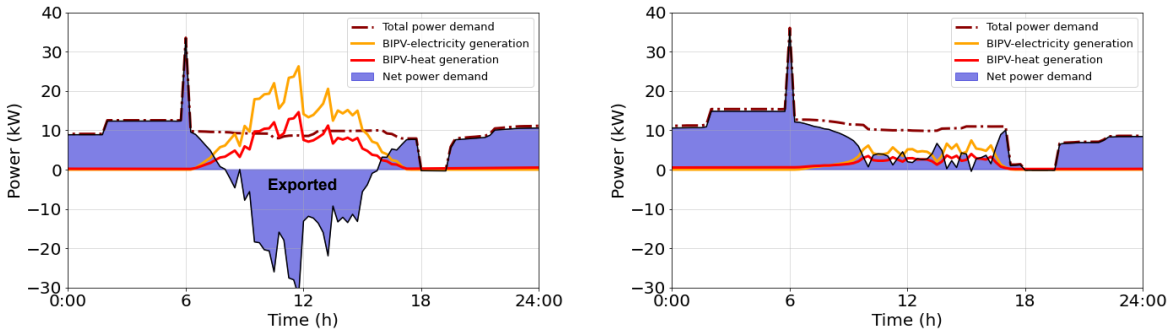

a) Sunny day b) Cloudy day

Figure 6-16: Power demand under BAU (PV/T)

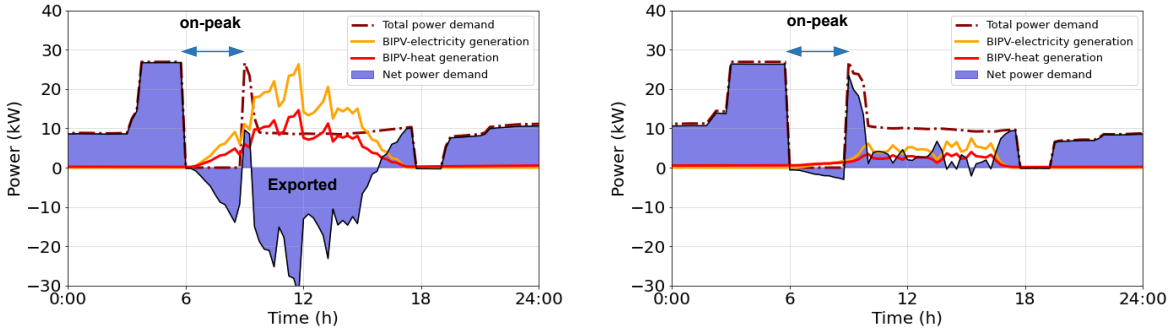

a) Sunny day b) Cloudy day

Figure 6-17: Power demand under morning event (PV/T)

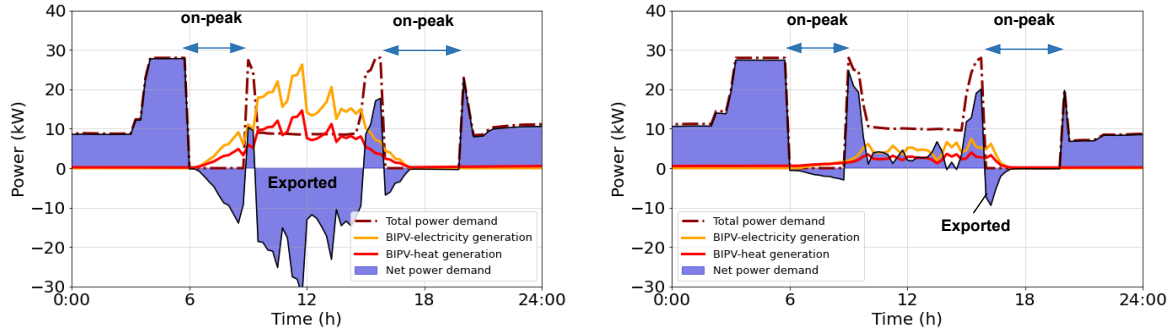

a) Sunny day b) Cloudy day

Figure 6-18: Power demand under morning and evening events (PV/T)

As shown in these graphs, the amount of PV self-consumption is 100% on cold cloudy days. In cold sunny days, the surplus energy is exported to the grid. These results demonstrate the potential of integrating MPC control strategies and PV/T to enhance energy flexibility in school buildings. This approach also can help reduce the carbon footprint of school buildings and contribute to a more sustainable future.

6.4.3 Energy Flexibility Quantification

Figure 6-19 and Figure 6-20 present the energy flexibility provided by using PV/T and appropriate predictive control strategies. As observed in Figure 6-19, the MPC for integrating the PV/T system in school buildings could provide around 20 kW energy flexibility during on-peak hours, meaning 100% power demand reduction. In this case, energy flexibility for the three h in the morning equals 61 Wh/m^2, and the four h in the afternoon is 31 Wh/m^2 of floor area. For sunny days, shown in Figure 6-20, the energy flexibility for the three hours in the morning equals 65 Wh/m^2, and for the four hours in the afternoon, it is 37 Wh/m^2. To achieve this energy flexibility while considering the thermal comfort of the students and teachers, the heating system turns on three hours before the morning event for cloudy days. In comparison, it must be turned on for two hours on sunny days.

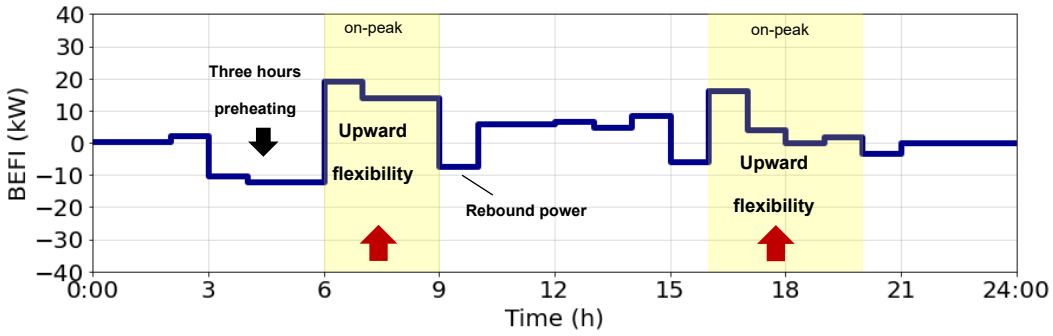

Figure 6-19: BEFI in the school with PV/T system – Cloudy day

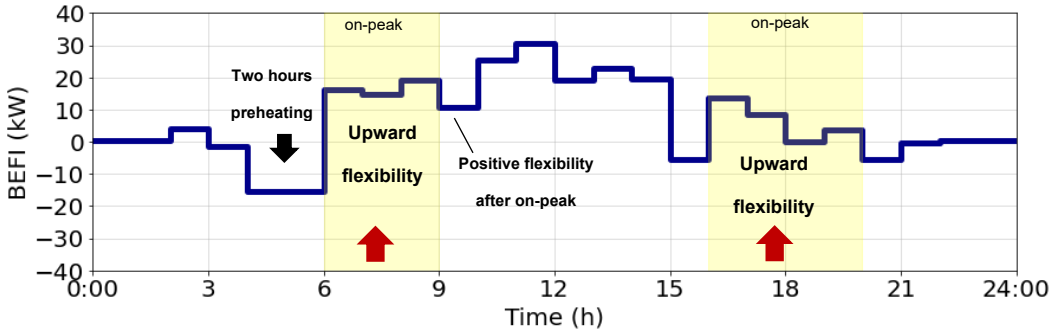

Figure 6-20: BEFI in the school with PV/T system – Sunny day

Table 12 provides an overview of the energy flexibility quantification for the model predictive control and PV/T system for sunny and cloudy days. This table presents average BEFI (kW), BEFI as a percentage (%), and energy reduction (kWh) during the morning (6:00 to 9:00 a.m.) and evening (4:00 to 8:00 p.m.) on-peak hours. Also, it presents energy reduction (kWh)due to MPC and PV/T systems over 24 hours. This table shows that maximum energy flexibility can be achieved by integrating MPC and rate flex M in morning and evening peak hours.

Table 12: Energy flexibility and energy consumption reduction by PV/T and MPC

Scenarios		6:00 to 9:00 a.m.			4:00 to 8:00 p.m.		
		BEFI (kW)	BEFI (%)	Energy reduction (kWh)	BEFI (kW)	BEFI (%)	Energy reduction (kWh)
PV/T compared to reference case							
Sunny day	Case 1a	5.16	45	27.55	1.31	26	10.52
	Case 2a	16.72	144	50.17	0.78	15	3.13
	Case 3a	16.72	144	50.17	6.44	125	25.79
Cloudy day	Case 1b	1.31	9	9.20	1.44	35	10.85
	Case 2b	15.70	110	47.12	0.58	14	2.33
	Case 3b	15.70	110	47.12	5.55	135	22.20
PV/T compared to PV case							
Sunny day	Case 1a	1.34	35	4.02	0.62	50	1.86
	Case 2a	1.34	35	4.02	0.62	50	1.86
	Case 3a	1.34	35	4.02	0.62	50	1.86
Cloudy day	Case 1b	0.58	22	1.75	0.56	6	1.69
	Case 2b	0.58	22	1.75	0.56	6	1.69
	Case 3b	0.58	22	1.75	0.56	6	1.69

Results showed that while the amount of energy reduction in a day could increase by 52%, the amount of energy flexibility increased by 100%. At the same time, the integration of MPC could

enhance the energy flexibility of the building during high-demand hours when needed by the grid. As shown in Table 2, using PV/T can enhance energy flexibility by 35% during the morning and 50% during the afternoon compared to the case with just PV (i.e., without heat generation). Also, the preheated fresh air could increase the air quality of the building. These results show the importance of designing for energy flexibility in buildings. It can be achieved by integrating technologies such as PV/T systems and predictive control strategies using the MPC approach.

6.5 Conclusion

This chapter presented an MPC methodology for integration of air-based PV/T system as a renewable energy retrofit for energy efficiency and flexibility in school buildings. The methodology was developed based on a case study for an archetype fully-electric school building in Québec, Canada. A third-order thermal network model for the classrooms was calibrated with measured data, and a PV/T model was developed. These models were integrated to apply MPC to the school building using the established dynamic tariffs for morning and evening peaks. In this study, three scenarios have been investigated and compared: 1) A reference case without a PV or air-based PV/T system, 2) Integration of a PV system and MPC strategies under a demand response scenario, and 3) Integration of an air-based PV/T system and MPC strategies under a demand response scenario. The results showed that applying a predictive control strategy with PV/T integration results in a 100 % reduction in the peak demand compared to the reference case during peak hours and the export of surplus power to the grid. Also, the PV self-consumption increased by up to 50% compared to the case without a predictive control strategy. This methodology is scalable and can be transferable to other institutional buildings. Future research should focus on a comparative analysis of various MPC strategies and optimization algorithms to identify the most effective approach for PV/T integration in school buildings.

Chapter 7: Conclusion

This thesis investigated the energy flexibility potential in school buildings through simulation and experimental studies. It contributed a general methodology for the development of data-driven grey-box thermal models and the implementation of MPC. The methodology is applied to an archetype fully-electric school building near Montréal, Québec, Canada. This approach is scalable and transferable to other institutional or mid-size commercial buildings.

In grey-box models, obtaining a model that provides reliable predictions and can be implemented in smart controllers is crucial for optimal building performance. A data-driven grey-box approach was used to create archetype models for different thermal zones; this approach enables rapid development and requires much less calibration data than black-box models. Grey-box models of different orders were designed to capture different phenomena. Archetype control-oriented models for zones with convective systems and zones with radiant floor systems are developed and calibrated with measured data. The impact of model resolution and structure on the energy flexibility quantification is investigated. Results showed a third-order RC thermal network for zones with convective systems and a fourth-order model for zones with radiant floor systems are able to capture the dynamic of the system for control purposes. Higher-order models can be used to increase accuracy, but they contain too many parameters and require information that is not often available with adequate accuracy.

Using these models, predictive control strategies were investigated with the aim of reducing peak demand in response to grid requirements and incentives. A key aim was to evaluate the potential of shifting electricity use in different archetype zones from on-peak hours to off-peak grid periods. Also, a methodology for defining and calculating a dynamic energy flexibility index for buildings was presented. The building energy flexibility index (BEFI) has been defined in terms of key performance indicators relative to a reference energy consumption profile at zone level, building level, and as a percentage.

To streamline the implementation of MPC, the proposed approach employs low-order resistance-capacitance (RC) thermal network models, a clustering of weather conditions to identify typical scenarios, and a number of near-optimal setpoint profiles corresponding to each cluster. The calibrated RC models are used to apply MPC to the school building using the established

dynamic tariffs for morning and evening peaks. The weather data were clustered into several categories, representing different weather conditions (6 clusters representing two ambient temperature ranges and three solar radiation ranges). For each heuristic MPC scenario, the model runs a simulation using forecast weather data to quantify and activate energy flexibility in response to grid requirements. The developed MPC framework was applied in the school used as case study. The developed MPC framework is applied in six classrooms, and the results are compared with four classrooms with the reactive control system as reference cases. Results indicated that the school building can provide 45% to 95% energy flexibility (load shifting relative to reference) during on-peak hours while satisfying thermal comfort constraints.

Finally, this thesis presented an MPC methodology for the integration of air-based PV/T system to enhance energy flexibility in school buildings so that in addition to production of solar electricity they can be used to preheat fresh air for the classrooms during the heating season. The PV/T system electrical capacity was set equal to peak electricity demand in the classrooms. A data-driven grey-box model for the classrooms is calibrated with measured data, and a PV/T model as a renewable energy retrofit measure for energy efficiency and flexibility is developed. These models are integrated to apply MPC to the school building and reduce peak demand during morning and evening. Three scenarios are investigated and compared: 1) A reference case without a PV or air-based PV/T system, 2) Integration of a PV system and MPC strategies under a demand response scenario, and 3) Integration of an air-based PV/T system and MPC strategies under a demand response scenario. Results showed that using a predictive control strategy with PV/T integration can significantly reduce peak demand, or even eliminating it, during morning and evening high-demand periods for the grid. The proposed methodology helps institutional buildings adapt smoothly to the necessities of the future smart grid and smart cities.

The proposed framework can be generalized and replicated in other institutional buildings and help institutional buildings adapt smoothly to the necessities of the future smart grid and smart cities.

7.1 Contributions

The major contributions from this thesis are listed below:

- Development of archetype models for zones with convective systems and zones with radiant floor systems in school buildings, which can be used in other mid-size institutional/commercial buildings. The models can capture the dynamics of the indoor temperature variations and the power demand of the HVAC system. The developed models are calibrated with measured data.
- Development of a new index, the Building Flexibility Index (BEFI), to be used to evaluate potential flexibility control scenarios for improved building-grid interaction. This was a collaborative effort with Hydro-Québec researchers, my supervisor, and other students in the lab. This methodology can be applied to different energy storage and generation systems, as well as to different levels of buildings from a cluster of buildings to district energy systems.
- A comprehensive heuristic MPC methodology to activate energy flexibility in buildings is proposed. The framework offers a practical method for the implementation of MPC as a supervisory control in buildings. The methodology is scalable and can be transferable to other buildings.
- Implementation of the developed MPC framework in a school building during heating season and analyze its performance for both unoccupied and occupied conditions.
- Design of a general MPC methodology for integrating air-based PV/T systems in school buildings is presented. This approach offers a renewable energy retrofit measure to enhance energy efficiency and flexibility so that in addition to production of solar electricity they can be used to preheat fresh air during the heating season.
- Collaboration with industry partners (Hydro-Québec and CanmetEnergy) and school board (CSSMI) to address practical challenges in implementing the proposed methodology, fostering a bridge between academic research and real-world applications in the context of school building energy management.

Overall, this thesis represents steps forward in developing and implementing model-based control strategies and renewable energy integration for energy flexibility in school buildings, applicable in other mid-size institutional and commercial buildings.

7.1.1 Publications

The published papers and conferences from this thesis, as well as the submitted papers that are under review are listed below:

Journal articles:

1. **Morovat, N.,** Athienitis, A. K., Candanedo, J. A., Delcroix, B. (2022). "Data-driven model-based control strategies to enhance energy flexibility in electrically heated school buildings", *Buildings,* 12(5), 581. *(Published)*

2. Candanedo, J. A., Vallianos, C., Delcroix, B., Date, J., Saberi, A., **Morovat, N.**, John C., and Athienitis, A. K. (2022), "Control-oriented archetypes: a pathway for the systematic application of advanced controls in buildings", *Journal of Building Performance Simulation*, 1-12. *(Published)*

3. **Morovat, N.,** Athienitis, A. K., Candanedo, J. A., Nouanegue, H. F. (2023). ""Heuristic Model Predictive Control Implementation to Activate Energy Flexibility in a Fully Electric School Building", *Energy Journal. (Accepted)*

4. **Morovat, N.,** Athienitis, A. K., Candanedo, J. A. (2023), "Design of a model predictive control methodology for integration of retrofitted air-based PV/T system in school buildings", *Journal of building performance simulation*. *(Submitted - Under review)*

Conference Proceedings:

1. **Morovat, N.,** Athienitis, A. K., Candanedo, J. A. (2023), "*Model Predictive Control for Integration of PV/T system in School Buildings*", The 18th Conference on Sustainable Development of Energy, Water and Environment Systems (SDEWES), Dubrovnik, Croatia, 24–29 September 2023.

2. **Morovat, N.,** Athienitis, A. K., Candanedo, J. A. (2023), "*Model predictive control for demand response in all-electric school buildings*", 13th Nordic Symposium on Building Physics (NSB 2023), Aalborg, Denmark, 12-14 June 2023.

3. **Morovat, N.,** Athienitis, A. K., Candanedo, J. A. (2022), "*A Heuristic Model Predictive Control Method to Activate the Energy Flexibility of School Buildings*", 7th International High-Performance Buildings Conference 2022, Purdue University, West Lafayette, IN, USA, July 10-14.

4. **Morovat, N.,** Athienitis, A. K., Candanedo, J. A. (2022), "*Enhancing energy flexibility of a school building using local setpoint adjustment in classrooms*", 5th International

Conference on Building Energy and Environment, Concordia University, Montreal, Québec, Canada, July 25-29.

5. **Morovat, N.,** Athienitis, A. K.**,** Candanedo, J. A. (2021). "Modeling energy performance and real-time energy flexibility of a floor heating system in a school building", Building Simulation 2021 Conference, Bruges, Belgium, September 1-3.

6. **Morovat, N.,** Candanedo, J. A., Athienitis, A. K. (2021). "*Application of grey-box models for the quantification of the energy flexibility of a school building in Canada*", 2021 ASHRAE Annual Conference, Phoenix, USA, June 28-30.

7. **Morovat, N.,** Candanedo, J. A., Athienitis, A. K. (2020), "*Data analysis, modelling, and energy flexibility assessment of an educational building in Canada*", eSIM 2021 Conference, Vancouver, BC, Canada, June 14 -16.

8. Athienitis, AK., Dumont, E., **Morovat, N.,** Lavigne, K., Date, J. (2020), "*Development of a dynamic energy flexibility index for buildings and their interaction with smart grids*", ACEEE Summer Study on Energy Efficiency in Buildings, California, USA, August 17-2.

Non-Refereed Contributions

1. Li, A., Du, B., **Morovat, N.,** Candanedo, J. A. (2024), "*Seminar 47: The Future is Electrifying Zero-Carbon Case Studies under Moderate Climates*", ASHRAE winter conference, January 20-24, Chicago, US.

2. Candanedo, J. A., **Morovat, N.,** Vallianos, C., John, C., and Athienitis, A. K. (2022), "*Contrôle avancé basé sur les données: Son rôle dans la gestion de la puissance électrique et de la flexibilité énergétique*", Symposium – Réseau Énergie et Bâtiments, Montreal, Canada, December 12.

3. **Morovat, N.,** Athienitis, A. K.**,** Candanedo, J. A. (2022), "*Model-Based Control Strategies for Energy Flexibility in School Buildings*", IEA EBC Annex 81: Data-driven smart buildings, October 12-14, Gothenburg, Sweden.

7.2 Recommendation for future works

The future work involves extending and enhancing the presented methodology in the following directions:

- *Diversity in Energy Sources:* The presented methodology can also be applied to buildings with different energy sources, such as dual fuel buildings with electricity and gas. Also assess the adaptability of the presented methodology to other types of buildings, such as residential buildings, commercial buildings, and cluster of buildings.
- *Integration of Energy Storage Systems:* Explore the integration of different energy storage systems, such as battery storage and Electric Vehicles (EVs) as mobile energy storage, using the same methodology. Investigate the impact of these storage technologies on overall energy flexibility and identify optimal control strategies.
- *Integration of Machine Learning Techniques:* Investigate how machine learning algorithms can improve the accuracy of predictions, particularly in dynamic weather conditions, and optimize the responsiveness and adaptability of the system. Using Reinforcement Learning (RL) with self-learning capability for online calibration of MPC is a promising method to develop automated building control in buildings.
- *Occupancy Modeling:* Integrate occupancy modeling into the developed methodology to account for the influence of building occupancy on energy flexibility and thermal comfort. Explore how to optimize the MPC system in order to respond dynamically to varying occupancy levels.
- *Online Recursive Calibration:* Implement online recursive calibration of models within the methodology to enhance accuracy over time. Explore adaptive techniques that continuously update the models based on real-time data, ensuring the system is robust.

References

Abdelrazik, A., B. Shboul, M. Elwardany, R. Zohny and A. Osama (2022). "The recent advancements in the building integrated photovoltaic/thermal (BIPV/T) systems: An updated review." *Renewable and Sustainable Energy Reviews 170*: 112988.

Afram, A. and F. Janabi-Sharifi (2014). "Theory and applications of HVAC control systems–A review of model predictive control (MPC)." *Building and Environment 72*: 343-355.

Afroz, Z., G. Shafiullah, T. Urmee and G. Higgins (2018). "Modeling techniques used in building HVAC control systems: A review." *Renewable and Sustainable Energy Reviews 83*: 64-84.

Amadeh, A., Z. E. Lee and K. M. Zhang (2022). "Quantifying demand flexibility of building energy systems under uncertainty." *Energy 246*: 123291.

Amara, F., V. Dermardiros and A. K. Athienitis (2019). Energy Flexibility for an Institutional Building with Integrated Solar System: Case Study Analysis. *IOP Conference Series: Earth and Environmental Science*, IOP Publishing.

Arroyo, J., F. Spiessens and L. Helsen (2020). "Identification of multi-zone grey-box building models for use in model predictive control." *Journal of Building Performance Simulation 13(4)*: 472-486.

Asaee, S. R., S. Nikoofard, V. I. Ugursal and I. Beausoleil-Morrison (2017). "Techno-economic assessment of photovoltaic (PV) and building integrated photovoltaic/thermal (BIPV/T) system retrofits in the Canadian housing stock." *Energy and Buildings 152*: 667-679.

ASHRAE 55 (2017). "Thermal Environmental Conditions for Human Occupancy."

ASHRAE Guideline 14 (2002). "Guideline 14-2002, Measurement of energy and demand savings." *American Society of Heating, Ventilating, and Air Conditioning Engineers, Atlanta, Georgia*.

ASHRAE, I. (2009). *2009 ASHRAE handbook: fundamentals*, American Society of Heating, Refrigeration and Air-Conditioning Engineers.

Aspetakis, G. and Q. Wang (2023). "Critical Review of Air-Based PVT Technology and Its Integration to Building Energy Systems." *Energy and Built Environment*.

Aswani, A., N. Master, J. Taneja, D. Culler and C. Tomlin (2011). "Reducing transient and steady state electricity consumption in HVAC using learning-based model-predictive control." *Proceedings of the IEEE 100(1)*: 240-253.

Athienitis, A. K. (2013). *Thermal analysis and design of passive solar buildings*, Routledge.

Athienitis, A. K., E. Dumont, N. Morovat, K. Lavigne and J. Date (2020). Development of a dynamic energy flexibility index for buildings and their interaction with smart grids. 2020 Summer Study on Energy Efficiency in Buildings. California, USA.

Athienitis, A. K. and W. O'Brien (2015). *Modeling, design, and optimization of net-zero energy buildings*, Wiley Online Library.

Attoye, D. E., T. O. Adekunle, K. A. Tabet Aoul, A. Hassan and S. O. Attoye (2018). "A conceptual framework for a building integrated photovoltaics (BIPV) educative-communication approach." *Sustainability 10(10)*: 3781.

Bacher, P. and H. Madsen (2011). "Identifying suitable models for the heat dynamics of buildings." *Energy and Buildings 43(7)*: 1511-1522.

Bai, Y., W. Zhang, T. Yu, J. Wang, G. Deng, J. Yan and J. Liu (2023). "Flexibility quantification and enhancement of flexible electric energy systems in buildings." *Journal of Building Engineering*: 106114.

Battaglini, A., J. Lilliestam, A. Haas and A. Patt (2009). "Development of SuperSmart Grids for a more efficient utilisation of electricity from renewable sources." *Journal of Cleaner Production 17(10)*: 911-918.

Bengea, S. C., A. D. Kelman, F. Borrelli, R. Taylor and S. Narayanan (2014). "Implementation of model predictive control for an HVAC system in a mid-size commercial building." *HVAC&R Research 20(1)*: 121-135.

Blum, D., Z. Wang, C. Weyandt, D. Kim, M. Wetter, T. Hong and M. A. Piette (2022). "Field demonstration and implementation analysis of model predictive control in an office HVAC system." *Applied Energy 318*: 119104.

Braun, J. E. (2003). "Load control using building thermal mass." *J. Sol. Energy Eng. 125(3)*: 292-301.

Braun, J. E. and N. Chaturvedi (2002). "An inverse gray-box model for transient building load prediction." *Hvac&R Research 8(1)*: 73-99.

Bruno, S., G. Giannoccaro and M. La Scala (2019). "A demand response implementation in tertiary buildings through model predictive control." *IEEE Transactions on Industry Applications 55(6)*: 7052-7061.

Buker, M. S. and S. B. Riffat (2015). "Building integrated solar thermal collectors–A review." *Renewable and Sustainable Energy Reviews 51*: 327-346.

Bünning, F., B. Huber, P. Heer, A. Aboudonia and J. Lygeros (2020). "Experimental demonstration of data predictive control for energy optimization and thermal comfort in buildings." *Energy and Buildings 211*: 109792.

Cabovská, B., G. Bekö, D. Teli, L. Ekberg, J.-O. Dalenbäck, P. Wargocki, T. Psomas and S. Langer (2022). "Ventilation strategies and indoor air quality in Swedish primary school classrooms." *Building and Environment 226*: 109744.

Canada energy regulator (2021). "Provincial and Territorial Energy Profiles – Quebec." 2021, from https://www.cer-rec.gc.ca/en/data-analysis/energy-markets/provincial-territorial-energy-profiles/provincial-territorial-energy-profiles-quebec.html.

Candanedo, J. A., V. R. Dehkordi and P. Lopez (2013). A control-oriented simplified building modelling strategy. *13th Conf. Intl. Building Perf. Simulation Ass*.

Candanedo, J. A., C. Vallianos, B. Delcroix, J. Date, A. Saberi Derakhtenjani, N. Morovat, C. John and A. K. Athienitis (2022). "Control-oriented archetypes: a pathway for the systematic application of advanced controls in buildings." *Journal of Building Performance Simulation 15(4)*: 433-444.

Chen, X., B. Cao and S. Pouramini (2023). "Energy cost and consumption reduction of an office building by Chaotic Satin Bowerbird Optimization Algorithm with model predictive control and artificial neural network: A case study." *Energy 270*: 126874.

Chen, Y. (2013). Methodology for Design and Operation of Active Building-Integrated Thermal Energy Storage Systems, Concordia University.

Chen, Y., Z. Chen, P. Xu, W. Li, H. Sha, Z. Yang, G. Li and C. Hu (2019). "Quantification of electricity flexibility in demand response: Office building case study." *Energy 188*: 116054.

Chen, Y., M. Guo, Z. Chen, Z. Chen and Y. Ji (2022). "Physical energy and data-driven models in building energy prediction: A review." *Energy Reports 8*: 2656-2671.

Coakley, D., P. Raftery and M. Keane (2014). "A review of methods to match building energy simulation models to measured data." *Renewable and Sustainable Energy Reviews 37*: 123-141.

Cotrufo, N., E. Saloux, J. Hardy, J. Candanedo and R. Platon (2020). "A practical artificial intelligence-based approach for predictive control in commercial and institutional buildings." *Energy and Buildings 206*: 109563.

Crawley, D. B., L. K. Lawrie, F. C. Winkelmann, W. F. Buhl, Y. J. Huang, C. O. Pedersen, R. K. Strand, R. J. Liesen, D. E. Fisher and M. J. Witte (2001). "EnergyPlus: creating a new-generation building energy simulation program." *Energy and Buildings 33(4)*: 319-331.

David Blum, J. C., Zhelun Chen, Gabe Fierro, Virginia Gori, Hicham Johra, Henrik Madsen, Anna Marszal-Pomianowska, Zheng O'Neill , Ojas Pradhan, Dimitrios Rovas, Francesco Sacco, Sofia Stensson , Christian A. Thilker, Charalampos Vallianos, Jin Wen , Stephen D. White (2023). Data-Driven Smart Buildings: State-of-the-Art Review.

Davito, B., H. Tai and R. Uhlaner (2010). "The smart grid and the promise of demand-side management." *McKinsey on Smart Grid 3*: 8-44.

De Coninck, R. and L. Helsen (2016). "Practical implementation and evaluation of model predictive control for an office building in Brussels." *Energy and Buildings 111*: 290-298.

De Coninck, R. and L. Helsen (2016). "Quantification of flexibility in buildings by cost curves–Methodology and application." *Applied energy 162*: 653-665.

De Coninck, R., F. Magnusson, J. Åkesson and L. Helsen (2016). "Toolbox for development and validation of grey-box building models for forecasting and control." *Journal of Building Performance Simulation 9(3)*: 288-303.

Delisle, V. and M. Kummert (2016). "Cost-benefit analysis of integrating BIPV-T air systems into energy-efficient homes." *Solar energy 136*: 385-400.

Denholm, P., M. O'Connell, G. Brinkman and J. Jorgenson (2015). Overgeneration from solar energy in california. a field guide to the duck chart, National Renewable Energy Lab.(NREL), Golden, CO (United States).

Dermardiros, V. and P. Scott Bucking PhD (2019). "Energy performance, comfort, and lessons learned from an institutional building designed for net zero energy." *ASHRAE Transactions 125*: 682-695.

Diakaki, C., E. Grigoroudis and D. Kolokotsa (2008). "Towards a multi-objective optimization approach for improving energy efficiency in buildings." *Energy and Buildings 40(9)*: 1747-1754.

Diamond, S. and S. Boyd (2016). "CVXPY: A Python-embedded modeling language for convex optimization." *The Journal of Machine Learning Research 17(1)*: 2909-2913.

Distribution., H.-Q. "État D'Avancement 2012 du Plan D'Approvisionnement 2011–2020. 2012.". Retrieved 12 January, 2022, from http://www.regie-energie.qc.ca/audiences/TermElecDistrPlansAppro_Suivis.html

Domahidi, A., E. Chu and S. Boyd (2013). ECOS: An SOCP solver for embedded systems. *2013 European Control Conference (ECC)*, IEEE.

Drgoňa, J., J. Arroyo, I. Cupeiro Figueroa, D. Blum, K. Arendt, D. Kim, E. P. Ollé, J. Oravec, M. Wetter, D. L. Vrabie and L. Helsen (2020). "All you need to know about model predictive control for buildings." *Annual Reviews in Control 50*: 190-232.

Drgoňa, J., J. Arroyo, I. C. Figueroa, D. Blum, K. Arendt, D. Kim, E. P. Ollé, J. Oravec, M. Wetter and D. L. Vrabie (2020). "All you need to know about model predictive control for buildings." *Annual Reviews in Control 50*: 190-232.

Drgoňa, J., D. Picard and L. Helsen (2020). "Cloud-based implementation of white-box model predictive control for a GEOTABS office building: A field test demonstration." *Journal of Process Control 88*: 63-77.

Droutsa, K. G., S. Kontoyiannidis, C. A. Balaras, S. Lykoudis, E. G. Dascalaki and A. A. Argiriou (2021). "Unveiling the existing condition and energy use in Hellenic school buildings." *Energy and Buildings 247*: 111150.

Dumoulin, R., E. D. Rounis and A. Athienitis (2021). "Operation and grid interaction modeling of a house with a building integrated photovoltaic thermal (BIPV/T) system coupled to an air-source heat pump." *Science and Technology for the Built Environment 27(9)*: 1311-1329.

Farrokhifar, M., H. Bahmani, B. Faridpak, A. Safari, D. Pozo and M. Aiello (2021). "Model predictive control for demand side management in buildings: A survey." *Sustainable Cities and Society 75*: 103381.

Fernández Bandera, C., G. Bastos Porsani and M. Fernández-Vigil Iglesias (2023). A demand side management approach to increase self-consumption in buildings. *Building Simulation*, Springer.

Finck, C., R. Li and W. Zeiler (2019). "Economic model predictive control for demand flexibility of a residential building." *Energy 176*: 365-379.

Finck, C., R. Li and W. Zeiler (2020). "Optimal control of demand flexibility under real-time pricing for heating systems in buildings: A real-life demonstration." *Applied energy 263*: 114671.

Foteinaki, K., R. Li, A. Heller and C. Rode (2018). "Heating system energy flexibility of low-energy residential buildings." *Energy and Buildings 180*: 95-108.

Fraisse, G., C. Viardot, O. Lafabrie and G. Achard (2002). "Development of a simplified and accurate building model based on electrical analogy." *Energy and Buildings 34(10)*: 1017-1031.

Fu, Y., Z. O'Neill, J. Wen, A. Pertzborn and S. T. Bushby (2022). "Utilizing commercial heating, ventilating, and air conditioning systems to provide grid services: A review." *Applied energy 307*: 118133.

Gao, Y., Y. Matsunami, S. Miyata and Y. Akashi (2023). "Model predictive control of a building renewable energy system based on a long short-term hybrid model." *Sustainable Cities and Society 89*: 104317.

Gaucher-Loksts, E., A. Athienitis and M. Ouf (2022). "Design and energy flexibility analysis for building integrated photovoltaics-heat pump combinations in a house." *Renewable Energy 195*: 872-884.

Gibbons, L. and S. Javed (2022). "A review of HVAC solution-sets and energy performace of nearly zero-energy multi-story apartment buildings in Nordic climates by statistical analysis of environmental performance certificates and literature review." *Energy 238*: 121709.

Golshan, M., H. Thoen and W. Zeiler (2018). "Dutch sustainable schools towards energy positive." *Journal of Building Engineering 19*: 161-171.

Gouda, M., S. Danaher and C. Underwood (2002). "Building thermal model reduction using nonlinear constrained optimization." *Building and Environment 37(12)*: 1255-1265.

Haakenstad, L. K. (1999). The open protocol standard for computerized building systems: BACnet. *Proceedings of the 1999 IEEE International Conference on Control Applications (Cat. No. 99CH36328)*, IEEE.

Haberl, J. S., D. E. Claridge and C. Culp (2005). "ASHRAE's Guideline 14-2002 for Measurement of Energy and Demand Savings: How to Determine what was really saved by the retrofit."

Ham, S., D. Kim, T. Barham and K. Ramseyer (2023). "The first field application of a low-cost MPC for grid-interactive K-12 schools: Lessons-learned and savings assessment." *Energy and Buildings 296*: 113351.

Hao, K., D. Kim and J. E. Braun (2022). "Comparing the economic performance of ice storage and batteries for buildings with on-site PV through model predictive control and optimal sizing." *Journal of Building Performance Simulation 15(5)*: 691-715.

Heidrich-Meisner, V. and R. F. Wimmer-Schweingruber (2018). *Solar wind classification via k-means clustering algorithm*. Machine learning techniques for space weather, Elsevier: 397-424.

Hensen, J. L. and R. Lamberts (2012). *Building performance simulation for design and operation*, Routledge.

Henze, G. P. (2003). "An overview of optimal control for central cooling plants with ice thermal energy storage." *J. Sol. Energy Eng. 125(3)*: 302-309.

Henze, G. P., D. E. Kalz, S. Liu and C. Felsmann (2005). "Experimental analysis of model-based predictive optimal control for active and passive building thermal storage inventory." *HVAC&R Research 11(2)*: 189-213.

Hong, T. and S. H. Lee (2019). "Integrating physics-based models with sensor data: An inverse modeling approach." *Building and Environment 154*: 23-31.

Hu, J. and P. Karava (2014). "Model predictive control strategies for buildings with mixed-mode cooling." *Building and Environment 71*: 233-244.

Hu, M., F. Xiao, J. B. Jørgensen and R. Li (2019). "Price-responsive model predictive control of floor heating systems for demand response using building thermal mass." *Applied Thermal Engineering 153*: 316-329.

Huang, S., Y. Ye, D. Wu and W. Zuo (2021). "An assessment of power flexibility from commercial building cooling systems in the United States." *Energy 221*: 119571.

Hydro-Québec (2020). "Simulation énergétique des bâtiments." 2020, from https://www.simeb.ca:8443/index_fr.jsp.

Hydro-Québec (2023). "History of electricity demand in Québec." from https://www.hydroquebec.com/documents-data/open-data/history-electricity-demand-quebec/.

Hydro Québec (2022). "Hydro-Québec—Rates for Business Customers, 2022.". Retrieved 10 April, 2022, from http://www.hydroquebec.com/business/customer-space/rates/.

HydroQuebec (2023). Retrieved May, 2023, from https://www.hydroquebec.com/data/documents-donnees/pdf/electricity-rates.pdf?v=20230401.

Ilic, D., P. G. Da Silva, S. Karnouskos and M. Griesemer (2012). An energy market for trading electricity in smart grid neighbourhoods. *2012 6th IEEE international conference on digital ecosystems and technologies (DEST)*, IEEE.

Jensen, S. Ø., A. Marszal-Pomianowska, R. Lollini, W. Pasut, A. Knotzer, P. Engelmann, A. Stafford and G. Reynders (2017). "IEA EBC annex 67 energy flexible buildings." *Energy and Buildings 155*: 25-34.

Joe, J., P. Im, B. Cui and J. Dong (2023). "Model-based predictive control of multi-zone commercial building with a lumped building modelling approach." *Energy 263*: 125494.

Joe, J. and P. Karava (2019). "A model predictive control strategy to optimize the performance of radiant floor heating and cooling systems in office buildings." *Applied energy 245*: 65-77.

Junker, R. G., A. G. Azar, R. A. Lopes, K. B. Lindberg, G. Reynders, R. Relan and H. Madsen (2018). "Characterizing the energy flexibility of buildings and districts." *Applied energy 225*: 175-182.

Killian, M. and M. Kozek (2016). "Ten questions concerning model predictive control for energy efficient buildings." *Building and Environment 105*: 403-412.

Kim, D. and J. E. Braun (2018). "Development, implementation and performance of a model predictive controller for packaged air conditioners in small and medium-sized commercial building applications." *Energy and Buildings 178*: 49-60.

Kim, D. and J. E. Braun (2022). "MPC solution for optimal load shifting for buildings with ON/OFF staged packaged units: Experimental demonstration, and lessons learned." *Energy and Buildings 266*: 112118.

Klein, K., S. Herkel, H.-M. Henning and C. Felsmann (2017). "Load shifting using the heating and cooling system of an office building: Quantitative potential evaluation for different flexibility and storage options." *Applied Energy 203*: 917-937.

Knudsen, M. D., L. Georges, K. S. Skeie and S. Petersen (2021). "Experimental test of a black-box economic model predictive control for residential space heating." *Applied Energy 298*: 117227.

Koskela, J. and P. Järventausta (2023). "Demand Response with Electrical Heating in Detached Houses in Finland and Comparison with BESS for Increasing PV Self-Consumption." *Energies 16(1)*: 497.

Le Dréau, J. and P. Heiselberg (2016). "Energy flexibility of residential buildings using short term heat storage in the thermal mass." *Energy 111*: 991-1002.

Leprince, J., H. Madsen, C. Miller, J. P. Real, R. van der Vlist, K. Basu and W. Zeiler (2022). "Fifty shades of grey: Automated stochastic model identification of building heat dynamics." *Energy and Buildings 266*: 112095.

Li, B., R. Roche, D. Paire and A. Miraoui (2019). "A price decision approach for multiple multi-energy-supply microgrids considering demand response." *Energy 167*: 117-135.

Li, G., Y. Fu, A. Pertzborn, Z. O'Neill and J. Wen (2022). Demand flexibility evaluation for building energy systems with active thermal storage using model predictive control. *2022 ASHRAE Annual Conference, Toronto, Canada*.

Li, R., G. Dane, C. Finck and W. Zeiler (2017). "Are building users prepared for energy flexible buildings?—A large-scale survey in the Netherlands." *Applied energy 203*: 623-634.

Li, R., A. J. Satchwell, D. Finn, T. H. Christensen, M. Kummert, J. Le Dréau, R. A. Lopes, H. Madsen, J. Salom and G. Henze (2022). "Ten questions concerning energy flexibility in buildings." *Building and Environment 223*: 109461.

Li, X. and J. Wen (2014). "Review of building energy modeling for control and operation." *Renewable and Sustainable Energy Reviews 37*: 517-537.

Li, Y., Z. O'Neill, L. Zhang, J. Chen, P. Im and J. DeGraw (2021). "Grey-box modeling and application for building energy simulations-A critical review." *Renewable and Sustainable Energy Reviews 146*: 111174.

Liu, X., Y. Zuo, Z. Yin, C. Liang, G. Feng and X. Yang (2023). "Research on an evaluation system of the application effect of ground source heat pump systems for green buildings in China." *Energy 262*: 125374.

Liu, Z., Y. Chen, X. Yang and J. Yan (2023). "Power to Heat: Opportunity of Flexibility Services Provided by Building Energy Systems." *Advances in Applied Energy*: 100149.

Liu, Z., H. Zhang, Y. Wang, X. Fan, S. You and A. Li (2023). "Data-driven predictive model for feedback control of supply temperature in buildings with radiator heating system." *Energy*: 128248.

Lopes, R. A., A. Chambel, J. Neves, D. Aelenei and J. Martins (2016). "A literature review of methodologies used to assess the energy flexibility of buildings." *Energy Procedia 91*: 1053-1058.

Lourenço, P., M. D. Pinheiro and T. Heitor (2014). "From indicators to strategies: Key Performance Strategies for sustainable energy use in Portuguese school buildings." *Energy and Buildings 85*: 212-224.

Luo, Z., J. Peng, J. Cao, R. Yin, B. Zou, Y. Tan and J. Yan (2022). "Demand flexibility of residential buildings: definitions, flexible loads, and quantification methods." *Engineering 16*: 123-140.

MacDougall, P., B. Ran, G. B. Huitema and G. Deconinck (2017). "Performance assessment of black box capacity forecasting for multi-market trade application." *Energies 10(10)*: 1673.

Maghrabie, H. M., K. Elsaid, E. T. Sayed, M. A. Abdelkareem, T. Wilberforce and A. Olabi (2021). "Building-integrated photovoltaic/thermal (BIPVT) systems: Applications and challenges." *Sustainable energy technologies and assessments 45*: 101151.

Manojkumar, R., C. Kumar, S. Ganguly and J. P. Catalão (2021). "Optimal peak shaving control using dynamic demand and feed-in limits for grid-connected PV sources with batteries." *IEEE Systems Journal 15(4)*: 5560-5570.

Marshall, A. (1972). "The thermal properties of concrete." *Building Science 7(3)*: 167-174.

Maurer, C., T. Baumann, M. Hermann, P. Di Lauro, S. Pavan, L. Michel and T. E. Kuhn (2013). "Heating and cooling in high-rise buildings using facade-integrated transparent solar thermal collector systems." *Journal of Building Performance Simulation 6(6)*: 449-457.

Mehigan, L., J. P. Deane, B. Ó. Gallachóir and V. Bertsch (2018). "A review of the role of distributed generation (DG) in future electricity systems." *Energy 163*: 822-836.

Merei, G., J. Moshövel, D. Magnor and D. U. Sauer (2016). "Optimization of self-consumption and techno-economic analysis of PV-battery systems in commercial applications." *Applied Energy 168*: 171-178.

Merema, B., D. Saelens and H. Breesch (2022). "Demonstration of an MPC framework for all-air systems in non-residential buildings." *Building and Environment 217*: 109053.

Mitterrutzner, B., C. Z. Callegher, R. Fraboni, E. Wilczynski and S. Pezzutto (2023). "Review of heating and cooling technologies for buildings: A techno-economic case study of eleven European countries." *Energy*: 129252.

Morovat, N., A. K. Athienitis, J. A. Candanedo and V. Dermardiros (2019). "Simulation and performance analysis of an active PCM-heat exchanger intended for building operation optimization." *Energy and Buildings 199*: 47-61.

Natural resources Canada (2022). "Survey of Commercial and Institutional Energy Use (SCIEU)." Retrieved 02/03, 2023, from https://www23.statcan.gc.ca/imdb/p2SV.pl?Function=getSurvey&SDDS=5034#a4.

NRCan (2021). "CanMETEO." 2021, from https://www.nrcan.gc.ca/energy/canmeteo/19908

O'Connell, S., G. Reynders, F. Seri and M. Keane (2019). Validation of a Flexibility Assessment Methodology for Demand Response in Buildings. *IOP Conference Series: Earth and Environmental Science*, IOP Publishing.

Ouf, M., M. Issa and P. Merkel (2016). "Analysis of real-time electricity consumption in Canadian school buildings." *Energy and Buildings 128*: 530-539.

Ouf, M. M. and M. H. Issa (2017). "Energy consumption analysis of school buildings in Manitoba, Canada." *International Journal of Sustainable Built Environment 6(2)*: 359-371.

Oviedo-Cepeda, J. C., F. Z. Amara and A. K. Athienitis (2021). Model Predictive Control Horizon Impact Over the Flexibility of a Net Zero Energy Building. *IECON 2021–47th Annual Conference of the IEEE Industrial Electronics Society*, IEEE.

Papachristou, A. C. and A. K. Athienitis (2016). The importance of thermal mass in predictive control case study: a zone with floor heating and a chilled beam. *Proceedings of the eSim Buildings Performance Simulations Conference*.

Pochwała, S., S. Anweiler, M. Tańczuk, I. Klementowski, D. Przysiężniuk, Ł. Adrian, G. McNamara and Ž. Stevanović (2023). "Energy source impact on the economic and environmental effects of retrofitting a heritage building with a heat pump system." *Energy*: 128037.

Policy, I. E. A. D. o. S. E. (2013). *Transition to sustainable buildings: strategies and opportunities to 2050*, Organization for Economic Co-Operation & Development.

Qu´ebec, G. d. Plan directeur en transition, innovation et efficacit energetiques du Quebec 2018 - 2023.

Reynders, G., J. Diriken and D. Saelens (2014). "Quality of grey-box models and identified parameters as function of the accuracy of input and observation signals." *Energy and Buildings 82*: 263-274.

Reynders, G., R. A. Lopes, A. Marszal-Pomianowska, D. Aelenei, J. Martins and D. Saelens (2018). "Energy flexible buildings: An evaluation of definitions and quantification methodologies applied to thermal storage." *Energy and Buildings 166*: 372-390.

Rounis, E. D., A. K. Athienitis and T. Stathopoulos (2021). "BIPV/T curtain wall systems: Design, development and testing." *Journal of Building Engineering 42*: 103019.

Rounis, E. D., Z. Ioannidis, A.-M. Sigounis, A. Athienitis and T. Stathopoulos (2022). "A novel approach for the modelling of convective phenomena for building integrated photovoltaic thermal (BIPV/T) systems." *Solar Energy 232*: 328-343.

Sadrizadeh, S., R. Yao, F. Yuan, H. Awbi, W. Bahnfleth, Y. Bi, G. Cao, C. Croitoru, R. de Dear and F. Haghighat (2022). "Indoor air quality and health in schools: A critical review for developing the roadmap for the future school environment." *Journal of Building Engineering*: 104908.

Sakellariou, F. (2011). "Model predictive control for thermally activated building systems." *Eindhoven: TU Eindhoven*: 1-91.

Sari, Y. A. and S. M. Said (2021). "Review of Building Integrated Photovoltaic-Thermal (BIPV/T) Systems: Current and Potential Technology Development." *Journal of Engineering Science & Technology Review 14(4)*.

Široký, J., F. Oldewurtel, J. Cigler and S. Prívara (2011). "Experimental analysis of model predictive control for an energy efficient building heating system." *Applied Energy 88(9)*: 3079-3087.

Sohani, A., C. Cornaro, M. H. Shahverdian, S. Samiezadeh, S. Hoseinzadeh, A. Dehghani-Sanij, M. Pierro and D. Moser (2022). *Using Building Integrated Photovoltaic Thermal (BIPV/T) systems to achieve net zero goal: Current trends and future perspectives*. Towards Net Zero Carbon Emissions in the Building Industry, Springer: 91-107.

Statistic Canada (2017). "Elementary–Secondary Education Survey for Canada, the provinces and territories. ." Retrieved November 6, 2020, from https://www150.statcan.gc.ca/n1/daily quotidien/171103/dq171103c-eng.htm.

Tabares-Velasco, P., C. Christensen and M. Bianchi (2012). "Simulated peak reduction and energy savings of residential building envelope with phase change materials." *ASHRAE Transactions 118*: 90-97.

Taheri, S., P. Hosseini and A. Razban (2022). "Model predictive control of heating, ventilation, and air conditioning (HVAC) systems: A state-of-the-art review." *Journal of Building Engineering*: 105067.

Tang, H., S. Wang and H. Li (2021). "Flexibility categorization, sources, capabilities and technologies for energy-flexible and grid-responsive buildings: State-of-the-art and future perspective." *Energy 219*: 119598.

Torres Ruilova, B. (2017). "Evaluation of energy flexibility of buildings using structural thermal mass."

Tripanagnostopoulos, Y., M. Souliotis, R. Battisti and A. Corrado (2006). "Performance, cost and life-cycle assessment study of hybrid PVT/AIR solar systems." *Progress in Photovoltaics: Research and applications 14(1)*: 65-76.

Tumminia, G., F. Sergi, D. Aloisio, S. Longo, M. A. Cusenza, F. Guarino, S. Cellura and M. Ferraro (2021). "Towards an integrated design of renewable electricity generation and storage systems for NZEB use: A parametric analysis." *Journal of Building Engineering 44*: 103288.

U.S. Energy Information Administration (EIA), C. b. e. c. s. C. d. T. B.-B., Tech. rep., U.S. Department of Energy, Washington, DC (2012).

US Energy Information Administration (2023). "As solar capacity grows, duck curves are getting deeper in California." Retrieved 07/02, 2023, from https://www.eia.gov/todayinenergy/detail.php?id=56880#.

Vallianos, C., A. Athienitis and B. Delcroix (2022). "Automatic generation of multi-zone RC models using smart thermostat data from homes." *Energy and Buildings 277*: 112571.

Villar, C. H., D. Neves and C. A. Silva (2017). "Solar PV self-consumption: An analysis of influencing indicators in the Portuguese context." *Energy strategy reviews 18*: 224-234.

Vivian, J., L. Croci and A. Zarrella (2022). "Experimental tests on the performance of an economic model predictive control system in a lightweight building." *Applied Thermal Engineering 213*: 118693.

Wang, D., Y. Chen, W. Wang, C. Gao and Z. Wang (2023). "Field test of Model Predictive Control in residential buildings for utility cost savings." *Energy and Buildings 288*: 113026.

Wang, D., W. Zheng, Z. Wang, Y. Wang, X. Pang and W. Wang (2023). "Comparison of reinforcement learning and model predictive control for building energy system optimization." *Applied Thermal Engineering 228*: 120430.

Wang, J., Z. Wei, Y. Zhu, C. Zheng, B. Li and X. Zhai (2023). "Demand response via optimal pre-cooling combined with temperature reset strategy for air conditioning system: A case study of office building." *Energy 282*: 128751.

Wang, J. C. (2019). "Energy consumption in elementary and high schools in Taiwan." *Journal of Cleaner Production 227*: 1107-1116.

Wang, Q., Y. Ding, X. Kong, Z. Tian, L. Xu and Q. He (2022). "Load pattern recognition based optimization method for energy flexibility in office buildings." *Energy 254*: 124475.

Wang, S. and Z. Ma (2008). "Supervisory and optimal control of building HVAC systems: A review." *Hvac&R Research 14(1)*: 3-32.

Weiß, T., A. M. Fulterer and A. Knotzer (2019). "Energy flexibility of domestic thermal loads–a building typology approach of the residential building stock in Austria." *Advances in Building Energy Research 13(1)*: 122-137.

Yang, S., A. Cannavale, D. Prasad, A. Sproul and F. Fiorito (2019). Numerical simulation study of BIPV/T double-skin facade for various climate zones in Australia: Effects on indoor thermal comfort. *Building Simulation*, Springer.

Yang, S., F. Fiorito, D. Prasad, A. Sproul and A. Cannavale (2021). "A sensitivity analysis of design parameters of BIPV/T-DSF in relation to building energy and thermal comfort performances." *Journal of building engineering 41*: 102426.

Yu, H. J. J. (2021). "System contributions of residential battery systems: New perspectives on PV self-consumption." *Energy Economics 96*: 105151.

Zhan, S., B. Dong and A. Chong (2023). "Improving energy flexibility and PV self-consumption for a tropical net zero energy office building." *Energy and Buildings 278*: 112606.

Zhang, K., A. Prakash, L. Paul, D. Blum, P. Alstone, J. Zoellick, R. Brown and M. Pritoni (2022). "Model predictive control for demand flexibility: Real-world operation of a commercial building with photovoltaic and battery systems." *Advances in Applied Energy 7*: 100099.

Zhao, G., J. Clarke, J. Searle, R. Lewis and J. Baker (2023). "Economic analysis of integrating photovoltaics and battery energy storage system in an office building." *Energy and Buildings 284*: 112885.

Zhao, J., L. Shi, J. Li, H. Li and Q. Han (2022). "A model predictive control regulation model for radiant air conditioning system based on delay time." *Journal of Building Engineering 62*: 105343.

Zhao, O., W. Zhang, L. Xie, W. Wang, M. Chen, Z. Li, J. Li, X. Wu, X. Zeng and S. Du (2022). "Investigation of indoor environment and thermal comfort of building installed with bifacial PV modules." *Sustainable Cities and Society 76*: 103463.

Zhou, Y. and S. Cao (2019). "Energy flexibility investigation of advanced grid-responsive energy control strategies with the static battery and electric vehicles: A case study of a high-rise office building in Hong Kong." *Energy Conversion and Management 199*: 111888.

Appendix A: School Building Details and Description

The case study school (Figure A-1) is a fully electric building located in Sainte Marthe-sur-le-Lac (near Montreal, QC, Canada). The school includes the following features:

- **Location:** Quebec, Canada
- **Electricity** only (no natural gas)
- In operation since **2017**
- **Floor Area**: 2,600 m^2 (28,000 ft^2) per storey with two storeys
- 24 regular classrooms with 4 mobile classrooms
- Approx. 570 students
- Double-glazed window with argon gas and low-e coating
- **Geothermal** - 28 loops with a depth of 100 m (330 ft)
- **ThermElect** for energy storage with a max 80 kW heat output
- **DHW:** two electric boilers with a capacity of 15 kW each
- **Heat Pumps**:
    - Large ground source water-to-water HP
    - 36 terminal fan coil units with heat pumps
- **Heating and cooling:**
    - All zones with **forced air systems**
    - Several zones with **radiant floors** (Gym and offices)
- Centralized **reverse flow heat recovery system** modulated based on schedule and CO_2 (100% outdoor air during our study period)

Figure A-1: Case study school – Horizon-du-Lac

Figure A-2 and A-3 present different zones in the school with the HVAC system in each zone. In this school, classrooms, kindergarten, and multipurpose room are equipped with convective system and the gym and offices also has radiant floor system.

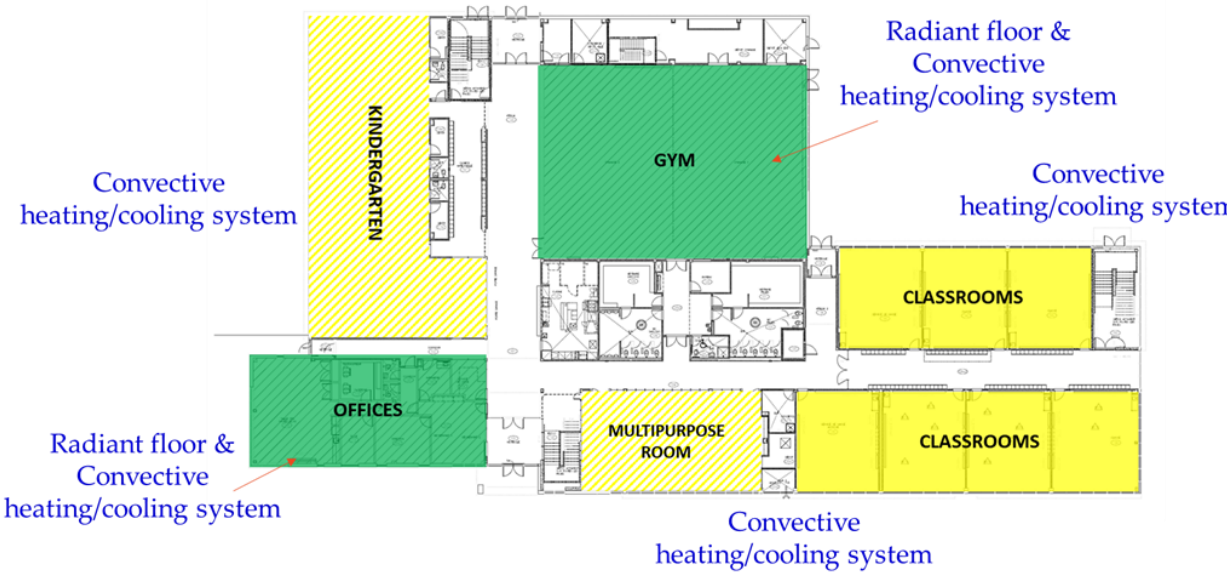

Figure A-2 : Plan view of the school and the HVAC system in each zones – First floor

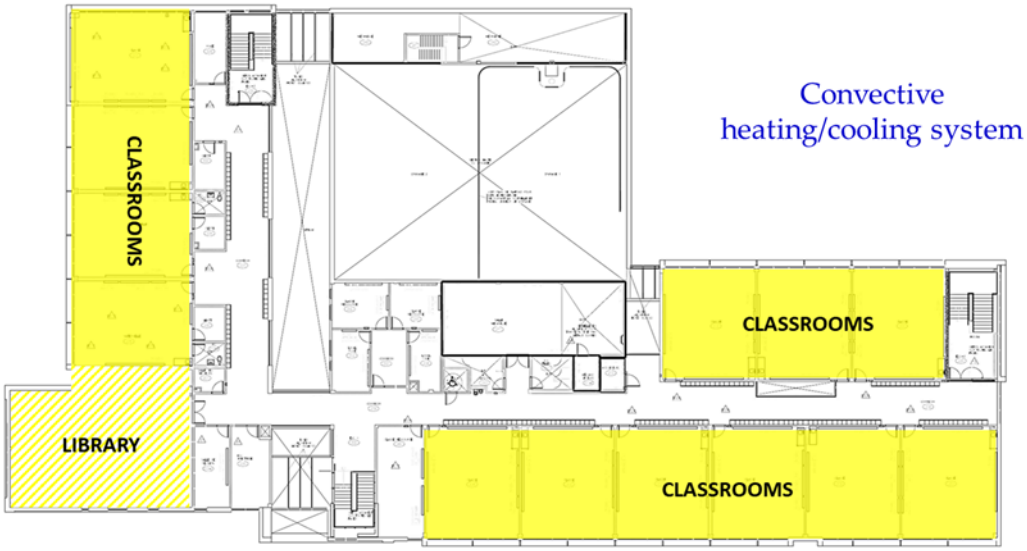

Figure A-3: Plan view of the school and the HVAC system in each zone – Second floor

Figure A-4 presents the gym, a classroom, and mechanical room in the school.

a) Gym

b) Classroom

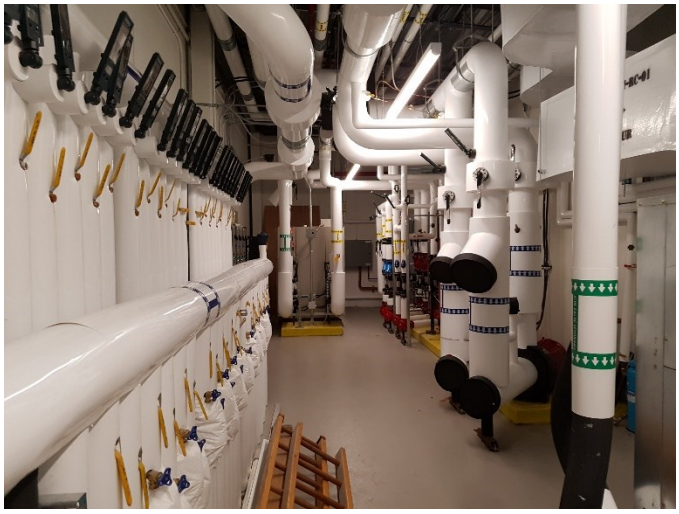

c) Mechanical room

Figure A-4: Some photo of the school building, the gym, a classroom, and the mechanical room

Appendix B: HVAC system Control

The HVAC system in the school includes a combination of a geothermal system, an electrically heated thermal energy storage device (ThermElect), a water-to-water heat pump (HP), several local water-to-air HPs, and a floor heating system. All heating systems are powered by electricity and connect to the electrical grid. The primary water-to-water HP, used for space heating, has a nominal output of 33 kW in two stages (16.5 kW per stage) and a maximum water supply temperature of 48.8 °C. The geothermal system with 28 loops generates low-temperature heat for the HP's evaporator side. ThermElect can preheat water for local water-to-air HPs and the water-

to-water HP. A three-way valve controls the HP's supply water temperature to the zones, with a maximum setting of 60 °C. Additionally, there's an integrated floor heating system for space heating and a convective ceiling system in offices and the gym, with thermostats regulating each zone's indoor temperature.

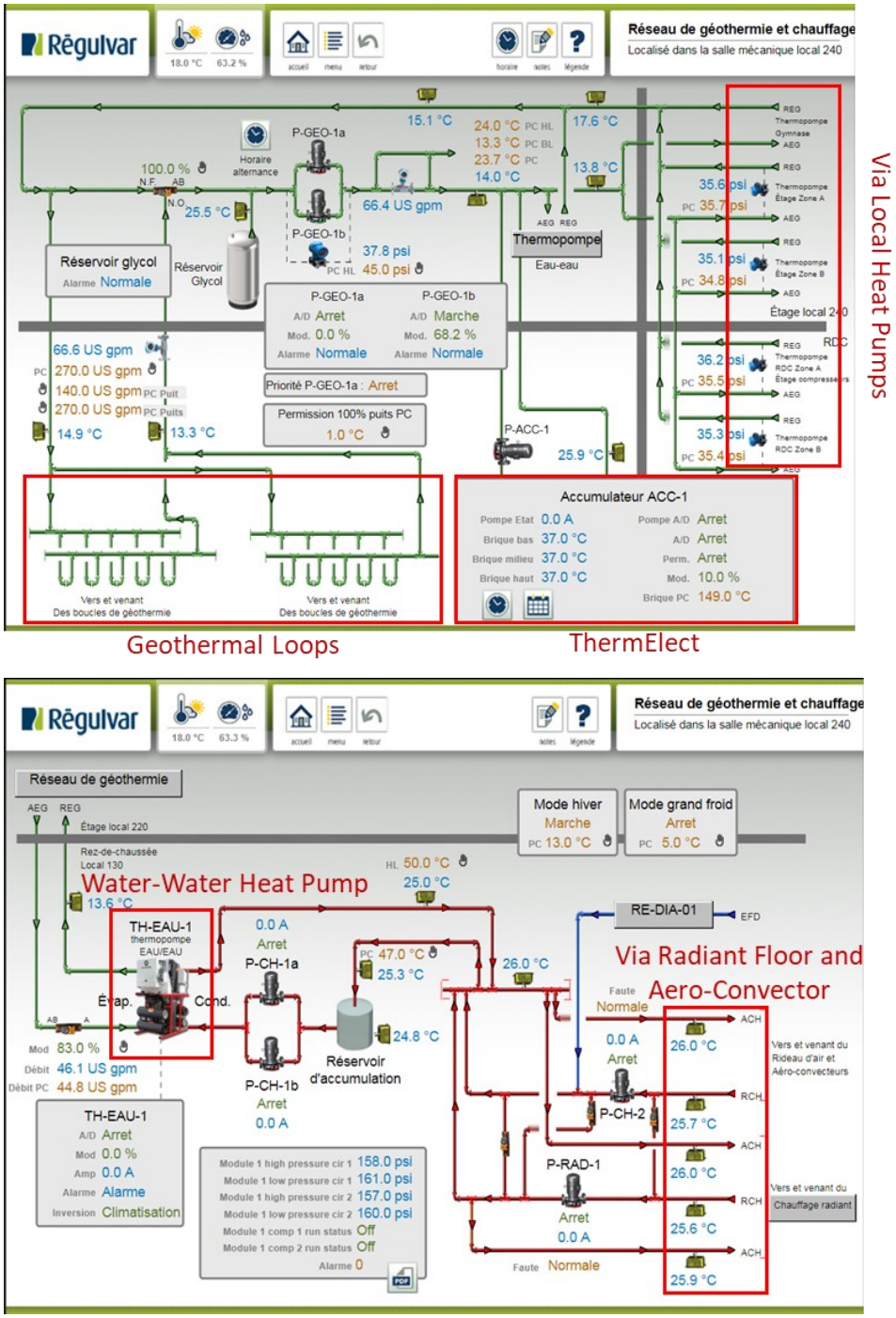

Figure B-1: HVAC system control graphical user interface

The HVAC system also has a reverse flow design with two exchangeable air intake and exhaust units, along with a two-positional damper located within the central air handling unit (shown in Figure B-2). Through changing position, this damper alternates the flow of outdoor intake and exhausted air thorough two heat exchanger cassettes to recover the heat (or cooling energy) stored within the cassette.

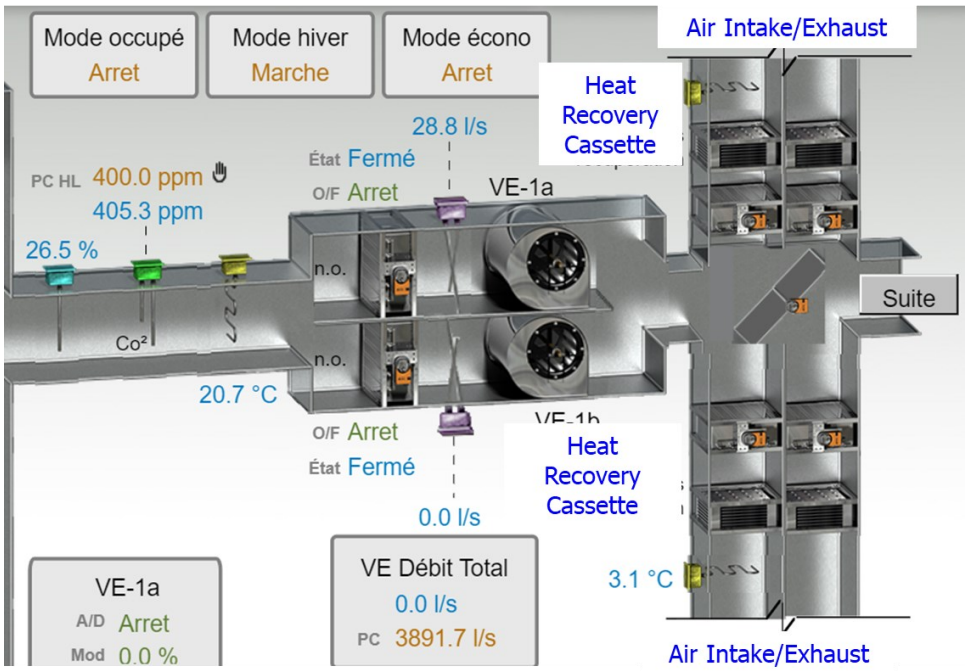

Figure B-2: Heat recovery system control graphical user interface

Table below presents the heat pumps' characteristics in the case study school building. There is a water-to-water heat pump for radiant floor system and aero-convectors, and 36 terminal fan coil units with water-to-air heat pumps.

TABLEAU DES THERMOPOMPES

NO.	LOCAL	MARQUE	MODÈLE	ÉLECTRICITÉ	VENTILATEUR D'ALIMENTATION				DÉBIT D'EAU GLYCOLÉE PROPYLÈNE GLYCOL 30% GPM (L/s)	DIMENSIONS ALIMENTATION	DIMENSIONS RETOUR	CHAUFFAGE				CAPACITÉ REFROIDISSEMENT (BTU/HR)
				VOLTAGE	DÉBIT (PCM)	DÉBIT A/N (9,5°C)(PCM)	P.S EXT. (poH²O)	MOTEUR (HP)				TEMP. ENTRÉE D'EAU °F (°C)	TEMP. SORTIE D'EAU °F (°C)	TEMP. ENTRÉE D'AIR °F (°C)	CAPACITÉ TOTAL (BTU/HR)	
TH-RC-01	GYMNASE 132	TRANE	GEVE 120	575/3/60	4510	2482	0,5	3	18 (1.134)	397x340	1008x987	27 (-2,8)	21,04 (-6,09)	70 (21)	80 840	114 900
TH-RC-02	MATERNELLE 119	TRANE	EXHF 036	208/1/60	1140	448	0,5	0,510	9 (0,567)	432x432	635x483	27 (-2,8)	22,87 (-5,07)	75 (23,9)	25 770	34 660
TH-RC-03	MATERNELLE 118	TRANE	EXHF 024	208/1/60	760	471	0,5	0,309	6 (0,378)	343x343	584x457	27 (-2,8)	23,22 (-4,88)	70 (21)	15 520	23 300
TH-RC-04	MATERNELLE 117	TRANE	EXHF 024	208/1/60	760	472	0,5	0,309	6 (0,378)	343x343	584x457	27 (-2,8)	23,22 (-4,88)	70 (21)	15 520	23 300
TH-RC-05	SERVICE DE GARDE 116	TRANE	EXHF 024	208/1/60	836	541	0,5	0,241	6 (0,378)	343x343	584x457	27 (-2,8)	23,13 (-4,93)	70 (21)	16 430	23 860
TH-RC-06	SALLE DES PROFS. 112	TRANE	EXHF 048	208/1/60	1520	442	0,5	0,751	12 (0,756)	457x457	749x533	27 (-2,8)	22,74 (-5,14)	70 (21)	34 920	46 310
TH-RC-07	SERV. DE GARDE 104 INFIRMERIE 105	TRANE	GEHE 006	208/1/60	200	51	0,506	0,083	1,5 (0,095)	292x292	508x356	27 (-2,8)	22,9 (-5,06)	70 (21)	5 870	7 110
TH-RC-08	CUISINE	TRANE	GEHE 012	208/1/60	400	26	0,532	0,125	3 (0,189)	292x292	508x356	27 (-2,8)	22,9 (-5,06)	70 (21)	8 760	11 200
TH-RC-09	SALLE POLY. 135	TRANE	EXHF 048	208/1/60	1520	1500	0,5	0,751	12 (0,756)	457x457	749x533	27 (-2,8)	22,74 (-5,14)	70 (21)	34 920	46 310
TH-RC-10	CORRIDOR 124, 123 VESTIAIRE 127 ET 129	TRANE	EXHF 024	208/1/60	836	174	0,5	0,241	6 (0,378)	343x343	584x457	27 (-2,8)	23,13 (-4,93)	70 (21)	16 430	23 860
TH-RC-11	SERVICE DE GARDE / MUSIQUE 139	TRANE	EXHF 024	208/1/60	760	445	0,5	0,309	6 (0,378)	343x343	584x457	27 (-2,8)	23,22 (-4,88)	70 (21)	15 520	23 300
TH-RC-12	SERVICE DE GARDE 140	TRANE	EXHF 024	208/1/60	760	440	0,5	0,309	6 (0,378)	343x343	584x457	27 (-2,8)	23,22 (-4,88)	70 (21)	15 520	23 300
TH-RC-13	CLASSE 142	TRANE	EXHF 024	208/1/60	760	445	0,5	0,309	6 (0,378)	343x343	584x457	27 (-2,8)	23,22 (-4,88)	70 (21)	15 520	23 300
TH-RC-14	CLASSE 143	TRANE	EXHF 024	208/1/60	760	440	0,5	0,309	6 (0,378)	343x343	584x457	27 (-2,8)	23,22 (-4,88)	70 (21)	15 520	23 300
TH-RC-15	CLASSE 144	TRANE	EXHF 024	208/1/60	760	445	0,5	0,309	6 (0,378)	343x343	584x457	27 (-2,8)	23,22 (-4,88)	70 (21)	15 520	23 300
TH-RC-16	CLASSE 145	TRANE	EXHF 024	208/1/60	760	440	0,5	0,309	6 (0,378)	343x343	584x457	27 (-2,8)	23,22 (-4,88)	70 (21)	15 520	23 300
TH-RC-17	CLASSE 146	TRANE	EXHF 030	208/1/60	1045	449	0,5	0,255	8,5 (0,410)	432x432	635x483	27 (-2,8)	22,40 (-5,33)	70 (21)	20 090	30 610
TH-RC-18	DIRECTION 106 PNE 111	TRANE	GEHE 009	208/1/60	300	32	0,258	0,083	2,25 (0,142)	292x292	508x356	27 (-2,8)	22,9 (-5,06)	70 (21)	6 630	8 620
TH-RC-19	SECRÉTARIAT 103	TRANE	GEHE 009	208/1/60	300	30	0,258	0,083	2,25 (0,142)	292x292	508x356	27 (-2,8)	22,9 (-5,06)	70 (21)	6 630	8 620
TH-ET-01	CLASSE 223	TRANE	EXHF 036	208/1/60	1026	438	0,5	0,402	9 (0,567)	432x432	635x483	27 (-2,8)	22,89 (-5,01)	70 (21)	25 280	34 240
TH-ET-02	CLASSE 226	TRANE	EXHF 024	208/1/60	760	461	0,5	0,309	6 (0,378)	343x343	584x457	27 (-2,8)	23,22 (-4,88)	70 (21)	15 520	23 300
TH-ET-03	CLASSE 227	TRANE	EXHF 024	208/1/60	760	461	0,5	0,309	6 (0,378)	343x343	584x457	27 (-2,8)	23,22 (-4,88)	70 (21)	15 520	23 300
TH-ET-04	CLASSE 228	TRANE	EXHF 024	208/1/60	760	464	0,5	0,309	6 (0,378)	343x343	584x457	27 (-2,8)	23,22 (-4,88)	70 (21)	15 520	23 300
TH-ET-05	CORRIDOR 201 ATRIUM 120	TRANE	EXHF 024	208/1/60	760	185	0,5	0,309	6 (0,378)	343x343	584x457	27 (-2,8)	23,22 (-4,88)	70 (21)	15 520	23 300
TH-ET-06	BIBLIOTHÈQUE 212	TRANE	EXHF 048	208/1/60	1672	728	0,5	0,376	12 (0,756)	457x457	749x533	27 (-2,8)	22,67 (-5,18)	70 (21)	34 030	48 000
TH-ET-07	CLASSE RESSOURCE 2XX	TRANE	GEHE 012	208/1/60	400	40	0,532	0,125	3 (0,189)	292x292	508x356	27 (-2,8)	22,9 (-5,06)	70 (21)	8 760	11 200
TH-ET-08	ADJ.DIR. 236, PNE 229 SALLE RÉUNION 212,1	TRANE	EXHF 018	208/1/60	627	51	0,5	0,094	4,5 (0,284)	343x343	584x457	27 (-2,8)	22,79 (-5,12)	70 (21)	12 910	18 510
TH-ET-09	CORRIDOR 202, 218 203, 205, 206, 136	TRANE	EXHF 024	208/1/60	760	239	0,5	0,309	6 (0,378)	343x343	584x457	27 (-2,8)	23,22 (-4,88)	70 (21)	15 520	23 300
TH-ET-10	CLASSE 204	TRANE	EXHF 024	208/1/60	760	449	0,5	0,309	6 (0,378)	343x343	584x457	27 (-2,8)	23,22 (-4,88)	70 (21)	15 520	23 300
TH-ET-11	CLASSE 209	TRANE	EXHF 024	208/1/60	760	449	0,5	0,309	6 (0,378)	343x343	584x457	27 (-2,8)	23,22 (-4,88)	70 (21)	15 520	23 300
TH-ET-12	CLASSE 215	TRANE	EXHF 024	208/1/60	760	449	0,5	0,309	6 (0,378)	343x343	584x457	27 (-2,8)	23,22 (-4,88)	70 (21)	15 520	23 300
TH-ET-13	CLASSE 214	TRANE	EXHF 024	208/1/60	760	440	0,5	0,309	6 (0,378)	343x343	584x457	27 (-2,8)	23,22 (-4,88)	70 (21)	15 520	23 300
TH-ET-14	CLASSE 217	TRANE	EXHF 024	208/1/60	760	449	0,5	0,309	6 (0,378)	343x343	584x457	27 (-2,8)	23,22 (-4,88)	70 (21)	15 520	23 300
TH-ET-15	CLASSE 216	TRANE	EXHF 024	208/1/60	760	440	0,5	0,309	6 (0,378)	343x343	584x457	27 (-2,8)	23,22 (-4,88)	70 (21)	15 520	23 300
TH-ET-16	CLASSE 219	TRANE	EXHF 024	208/1/60	760	449	0,5	0,309	6 (0,378)	343x343	584x457	27 (-2,8)	23,22 (-4,88)	70 (21)	15 520	23 300
TH-ET-17	CLASSE 218	TRANE	EXHF 024	208/1/60	760	440	0,5	0,309	6 (0,378)	343x343	584x457	27 (-2,8)	23,22 (-4,88)	70 (21)	15 520	23 300
TH-ET-18	CLASSE 220	TRANE	EXHF 030	208/1/60	1045	449	0,5	0,255	8,5 (0,410)	432x432	635x483	27 (-2,8)	22,40 (-5,33)	70 (21)	20 090	30 610

REMARQUE:

⚠1

• FAIRE LES AJUSTEMENTS NÉCESSAIRES AFIN QUE LE VENTILATEUR DE LA THERMOPOMPE FONCTIONNE À DÉBIT CONSTANT EN TOUT TEMPS.

• LES THERMOPOMPES TH-RC-06, TH-RC-07, TH-RC-08, TH-RC-18, TH-RC-19, TH-ET-07, TH-ET-08 SERONT FOURNIES AVEC SOUPAPE RÉGULATRICE DE DÉBIT D'EAU EN FONCTION DE LA PRESSION DE RÉFRIGÉRANT DE LA THERMOPOMPE (PAR MANUFACTURIER). CETTE SOUPAPE EST DONC FOURNIE PAR L'ENTREPRENEUR EN VENTILATION ET INSTALLÉE SUR LA TUYAUTERIE PAR L'ENTREPRENEUR EN CHAUFFAGE/REFOIDISSEMENT. L'ENTREPRENEUR EN VENTILATION EST RESPONSABLE DU RACCORDEMENT DU CAPILLAIRE DE LA SOUPAPE JUSQU'AU POINT DE RACCORDEMENT PRÉVU À CET EFFET SUR LE CONDENSEUR DE LA THERMOPOMPE ET L'AJUSTEMENT DU RESSORT DE LA SOUPAPE.

Appendix C: Sample of Python Codes for RC Model Identification, Weather Clustering, and MPC strategies

RC model Identification

```
"""
Variable Names
Uin: Conductance matrix input by user, upper triangle only, (nN x nN) (W/K)
U: Conductance matrix (symmetrical) with added capacitance for diagonal term, (nN x
nN) (W/K)
C: Capacitance vector, (nN x 1) (J/K)
F: Conductance matrix of nodes connected to a known temperature source, (nN x nM)
(W/K)
T: Temperature vector per timestep, (nT x nN) (degC)
TK: Temperature vector of known temperatures per timestep, (nT x nM) (degC)
Qin: Heat flow, only external sources, (nN x 1) (W)
Q: Heat flow vector + external sources + capacitance from previous timestep (implicit
only), (nN x 1) (W)

nN: Number of nodes
nM: Number of nodes with known temperatures
nT: Number of timesteps

Node Number: Object
0: effective room node, connected to capacitor and T_ambient (in the Ms)

Node Number with known temperatures: Object
0: ambient air
"""

def mU4C3(U_env, C_env, U_air, C_air, U_floor, C_floor,U_inf, dt):
    # Load dependencies
    from numpy import zeros
    from numpy import sum as npsum
    from numpy.linalg import inv

    # #### Control
    nN = 3          # number of nodes
    nM = 1          # number of nodes with known temperatures

    #%% Nodal Connections
    # Declare variables
    Uin = zeros((nN,nN))      # K/W
    F = zeros((nN,1))         # K/W
    C = zeros((nN,1))         # J/K

    # How are the nodes connected?
    Uin[0,1] = U_air    #(1/R + U + dx/kA)**-1
    Uin[1,2] = U_floor
#   Uin[1,2] = (1/U_air)**-1

    # Connected to temperature sources
    F[0,0] = U_env
    F[1,0] = U_inf
#    F[2] = 0 #(1/U_in)**-1

    # Nodes with capacitance
    C[0,0] = C_env
```

```
#    C[1] = 0
    C[1,0] = C_air
    C[2,0] = C_floor

    #%% U-matrix completion, and its inverse
    U = -Uin - Uin.T  # U is symmetrical, non-diagonals are -ve
    s = -npsum(U,1)
    for i in range(0,nN):
        U[i,i] = s[i] + F[i] + C[i]/dt
    U_inv = inv(U)

    #%% Ship it
    return (U_inv, F, C, nN, nM)
# Import dependencies
# import numpy as np
from numpy import reshape, multiply, dot, cos, pi, zeros, shape, tile

# Calculate temperatures for next timesteps: T(t+1) = U^-1 * Q(t)
# Seperated in case the explicit scheme is needed
def calcT(U_inv, F, C, Qint, Tt, TKt, dt):
    # Q-vector: Q = Qin + F*TM(t) + C/dt*T(t)
    nN = U_inv.shape[0]
    Q = Qint + reshape(dot(F,TKt),(nN,1)) + multiply(C/dt,reshape(Tt,(nN,1)))
    return (dot(U_inv, Q)).T

# Function to calculate future temperatures
def futureT(Q, initialT, TK, U_inv, F, C, nN, dt):
    ft, nM = shape(TK)           # Temperature matrices
    T = zeros((ft, nN)) # degC
    T[0,] = initialT

    for i in range(ft-1):  # Calculate future states
        T[i+1,] = calcT(U_inv, F, C, Q[i,].reshape(nN,1), T[i,].reshape(nN,1),
TK[i+1,].reshape(nM,1), dt)
    return T
# Generate a periodic input
def periodic(mean, diff, peak_time, period, dt, nt, days):
    # peak_time in hour of day; 3PM is 15
    # (period, dt, nt) in seconds; 1 day = 86400s
    # days in days, obviously
    theta = peak_time*pi/12
    omega = 2*pi/period
    return days*[mean + diff/2*cos(omega*dt*t - theta) for t in range(nt)]
# Linear ramps
def linearRamp(T_SP_day, T_SP_dT, setback_beg, setback_end, ramp_dur, dt, nt, days=1):
    # T_SP_day:    daytime setpoint to maintain
    # T_SP_dT:     setback amount
    # setback_beg: setback beginning time (occupancy departure)
    # setback_end: setback end time (occupancy arrival)
    # ramp_dur:    hours, ramp duration; "0" equals to a step change
    T_SP = zeros((nt,1)) # degC; Interior temperature setpoint per timestep
    for t in range(nt):
        time = t*dt/3600.
        if (setback_beg <= time and time < (setback_beg+ramp_dur)):              #
begin setback
            T_SP[t] = T_SP_day - (time-setback_beg)*T_SP_dT/ramp_dur
        elif ((setback_beg+ramp_dur) <= time or time < (setback_end-ramp_dur)): #
night time
            T_SP[t] = T_SP_day - T_SP_dT
        elif ((setback_end-ramp_dur) <= time and time < setback_end):            #
revert setback
            T_SP[t] = T_SP_day - (setback_end-time)*T_SP_dT/ramp_dur
```

```
        else:                                                                  # day
time
            T_SP[t] = T_SP_day
    return tile(T_SP, (days,1))
#Load Dependencies
import numpy as np
import matplotlib.pylab as plt
import matplotlib as mpl
# Plot in notebook; comment out the line below for windowed plots %matplotlib inline
# mpl.rc('figure', figsize=(10, 10))
from scipy.optimize import minimize
import pandas as pd
#from scipy.optimize import curve_fit
# Import mU1C1 script
import mU4C3
# Extra scripts to keep this notebook simple and tidy
import simfun
mpl.rc('figure', figsize=(10, 8))

#%%
# Temperatures and setpoints
T_amb = data['Tout'].values
T_opr = data['Tinside'].values
Diffuse_Solar_radiation = data['Diffuse Solar Radiation'].values
Direct_Solar_radiation = data['Direct Solar Radiation'].values
Power = data['Power'].values
People = data['People'].values

# Total
ntt = len(Power)
Q_total = np.zeros((ntt,3))
Q_total[:,0] = 0.4*Power
#Q_total[:,1] = 0#0.03*Power   #0.6*Power #+ Direct_Solar_radiation
Q_total[:,1] = Power #+0.2*Direct_Solar_radiation #Diffuse_Solar_radiation#
0.2*Direct_Solar_radiation #+ Diffuse_Solar_radiation + People#+
Direct_Solar_radiation
Q_total[:,2] = Power
#Q_total = data['Power'].values
# Number of timesteps = number of data points loaded
nt = len(Q_total)
split = int(4.2/7*nt) # use 3.5 days out of 5 for training, and the rest for cross-
validation
#Plot Imported Data
plt.figure()
plt.plot(Q_total[:,0],'b', lw=3,label='HP Power')
plt.plot(Q_total[:,1],'g', lw=3,label='HP Power')
#plt.plot(Diffuse_Solar_radiation,'m',lw=3, label='Diffuse Solar radiation')
#plt.plot(0.2*Direct_Solar_radiation,'y',lw=3, label='Direct Solar radiation')
#plt.plot(Equip,'r', label='Equipment')
plt.xlabel('Timestep', fontsize = 'large')
plt.ylabel('Heat, W', fontsize = 'large')
plt.legend(loc='best', fontsize = 'large')
plt.xlim(0,672)
plt.ylim(0,4500)
plt.grid()
plt.show()
#%%
plt.figure()
plt.plot(T_opr,'g',lw=3, label='Indoor Temperature')
plt.plot(T_amb,'b',lw=3, label='Outdoor Temperature')
plt.xlabel('Timestep', fontsize = 'large')
plt.ylabel('Temperature, Deg C', fontsize = 'large')
plt.legend(loc='best', fontsize = 'large')
```

```
plt.xlim(0,480)
plt.ylim(-30,25)
plt.grid()
plt.show()
#%%
#Cost functions for the calibration
# Euclidean distance based cost function
def costEuclidean(x, Q, initialT, TK, dt, testT):
    U_in, C_in = x
    U_inv, F, C, nN, nM = mU4C3.mU4C3(U_in, C_in, dt)
    # Calculate the future temperatures
    T = simfun.futureT(Q, initialT, TK, U_inv, F, C, nN, dt)
    err = T - testT                    # setpoint error
    return np.sqrt(np.dot(err.T, err)) # sqrt[sum(error^2)]
## NMBE based cost function [normalized mean bias error]
def costNMBE(x, Q, initialT, TK, dt, testT):
    U_in, C_in = x
    U_inv, F, C, nN, nM = mU4C3.mU4C3(U_in, C_in, dt)
    # Calculate the future temperatures
    T = simfun.futureT(Q, initialT, TK, U_inv, F, C, nN, dt)
    err = T - testT                    # setpoint error
    return np.abs(np.sum(err))/(np.mean(testT)*(len(testT)-1))
# CV(RMSE) based cost function
# [coefficient of variance of the root mean square error]
def costCVRMSE(x, Q, initialT, TK, dt, testT):
    U_env, C_env, U_air, C_air, U_floor, C_floor,U_inf= x
    U_inv, F, C, nN, nM = mU4C3.mU4C3(U_env, C_env, U_air, C_air, U_floor,
C_floor,U_inf, dt)
    # Calculate the future temperatures
    T = simfun.futureT(Q, initialT, TK, U_inv, F, C, nN, dt)
    err = T[:,1] - testT.squeeze()                  # setpoint error
    return 1/np.mean(testT)*np.sqrt(np.dot(err.T, err)/(len(testT)-2)) #-
np.std(T[:,0])

#%%
#x0 = [U_env, C_env, U_air, C_air, U_floor, C_floor,U_inf]
x0 = [50, 4.9e7, 2.4e3, 2.3e6, 50, 5e3,1000]              # initial guess
#x0 = [1000, 1.9e7, 1000, 0.3e7, 100]              # initial guess
iniT = np.array([[20 ,20,20]])
#iniT = [19,19]
# Extra arguments to send to cost function, Q_total, temperatures, timestep...
args = Q_total[0:split,:].reshape(split,3), iniT, T_amb[0:split].reshape(split,1), dt,
T_opr[0:split].reshape(split,1)
bnds = ((0, 100), (0, 1e10), (0, 1e8), (1e5, 1e10), (0, 1e6), (0, 1e10), (0, 1e6)) #
bounds, None = not bounded
# minimization algorithms. The "simplex-based" Nelder-Mead algorithm
res = minimize(costCVRMSE, x0, method='Nelder-Mead', args=args, options={'ftol': 1e-
12, 'disp': True, 'maxiter': 10000})
#res = minimize(costCVRMSE, x0, method='SLSQP', args=args, bounds=bnds,
options={'ftol': 1e-15, 'disp': True, 'maxiter': 2000, 'eps': 1.4901161193847656e-08})
print("Best values for U and C: %s" % res.x)
U_env_best, C_env_best, U2_air_best, C2_air_best ,U_floor_best, C_floor_best,
U_inf_best = res.x

# Calculate T for the U1C1 model using the obtained results
U_inv, F, C, nN, __ = mU4C3.mU4C3(U_env_best, C_env_best, U2_air_best, C2_air_best
,U_floor_best, C_floor_best, U_inf_best, dt)
T_train = simfun.futureT(args[0], args[1], args[2], U_inv, F, C, nN, dt)
T_cross = simfun.futureT(Q_total[split::].reshape(nt-split,3),
                         T_train[-1], T_amb[split::].reshape(nt-split,1),
                         U_inv, F, C, nN, dt)
```

Clustering:

```
import numpy as np
import pandas as pd
import matplotlib.pyplot as plt
from matplotlib.ticker import MaxNLocator
from sklearn.cluster import KMeans
from sklearn.preprocessing import MinMaxScaler
from sklearn.metrics import silhouette_score
from sklearn.manifold import TSNE
from google.colab import data_table

def set_plot_info(ax, title='', xlabel='', ylabel='', xlim=[], ylim=[], xticks=[],
yticks=[]):
    # set main plot attributes
    if len(title) > 0:
        ax.set_title(title)
    if len(xticks) > 0:
        ax.set_xticks(xticks)
        ax.set_xticklabels([str(n) for n in xticks])
    if len(yticks) > 0:
        ax.set_yticks(yticks)
        ax.set_yticklabels([str(n) for n in yticks])
    if len(xlim) > 0:
        ax.set_xlim(xlim)
    if len(ylim) > 0:
        ax.set_ylim(ylim)
        print('set ylim')
    if len(xlabel) > 0:
        ax.set_xlabel(xlabel)
    if len(ylabel) > 0:
        ax.set_ylabel(ylabel)

def text_on_plot(ax, text, x_pos_ratio=0.0, y_pos_ratio=1.0):
    ya, yb = ax.get_ylim()
    xa, xb = ax.get_xlim()
    txt_handle = ax.text(xa + x_pos_ratio * (xb - xa), ya + y_pos_ratio * (yb - ya),
text, verticalalignment ='top', horizontalalignment='left')
    return txt_handle

# assign function
def df_assign(df):
    var_list=[]
    for i in range(len(df.columns)):
        var_list.append(df.iloc[:,i].to_numpy())
    return var_list

# data
def load_data(source='pkl'):
    if source != 'pkl':
        df = pd.read_excel (r'vl_cluster_winter.xlsx',0)
        col = df.columns[0]
        df[col] = pd.to_datetime(df[col], format='%Y-%m-%d %H:%M:%S:%f')
        df = df.set_index(df[col])
        df = df.drop(columns=col, axis=1)
        df[df>1e6]=np.nan
        df.to_pickle('vl_cluster_winter.pkl')

    else:

        df = pd.read_pickle('vl_cluster_winter.pkl')

    return df
```

```
df = load_data(source='excel')
#df = load_data(source='pkl')


# define the model inputs
prod = df[["GHI"]].sum(axis=1)
cons = df[["GHI"]].sum(axis=1)
df = pd.concat([prod, cons], axis=1, sort=False)
df.columns = 'prod, cons'.split(', ')

#df = df['2022-01-01':'2023-01-01']
df_hourly = df.resample('H').mean()
df_hourly['hour'] = df_hourly.index.hour


df_prod =df_hourly[[df_hourly.columns[0], 'hour']]
df_prod.index = df_prod.index.date
df_prod_pivot = df_prod.pivot(columns='hour')

df_cons =df_hourly[[df_hourly.columns[1], 'hour']]
df_cons.index = df_cons.index.date
df_cons_pivot = df_cons.pivot(columns='hour')


#PV GEN
# parameter selection
df_pivot = df_prod_pivot #here choose what is going to be clustered
for col in df_prod_pivot.columns: #here put the other param if pivoting
    df_pivot[col]=df_prod_pivot[col] #here put the other param if pivoting

# to be renamed after parameter selection
param = 'PV Generation'

# colors
col_list = []
for i, col in enumerate(df.columns):
    col_list.append( (param, i) )
df.columns = col_list
color_list = ['darkblue', 'darkred', 'darkgreen', 'orange', 'purple','yellow', 'cyan',
'black', 'magenta', 'gray', 'brown', 'pink', 'violet']

# number of clusters
m_cluster = 3

# make copy to df_pivot for cluster analysis
X = df_pivot.values.copy()
sc = MinMaxScaler()
X = sc.fit_transform(X)
silhouette_scores = []
n_cluster_list = np.arange(2,13).astype(int)

# k-means
kmeans = KMeans(n_clusters=m_cluster, init='k-means++', max_iter=100000, n_init=1,
verbose=0, random_state=10)
cluster_found = kmeans.fit_predict(X)
cluster_found_sr = pd.Series(cluster_found, name='cluster')
df_pivot = df_pivot.set_index(cluster_found_sr, append=True )
cluster_values = sorted(df_pivot.index.get_level_values('cluster').unique())

# average silhouette test
for n_cluster in n_cluster_list:
    # initiate k-means with the same random state
```

```
    kmeans = KMeans(n_clusters=n_cluster, init='k-means++', max_iter=100000, n_init=1,
verbose=0, random_state=10)
    cluster_found = kmeans.fit_predict(X)
    silhouette_scores.append(silhouette_score(X, kmeans.labels_))

# plot
fig = plt.figure(constrained_layout=False, figsize=(14,10))
gs = fig.add_gridspec(nrows=2, ncols=2)
ax0 = fig.add_subplot(gs[:-1, :]) # traces and centroids
plt.xticks(fontsize= 20)
plt.yticks(fontsize= 20)
plt. xlabel('x-axis', fontsize=24)
plt. ylabel('y-axis', fontsize=24)
ax1 = fig.add_subplot(gs[-1, 0])  # average silhouette
ax2 = fig.add_subplot(gs[-1, 1])  # centroids

for cluster, color in zip(cluster_values, color_list):
    df_pivot.xs(cluster, level=1).T.plot(ax=ax0, legend=False, alpha=0.15,
color=color, label= f'Cluster (cluster)', lw=2)
    df_pivot.xs(cluster, level=1).median().plot(ax=ax0, color=color, alpha=1, ls='-',
lw = 2)
    df_pivot.xs(cluster, level=1).median().plot(ax=ax2, color=color, alpha=1, ls='-',
lw=2 )

# ax0: to be renamed and scaled
set_plot_info(ax0, 'Daily profile of ' + param + ' - ' + str(m_cluster) + ' Clusters
','Time (Hour)', 'GHI (W/m^2)', [0, 23], [0,700], range(0,24,2))
plt. xlabel('x-axis', fontsize=24)
plt. ylabel('y-axis', fontsize=24)
# ax1
ax1.plot(silhouette_scores, color='darkblue', lw=1)
ax1.plot(silhouette_scores,'o', color = 'darkred')
set_plot_info(ax1,'Average Silhouette','Number of Clusters','Average Silhouette', [2,
10], [])
ax1.xaxis.set_major_locator(MaxNLocator(integer=True))
plt. xlabel('x-axis', fontsize=24)
plt. ylabel('y-axis', fontsize=24)
# ax2: to be renamed and scaled
set_plot_info(ax2, 'Daily Profiles', 'Hour', 'kW', [0, 23], [0,1000], range(0,24,2))
plt. xlabel('x-axis', fontsize=24)
plt. ylabel('y-axis', fontsize=24)
# validating results with t-SNE
tsne = TSNE()
results_tsne = tsne.fit_transform(X)

# summary text
dpt_text = ''
for cluster, color in zip(cluster_values, color_list):
    level_list = df_pivot.index.get_level_values('cluster').to_list()
    pt_idx = [i for i, lv in enumerate(level_list) if lv == cluster]
    X = results_tsne[pt_idx,0]
    Y = results_tsne[pt_idx,1]
    print(len(pt_idx), 'days in cluster',cluster+1)
    # summary text on the main plot ax0
    dpt_text += str(cluster+1) +' - '+  color + ' cluster' +' : '+ str(len(pt_idx)) +'
days \n'
#text_on_plot(ax0, 'Cluster Analysis Results:\n' + dpt_text, 0, 1)

plt.style.use('seaborn')
plt.tight_layout()
plt.show()
print('\n')
```

```
#df11 = df_pivot.xs(3, level=1).median()
#print(df11)


#-------------------------------------------------------------------------------------------
-------------------------------------------------------------------------
#CONS
# parameter selection
df_pivot = df_cons_pivot #here choose what is going to be clustered
for col in df_cons_pivot.columns: #here put the other param
    df_pivot[col]=df_cons_pivot[col] #here put the other param

# to be renamed after parameter selection
param = 'Consumption'

# colors
col_list = []
for i, col in enumerate(df.columns):
    col_list.append( (param, i) )
df.columns = col_list
color_list = ['darkblue', 'darkred', 'darkgreen', 'orange', 'purple','yellow', 'cyan',
'black', 'magenta', 'gray', 'brown', 'pink', 'violet']

# number of clusters
m_cluster = 4

# make copy to df_pivot for cluster analysis
X = df_pivot.values.copy()
sc = MinMaxScaler()
X = sc.fit_transform(X)
silhouette_scores = []
n_cluster_list = np.arange(2,13).astype(int)

# k-means
kmeans = KMeans(n_clusters=m_cluster, init='k-means++', max_iter=100000, n_init=1,
verbose=0, random_state=10)
cluster_found = kmeans.fit_predict(X)
cluster_found_sr = pd.Series(cluster_found, name='cluster')
df_pivot = df_pivot.set_index(cluster_found_sr, append=True )
cluster_values = sorted(df_pivot.index.get_level_values('cluster').unique())

# average silhouette test
for n_cluster in n_cluster_list:
    # initiate k-means with the same random state
    kmeans = KMeans(n_clusters=n_cluster, init='k-means++', max_iter=100000, n_init=1,
verbose=0, random_state=10)
    cluster_found = kmeans.fit_predict(X)
    silhouette_scores.append(silhouette_score(X, kmeans.labels_))

# plot
fig = plt.figure(constrained_layout=False, figsize=(9,6))
gs = fig.add_gridspec(nrows=2, ncols=2)
ax0 = fig.add_subplot(gs[:-1, :]) # traces and centroids
ax1 = fig.add_subplot(gs[-1, 0])  # average silhouette
ax2 = fig.add_subplot(gs[-1, 1])  # centroids

for cluster, color in zip(cluster_values, color_list):
    df_pivot.xs(cluster, level=1).T.plot(ax=ax0, legend=False, alpha=0.15,
color=color, label= f'Cluster (cluster)', lw=1)
    df_pivot.xs(cluster, level=1).median().plot(ax=ax0, color=color, alpha=1, ls='-',
lw = 1)
    df_pivot.xs(cluster, level=1).median().plot(ax=ax2, color=color, alpha=1, ls='-',
lw=1 )
```

```
# ax0: to be renamed and scaled
set_plot_info(ax0, 'Daily profile of ' + param + ' - ' + str(m_cluster) + ' Clusters
', 'Hour', 'kW', [0, 23], [10,25], range(0,24,1))
# ax1
ax1.plot(silhouette_scores, color='darkblue', lw=1)
ax1.plot(silhouette_scores,'o', color = 'darkred')
set_plot_info(ax1,'Average Silhouette','Number of Clusters','Average Silhouette', [2,
10], [])
ax1.xaxis.set_major_locator(MaxNLocator(integer=True))
# ax2: to be renamed and scaled
set_plot_info(ax2, 'Daily Profiles', 'Hour', 'kW', [0, 23], [0,50], range(0,24,2))

# validating results with t-SNE
tsne = TSNE()
results_tsne = tsne.fit_transform(X)

# summary text
dpt_text = ''
for cluster, color in zip(cluster_values, color_list):
    level_list = df_pivot.index.get_level_values('cluster').to_list()
    pt_idx = [i for i, lv in enumerate(level_list) if lv == cluster]
    X = results_tsne[pt_idx,0]
    Y = results_tsne[pt_idx,1]
    print(len(pt_idx), 'days in cluster',cluster+1)
    # summary text on the main plot ax0
    dpt_text += str(cluster+1) +' - '+  color + ' cluster' +' : '+ str(len(pt_idx)) +'
days \n'
text_on_plot(ax0, 'Cluster Analysis Results:\n' + dpt_text, 0, 1)

plt.style.use('seaborn-whitegrid')
plt.tight_layout()
plt.show()
print('\n')


#PV GEN AGAINST CONS
# parameter selection
df_pivot = df_prod_pivot #here choose what is going to be clustered
for col in df_cons_pivot.columns: #here put the other param
    df_pivot[col]=df_cons_pivot[col] #here put the other param

# to be renamed after parameter selection
param = 'PV Generation'

# colors
col_list = []
for i, col in enumerate(df.columns):
    col_list.append( (param, i) )
df.columns = col_list
color_list = ['darkblue', 'darkred', 'darkgreen', 'orange', 'purple','yellow', 'cyan',
'black', 'magenta', 'gray', 'brown', 'pink', 'violet']

# number of clusters
m_cluster = 6

# make copy to df_pivot for cluster analysis
X = df_pivot.values.copy()
sc = MinMaxScaler()
X = sc.fit_transform(X)
silhouette_scores = []
n_cluster_list = np.arange(2,13).astype(int)
```

```
# k-means
kmeans = KMeans(n_clusters=m_cluster, init='k-means++', max_iter=100000, n_init=1,
verbose=0, random_state=10)
cluster_found = kmeans.fit_predict(X)
cluster_found_sr = pd.Series(cluster_found, name='cluster')
df_pivot = df_pivot.set_index(cluster_found_sr, append=True )
cluster_values = sorted(df_pivot.index.get_level_values('cluster').unique())

# average silhouette test
for n_cluster in n_cluster_list:
    # initiate k-means with the same random state
    kmeans = KMeans(n_clusters=n_cluster, init='k-means++', max_iter=100000, n_init=1,
verbose=0, random_state=10)
    cluster_found = kmeans.fit_predict(X)
    silhouette_scores.append(silhouette_score(X, kmeans.labels_))

# plot
fig = plt.figure(constrained_layout=False, figsize=(9,6))
gs = fig.add_gridspec(nrows=2, ncols=2)
ax0 = fig.add_subplot(gs[:-1, :]) # traces and centroids
ax1 = fig.add_subplot(gs[-1, 0])  # average silhouette
ax2 = fig.add_subplot(gs[-1, 1])  # centroids

for cluster, color in zip(cluster_values, color_list):
    df_pivot.xs(cluster, level=1).T.plot(ax=ax0, legend=False, alpha=0.15,
color=color, label= f'Cluster (cluster)', lw=1)
    df_pivot.xs(cluster, level=1).median().plot(ax=ax0, color=color, alpha=1, ls='-',
lw = 1)
    df_pivot.xs(cluster, level=1).median().plot(ax=ax2, color=color, alpha=1, ls='-',
lw=1 )

# ax0: to be renamed and scaled
set_plot_info(ax0, 'Daily profile of ' + param + ' - ' + str(m_cluster) + ' Clusters
', 'Hour', 'GHI (W/m^2)', [0, 24], [0,1000], range(0,24,1))
# ax1
ax1.plot(silhouette_scores, color='darkblue', lw=1)
ax1.plot(silhouette_scores,'o', color = 'darkred')
set_plot_info(ax1,'Average silhouette index','K (Number of Clusters)','Average
Silhouette', [2, 10], [])
ax1.xaxis.set_major_locator(MaxNLocator(integer=True))
# ax2: to be renamed and scaled
set_plot_info(ax2, 'Daily Profiles', 'Hour', 'kW', [0, 23], [0,100], range(0,24,2))

# validating results with t-SNE
tsne = TSNE()
results_tsne = tsne.fit_transform(X)

# summary text
dpt_text = ''
for cluster, color in zip(cluster_values, color_list):
    level_list = df_pivot.index.get_level_values('cluster').to_list()
    pt_idx = [i for i, lv in enumerate(level_list) if lv == cluster]
    X = results_tsne[pt_idx,0]
    Y = results_tsne[pt_idx,1]
    print(len(pt_idx), 'days in cluster',cluster+1)
    # summary text on the main plot ax0
    dpt_text += str(cluster+1) +' - '+  color + ' cluster' +' : '+ str(len(pt_idx)) +'
days \n'
text_on_plot(ax0, 'Cluster Analysis Results:\n' + dpt_text, 0, 1)

plt.style.use('seaborn-whitegrid')
plt.tight_layout()
plt.show()
```

```
print('\n')

#df11 = df_pivot.xs(3, level=1).median()
#print(df11)



# parameter selection
df_pivot = df_cons_pivot #here choose what is going to be clustered
for col in df_prod_pivot.columns: #here put the other param
    df_pivot[col]=df_prod_pivot[col] #here put the other param

# to be renamed after parameter selection
param = 'Consumption'

# colors
col_list = []
for i, col in enumerate(df.columns):
    col_list.append( (param, i) )
df.columns = col_list
color_list = ['darkblue', 'darkred', 'darkgreen', 'orange', 'purple','yellow', 'cyan',
'black', 'magenta', 'gray', 'brown', 'pink', 'violet']

# number of clusters
m_cluster = 2

# make copy to df_pivot for cluster analysis
X = df_pivot.values.copy()
sc = MinMaxScaler()
X = sc.fit_transform(X)
silhouette_scores = []
n_cluster_list = np.arange(2,13).astype(int)

# k-means
kmeans = KMeans(n_clusters=m_cluster, init='k-means++', max_iter=100000, n_init=1,
verbose=0, random_state=10)
cluster_found = kmeans.fit_predict(X)
cluster_found_sr = pd.Series(cluster_found, name='cluster')
df_pivot = df_pivot.set_index(cluster_found_sr, append=True )
cluster_values = sorted(df_pivot.index.get_level_values('cluster').unique())

# average silhouette test
for n_cluster in n_cluster_list:
    # initiate k-means with the same random state
    kmeans = KMeans(n_clusters=n_cluster, init='k-means++', max_iter=100000, n_init=1,
verbose=0, random_state=10)
    cluster_found = kmeans.fit_predict(X)
    silhouette_scores.append(silhouette_score(X, kmeans.labels_))

# plot
fig = plt.figure(constrained_layout=False, figsize=(14,10))
gs = fig.add_gridspec(nrows=2, ncols=2)
ax0 = fig.add_subplot(gs[:-1, :]) # traces and centroids
plt.xticks(fontsize= 20)
plt.yticks(fontsize= 20)
plt. xlabel('x-axis', fontsize=24)
plt. ylabel('y-axis', fontsize=24)
ax1 = fig.add_subplot(gs[-1, 0])  # average silhouette
ax2 = fig.add_subplot(gs[-1, 1])  # centroids

for cluster, color in zip(cluster_values, color_list):
    df_pivot.xs(cluster, level=1).T.plot(ax=ax0, legend=False, alpha=0.15,
color=color, label= f'Cluster (cluster)', lw=2)
```

```
    df_pivot.xs(cluster, level=1).median().plot(ax=ax0, color=color, alpha=1, ls='-',
lw = 3)
    df_pivot.xs(cluster, level=1).median().plot(ax=ax2, color=color, alpha=1, ls='-',
lw=3 )
#print(df_pivot.xs(1, level=1).median())
#print(data_table.DataTable(df_pivot.xs(1, level=1).median()))

#df11 = df_pivot.xs(3, level=1).median()
#print(df11)
# ax0: to be renamed and scaled
set_plot_info(ax0, [], 'Time (Hour)', 'Power (kW)', [0, 23], [0,2.5], range(0,24,2))

ax0.yaxis.set_major_locator(MaxNLocator(integer=True))
# ax1
ax1.plot(silhouette_scores, color='black', lw=3)
ax1.plot(silhouette_scores,'o', color = 'darkblue')
set_plot_info(ax1,'Average silhouette index','K (Number of Clusters)','Average
silhouette index', [1, 10], [])
ax1.xaxis.set_major_locator(MaxNLocator(integer=True))
#ax2: to be renamed and scaled
#set_plot_info(ax2, 'Daily Profiles', 'Time (Hour)', 'Indoor Temperature (˚C)', [0,
23], [0,150], range(0,24,2))
plt. xlabel('x-axis', fontsize=24)
plt. ylabel('y-axis', fontsize=24)
# validating results with t-SNE
tsne = TSNE()
results_tsne = tsne.fit_transform(X)

# summary text
dpt_text = ''
for cluster, color in zip(cluster_values, color_list):
    level_list = df_pivot.index.get_level_values('cluster').to_list()
    pt_idx = [i for i, lv in enumerate(level_list) if lv == cluster]
    X = results_tsne[pt_idx,0]
    Y = results_tsne[pt_idx,1]
    print(len(pt_idx), 'days in cluster',cluster+1)
    # summary text on the main plot ax0
    dpt_text += str(cluster+1) +' - '+  color + ' cluster' +' : '+ str(len(pt_idx)) +'
days \n'
text_on_plot(ax0, 0, 1)

plt.style.use('seaborn-whitegrid')
plt.tight_layout()
plt.show()
print('\n')
```

MPC Code:

```
import numpy as np
import pandas as pd
import cvxpy as cp
import matplotlib.pyplot as plt
#import scipy.optimize as so
#from numpy.linalg import norm as norm2
#from sklearn.model_selection import train_test_split as tts
#from sklearn.metrics import mean_squared_error
#from sklearn.metrics import r2_score
#from math import sqrt
#from google.colab import files
#import io
import importlib
importlib.reload(plt)
```

```
"""#**Data**"""


#%%

def df_assign(df):
    var_list=[]
    for i in range(len(df.columns)):
        var_list.append(df.iloc[:,i].to_numpy())
    return var_list
# process data
#data = files.upload()
df = pd.read_excel(r'Feb.xlsx') #import data
col = df.columns[0]
df[col] = pd.to_datetime(df[col], format='%Y-%m-%d %H:%M:%S') #change to datetime
df = df.set_index(df[col])
df = df.drop(columns=col, axis=1)
dt = 900  #sampling rate (sec)
Tout = df[["Text"]].sum(axis=1) #outside ambient temperature
Tgrd = df[['Tgrd']] #ground temperature
GVI = df[["Sol.Vert"]].sum(axis=1) * 4 #global vertical irradiance
GVI[GVI<0] = 0
GHI = df[["Sol.Hor"]].sum(axis=1) * 4 #global horizontal irradiance
GHI[GHI<0] = 0
P_pv = df[["PV-1"]].sum(axis=1) * 0 #total PV generation
P_tot = df[["TOT-1"]].sum(axis=1) * 4 #total electrical load
Q_sol = GVI * Awin #total incident solar radiation
Q_hp = P_hp * COP #heat from heat pump
P_heat = P_bb1 + P_bb2 + P_bb3 + P_hp

#%%
"""#**Simulation Setup**"""

# parameters
sph = 4 #steps per hour
ph = int(len(df_sim.index)-1) #prediction horizon (number of steps)
num_day = int(ph*900/3600/24) #prediction horizon (number of days)
control_factor = 4
ch = int(ph/control_factor) #control horizon (number of steps)
st = 1 #start point of algorithm
t = (np.arange(ph))*900/3600*4 #time array
#%%
"""#**Predictive Control**"""
#Business as Usual case

# states, inputs and disturbances
nx, nu, nd = 4, 4, 4 #third-order(3) + battery(1)
x = cp.Variable((nx, ph))
u = cp.Variable((nu, ph))
d = cp.Variable((nd, ph))

comfort_min, comfort_max = 18*np.ones(ph), 27*np.ones(ph) #thermal comfort boundaries
for i in range(num_day):
  comfort_min[int(sph*(24*i+6)):int(sph*(24*i+18))] = 21
  comfort_max[int(sph*(24*i+6)):int(sph*(24*i+18))] = 24
comfort_base_min, comfort_base_max = 16*np.ones(ph), 18*np.ones(ph)

price = 1*np.ones(ph) #price of consumption (For BAU)
#price = 4.33*np.ones(ph) #price of consumption (Correct)
#for i in range(num_day):
  #price[int(sph*(24*i+6)):int(sph*(24*i+9))] = 50.65
  #price[int(sph*(24*i+16)):int(sph*(24*i+20))] = 50.65
```

```
penalty = 2000*100*np.ones(ph) #comfort violation penalty
penalty_base = 100*100*np.ones(ph)
#penalty_peak = 100*10 #penalty of peak demand
penalty_peak = 1 #penalty of peak demand (For BAU)
constraints = cons = []

cons.append(x[0,0] == 18.3,)
cons.append(x[1,0] == 17.9,)
cons.append(x[2,0] == 17,)

cons.append(u[0,:] >= heating_min,)
cons.append(u[0,:] <= heating_max,)
cons.append(u[1,:] >= heating_min,)
cons.append(u[1,:] <= heating_max,)
cons.append(u[2,:] >= heating_min,)
cons.append(u[2,:] <= heating_max,)

cons.append(d[0,:] == df_sim['Tout'][st:st+ph],) #ambient air temperature
cons.append(d[1,:] == df_sim['P_pv'][st:st+ph],) #PV generation
cons.append(d[2,:] == df_sim['Q_sol'][st:st+ph],) #solar gains
cons.append(d[3,:] == df_sim['Tgrd'][st:st+ph],) #ground temperature

cost = 0 #cost initialization

for j in range(0,control_factor): #control horizon loop
  cons.append(x[0,ch*j] == x[0,ch*j-1],) #initialization of temp1
  cons.append(x[1,ch*j] == x[1,ch*j-1],) #initialization of temp2
  cons.append(x[2,ch*j] == x[2,ch*j-1],) #initialization of temp2
  cons.append(x[3,ch*j] == x[3,ch*j-1],) #initialization of battery soc

  for k in range((ch*j)+1,ch*(j+1)): #step loop
    cons.append(x[0,k] == x[0,k-1] + (dt/C1)*(u[0,k] + (d[0,k]-x[0,k-1])/R1 + (x[1,k-
1]-x[0,k-1])/R2),) #state estimator 0
    cons.append(x[1,k] == x[1,k-1] + (dt/C2)*(u[1,k] + (d[0,k]-x[1,k-1])/R3 + (x[0,k-
1]-x[1,k-1])/R2 + (x[2,k-1]-x[1,k-1])/R4),) #state estimator 1
    cons.append(x[2,k] == x[2,k-1] + (dt/C3)*(u[2,k] + alpha3*d[2,k] + (x[1,k-1]-
x[2,k-1])/R4),) #state estimator 2
    #cons.append(x[3,k] == x[3,k-1] + (u[3,k]*dt,) #state estimator 3

    #cons.append(x[0,k] == x[0,k-1] + (dt/C1)*(u[0,k] + alpha1*d[2,k] + (d[0,k]-x[0,k-
1])/R1 + (x[1,k-1]-x[0,k-1])/R4 + (x[2,k-1]-x[0,k-1])/R5),) #state estimator 0
    #cons.append(x[1,k] == x[1,k-1] + (dt/C2)*(u[1,k] + alpha2*d[2,k] + (d[0,k]-x[1,k-
1])/R2 + (x[0,k-1]-x[1,k-1])/R4 + (x[2,k-1]-x[1,k-1])/R6),) #state estimator 1
    #cons.append(x[2,k] == x[2,k-1] + (dt/C3)*(u[2,k] + alpha3*d[2,k] + (d[0,k]-x[2,k-
1])/R3 + (x[0,k-1]-x[2,k-1])/R5 + (x[1,k-1]-x[2,k-1])/R6 + (d[3,k]-x[2,k-1])/R7),)
#state estimator 2
    #cons.append(x[3,k] == x[3,k-1] + (u[3,k]*dt,) #state estimator 3

    cost += (u[0,k] + u[1,k] + u[2,k]) * price[k] #minimize heating energy cost based
on rate flex-M (For BAU)
    #cost += (u[0,k] + u[1,k] + u[2,k]) * 100*price[k] #minimize heating energy cost
based on rate flex-M (Correct)

    cost += cp.norm2(u[0,k] + u[1,k] + u[2,k] + u[3,k] - d[1,k]) #maximize self-
consumtion

    cost += cp.maximum(comfort_min[k] - x[0,k], 0, x[0,k] - comfort_max[k]) *
penalty[k] #penalize comfort violation
    cost += cp.maximum(comfort_min[k] - x[1,k], 0, x[1,k] - comfort_max[k]) *
penalty[k]
    cost += cp.maximum(comfort_base_min[k] - x[2,k], 0, x[2,k] - comfort_base_max[k])
* penalty_base[k]
```

```
    cost += cp.norm2(u[0,k] - u[0,k-1]) #penalize high slew rate
    cost += cp.norm2(u[1,k] - u[1,k-1])
    cost += cp.norm2(u[2,k] - u[2,k-1])
    cost += cp.norm2(u[3,k] - u[3,k-1])

  cost += (cp.norm_inf(u[0,:]) + cp.norm_inf(u[1,:]) + cp.norm_inf(u[2,:])) *
penalty_peak #penalize peak demand

  constraints.extend(cons)
  # form and solve the problem
  problem = cp.Problem(cp.Minimize(cost), constraints)
  problem.solve(verbose=True, solver=cp.ECOS)

# value retrieval
T_out = d[0,:].value
T1_flx = x[0,:].value
T2_flx = x[1,:].value
T3_flx = x[2,:].value
Q1_flx = u[0,:].value
Q2_flx = u[1,:].value
Q3_flx = u[2,:].value
Q_flx = Q1_flx + Q2_flx + Q3_flx
#Q_flx = Q2_flx
P_flx = Q_flx
Ppv = d[1,:].value
P_net_BAU = P_flx # - Ppv
#%%
# Flat rate price
"""#**Predictive Control**"""

# states, inputs and disturbances
nx, nu, nd = 3, 4, 4
x = cp.Variable((nx, ph))
u = cp.Variable((nu, ph))
d = cp.Variable((nd, ph))

comfort_min, comfort_max = 18*np.ones(ph), 27*np.ones(ph) #thermal comfort boundaries
for i in range(num_day):
  comfort_min[int(sph*(24*i+6)):int(sph*(24*i+18))] = 21
  comfort_max[int(sph*(24*i+6)):int(sph*(24*i+18))] = 24
comfort_base_min, comfort_base_max = 16*np.ones(ph), 18*np.ones(ph)

price = 1*np.ones(ph) #price of consumption (For BAU)
#price = 4.33*np.ones(ph) #price of consumption (Flat rate - Active this line only)
#for i in range(num_day):
  #price[int(sph*(24*i+6)):int(sph*(24*i+9))] = 50.65
  #price[int(sph*(24*i+16)):int(sph*(24*i+20))] = 50.65

penalty = 2000*100*np.ones(ph) #comfort violation penalty
penalty_base = 100*100*np.ones(ph)
#penalty_peak = 100*10 #penalty of peak demand (Correct)
penalty_peak = 1000 #penalty of peak demand (For BAU)
constraints = cons = []

cons.append(x[0,0] == 18.3,)
cons.append(x[1,0] == 17.9,)
cons.append(x[2,0] == 17,)

cons.append(u[0,:] >= heating_min,)
cons.append(u[0,:] <= heating_max,)
cons.append(u[1,:] >= heating_min,)
cons.append(u[1,:] <= heating_max,)
cons.append(u[2,:] >= heating_min,)
```

```
cons.append(u[2,:] <= heating_max,)

cons.append(d[0,:] == df_sim['Tout'][st:st+ph],) #ambient air temperature
cons.append(d[1,:] == df_sim['P_pv'][st:st+ph],) #PV generation
cons.append(d[2,:] == df_sim['Q_sol'][st:st+ph],) #solar gains
cons.append(d[3,:] == df_sim['Tgrd'][st:st+ph],) #ground or adjacent zone temperature

cost = 0 #cost initialization

for j in range(0,control_factor): #control horizon loop
  cons.append(x[0,ch*j] == x[0,ch*j-1],) #initialization of temp1
  cons.append(x[1,ch*j] == x[1,ch*j-1],) #initialization of temp2
  cons.append(x[2,ch*j] == x[2,ch*j-1],) #initialization of temp2
  cons.append(x[3,ch*j] == x[3,ch*j-1],) #initialization of battery soc

  for k in range((ch*j)+1,ch*(j+1)): #step loop
    cons.append(x[0,k] == x[0,k-1] + (dt/C1)*(u[0,k] + (d[0,k]-x[0,k-1])/R1 + (x[1,k-
1]-x[0,k-1])/R2),) #state estimator 0
    cons.append(x[1,k] == x[1,k-1] + (dt/C2)*(u[1,k] + (d[0,k]-x[1,k-1])/R3 + (x[0,k-
1]-x[1,k-1])/R2 + (x[2,k-1]-x[1,k-1])/R4),) #state estimator 1
    cons.append(x[2,k] == x[2,k-1] + (dt/C3)*(u[2,k] + alpha3*d[2,k] + (x[1,k-1]-
x[2,k-1])/R4),) #state estimator 2
    #cons.append(x[3,k] == x[3,k-1] + (u[3,k]*dt),) #state estimator 3

    #cons.append(x[0,k] == x[0,k-1] + (dt/C1)*(u[0,k] + alpha1*d[2,k] + (d[0,k]-x[0,k-
1])/R1 + (x[1,k-1]-x[0,k-1])/R4 + (x[2,k-1]-x[0,k-1])/R5),) #state estimator 0
    #cons.append(x[1,k] == x[1,k-1] + (dt/C2)*(u[1,k] + alpha2*d[2,k] + (d[0,k]-x[1,k-
1])/R2 + (x[0,k-1]-x[1,k-1])/R4 + (x[2,k-1]-x[1,k-1])/R6),) #state estimator 1
    #cons.append(x[2,k] == x[2,k-1] + (dt/C3)*(u[2,k] + alpha3*d[2,k] + (d[0,k]-x[2,k-
1])/R3 + (x[0,k-1]-x[2,k-1])/R5 + (x[1,k-1]-x[2,k-1])/R6 + (d[3,k]-x[2,k-1])/R7),)
#state estimator 2
    #cons.append(x[3,k] == x[3,k-1] + (u[3,k]*dt),) #state estimator 3

    #cost += (u[0,k] + u[1,k] + u[2,k]) * price[k] #minimize heating energy cost based
on rate flex-M (For BAU)
    cost += (u[0,k] + u[1,k] + u[2,k]) * 100*price[k] #minimize heating energy cost
based on rate flex-M (Correct)

    cost += cp.norm2(u[0,k] + u[1,k] + u[2,k] + u[3,k] - d[1,k]) #maximize self-
consumtion

    cost += cp.maximum(comfort_min[k] - x[0,k], 0, x[0,k] - comfort_max[k]) *
penalty[k] #penalize comfort violation
    cost += cp.maximum(comfort_min[k] - x[1,k], 0, x[1,k] - comfort_max[k]) *
penalty[k]
    cost += cp.maximum(comfort_base_min[k] - x[2,k], 0, x[2,k] - comfort_base_max[k])
* penalty_base[k]

    cost += cp.norm2(u[0,k] - u[0,k-1]) #penalize high slew rate
    cost += cp.norm2(u[1,k] - u[1,k-1])
    cost += cp.norm2(u[2,k] - u[2,k-1])
    cost += cp.norm2(u[3,k] - u[3,k-1])

  cost += (cp.norm_inf(u[0,:]) + cp.norm_inf(u[1,:]) + cp.norm_inf(u[2,:])) *
penalty_peak #penalize peak demand

  constraints.extend(cons)
  # form and solve the problem
  problem = cp.Problem(cp.Minimize(cost), constraints)
  problem.solve(verbose=True, solver=cp.ECOS)

# value retrieval
T_out = d[0,:].value
```

```
T1_flx = x[0,:].value
T2_flat_rate = x[1,:].value
T3_flx = x[2,:].value
Q1_flx = u[0,:].value
Q2_flx = u[1,:].value
Q3_flx = u[2,:].value
Q_flx = Q1_flx + Q2_flx + Q3_flx
#Q_flx = Q2_flx
P_flx = Q_flx
#P_bat = u[3,:].value
#soe_bat = x[3,:].value * 100
Ppv = d[1,:].value
P_net_predictive_flat_rate = P_flx

#%%
# Rate flex M price

"""#**Predictive Control**"""

# states, inputs and disturbances
nx, nu, nd = 4, 4, 4 #third-order(3)
x = cp.Variable((nx, ph))
u = cp.Variable((nu, ph))
d = cp.Variable((nd, ph))

comfort_min, comfort_max = 18*np.ones(ph), 27*np.ones(ph) #thermal comfort boundaries
for i in range(num_day):
  comfort_min[int(sph*(24*i+6)):int(sph*(24*i+18))] = 21
  comfort_max[int(sph*(24*i+6)):int(sph*(24*i+18))] = 24
comfort_base_min, comfort_base_max = 16*np.ones(ph), 18*np.ones(ph)

#price = 1*np.ones(ph) #price of consumption (For BAU)
price = 4.33*np.ones(ph) #price of consumption (Flat reat - Active this line only)
for i in range(num_day):
  price[int(sph*(24*i+6)):int(sph*(24*i+9))] = 50.65 #price of consumption (Rate flex
M - Morning - Active this line only)
  #price[int(sph*(24*i+16)):int(sph*(24*i+20))] = 50.65

penalty = 2000*100*np.ones(ph) #comfort violation penalty
penalty_base = 100*100*np.ones(ph)
penalty_peak = 1000
constraints = cons = []

cons.append(x[0,0] == 18.3,)
cons.append(x[1,0] == 17.9,)
cons.append(x[2,0] == 17,)

cons.append(u[0,:] >= heating_min,)
cons.append(u[0,:] <= heating_max,)
cons.append(u[1,:] >= heating_min,)
cons.append(u[1,:] <= heating_max,)
cons.append(u[2,:] >= heating_min,)
cons.append(u[2,:] <= heating_max,)

cons.append(d[0,:] == df_sim['Tout'][st:st+ph],) #ambient air temperature
cons.append(d[1,:] == df_sim['P_pv'][st:st+ph],) #PV generation
cons.append(d[2,:] == df_sim['Q_sol'][st:st+ph],) #solar gains
cons.append(d[3,:] == df_sim['Tgrd'][st:st+ph],) #ground or adjacent zone temperature

cost = 0 #cost initialization

for j in range(0,control_factor): #control horizon loop
  cons.append(x[0,ch*j] == x[0,ch*j-1],) #initialization of temp1
```

```
  cons.append(x[1,ch*j] == x[1,ch*j-1],) #initialization of temp2
  cons.append(x[2,ch*j] == x[2,ch*j-1],) #initialization of temp2
  cons.append(x[3,ch*j] == x[3,ch*j-1],) #initialization of battery soc

  for k in range((ch*j)+1,ch*(j+1)): #step loop
    cons.append(x[0,k] == x[0,k-1] + (dt/C1)*(u[0,k] + (d[0,k]-x[0,k-1])/R1 + (x[1,k-
1]-x[0,k-1])/R2),) #state estimator 0
    cons.append(x[1,k] == x[1,k-1] + (dt/C2)*(u[1,k] + (d[0,k]-x[1,k-1])/R3 + (x[0,k-
1]-x[1,k-1])/R2 + (x[2,k-1]-x[1,k-1])/R4),) #state estimator 1
    cons.append(x[2,k] == x[2,k-1] + (dt/C3)*(u[2,k] + alpha3*d[2,k] + (x[1,k-1]-
x[2,k-1])/R4),) #state estimator 2
    #cons.append(x[3,k] == x[3,k-1] + (u[3,k]*dt),) #state estimator 3

    #cons.append(x[0,k] == x[0,k-1] + (dt/C1)*(u[0,k] + alpha1*d[2,k] + (d[0,k]-x[0,k-
1])/R1 + (x[1,k-1]-x[0,k-1])/R4 + (x[2,k-1]-x[0,k-1])/R5),) #state estimator 0
    #cons.append(x[1,k] == x[1,k-1] + (dt/C2)*(u[1,k] + alpha2*d[2,k] + (d[0,k]-x[1,k-
1])/R2 + (x[0,k-1]-x[1,k-1])/R4 + (x[2,k-1]-x[1,k-1])/R6),) #state estimator 1
    #cons.append(x[2,k] == x[2,k-1] + (dt/C3)*(u[2,k] + alpha3*d[2,k] + (d[0,k]-x[2,k-
1])/R3 + (x[0,k-1]-x[2,k-1])/R5 + (x[1,k-1]-x[2,k-1])/R6 + (d[3,k]-x[2,k-1])/R7),)
#state estimator 2
    #cons.append(x[3,k] == x[3,k-1] + (u[3,k]*dt),) #state estimator 3

    #cost += (u[0,k] + u[1,k] + u[2,k]) * price[k] #minimize heating energy cost (For
BAU)
    cost += (u[0,k] + u[1,k] + u[2,k]) * 100*price[k] #minimize heating energy cost
based on rate flex-M (Correct)

    cost += cp.norm2(u[0,k] + u[1,k] + u[2,k] + u[3,k] - d[1,k]) #maximize self-
consumtion

    cost += cp.maximum(comfort_min[k] - x[0,k], 0, x[0,k] - comfort_max[k]) *
penalty[k] #penalize comfort violation
    cost += cp.maximum(comfort_min[k] - x[1,k], 0, x[1,k] - comfort_max[k]) *
penalty[k]

    cost += cp.norm2(u[0,k] - u[0,k-1]) #penalize high slew rate
    cost += cp.norm2(u[1,k] - u[1,k-1])
    cost += cp.norm2(u[2,k] - u[2,k-1])
    cost += cp.norm2(u[3,k] - u[3,k-1])

  cost += (cp.norm_inf(u[0,:]) + cp.norm_inf(u[1,:]) + cp.norm_inf(u[2,:])) *
penalty_peak #penalize peak demand

  constraints.extend(cons)
  # form and solve the problem
  problem = cp.Problem(cp.Minimize(cost), constraints)
  problem.solve(verbose=True, solver=cp.ECOS)

# value retrieval
T_out = d[0,:].value
T1_flx = x[0,:].value
T2_flexM_morning = x[1,:].value
T3_flx = x[2,:].value
Q1_flx = u[0,:].value
Q2_flx = u[1,:].value
Q3_flx = u[2,:].value
Q_flx = Q1_flx + Q2_flx + Q3_flx
#Q_flx = Q2_flx
P_flx = Q_flx
Ppv = d[1,:].value
P_net_predictive_flexM_morning = P_flx
```